Catalytic Degradation of Waste Polymers

by

Tina Gornall, MPhys, MSc

Submitted in partial fulfilment of the requirements for the degree of Doctor of

Philosophy at the University of Central Lancashire

January 2011

Declaration

The work described in this thesis was conducted at the Centre for Materials Science, University of Central Lancashire, between July 2005 and November 2008. Unless otherwise stated, it is the work of the author and has not been submitted in support of any other degree.

Signature:……………………………..

Tina Gornall

January 2011

Abstract

Plastics have become an integral part of our lives. However, the disposal of plastic waste poses an enormous problem to society. An ideal solution would be to break down a polymer into its monomer, which could then be used as the building-blocks to recreate the polymer. Unfortunately, the majority of plastics do not degrade readily into their monomer units. Thermal degradation of polymers usually follows a radical mechanism (which is of high energy and requires high temperatures) and produces a large proportion of straight chain alkanes, which have low relative octane number (RON) and so cannot be used in internal combustion engines. However, a suitable catalyst can help to branch straight alkane chains and so give high RON fuels that can be blended into commercial fuels.

An extensive thermogravimetric study of polymer-catalyst mixtures was undertaken and produced dramatic reductions in the onset temperature of degradation and significant changes in the activation energy, suggesting a change to a desirable Brønsted- or Lewis-acid catalysed degradation mechanism in many cases. For example, GC-MS analysis of low-density polyethylene (LDPE) degraded with Fulcat 435 clay showed the polymer forming a large number of C_6-C_7 single-branched alkanes of intermediate RON value. In comparison, degradation of LDPE in the presence of a ZSM-5 zeolite (280z) resulted in the production of a large aromatic content (41% of Total Mass at 450ºC) together with branched C_6-C_8 hydrocarbons (40%). This formation of a large proportion of high RON components from polyethylene and other polymers could move us one step closer to tackling the enormous problem of plastic waste disposal that the world faces today.

Table of Contents

Table of Tables

Table of Figures

Acknowledgements

Firstly, I would like to thank my supervisors Dr. Richard McCabe and Prof. Gary Bond for their guidance and support throughout the project. Thank you to Jim Donnelly of the University of Central Lancashire Analytical Unit for his assistance, and Dr. Runjie Mao for helping me to couple together the equipment and understand the instruments. Thanks also to Pat Cookson for running some NMR experiments for me and to Dr Rongrong Zhou for teaching me how to use the new pyroprobe.

On a personal level, a special thank you goes to my husband Richard who has been an unbelievable support throughout the many years of my PhD. Also, to my two lovely children, James and Emily, who have changed my life. But mostly, this thesis is dedicated to my Dad who supported me all the way.

Abbreviations

General

APC	American Plastics Council
ATR	attenuated total reflectance
BET	Brunauer, Emmett and Teller
BTX	Benzene, Toluene, Xylene
CCD	charge coupled device
CEC	cation exchange capacity
CI-MS	chemical ionisation-mass spectrometry
CPP	Curie point pyrolysis
CV	calorific value
DCM	dichloromethane
DEFRA	Department for Environment Food and Rural Affairs
DT	differential thermogravimetry
DTA	differential thermal analysis
ECD	electron capture detector
EDX	energy dispersive X-ray
ELV	end-of-life vehicles
EPS	expanded polystyrene
FCC	fluidised catalytic cracking
FTIR	Fourier Transform Infrared
GC	gas chromatography
HDPE	high-density polyethylene
ICI	Imperial Chemical Industries
IR	Infrared
IRE	internal reflecting element
LDPE	low-density polyethylene
LHHW	Langmuir-Hinshelwood-Hougen-Watson
LLDPE	linear low-density polyethylene
LPG	liquefied petroleum gas
MAS	magic angle spinning
MIR	multiple internal reflectance
MS	mass spectrometry
MSW	municipal solid waste
NMR	nuclear magnetic resonance

ON	octane number
PA	polyamide
PAN	polyacrylonitrile
PB	polybutadiene
PE	polyethylene
PET	polyethylene terephthalate
PMMA	polymethyl methacrylate
PP	polypropylene
PS	polystyrene
PU	polyurethane
PVA	polyvinyl acetate
PVC	polyvinyl chloride
Py-GC	pyrolysis-gas chromatography
Py-GC-MS	pyrolysis-gas chromatography-mass spectrometry
Py-MS	pyrolysis-mass spectrometry
RDF	refuse derived fuel
RE	rare-earth
RF	radio frequency
RPI	Rensselaer Polytechnic Institute
S/N	signal to noise ratio
SEM	scanning electron microscopy
SPM	simultaneous pyrolysis methylation
SPM-GC	simultaneous pyrolysis methylation-gas chromatography
TG	thermogravimetry
TGA	thermogravimetric analyser
TPA	thermoplastic acrylic
TPD	temperature programmed desorption
V	vinyl
VAT	value added tax

Symbols

λ	wavelength/ nm or cm^{-1}, where appropriate
ν	frequency/ s^{-1}
ε_0	solvent strength parameter/ Jm^{-2}
C	concentration/ M or mol dm^{-3}
E_a	activation energy/ kJmol^{-1} or kcal mol^{-1}
C_v	heat capacity
C_p	specific heat
t_R	retention time/ mins

Constants

c	speed of light, 2.998 x 10^8 ms^{-1}
h	Planck's constant, 6.626 x 10^{-34} Js^{-1}

Chapter 1

Introduction

1 Introduction

1.1 Waste

'Waste' is defined as any substance or object which the holder discards or intends or is required to discard.[1] Municipal Solid Waste (MSW) is a term used to describe the waste produced by households or commercial establishments, *i.e.* food, paper, glass, textiles, cans and plastic, that is collected by a local Government authority. Currently, the majority of urban solid waste generated in the UK is disposed of in sanitary landfill sites, involving no sorting or recycling. However, with a massive growth in population, hence an increase in the generation of waste, a reduction in the amount of land available and the synthesis of more hazardous products such as pesticides, landfills are bigger and more toxic than ever before. The future of waste disposal must be based on the underlying principle of sustainable development and an effort must be made to conserve non-renewable resources to the maximum extent possible.

1.1.1 Energy Recovery from Municipal Solid Waste

Municipal Solid Waste can be incinerated according to the Kyoto Protocol[2] and the European Parliament guidelines on residues and emission values.[3] However, to consider a waste incineration plant as an energy-producing facility, the waste's calorific value must exceed the energy required for the construction and operation of the plant.[4] The calorific value (CV) of a material is an expression of the energy content, or heat value, released when burnt in air and is measured in terms of the

energy content per unit mass, or volume, hence MJ/kg for solids, MJ/l for liquid or MJ/Nm^3 for gases.[5]   The relatively high calorific values of modern packaging materials means that typical municipal solid waste has a heat content between one-third and one-half that of power station coal. The calorific values of numerous waste materials and fuels are displayed in Table 1.1.

Table 1.1: Calorific values of waste materials and fuels[6,7]

Material	Btu per pound	MJ/kg
Polyethylene	18000-20000	42-46
Polypropylene	20000	46
Polystyrene	18000-19500	42-45
Polyvinyl chloride	8000-9500	19-22
Polyurethane	10000	23
Polymethyl methacrylate	14000	33
Polyamide	13000-15000	30-35
Polyester	13000	30
Synthetic rubber (tyres)	14600	34
Paper	7700	18
Power station coal	11000	26
Oil	18000	42
Natural gas	23000	53
Brown coal	4200	10
Wood	9000	21

In 2003/04, England produced 29.1 million tonnes of municipal waste, of which 72% was disposed of at landfill (a reduction from 75% in 2002/03). The proportion of waste being recycled or composted was said to have increased from 15.6% in 2002/03 to 19.0% in 2003/04, whilst the proportion of waste incinerated with energy recovery

remained constant at 9%.[8] The national waste strategy targets involve recycling/composting 33% of household waste in the UK by 2015.[9]

Financial incentives (tax concessions or VAT differentiation) or disincentives can be used to change the generation, recycling, reuse and final disposal of waste.[10] In October 1996, a tax on disposal of waste to landfill in England and Wales was levied at £7 per tonne for active and £2 per tonne for inactive waste. The landfill tax credit scheme aimed to channel up to 20% of the funds from the tax towards bodies with environmental objectives.[11]

1.1.2   Plastic Waste

The modern plastics industry can trace its origins back to 1862 when Alexander Parkes unveiled *Parkesine* (cellulose-acetate plasticised with camphor) - the first man-made plastic.[12] Today, there are in excess of twenty different polymer types in common usage – all with different properties and functionalities. Plastics have become an integral part of our lives. Their low density, strength, low cost, user-friendly design and fabrication capabilities are the drivers to the steady growth in plastic consumption.[13] However, with a dramatic increase in the use of plastics over the last fifty years has come a major problem with its disposal. In sanitary landfill, polymers act essentially as inert materials and do not decompose readily, retarding the processes of settling and stabilisation of the refuse. An alternative to the landfilling of plastic waste must be sought.

Packaging represents the single largest sector of plastics use in the UK economy, with the majority comprising of polyethylene (PE) films (shrink wrap, sacks, industrial

liners). The EC Directive on Packaging and Packaging Waste 94/62/EC sets targets for the recovery and recycling of these packaging wastes.[14] The building and construction sector is the second-largest consumer of plastics in the UK. Common uses include insulation, flooring, windows, pipes and fitted furniture, with polyvinyl chloride (PVC) utilised the most. In terms of volume, automotive vehicles contain a larger proportion of plastics than any other material, but comprise only 10% of the total weight. The waste plastics from end-of-life vehicles (ELV), such as polypropylene battery cases and bumpers, are recycled under the ELV Directive 2000/53/EC.[15] The proportion of different types of polymers consumed in the UK (2000) is displayed in Figure 1.1.

Legend:
- Low-Density Polyethylene
- Polyvinyl Chloride
- Polypropylene
- High-Density Polyethylene
- Expanded Polystyrene
- Acrylonitrile Butadiene Styrene
- Polyethylene Terephthalate
- Polystyrene
- Other
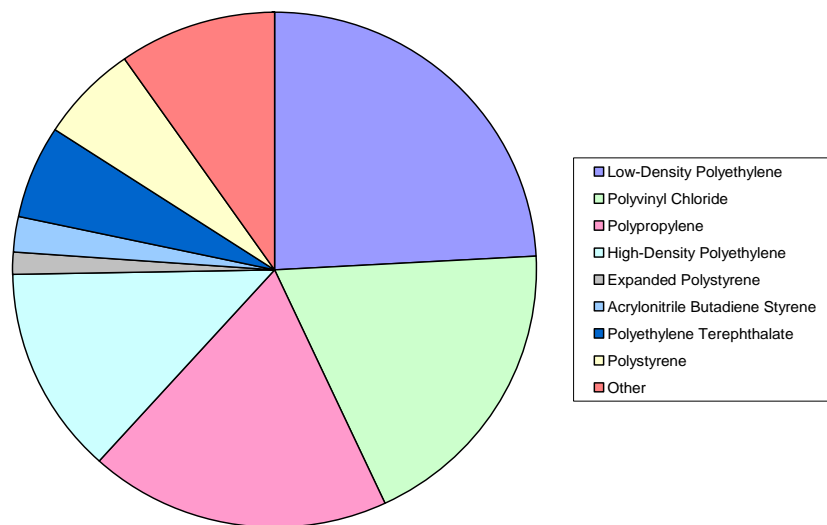
Figure 1.1: Percentage of UK consumption of plastics by polymer type, 2000[16]

In the UK in 2003, 287,000 tonnes of plastic waste was reprocessed, with 114,000 tonnes exported for reprocessing – an achievement of 22.4%. In 2004, nearly 170,000 tonnes of plastic waste was reprocessed domestically, with 174,000 tonnes exported for reprocessing - an achievement of 18.6%.[17]

1.1.2.1 Reuse of Plastic Waste

Recycling plastics encompasses four phases of activity: collection, separation, processing/manufacturing and marketing. As only clean, homogeneous resins can produce the highest-quality recycled plastic products, an effective separation of plastics waste is necessary.[18] Most plastics have densities within the range 900-1500 kg/m^3,[19] therefore flotation methods can provide crude separation. Some plastics, *e.g.* polyvinyl chloride and polypropylene can be separated by applying gravity separation, whilst the separation of PVC and polyethylene terephthalate is very difficult, due to the two polymers having only a slight difference in density.[20] A new rapid-identification system produced by the American Plastics Council (APC) uses mid-infared wavelength technology to distinguish up to twenty-three different plastics, identifying the chemical compositions of each plastic within five seconds.[21]

Rensselaer Polytechnic Institute (RPI) has developed a technique for the recycling of plastics that are not cross-linked.[22] The process uses unsorted plastic that has been coarse-shredded. Xylene is added to the mixture and any polystyrene present dissolves in the solvent. The xylene/polystyrene liquid is obtained from the vessel, decontaminated and the solvent and the plastic are separated by distillation. The xylene distillate is then re-heated and reintroduced into the plastic mixture. As the solvent is at a slightly higher temperature, low-density polyethylene is dissolved and removed in the same way. The process is repeated several times, each time with the xylene being reintroduced into the plastic mixture at a higher temperature; hence a different plastic is dissolved for each cycle. The end result is that the mixture of plastics has been separated and recycled into pure plastic pellets. This dissolution/reprecipitation technique was used by Poulakis and Papaspyrides for the

recycling of polypropylene.[23]   Polypropylene was dissolved in a combination of xylene and acetone, with the xylene being an effective solvent and the acetone acting as a non-solvent to precipitate the polymer in the form of powder without gelling lumps.   Excellent recoveries in polymer and solvent were achieved, with good retention of mechanical properties of the recycled polypropylene.   Pappa *et al*., investigated the recycling of PP, rigid PVC bottles, PS foam, LDPE film and HDPE bottles.[24]   The LDPE:HDPE:PP mixture was separated successfully using a xylene/propanol system at different temperatures.   PVC was separated from PS by dissolving it in cyclohexanone and precipitating it with hexane.   The cost of the recycled polymer was found to be comparable to the commercial price of the virgin one, with no difference in quality.

Table 1.2 lists the recycling codes currently used in the UK today.   These inform the consumer as to the type of polymer they are discarding and enables the correct recycling of the waste plastic wherever possible.

Table 1.2: Recycling codes

PETE (1)	Polyethylene Terephthalate (PET) - recycled into carpets, fibre fillings.
HDPE (2)	High-Density Polyethylene (HDPE) – recycled into plastic pipes, flower pots.
V (3)	Vinyl (V) / Polyvinyl Chloride (PVC).
LDPE (4)	Low-Density Polyethylene (LDPE) – recycled into rubbish bags, plastic tubing.
PP (5)	Polypropylene (PP).
PS (6)	Polystyrene (PS).
OTHER (7)	Other (layered or mixed plastic).

1.1.3   Aims of the Project

The disposal of vast amounts of non-degradable plastic waste in landfill is not acceptable long-term. This study aims to investigate the thermal degradation of a variety of waste polymers in the presence of catalysts in an attempt to convert this valuable waste stream into high-grade fuel.

1.2 Polymers

In simple terms, a polymer can be described as a large molecule, built up from numerous smaller molecules known as monomers. A polymer may be linear, slightly branched or highly interconnected. There are two main systems used to classify polymers: one based on their response to thermal treatment (thermoplastics and thermosets) and the other based on the nature of the chemical reactions employed in the polymerisation (condensation and addition polymers).[25] Addition polymerisation involves the combination of simple molecules without the formation of any new products. In contrast, condensation polymerisation is the combination of simple, dissimilar molecules, with the formation of by-products such as water or ammonia.

By understanding the structures of the different types of polymers found in municipal solid waste, their mechanisms of degradation can be studied (and perhaps altered by the presence of catalysts) in order to achieve the most useful decomposition products.

1.2.1 Polymerisation Mechanisms

1.2.1.1 Addition Polymerisation

Addition polymers are those formed by the addition reaction of an unsaturated monomer, where the molecular formula of the structural unit (or units) is identical with that of the monomer from which the polymer is derived. Some examples of addition polymers are shown in Figure 1.2.
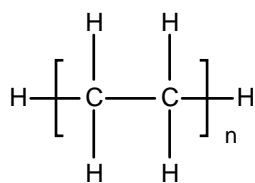
Polyethylene
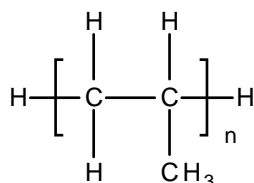
Polypropylene
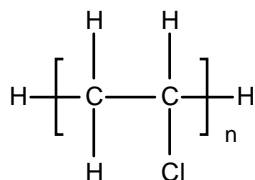
Polyvinyl chloride
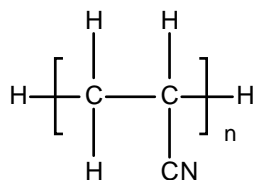
Polyacrylonitrile
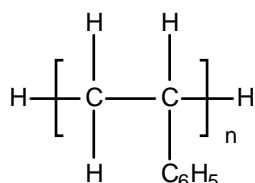
Polystyrene
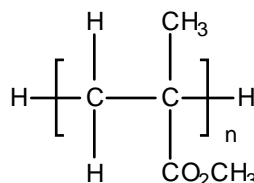
Polymethyl methacrylate

Figure 1.2: Examples of addition polymers

1.2.1.2 Condensation Polymerisation

Condensation polymers, such as polyester, are prepared from monomers where the reaction is accompanied by the loss of a small molecule (*i.e.* water). Condensation polymers are usually formed by the stepwise intermolecular condensation of reactive groups, whereas addition polymers result ordinarily from chain reactions involving some sort of active centre.[26] A notable exception occurs with the synthesis of polyurethanes which are formed by reaction of isocyanates with hydroxyl compounds and follow step kinetics, without elimination of small molecules from the respective units.[27]

1.2.2 Thermoplastics

1.2.2.1 Polyalkenes

Polyethylene (see Figure 1.2) is the most fundamental plastic due to its simple structure, low cost and useful balance of properties. High-density (linear) polyethylene (HDPE) is a flexible regular molecule that crystallises readily to rigid, strong products of good electrical and chemical resistance.

Typically, linear polyethylene contains less than one side chain per two hundred carbon atoms in the main chain, whereas a typical low-density polyethylene (LDPE) molecule may contain, on average, fifty short branches and less than one long branch. These side groups break up the regularity of the chain, so reducing the crystallinity of the polymer and producing a lower density, lower melting and more flexible product.

Polypropylene can be similar to polyethylene but with greater rigidity and hardness, or amorphous and of little strength. The rigid form of polypropylene is *isotactic*, with a regular stereochemistry at each alternating carbon atom (see Figure 1.2). The amorphous form is *atactic*, with a random distribution of different stereochemical arrangements at each methyl-bearing carbon atom. The isotactic molecule is forced into a preferred helical-coil formation whose regularity produces high crystallinity. The helical structure gives the best balance between the interatomic repulsive forces and the van der Waals attractive forces between the methyl groups.[28] In the syndiotactic form, the polymer-monomer units are arranged in repeating pairs so that the methyl groups alternate between the two sides of the stretched chain. There is little structure in the polymer backbone, resulting in poor strength and high tackiness. Commercial polypropylene is typically 90-95% isotactic.

1.2.2.2 Polystyrene

Polystyrene is an amorphous polymer of good transparency, rigidity and low water absorption. The monomer, *styrene*, is a derivative of benzene (vinyl benzene) that polymerises readily. Polystyrene has a succession of bulky phenyl groups on alternate carbon atoms which stiffen the main chain considerably, producing a clear, amorphous, glassy solid that is brittle at room temperature (see Figure 1.2). Polystyrene film is strong, light and durable, and at a thickness of around 30 μm, is used for envelope windows. Expanded polystyrene (EPS) is a closed-cell foam composed of small, interconnected beads. The polystyrene beads are heated with hot air or steam to drastically reduce their density, then cooled and moulded. Applications of EPS include drink cups, cavity wall insulation and packaging.

1.2.2.3 Polyvinyl Chloride

The monomer of PVC, vinyl chloride, is produced in a two-stage process in which the ethylene is first reacted catalytically with HCl and oxygen to yield 1,2-dichloroethane, and then pyrolysed to vinyl chloride and HCl. In general, polyvinyl chloride is a partially syndiotactic material, with sufficient irregularity of structure that crystallinity is low (see Figure 1.2).

1.2.2.4 Polymethyl Methacrylate

Polymethyl methacrylate (PMMA) is a clear, colourless, transparent linear thermoplastic, approximately 70-75% atactic in structure (see Figure 1.2). Because of its lack of complete stereoregularity and its bulky side groups, it is amorphous and is the most important of the commercial acrylic polymers. PMMA is made by free radical vinyl polymerisation from the monomer, methyl methacrylate. PMMA is

stiffened by the distribution of successive quaternary carbon atoms along the main chain, which yields hard, rigid products. Their normal random configuration prevents crystallisation, so producing an amorphous glassy solid.

1.2.2.5 Polyacrylonitrile

When polyacrylonitrile (PAN) was first developed, it was considered a useless material because it could not be dissolved or plasticised and was not soluble in the monomer and therefore could not be polymerised into useful shapes by casting. Nowadays, solvents such as dimethyl formamide have been discovered which are able to interact with the highly polar $-C{\equiv}N$ groups and cause solution of the polymer. Acrylic fibres exhibit the properties of high strength, stiffness and toughness, with good weatherability and stain resistance (see Figure 1.2).

1.2.3 Thermosets

1.2.3.1 Polyesters

Condensation polymers are formed *via* a succession of condensation reactions between two appropriate monomers. The polymerisation of polyester begins with the formation of an ester linkage in a condensation reaction involving a carboxylic acid group of one material and the hydroxyl group of another. The product has a free hydroxyl group at one end and a free carboxyl group at its other, allowing reaction with additional monomer units, forming new ester linkages and lengthening the polymer chain. Linear aliphatic polyesters have low melting points and high solubility, therefore are suitable for applications as fibres. However, the stiffening action of the *p-phenylene* group in a polymer chain leads to high melting points and good fibre-forming properties. It was discovered that by reacting ethylene glycol and

dimethyl terephthalate, a suitable polyester could be produced. The formation of polyethylene terephthalate is displayed in Figure 1.3.
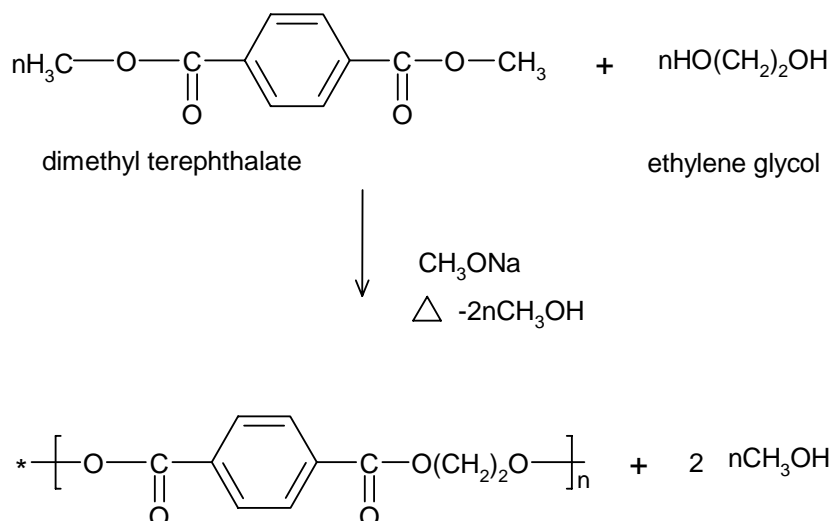
Figure 1.3: Formation of polyethylene terephthalate[29]

Nowadays, terephthalic acid is used directly to form polyethylene terephthalate (PET). The acid is converted to the dimethyl ester, which can be purified easily by distillation or crystallisation. This then reacts with the glycol by ester interchange. PET has a high crystalline melting point and glass transition temperature, therefore it retains good mechanical properties at temperatures up to 150°-175°C. Polyethylene terephthalate fibres display exceptional crease resistance and low moisture absorption, making them highly suitable in the textiles industry.

1.2.3.2 Polyamide

The word 'nylon' is often used as a generic term for synthetic polyamides. Nylons are composed of flexible hydrocarbon chains alternating with regularly repeating polar amide groups. The regular structure and the intermolecular attraction due to

polarity and hydrogen bonding result in high crystallinity (rigidity and strength), whilst the hydrocarbon segments give the polyamide its flexible property. Nylons are described by a numbering system, which indicates the number of carbon atoms in the monomer chains, with 6, 66, 610 and 11 nylon being of greatest commercial importance. The structures of Nylon 6 and Nylon 66 are displayed in Figure 1.4.
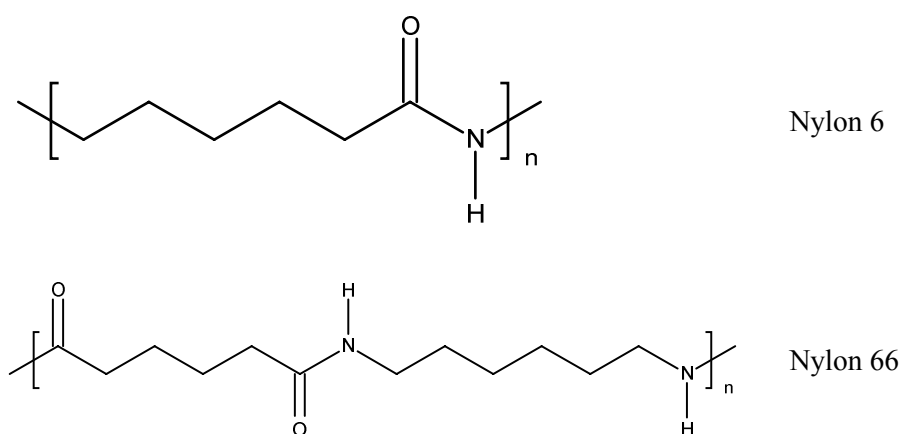
Figure 1.4: Nylons 6 and 66

Since the chains of nylons having an even number of carbon atoms between the amide groups pack better, their melting points are higher than comparable nylons with odd numbers of carbon atoms, such as nylon 11 (the odd-even effect). The melting point decreases and the water resistance increases as the number of methylene groups between amide groups is increased. The thermal degradation of nylon is said to include primary reactions below 300°C, which produces mainly light molecules such as H_2O, CO_2 and NH_3. Secondary reactions, occurring above 300°C, result in a large amount of crosslinking.[30] Nylons, because of their linear structure, can be drawn into excellent fibres of high strength, toughness and flexibility which are insoluble in all common solvents.

1.2.3.3   Polyurethane

Urethanes are formed from reacting an *iso*cyanate group (-N=C=O) with a hydroxyl group (-OH). A polyurethane linkage is displayed in Figure 1.5. Polyurethanes are widely used in foams, fibres, elastomers and coatings. They are made in several steps, with the initial macromolecule being a low-molecular weight (1,000-2,000) polymer with hydroxyl end groups. This basic intermediate may be a polyester, polyether or a mixed polyester-polyamide, which undergoes linking or crosslinking with a di- or tri-*iso*cyanate to form the polyurethane structure. The urethane group is produced *via* an addition reaction of a hydroxyl compound across an *iso*cyanate group.
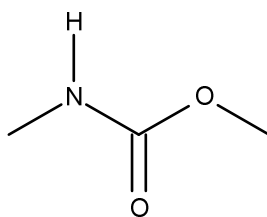
Figure 1.5: Polyurethane linkage

Polyurethane foams can be either rigid or flexible. Rigid foams are used in cavity wall insulation, whereas flexible urethane foams have applications in furniture and automobile cushioning. Flexible foams are made by liquid-phase reaction between low-molecular-weight polyols and polyisocyanates.

1.2.3.4   Polybutadiene

Polybutadiene was one of the first types of synthetic elastomer to be invented. Butadiene is derived exclusively from petroleum. Fractionation of the products of cracking petroleum yields a large amount of hydrocarbons of the butane and butene families. 1-Butene is separated and dehydrogenated catalytically in the vapour phase

to 1,3-butadiene. *cis*-1,4-Polybutadiene is made by coordination or anionic polymerisation and has high elasticity and good resistance to oxidation. *trans*-1,4-Polybutadiene has toughness, resilience and abrasion resistance. The structures of *cis*-polybuta-1,4-diene and *trans*-polybuta-1,4-diene are displayed in Figure 1.6.

cis-polybuta-1,4-diene   *trans*-polybuta-1,4-diene
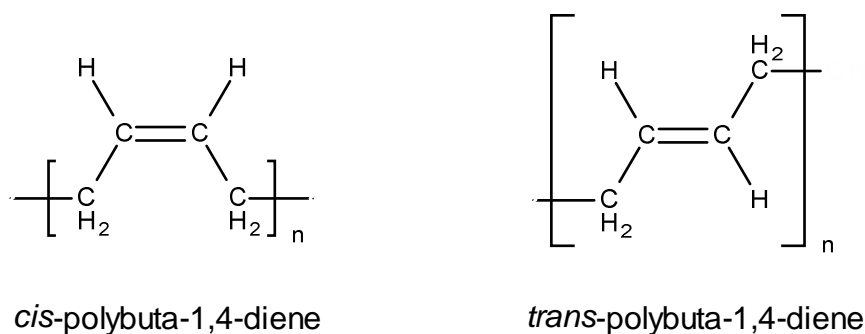
Figure 1.6: Structures of *cis*-polybuta-1,4-diene and *trans*-polybuta-1,4-diene

1.2.4   Additives and Plasticisers

Additives are essential in polymer processing to achieve desired characteristics. Additives can improve or modify the mechanical properties (fillers, reinforcements), colour and appearance (pigments, dyestuffs), give resistance to heat degradation (antioxidants, stabilisers), improve flame resistance (flame retardants) and improve the performance (plasticisers, preservatives).[31] Plasticisers have been used in many polymers for different applications where flexible properties are needed, and in many cases, more than one plasticiser is used to plasticise a polymer system. They may also serve as a lubricant, thermal stabiliser or flame retardant.[32]

1.3 Catalysts and Support Materials

A catalyst is defined as a material that accelerates a chemical reaction but remains unchanged chemically in the process. For a reaction to be possible, the process must be accompanied by a decrease of free energy. The reduction in activation energy is achieved by the catalyst providing an alternative pathway of lower energy for the reaction. Often products are formed in addition to those that are desired. The *selectivity* of a catalyst is a measure of the catalyst's ability to direct the conversion to the desired products. The greater the *stability* of a catalyst, the lower the rate at which the catalyst loses its activity or selectivity or both.[33]

Generally, catalysts consist of two or more components: the support and one or more active phases. The phase is principally responsible for the catalytic activity, whilst the support provides a vehicle for the active phase. The activity of a catalyst has been related to the number of active (acid) sites on the catalyst surface. Strong acids come in two fundamental types, *Brønsted* and *Lewis* acids. *Brønsted* acidity is provided by the very active hydrogen ion (H^+), which has a high positive charge density and seeks out negative charge, such as pi-electrons in aromatic centres. Brønsted acids can add to an olefinic double bond to form a carbocation. *Lewis* acids have high positive charge densities and can abstract a hydride ion from a saturated hydrocarbon, forming a carbenium ion. Catalysts employed in the petrochemical industry include amorphous silica-alumina (SiO_2/Al_2O_3), zeolites, acid-activated clays, and aluminium chloride ($AlCl_3$), amongst others.

1.3.1   Support Materials

1.3.1.1   Aluminosilicates

Aluminium is about the same size as silicon and readily substitutes for the latter in nature. However, since aluminium is a 3+ ion and silicon is 4+, an additional cation is required for charge balance. Thus, a Si^{4+} in the silicate framework can be substituted by the combination of an Al^{3+} with an additional (non-framework) ion. Aluminosilicates incorporating aluminium (Al), silicon (Si) and oxygen (O) find wide application as industrial catalysts.

1.3.1.2   Zeolites

Zeolites consist of atoms or ions arranged in a periodic array and are structurally unique in having cavities or pores with molecular dimensions, as part of their crystalline structures, which bear catalytic sites.

In zeolite ZSM-5, some of the silicon atoms in the SiO_4 tetrahedra are replaced by Al atoms. The tetrahedra are linked to form a chain-type building block, which are then connected to other chains. Rings consisting of 10 oxygen atoms provide access to a network of intersecting pores within the crystal. Many molecules are small enough to penetrate into this intracrystalline pore structure, where they may be catalytically converted. The aluminosilicate structure is ionic, incorporating Si^{4+}, Al^{3+} and O^{2-} ions. When some of the Si^{4+} ions in the SiO_4 tetrahedra are replaced by Al^{3+} ions, an excess negative charge is generated. To compensate for this negative charge, positive ions (cations) must be added to the framework Si^{4+} and Al^{3+}. These non-framework cations play a central role in determining the catalytic nature of the zeolite.

Faujasites consist of 12-membered oxygen rings (0.74 nm apertures) and a three-dimensional pore structure, and are able to admit hydrocarbon molecules larger than naphthalene. For this reason, faujasites have applications in the catalytic cracking of petroleum molecules into smaller gasoline-range molecules. Faujasites are made of *sodalite* cages – twenty-four primary building blocks of SiO_4 and AlO_4 tetrahedra in a truncated octahedron – arranged in a regular array. Each sodalite cage is connected to four other sodalite cages, with each connecting unit made of six bridging oxygen ions linking the hexagonal faces of two sodalite units. The *supercage* in faujasites, surrounded by 10 sodalite units, is large enough to contain a sphere of diameter 1.2 nm. The structure of faujasite is displayed in Figure 1.7.
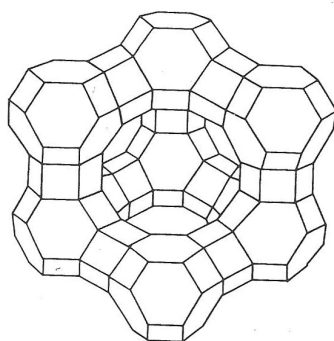
Figure 1.7: Structure of faujasite[34]

1.3.1.2.1 Adsorption in Zeolites

The void spaces in the crystalline structures of zeolites provide a high capacity for adsorbates. Chemisorption of polar molecules is influenced strongly by the nature of the cations and the interactions between the cations and guest molecules. Guest molecules can change the configuration of the aluminosilicate framework slightly. Adsorption in the pores cannot take place unless the guest molecules are small enough to fit through the apertures, and can be hindered by the cations.

1.3.1.2.2 Aluminium Content

The ion exchange capacity of a zeolite is equal to the concentration of Al^{3+} ions, therefore the structures with low Si/Al ratios are able to have higher concentrations of catalytic sites than the zeolites with high Si/Al ratios. However, the stability of the crystal framework increases with increasing Si/Al ratios. Table 1.3 lists the Si/Al ratios for four different types of zeolites.

Table 1.3: Si/Al ratios for four types of zeolite[35]

Zeolite	Name	Si/Al Ratio
Zeolite A	LTA	1
Zeolite Y	FAU	≈ 2.5
Mordenite	MOR	≈ 5
ZSM-5	MFI	> 12

1.3.1.2.3 Acidity of Zeolites

Both Brønsted and Lewis acid sites occur in zeolites. The hydrogen form zeolite contains protons (H^+) that are mobile within the structure. OH groups located near AlO_4^- tetrahedra are thought to be strong Brønsted acids, but are said to have a wide distribution of proton donor strengths.[36] Zeolites with low densities of proton donor groups, such as HZSM-5 and ultra-stable HY, have been found to have high proton donor strengths, with the highest strengths associated with AlO_4^- tetrahedra having the smallest number of Al neighbours. When a hydrogen form zeolite is heated to high temperatures, water is driven off and coordinatively unsaturated Al^{3+} ions are formed. These are strong Lewis acids, with one Lewis acid site formed from two Brønsted acid sites.

1.3.1.2.4 Ion Exchanged Zeolites

Most industrial cracking catalysts contain 10% to 25% rare-earth (RE) Y zeolites in a matrix of silica-alumina, and are generally obtained by ion-exchange of an NaY zeolite using a solution of mixed rare-earth chlorides containing salts of lanthanum, cerium and neodymium. Rabo, Angell and Schomaker[37] indicated three potential catalytic sites on La^{III}Y and Ce^{III}Y zeolites – surface hydroxyl groups, oxygen deficient silicon-aluminium linkages and rare-earth cations at surface sites (present at high temperatures). Rare-earth exchanged zeolites exhibit improved thermal and chemical stabilities over the pure H-forms, while still possessing good catalytic properties. The catalytic activity is ascribed to the hydroxyl groups (Brønsted sites) and trigonal aluminium (Lewis sites), which result from heat treatment of the exchanged zeolite.[38] The increase in proton activity and in cracking activity caused by exchange of HY by cerium cations can be explained by hydrolysis of these cations, yielding protons:[39]

$$Ce^{3+} + 2H_2O \rightarrow [Ce(OH)_2]^+ + 2H^+$$
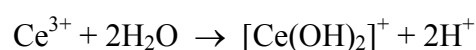
The significant increase in catalytic activity due to the presence of the RE cation has been linked to the formation of more Brønsted-acid sites.[40] Sherry[41] studied the ion-exchange properties of zeolites. He stated that all of the sites in a crystalline ion-exchanger may not be accessible to all cations and that the ion-exchange capacity of zeolites varied with the ingoing cation. Ward[42] studied the nature of active sites on RE Y-zeolites. Pyridine absorption produced bands near 3522 cm^{-1}, which were attributed to hydroxyl groups attached to the RE cations. The zeolite was found to contain several types of structural hydroxyl groups and to behave as a Brønsted acid.

Malinowski and Krzyzanowski found that exchange of cerium in a Y-zeolite had relatively small influence on the amount of strong acidic sites and on the catalytic activity of the zeolite. Further increase in the cerium cation content gave a fast increase in the acidity of the centres and a very fast rise of catalytic activity.[43] Gauthier *et al*., stated that the activity of Y-zeolites increased with the degree of exchange of Na^+ ions by Ce^{3+} cations. However, this increase was said not to be instantaneous nor linear, with no activity observed below a 20% exchange and a rapid increase in activity observed above this.[44] Lemos *et al*.,[45] found that the maximum was reached when the degree of rare-earth exchange was such that only one trivalent cation existed in the vicinity of the same supercage. This was said to occur at 42% exchange.

Lanthanum ions in the form of $[La_2(OH)_2]^{4+}$ or $La(OH)^{2+}$ species are believed to be responsible for the withdrawal of electrons from the framework hydroxyl groups, thus making the protons more acidic.[46] The effective charge on lanthanum has been found to be reduced from +3 to +2 between 200°C and 500°C, with the irreversible formation of a bridged hydroxyl group, suggesting each La cation creates one new Brønsted site. However, due to the different OH environments, these acid sites are not identical in strength. The hydrated La^{3+} cation has an ionic radius of 3.96 Å and remains in the supercage of the zeolite. On heating, the hydration sphere is lost and a number of lanthanum atoms migrate into the sodalite cage while sodium cations migrate from the sodalite cage to the supercage.[47] Lee and Rees[48] stated that lanthanum migration did not occur below 60°C, whilst the amount of lanthanum locked in the small cages became constant at temperatures greater than 300°C. The hydrated cerium(III) ions were also found to be too large to diffuse through the six-

membered ring which separates the supercage and small cages (hexagonal prism and sodalite cage). Hence, the cerium(III) ions in CeNaY were located in the supercages only, until a temperature of 250-300°C when the cerium ions migrated to the small cages.[49] Nery *et al.*,[50] showed that regardless of calcination mode, both La and Ce migrate to S2 sites that are located inside the sodalite cage, whereas Na cations migrate to S4 sites. The sites for non-framework atoms in Y-zeolites are displayed in Figure 1.8.
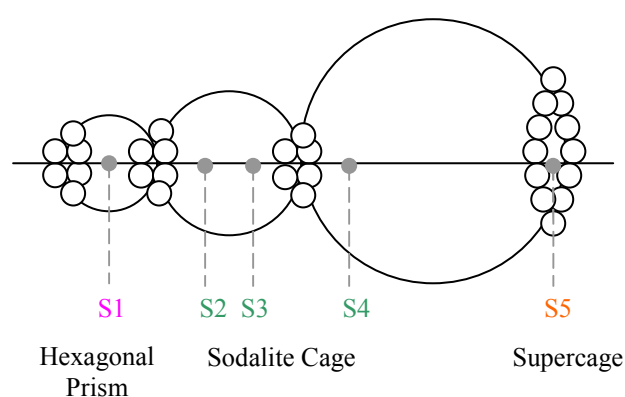
Figure 1.8: The crystallographic sites for non-framework atoms[50]

In relation to this study, a Ce^{3+} Y-zeolite and La^{3+} Y-zeolite were characterised and used for the catalytic degradation of various types of pure and waste plastic.

1.3.1.2.5 Selectivity of Zeolites

Zeolite catalysts often have a high selectivity for the following class of reaction:

$$olefins + cycloparaffins \rightarrow paraffins + aromatics$$
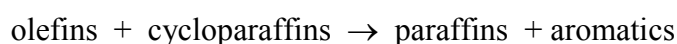
which is accounted for by hydrogen (hydride and proton) transfers. This makes zeolites important catalysts in the cracking of heavier petroleum fractions into smaller paraffins and olefins that boil in the gasoline range. Chatterjee *et al.*,[51] studied the interaction energy between organic molecules (reactant and product) and the zeolite host lattice to locate the reason for the selectivity order. It was found that the positive charges in the molecules have ionic interactions with the basic oxygen of the zeolite framework, allowing adsorption inside the zeolite void volume. The void dimensions of the zeolite were said to control product yield, whilst the electronic interactions played a vital role in the mechanism of the organic reaction. Woo, Lee and Lee[52] investigated the catalytic skeletal isomerisation of *n*-butenes to *iso*-butene over a natural clinoptilolite zeolite. It was found that proton exchange was essential for the zeolite to have isomerisation activity. The exchange created strong acid sites, with a zeolite of Si/Al ratio of 20 exhibiting greater activity than a zeolite with Si/Al ratio of 10. Buchanan[53] studied the effects of adding ZSM-5 to fluid catalytic cracking (FCC) units. The zeolite was found to catalyse C_5^+ olefin isomerisation, with ZSM-5 prepared with higher silica/alumina ratio exhibiting higher gasoline selectivity.

1.3.1.3 Clays

Clay minerals are found in soils, sediments and rocks and are classified as *phyllosilicates* (hydrous aluminosilicates). Generally, they are said to be composed of particles less than 2 μm in size. The vast majority of clays are aluminosilicates or magnesiosilicates, and consist of repeating layers of silicate $[SiO_4]^{4-}$ sheets (tetrahedral) and metal oxide sheets (octahedral) bonded together *via* shared oxygen atoms and combined in T:O (1:1) or T:O:T (2:1) arrangements, as shown in Figure 1.9.
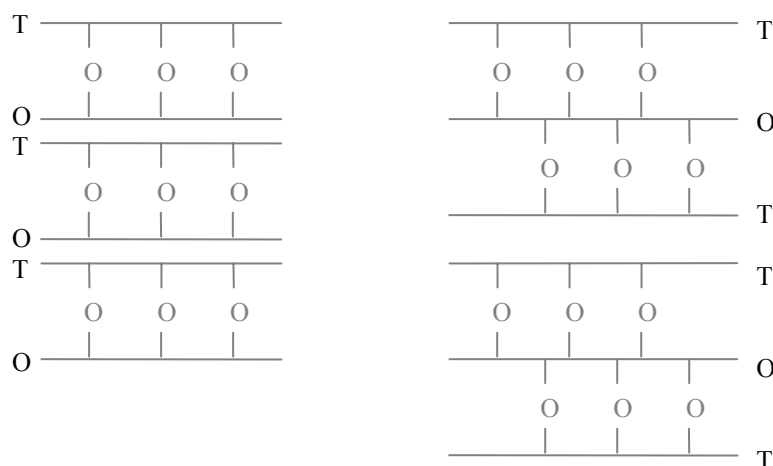
Figure 1.9: T:O and T:O:T arrangements in clays

The 1:1 arrangement of alternating tetrahedral and octahedral sheets uses hydrogen bonds between the —OH on one layer and a bridging —O— on the next layer as the main bonding force between layers. Smectites (*e.g.* montmorillonite) are composed of the 2:1 arrangement of repeating units of tetrahedral:octahedral:tetrahedral layers. If the layers are neutral and are simply held together by van der Waals forces (e.g. talc), then the layers can easily slip over one another.

1.3.1.3.1 Acidity of Clays

Clay minerals show both Brønsted and Lewis acidity. Brønsted acidity depends upon the water content of the clay and on whether the layer charge arises from substitution in the octahedral or tetrahedral sheet, and is derived from dissociation of water molecules in the interlayer exchangeable cations:[54]

$$[M(OH_2)_n]^{m+} \leftrightarrow [M(OH_2)_{n-1}OH]^{(m-1)+} + H^+$$
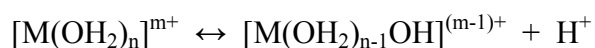
Brønsted acidity is greater when the water content of the clay is low and when highly polarising species (*i.e.* M^{3+} cations) are exchanged for the natural Na^+ and Ca^{2+} cations. Cr^{3+} and Fe^{3+} are the most active interlayer cations. Additionally, the —OH groups of the octahedral layer which protrude into the interlayer region through the holes in the silica ring are a minor contribution to the acidity of the clay.

Lewis acidity in clays is associated with exposed Al^{3+} and Fe^{3+} at the 'broken' crystallite edges. These defect Al sites are usually saturated at room temperature, but can be exposed on heating to around 300°C. The deposition of metal salts (*i.e.* copper, magnesium and zinc chlorides) on the clay surface has also been found to provide a source of Lewis acidity. The acidity of clays can be increased by removing interlayer water, through heating, desiccation, evacuation or addition of a non-polar solvent.

Natural montmorillonite has limited catalytic activity. Montmorillonite contains both Brønsted and Lewis acid sites and acid treatment can increase the Lewis acidity by breaking down the clay sheets. Ganguli and Bhagawati[55] compared the Lewis acidity of Na^+, Ca^{2+} and Zn^{2+}-loaded montmorillonite, acid-treated Zn^{2+}-loaded montmorillonite and Fe-pillared montmorillonite. Acid treated Zn^{2+}-loaded clay was found to exhibit the highest Lewis acidity.

Acid treatment of a clay is carried out by treating the clay with concentrated mineral acids such as sulphuric, phosphoric and hydrochloric acids. This results in changes to surface area, porosity and the type and concentration of the ions in the exchange sites. During acid activations, Al^{3+} and Mg^{2+} cations are removed from the octahedral sites

in the clay layers by the action of the acid, and are relocated in the interlayer space where they act as acid centres. This promotes catalytic activity by increasing the number of Brønsted and potential Lewis acid sites. On acid activation, some of the Al, Mg and Fe in the octahedral layer of the clay are dissolved out, leaving 'floppy' silica sheets. Folding of the sheets can form mesopores (100 Å) which are able to accommodate larger molecules for sorption and catalysis. The acid activation of a clay is shown in Figure 1.10.

Na$^+$ or Ca^{2+} cations $\xrightarrow[\text{Heat}]{\text{5M H}^+}$ Al^{3+} and H$^+$ cations
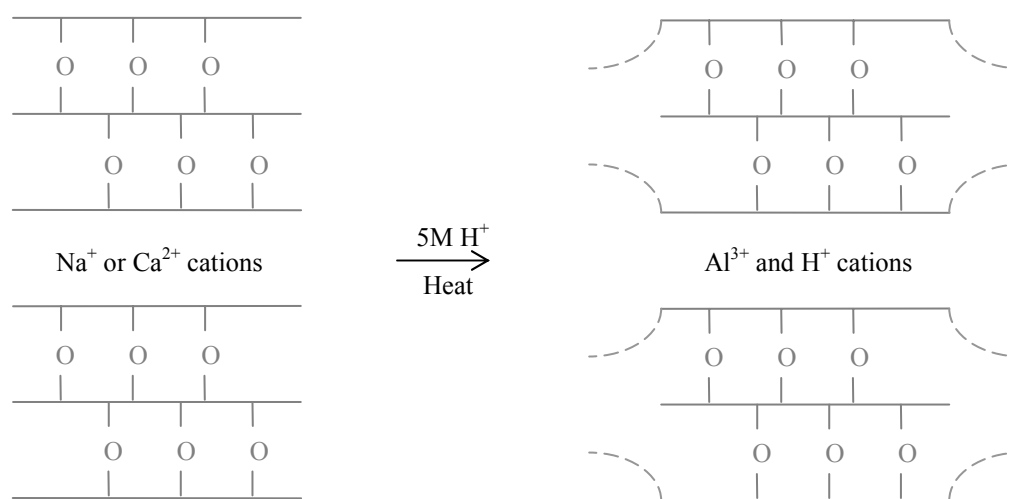
Figure 1.10: Acid activation of a clay

Thomas, Hickey and Stecker[56] investigated the effects of acid activation on montmorillonite clay. Cold (room temperature) acid was found to remove all of the calcium, sodium and potassium ions, and part of the magnesium, from the interplanar space within the clay, suggesting that cold acid does not attack the central layer. Hot acid (boiling) was found to remove some aluminium from the central layer. No significant amount of silica was removed by either treatment and an increase in catalytic activity of the clay was observed.

Montmorillonite, $Al_2(Si_4O_{10})(OH)_2$, is composed of SiO_2 (66.7%), Al_2O_3 (28.3%) and H_2O from hydroxyl groups (5%) and is formed of planes of two silicon tetrahedra and a central plane with aluminium octahedra. An important feature of the clay is that water and other polar molecules of an organic nature can enter between the unit layers, causing a displacement in the lattice in the direction of the *c*-axis. For a completely dry clay, the *c*-axis depends upon the size and type of the interlayer cation present. The interlayer spacing, Δd, is an important parameter of the clay system as it gives a measure of the available reaction space during a clay/organic molecule interaction. Dimensions of the *c*-axis for montmorillonite are not fixed and vary from 9.6 Å when no polar molecules are present between the layers, up to 15 Å (with polar molecules present).[57] Three of the catalysts investigated in this study (Fulacolor, Fulcat 435 and Fulmont) were derived from montmorillonite clays by acid activation. EPZE, EPZG and EPZ10 have Lewis acids deposited on the acid-activated montmorillonite K10.

At higher temperatures, clays have a tendency to dehydrate, resulting in ceramification and collapse of the layers. This is a major disadvantage as the clays are not stable to the hydrothermal treatment required to remove coke build-up and regenerate the catalyst. Pillaring is a process that uses inorganic cations to 'prop' the clay layers apart, so greatly improving the structural integrity of the clay. Additionally, the inorganic cation pillars themselves may be catalytically active, therefore their presence can increase the activity of the clay and enhance shape selectivity.

1.3.2 The Heating of Catalysts

In a zeolite, the aluminosilicate framework and the separate water molecules are held together by strong bonds, but the bond between the water molecules and the framework is relatively weak. Consequently, on heating to temperatures of approximately 100°C, water molecules are lost from the zeolite, without affecting the framework structure.[58] Liengme and Hall[59] stated that maximum activity for the zeolite was achieved when all residual hydroxyl groups associated with catalytically active sites were removed. Utterhoeven, Christner and Hall found that during this process, both Brønsted and Lewis sites were present on the silica-alumina surface, with Brønsted sites making up only a small portion of the surface hydroxyl groups.[60]

On heating a clay, desorption of H_2O on exterior surfaces and dehydration of interlayer H_2O occurs at low temperatures (< 100°C).[61] This endothermic effect is accompanied by a loss of mass as the absorbed water is removed. The second endothermic effect involves the removal of the hydroxyl groups from the lattice of the mineral in the form of water vapour. For montmorillonite, this is said to occur from 670°C to 710°C. On heating, kaolinite was found to show an endothermic effect at 560°C and two exothermic effects with maxima at 960°C and 1,250°C, with a total weight loss of 14%.[62]

Heating a clay is known to increase the Brønsted and Lewis acidity. However, care must be taken when dehydrating the clay as heating can cause layer collapse through layer crosslinking, along with elimination of water (ceramification). Depending on the degree of order, hydrogen bonding and layer spacing, ceramification of a clay occurs between 300°C and 700°C.

1.3.3   Catalyst Deactivation

Physical changes in a catalyst can lead to a decay in performance. The five main causes of deactivation are poisoning of the active sites, fouling by coke deposits, thermal degradation, mechanical damage and corrosion/leaching by the reaction mixture.[63] Poisoning occurs by adsorption of impurities in the feed, whilst fouling involves the covering of a surface with a deposit such as coke. If an impurity is not too strongly adsorbed on the catalyst and no reconstruction of the active site has occurred, regeneration of the catalyst may be possible. Many catalytic processes form carbonaceous deposits or 'coke' on the catalysts and this is the most common type of poisoning caused by reactants or products. Coke is produced by unwanted polymerisation and dehydrogenation (condensation) of organic molecules present in the feed or formed as a product. The reactions leave a layer of highly hydrogen deficient carbonaceous material on the catalyst surface, making the active sites inaccessible.

Holdeman and Botty[64] carried out electron microscopy studies to characterise the carbon deposits of silica-alumina catalysts. The results indicated that the coke deposited was a finely divided, highly dispersed phase present within the ultimate pore structure of the catalyst. Holmes *et al.*,[65] carried out sorption studies on a sample of ZSM-5 to locate coke within the zeolitic pores and to differentiate between poisoning and blockage of the active sites. The coke formation was found to involve two major steps. The initial cracking reaction generated alkenes, which then underwent secondary reactions (cyclisation, dehydrogenation) to form substituted benzenes and naphthalenes. These smaller aromatics then underwent further cyclisation and dehydrogenation to form larger insoluble aromatic compounds. The

coke was found to be located on both the external surface and within the zeolite pores. Hopkins *et al.*,[66] investigated the acidity and cracking activity during coke deactivation of ultrastable Y zeolite. Compared to a fresh USY zeolite, coke deactivated H-USY did not show significant changes in the acid strength distribution, number of acid sites, fraction of Brønsted and Lewis acid sites or pore size distribution. However, rapid loss in activity was observed and was said to be due to deposition of coke on active sites near the external crystal surface. Active sites in the inner portion of the zeolite particles were said to have remained unaffected by the coke.

1.4 Recycling of Plastics

This study involves the thermal and catalytic degradation of thirteen different polymers, from simple polyalkenes (polyethylene, polypropylene) to polystyrene, polyvinyl chloride, polyacrylonitrile, polymethyl methacrylate and polybutadiene. Decomposition of condensation polymers such as polyesters, polyamides and polyurethanes were also investigated. The main findings from previous research involving the decomposition of these plastics is summarised below, with more detailed reference tables collated in Appendix A.

1.4.1 Degradation of Polyalkenes

The non-catalytic degradation of polyethylene wax,[67] linear low-density polyethylene (LLDPE),[68,69] low-density polyethylene[70,71] and high-density polyethylene[72,73] was found to produce low yields of gases and oils and large amounts of residue. An increase in temperature gave greater polymer conversion and an increase in the gas

and liquid products (straight-chain hydrocarbons). The mechanism of the thermal degradation of polyalkenes occurs *via* a radical chain mechanism initiated by random scission of the polymer chain (see Figure 1.11). β-scission reactions of the radicals leads to gas and liquid olefins, whilst random propagation forms alkenes and dienes.
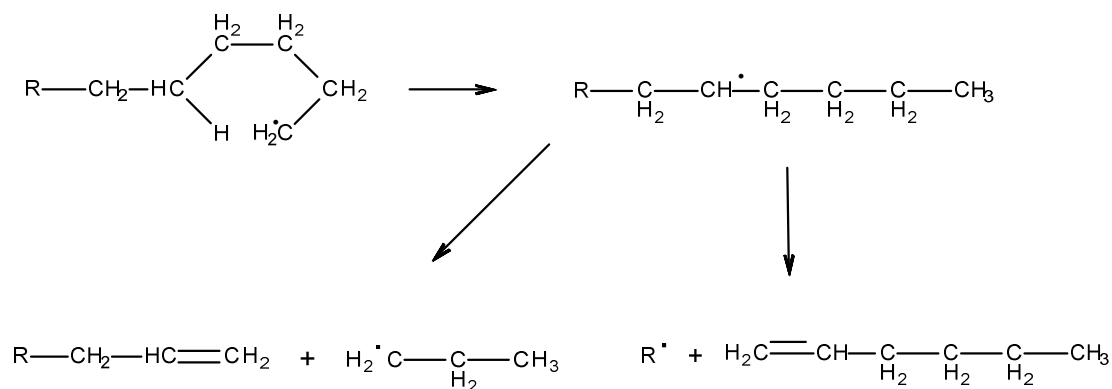
Figure 1.11: Thermal degradation mechanism of PE, with chain scission producing propene and 1-hexene *via* two different pathways[74]

Intermolecular hydrogen transfer of primary radicals leads to the formation of alkanes and more stable secondary radicals (see Figure 1.12).
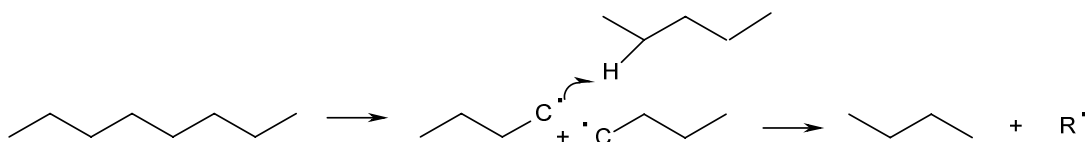
Figure 1.12: Free radical degradation mechanism

Catalytic degradation[75-82] produced a higher liquid yield (C_5-C_9), an increase in branched alkanes and aromatics, and decreases in the decomposition temperature and activation energies of degradation. The catalytic degradation of polyalkanes is thought to follow a carbocation mechanism initiated by either:

i. abstraction of a hydride ion (see Figure 1.13) that readily takes place when the molecule contains branched chains, *i.e.* tertiary hydrogens (LDPE, PP)

ii. addition of a proton to the double bonds of the molecule or to the olefins produced primarily from thermal degradation, that in turn produced the carbenium ion.[83]
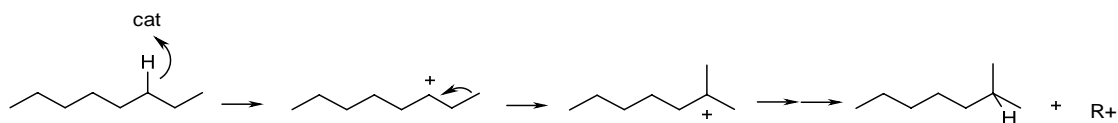
Figure 1.13: Carbocation formation and rearrangement reactions

The degradation of polypropylene[84-87] in the presence of catalysts resulted in the production of C_4-C_{12} olefins, *iso*-paraffins (branched alkanes) and aromatics. The polymer was said to have degraded *via* an ionic mechanism, with the abstraction of the hydride ion occurring as a result of the action of Lewis acid sites of the catalyst, or the addition of a proton to the olefins formed by thermal degradation being a result of the Brønsted acid sites.

Comparisons between the decomposition products of polypropylene and polyethylene[88-92] suggested that the presence of tertiary carbons on LDPE and PP

provided favourable positions for the initiation of polymer chain cracking. Polyethylene was said to have undergone greater scission of C-C chains than polypropylene, with PP producing a larger carbon distribution due to its side-chain methyl groups hindering access to the inner sites of the catalyst.

1.4.1.1 Polystyrene (PS)

Thermal degradation of polystyrene [93-95] produced approximately 70% conversion of PS into styrene, with yield increasing with temperature. Degradation occurred *via* a free-radical mechanism (see Figure 1.14A). In the presence of acid catalysts, polystyrene was said to degrade by mechanisms involving proton transfer from Brønsted acid sites, along with the generation of radical cations in aromatic compounds by Lewis sites (see Figure 1.14B). The addition of a catalyst[97-101] resulted in aromatics (benzene and toluene) from further cracking and hydrogenation of the styrene yield. Comparing the degradation of polystyrene and polyalkenes,[102-105] higher gaseous products were obtained with PE and PP, whilst PS produced 97% aromatics in liquid yield due to its polycyclic structure.

A
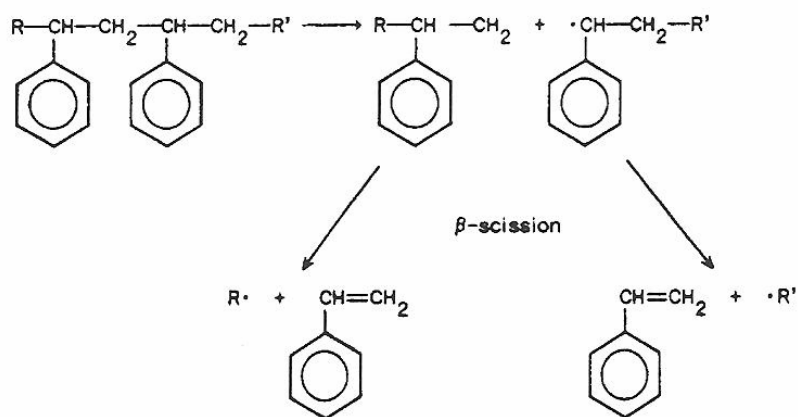
B
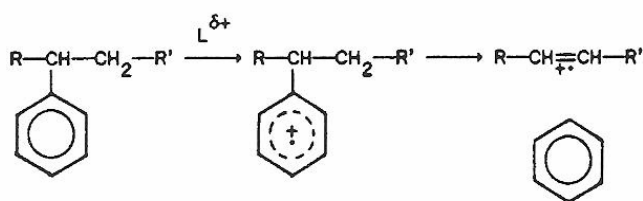
Figure 1.14: Initiation steps for thermal degradation (A) of polystyrene and degradation with acid catalysts having Lewis sites, $L^{\delta+}$ (B)[96]

1.4.1.2 Polybutadiene (PB)

The thermal degradation of polybutadiene[106-108] reported the decomposition of PB to be a two-step process yielding mainly CH_4 with only a small yield of monomer.

1.4.1.3 Polyvinyl Chloride (PVC)

On heating, PVC undergoes thermal dehydrochlorination to form a conjugated polyene. The polymer then unzips and undergoes a radical cyclisation to form benzene, chlorobenzene, dichlorobenzene and trichlorobenzene. As these chlorinated aromatics are so stable, the trimer formation pathway is found to be the major pyrolysis pathway for PVC degradation.[109] Dehydrochlorination is said to follow the mechanism of a chain reaction, with the activation energies of initiation, propagation and termination found to be 40-60 kcal/mol, 5 kcal/mol and 0 kcal/mol respectively.[110] These three steps of PVC degradation are displayed in Figure 1.15.

In the catalytic degradation of PVC, double bonds and tertiary carbon atoms are formed. The chlorine linked to the tertiary carbon atom can be easily removed to form a double bond and give an allylic structure from which HCl is removed. Thus,

the presence of the metal chlorides were found to bring about radical-type decomposition by providing unsaturated centres through an ionic mechanism.[111] The coke fraction was found to increase with the presence of Lewis acids.[112]

i. Initiation: $40 < E_1 < 60$ kcal/mol (167-251 kJ/mol)
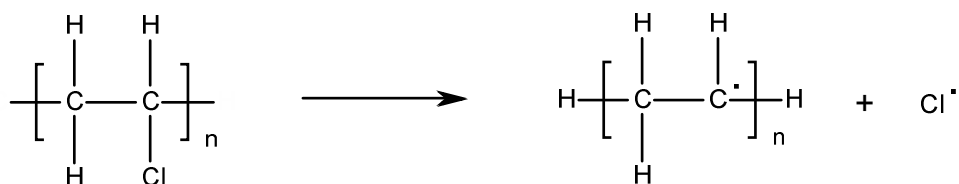
ii. Propagation: $E_2 \approx 5$ kcal/mol (21 kJ/mol)
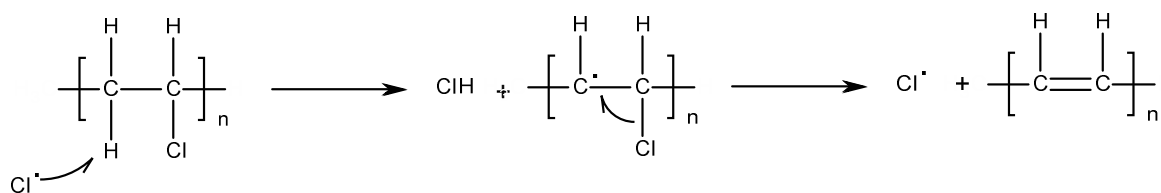
iii. Termination: $E_3 \approx 0$ kcal/mol

Figure 1.15: Degradation of polyvinyl chloride

1.4.1.4   Polyacrylonitrile (PAN)

No studies involved the presence of catalysts.   Thermal degradation of polyacrylonitrile[113-115] reported 'trace' or 'considerable' amounts of HCN evolved with acrylonitrile, acetonitrile and residue.

1.4.1.5 Polymethyl Methacrylate (PMMA)

The heating of polymethyl methacrylate[116-119] resulted in the degradation of PMMA primarily to its monomer, methyl methacrylate, *via* β-scission. The degradation of PMMA is displayed in Figure 1.16.
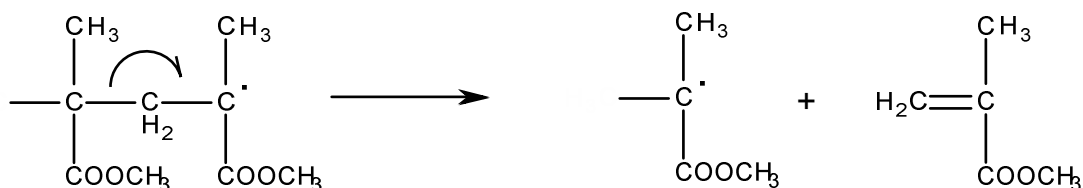
Figure 1.16: Degradation of polymethyl methacrylate

1.4.2 Degradation of Condensation Polymers

1.4.2.1 Polyesters (PE) - Polyethylene Terephthalate (PET)

The thermal degradation of polyethylene terephthalate[120-123] was said to have occurred *via* a molecular mechanism, with random chain scission at the ester links, with acetaldehyde as the major product (80%) of the gas yield. Other gaseous products include carbon monoxide, carbon dioxide, water, ethane and methane. Cyclic oligomers (mainly the trimer) were said to have been formed, with monomers of PET also produced.

1.4.2.2 Degradation of Polyamides (PA)

Nylon-6 was found to undergo major degradation from 300-400°C[124] with the maximum rate of volatilisation occurring at 30-40% volatilisation.[125] The gaseous product formed on thermal degradation of polyamide was predominantly carbon

dioxide and water, with small amounts of hydrocarbons (ethane, ethene, propane, propene) and cyclic compounds (benzene).

1.4.2.3 Degradation of Polyurethanes (PU)

The thermal degradation of polyurethane was found to occur in two steps[126] with the first stage resulting in the production of cyanates and substituted amines, and the second stage producing low molecular weight nitrogen-containing species. The PU chain is degraded by successive transerification reactions of the urethane bonds with low molecular weight glycols with the aid of a catalyst. The presence of catalysts allowed the complete recovery of polyols from the PU matrix.[127]

1.4.3 Degradation of Mixed Plastics

Heating different polymers together can have some effect on the yields of gases, liquids and residues[128-130] and on the rates of degradation.[131] Increasing the ratio of LDPE in a PE:PP mix produced a greater amount of C_{16+} paraffins in relation to PP alone (which produced no C_{16+} paraffins).[132] Adding polystyrene to a PE:PP mixture gave a higher aromatic content in the liquid component,[133] whilst the degradation of PS was found to be accelerated by the presence of carbenium ions from polypropylene decomposition.[134] The presence of polyvinyl chloride and polyethylene terephthalate in waste was said to have decreased the yield of liquid products and increased the amounts of gases and residues.[135,136]

The formation of branched alkanes, alkenes and aromatics from the degradation of various types of polymers has an application in the production of high octane fuel for motor vehicles. The use of catalysts in the decomposition of waste plastic at as low a temperature as possible could play a significant part in creating gasoline, whilst also reducing the impact of waste plastic on the environment.

1.5   Petroleum Chemistry

Many of the reactions encountered in the thermal and catalytic degradation of polymers are utilised by the petrochemicals industry to produce fuels and chemical precursors. In oil refineries, besides physical processes such as distillation and extraction, a large number of different chemical conversion processes are applied, with catalysis playing an important role. The four most important processes are:

  i. catalytic reforming

 ii. hydrotreatment

iii. fluid catalytic cracking (FCC)

iv. alkylation

Cracking reactions are carried out in order to reduce the molecular size and to produce more valuable fractions (*i.e.* gasoline), whilst FCC involves zeolites and a complex network of carbenium ion reactions for size reductions and isomerisation.[137]   By understanding the processes involved in the petrochemical industry, they can then be applied to the thermal degradation of polymers in order to create the highest octane number products as possible.

1.5.1   Crude Petroleum

Crude petroleum consists of mainly hydrocarbons, with small proportions of sulphur, nitrogen and oxygen as hydrocarbon derivatives. Three hydrocarbons in petroleum can be classified as *paraffins*, *naphthenes* (cylcoparaffins) and *aromatics*. It is mainly in the lower boiling ranges that hydrocarbons belong to one of these three types, whilst higher molecular weight hydrocarbons include complexes consisting of two or more radicals of the same type or different types, *i.e.* aromatics with paraffin side chains. It is only during the cracking process that unsaturated or olefinic hydrocarbons are formed.

1.5.2   Refining

The refining of petroleum is carried out for two reasons. Firstly, it is advantageous to extract from the petroleum all the products that are of high calorific value (*i.e.* gasoline, paraffin wax), and secondly, by removing the volatile light hydrocarbons and gasoline, the oil can be used safely as fuel oil. Petroleums are commonly classified according to their distillation residue. Asphaltic bases contain very little paraffin wax and the residue consists mainly of asphaltic matter that is predominantly condensed aromatics. They are relatively high in sulphur, nitrogen and oxygen content and the light and intermediate fractions have a high percentage of naphthenes, therefore asphaltic bases are suitable for high quality gasoline. Paraffin bases contain little or no asphaltic matter and less non-hydrocarbons, and are used to obtain paraffin wax and premium grade kerosene. Mixed bases are an intermediate class, containing appreciable quantities of asphalt as well as paraffin wax.[138] Refining also removes sulphur compounds (said to promote corrosion of engine parts and increase wear).

1.5.3 Distillation

The distillation process is used for the separation of vapour and liquid mixtures on the basis of their volatility. The components of petroleum can be defined by distilling a mixture of petroleum through an efficient fractionating column and identifying the boiling point and pressure of the vapours at the top of the column, along with the percentage by weight volume of distillate. Petroleum contains many thousands of different compounds which vary in molecular weight from methane (CH_4 = 16) to more than 2000 and boiling points that range from -160°C (-280°F) to temperatures of nearly 1100°C (2000°F). The main fractions obtained from the primary distillation of crude - gasoline, kerosene, gas oil and fuel oil – have much narrower and more sharply defined boiling ranges. Primary Distillation or 'topping' of petroleum is the most important and widely used method of separating petroleum into gasoline, kerosene, gas oil and reduced petroleum. The lowest boiling fractions, *i.e.* gases and some gasoline, leave from the top of the fractionating tower, while the heavier fractions *i.e.* naphthas, kerosene and gas oil are withdrawn as side streams. The various types of petroleum products, along with their uses, are displayed in Table 1.4.

Table 1.4: Petroleum Products

Product	Constituents	Boiling Temp.[139]	Uses
Reformed Natural Gas	Predominantly CH_4 (0-20% higher hydrocarbons)	-126ºC	Electricity generation through gas turbines
Liquefied Petroleum Gas (LPG)	Propane, *iso*-butane and propene or butene	-42ºC – 0ºC	Motor fuel, refrigeration
Gasoline (petrol)	C_4-C_{12} paraffins, olefins and aromatics	15ºC – 150ºC	Motor fuel
Solvents (Naphthas)	*Aliphatic* – paraffinic hydrocarbons, cycloparaffins (naphthenes) *Aromatic* – alkyl-substituted benzene	Light naphtha (C_5-C_6) 30ºC – 90ºC Heavy naphtha (C_6-C_{12}) 90ºC – 200ºC	Feedstock for high octane gasoline, solvents in paint, dry-cleaning, rubber industry and for industrial extraction
Kerosene (paraffin oil)	C_{10}-C_{16} *i.e.* *n*-dodecane, alkyl benzenes and naphthalene	115ºC – 220ºC	Jet fuel, rocket fuel
Distillate Fuel Oil (light) Residual Fuel Oil (heavy)	C_9-C_{20} C_{12}-C_{70}	175ºC – 600ºC	Domestic fuel oil (stove, furnace), diesel fuel oil
Lubricating Oil	C_{25}-C_{40}	> 400ºC	Motor, aviation oils
Paraffin Wax	C_{20}-C_{30} straight chain hydrocarbons	> 300ºC	Pharmaceuticals, cosmetics, candle making
Asphalt	Non-volatile hydrocarbons	> 300ºC	Paving roads, roofing
Coke			Carbon electrodes

1.5.4 Motor Fuels

Motor gasoline is a complicated mixture of hydrocarbons distilling between 30°C and 200°C and consisting of compounds in the range C_4-C_{12}. To obtain a gasoline that burns cleanly and effectively, the fuel must be blended from a number of components,

whilst the incorporation of additives improves the performance and maintains stability. The most important properties for satisfactory performance of the gasoline are *volatility*, as measured by distillation characteristics and vapour pressure, and *anti-knock value*, expressed as octane number.

The volatility of a gasoline is its tendency to pass from the liquid phase to the vapour phase under varying conditions of temperature and pressure. The engine may be cold, warm or hot, thus the volatility must be controlled within certain limits. Since gasoline is composed of a number of individual compounds whose boiling points cover a range of temperatures, the vapour pressure of the liquid will decrease as the lower boiling compounds evaporate. All hydrocarbons that boil within 30°C-200°C are satisfactory for applications in motor gasoline.

The ratio of fuel-to-air is an important factor for the performance of a combustion engine. Hydrocarbon-air mixtures are only flammable over a limited range of fuel:air ratios, if the concentration of hydrocarbon vapour is too low (weak mixture) or too high (rich mixture), the mixture will not be ignited by the spark. The most economic running condition has been found to be an air:fuel ratio of just over 17:1.[140]

Detonation, also known as 'knocking' or 'pinking' is the sharp, metallic sound emitted from the cylinders of spark-ignition engines under certain conditions.[141] When the fuel-air mixture, compressed by the piston, is ignited by the spark, a flame travels from the spark plug at a speed of around 22-45 ms^{-1}. A considerable increase in pressure results; hence the un-burnt mixture beyond the flame is rapidly compressed, and therefore raised in temperature. Under non-knocking conditions, the

flame travels at a fairly constant speed until combustion is complete. Under knocking conditions, the mixture ignites and begins to burn steadily, however, the end gas, heated by radiation and further compressed by the expanded products of combustion, reaches a temperature at which self-ignition occurs ahead of the flame. As the fuel has been raised above its self-ignition temperature, a sudden, very rapid burning (explosion) of the remaining un-burnt mixture ensues, resulting in the flame travelling at several thousand metres per second. The compression wave produces a characteristic 'knock' on the cylinder wall.

Aromatics (*i.e.* benzene, toluene), *iso*-paraffins (highly branched) and olefins are thought to have high anti-knock value. Mixed paraffins (*i.e. iso*-paraffins with limited branching) and naphthenes (*i.e.* cyclohexane) are said to exhibit intermediate anti-knock value, whilst paraffins such as *n*-heptane exhibit low anti-knock characteristics. In general, knock resistance is increased with the degree of branching and the number of double bonds as more stable radicals are formed allowing slower, smoother reactions.

The anti-knock property of gasoline is expressed as octane number (ON). Two pure paraffin hydrocarbons, with very similar physical properties, were selected as reference fuels. Heptane, C_7H_{16}, was found to knock in an engine under virtually any condition, whilst *iso*-octane, C_8H_{18} (2,2,4-trimethylpentane) was found to have a knock resistance higher than any gasoline. The former was ascribed an octane number rating of zero and the latter 100. By blending the two compounds across the full range of volumetric ratios, it was possible to set a scale from 0 to 100 against which any gasoline could be calibrated.[142]

It is the function of the internal combustion engine to convert heat into mechanical work; therefore the fuel that produces the greatest amount of heat during combustion is advantageous. On combustion, hydrogen gives out more heat than carbon; hence the hydrocarbons richest in hydrogen have the highest calorific value per unit weight. When comparing the same number of carbon atoms, paraffins (straight and branched chain) have the highest calorific value, followed by naphthenes and olefins, and then aromatics.

This study aims to produce the highest-grade fuel from the recycling of various types of waste plastic. To achieve this, the important mechanisms of thermal cracking must be understood.

1.5.4.1 Thermal Cracking

Thermal cracking involves the decomposition of petroleum at elevated temperatures (>350°C) through carbon-carbon bond rupture, without the aid of catalysts[143]. The larger molecules are split into fragments of lower molecular weight (lower boiling) products by the application of heat and pressure alone.[144] Two general types of free-radical reaction occur during cracking, which are displayed in Figure 1.17.

i. Primary reactions – decomposition of large molecules into small molecules (*i.e.* butane to methane and propene)
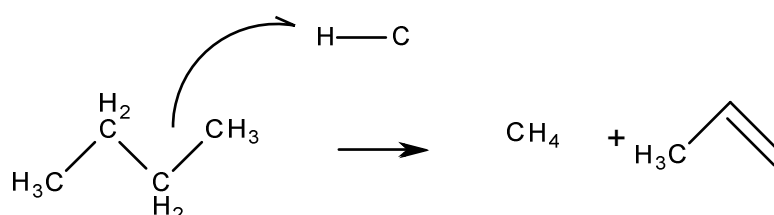
ii. Secondary reactions – interaction of primary products to form higher molecular weight materials:

$$R—HC=CH_2 \quad + \quad R'—HC=CH_2$$

$$\downarrow$$

Cracked residuum + coke + other products
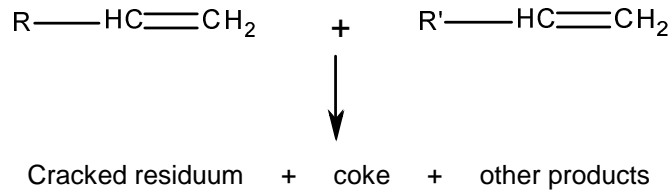
Figure 1.17: (i) Primary and (ii) secondary cracking reactions

Carbon-carbon bond scission of paraffinic molecules or side chains is an irreversible endothermic process that yields lower molecular weight molecules (*i.e.* olefinic hydrocarbons). Once formed, olefins can themselves crack, or can undergo further reactions. These isomerisation, dehydrogenation and polymerisation reactions are displayed in Figure 1.18.

i. Isomerisation (endothermic process)

$$H_3C—\underset{H_2}{C}—\underset{H}{C}=CH_2 \quad \rightleftharpoons \quad H_3C—\underset{H}{C}=\underset{H}{C}—CH_3$$
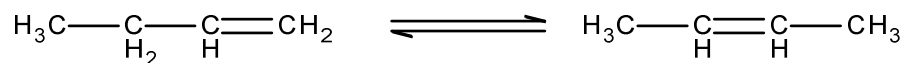
ii. Dehydrogenation (endothermic process)

$$H_3C—H_2C—HC=CH_2 \quad \rightleftharpoons \quad H_2C=CH—HC=CH_2 \quad + \quad H_2$$
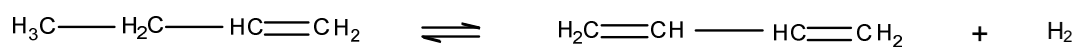
iii. Polymerisation (exothermic process)
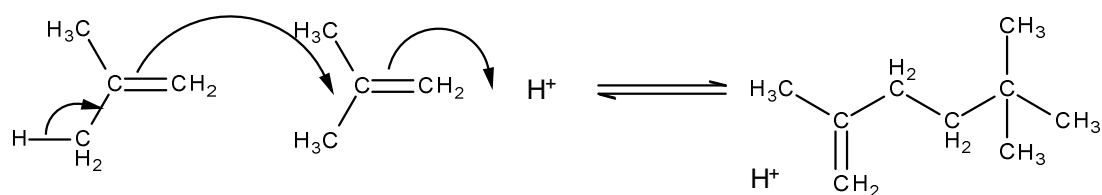
Figure 1.18: Isomerisation, dehydrogenation and polymerisation reactions[145]

1.5.4.1.1 β-scission

β-scission is one of the most important reactions in the thermal cracking of petroleum. On splitting the C-C bond, free radicals are formed and can undergo β-scission in which they break two carbons away from the charged carbon. This produces an olefin and a primary free radical which has two fewer carbon atoms.[146] An example of β-scission is displayed in Figure 1.19. However, one of the disadvantages of thermal cracking is that a high percentage of olefins formed during intermediate reactions polymerise directly to coke.
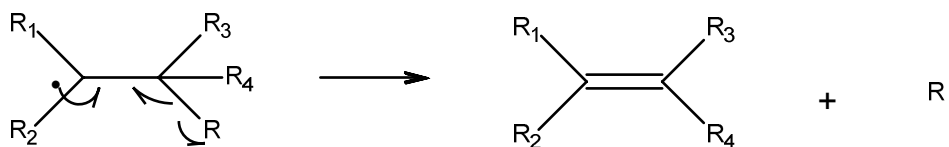
Figure 1.19: β-scission of petroleum

47

1.5.4.2 Catalytic Cracking

The catalytic cracking process uses a catalyst that enables the formation of more desired higher octane hydrocarbon products, consisting largely of branched paraffins, cycloparaffins and aromatics which have greater chemical stability than mono-olefins and diolefins. Additionally, catalytic cracking results in the production of the maximum amount of butenes and butanes (C_4H_8 and C_4H_{10}), rather than ethene and ethane (C_2H_4 and C_2H_6).

Catalytic cracking begins with the formation of a carbenium ion ($R\!-\!CH_2+$) either by the removal of a hydride ion (H^-) from a paraffin or by the addition of a proton (H^+) to the olefin. These ions are formed by reactions between hydrocarbon molecules and acidic sites on the catalyst.[147] Hydride removal by a Lewis site and hydrogen addition by a Brønsted site is displayed in Figure 1.20.

a) hydride removal by Lewis site

$$R\!-\!CH_2\!-\!CH_2\!-\!CH_3 \longrightarrow R\!-\!CH_2\!-\!\overset{+}{CH}\!-\!CH_3$$
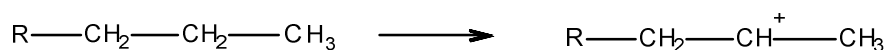
b) hydrogen addition by Brønsted site

$$R\!-\!CH\!=\!CH\!-\!CH_3 \longrightarrow R\!-\!\overset{+}{CH}\!-\!CH_2\!-\!CH_3$$
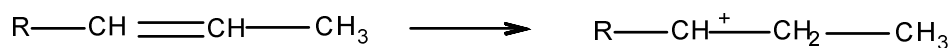
Figure 1.20: (a) Lewis and (b) Brønsted reactions

The ease of cracking of a paraffin is influenced by its structure as well as its molecular weight. Hydrocarbons containing tertiary carbon atoms crack most readily, while quaternary carbon atoms are most resistant.[148] In compounds containing both tertiary and quaternary carbon atoms, the accelerating influence of the former and retarding influence of the latter cancel each other out. Three major catalytic reforming reactions are dehydrogenation, isomerisation and hydrocracking.[149]

Dehydrogenation is essentially the removal of hydrogen from the parent molecule. The presence of hydrogen during a thermal reaction of a petroleum feedstock terminates many of the coke-forming reactions[150] and enhances the yields of the lower boiling components, such as gasoline and kerosene. An example of dehydrogenation is given in Figure 1.21, where methylcyclohexane (a naphthene) is converted to toluene (an aromatic):
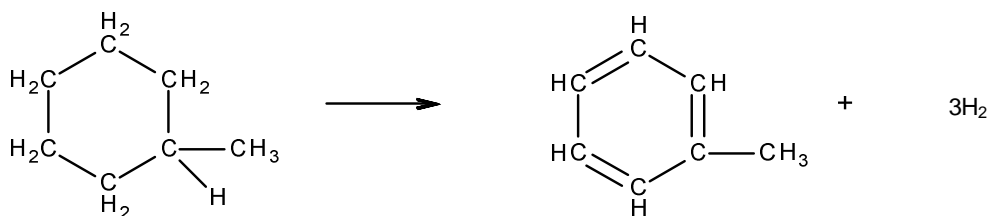
Figure 1.21: Dehydrogenation of methylcyclohexane

Isomerisation of *n*-paraffins to *iso*-paraffins refers to the rearrangement of the carbon and hydrogen atoms in a hydrocarbon molecule. An example of isomerisation is given in Figure 1.22, which displays the conversion of *n*-octane to 2,5-dimethylhexane (an *iso*-paraffin):
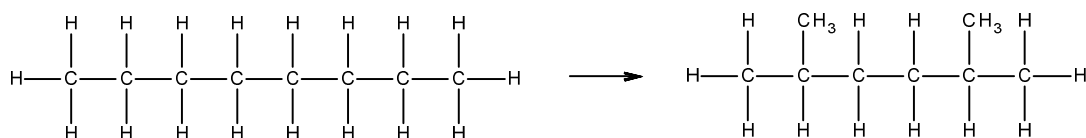
Figure 1.22: Isomerisation of *n*-octane

The isomerisation of naphthenes and paraffins is a reversible first-order reaction, propagated by carbenium ions to the formation of an intermediate complex followed by intramolecular rearrangement. The hydrocarbon is placed in contact with a catalyst of aluminium chloride promoted with anhydrous hydrogen chloride, under conditions to give favourable equilibria. The isomerisation of hexane is very desirable to improve octane number of petroleum fractions, but can be difficult to accomplish in practice.[151]

Hydrocracking of paraffins into smaller molecules, for example the cracking of *n*-heptane into *iso*pentane and ethane, is displayed in Figure 1.23:
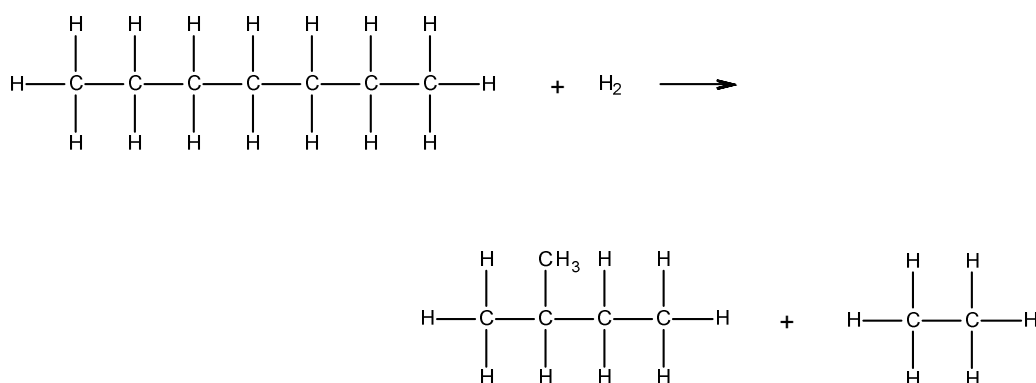
Figure 1.23: Hydrocracking of *n*-heptane

One of the most important reactions in hydrocracking is the partial hydrogenation of polycyclic aromatics followed by rupture of the saturated rings to form substituted monocyclic aromatics. The sidechains can then be split off to produce high-octane number *iso*-paraffins.[152] The products of hydrocracking are composed of either saturated or aromatic compounds and no olefins are produced. Hydrocracking catalysts are dual functional, containing both hydrogenation and cracking sites. The hydrogenation component is generally a mixture of sulphides of Ni and W or a noble metal (Pt or Pd), while the acid component (and also the support for the hydrogenation component) is amorphous silica-alumina or a zeolite.[153] For the production of gasoline, strongly acidic materials promote reactions which lead to low methane and ethane production and conservation of monocyclic rings.

During catalytic cracking, paraffins tend to crack at carbon-carbon bonds near the centre of the molecule, whilst *iso*-paraffins break between carbon atoms that are next to a tertiary carbon. This yields products containing more C_3 and C_4 species. Olefins are the most reactive hydrocarbons in catalytic cracking. They tend to undergo isomerisation, producing branched-chain olefins, which can then undergo hydrogen transfer reactions with naphthenes and other hydrocarbons. The cracking of naphthenes (cycloparaffins) involves both ring and chain rupture and occurs more readily than paraffins, but not as readily as olefins. Olefins and paraffins are yielded with only minor amounts of methane and C_2 hydrocarbons. Aromatic hydrocarbons exhibit wide variations in their susceptibility to catalytic cracking. The benzene ring is nearly inert and when aromatic rings such as naphthalene do crack, coke is often deposited on the catalyst.[154]

Fluidised Catalytic Cracking (FCC) is the most dynamic and versatile of the refining processes. Feed vapours come into contact with hot catalyst micro-spheres under fluidised conditions and the products are separated from the deactivated catalysts. The catalyst is then regenerated at high temperature, and the reaction-regeneration process continues. Fluidised-bed operation, with its excellent temperature control, is a major producer of olefins in the refinery[155] and prevents over- and under-reforming, resulting in more selectivity in the conditions needed for optimum yield of the desired product. The major process variables are temperature, pressure, catalyst-oil ratio (ratio of the weight of catalyst entering the reactor per hour to the weight of the oil charged per hour) and space velocity (weight of oil charged per hour per weight of catalyst in the reaction zone).

1.5.5 Optimisation Processes

High octane number gasoline is produced not only from the cracking of heavy fractions of petroleum, but also by converting the *n*-paraffin components of the lighter gasoline fraction (C_4 to C_6) into high octane number material. **Alkylation** is a process that combines olefins and paraffins for the production of high-octane motor fuel. The reaction proceeds through a carbenium ion, formed from an *iso*-butane and an olefin with sulphuric acid or hydrogen fluoride as the catalyst. The carbenium ion adds on to the olefin to form another ion which in turn reacts with *iso*-butane to produce the primary reaction product and a new carbenium ion to continue the general reaction. Side reaction products are both lighter and heavier than the primary products. For example, the combination of *iso*-butane with normal butanes (see Figure 1.24), in the presence of a catalyst, gives a saturated C_8 product known as an alkylate.[156] Butenes

produce the highest octane numbers, pentenes intermediate and propene the lowest, although all alkylates have octane numbers greater than 87.

iso-butane   1-butene   alkylate
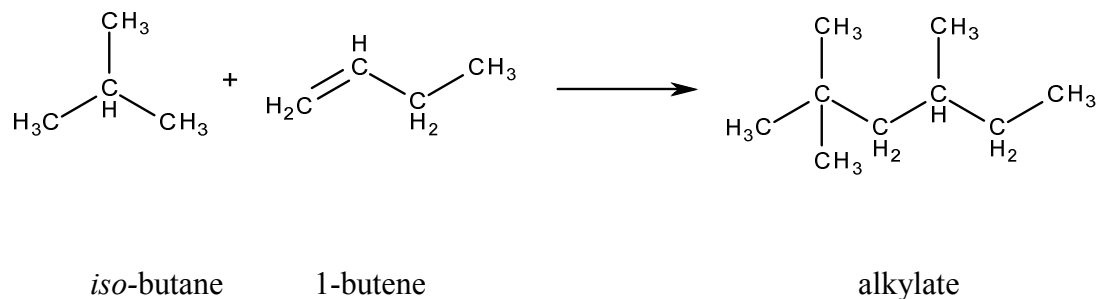
Figure 1.24: Production of an alkylate

Polymerisation combines unsaturated materials to yield products of higher molecular weight, while maintaining the atomic arrangement present in the basic molecule. Using this process, a hydrocarbon such as propene, can be polymerised in the presence of catalyst (*i.e.* sulphuric acid, copper pyrophosphate or phosphoric acid) to a material boiling in the gasoline range. When used for the manufacture of gasoline components the reaction is adjusted to give highly branched molecules that possess high octane ratings.

1.6 Summary

The disposal of waste plastic is known to be a worldwide problem. Any solution must be energetically viable and environmentally sound. By understanding the structures of the many different types of polymers used today and by understanding the mechanisms of their degradation, it may be possible to optimise the decomposition products of this waste stream to give useful products. In the presence of catalysts, the degradation pathways of a polymer may change from a high-energy free radical mechanism to a more stable carbocation mechanism that can result in higher proportions of high RON fuel, for example. By investigating the properties of selected clay and zeolite catalysts, the energy required to degrade a polymer may be reduced and so an energy saving may also be achieved.

Chapter 2

Catalyst Characterisation

2 Catalysts

For this study, six clays and four zeolites were used as the catalysts to aid polymer degradation. It was important to document the differences in the structure and properties of each of the catalysts in order to fully understand the effects they were having on the decomposition kinetics and degradation products of the plastics.

2.1 Montmorillonite Clay

Montmorillonite (the main mineral in bentonite clays) is a common clay mineral and member of the smectite group. It is formed from repeating layers of two tetrahedral sheets sandwiching a central octahedral sheet (2:1 structure). Montmorillonites are T:O:T clays in which substitution of some of the octahedral aluminium (Al^{3+}) atoms by magnesium (Mg^{2+}) or iron (Fe^{2+}) atoms has taken place, resulting in the octahedral sheet retaining a residual negative charge. In the naturally occurring form, this charge is balanced by the introduction of interlamellar cations (*i.e.* Na^{2+}, Ca^{2+}) into the water layer, with some cations also occupying broken edge sites.

Natural montmorillonite clays have almost no catalytic activity. Acid treatment of the clay can cause partial leaching of aluminium from the octahedral layer, resulting in de-lamination of the aluminosilicate sheets and hence a less crystalline structure. Considerable de-lamination results in an increase in surface area, particularly at the

sheet edges, as well as adsorption of protons and acid cations such as Al^{3+} onto external and internal surfaces.

2.1.1 Ful*

The three Ful* samples used in this study were obtained from Rockwood Additives Ltd. All were acid activated, which had opened up the clay structure in order to allow access to larger molecules. Acid activation had also increased the surface areas of the clays.

2.1.1.1 Fulacolor

Fulacolor is a reactive acid clay produced from a non-toxic, natural material. It is used as a catalyst for colour forming on carbonless copy paper and is thought to have good Brønsted and Lewis acidity. The Fulacolor sample used in this study was said to have been made by the acid activation of the Spanish montmorillonite clay, Los Trancos. Mean particle size was given as 4.6 ± 0.4 μm.[157]

2.1.1.2 Fulcat 435

Fulcat 435 is an inorganic acid activated montmorillonite clay industrial catalyst and adsorbent. The natural clay structure has undergone acid activation in order to develop Brønsted and Lewis acid sites and increase the surface area. Particle size was given as >75 μm (90%), with a surface area (BET) of 350 m^2g^{-1} and pore volume of 0.4 cm^3g^{-1}.[158]

2.1.1.3 Fulmont

Fulmont bleaching earth is an acid activated montmorillonite, but other clay minerals such as kaolinite, attapulgite and palygorskite can also occur in the product.[159] It is used in industry to decolourise edible food oils and animal fats and for the destruction of peroxides, which increases oxidation stability of the refined oil. Fulmont is known to have high surface area and high Brønsted and Lewis acidity.

2.1.2 Envirocats, EPZ*

Envirocats are heterogeneous, non-toxic, non-corrosive catalysts based on 'Clayzic' – clay supported zinc chloride. They are made from acid-activated K10 montmorillonite clay and are thought to be powerful Lewis acids. The EPZ* samples used in this study were obtained from Contract Chemicals Limited and were obtained on signing a "non-reverse engineering" agreement.

2.1.2.1 EPZE

EPZE was said to have been prepared by depositing microcrystalline $AlCl_3$ on Clayzic. EPZE is thought to display less activity than EPZG due to the deposited $AlCl_3$ coordinating to the oxygen (OH) in the clay and reducing the activity of the catalyst.

2.1.2.2 EPZG

EPZG was said to have been prepared by depositing microcrystalline $FeCl_3$ on acid activated montmorillonite K10 clay. EPZG is thought to display greater activity than EPZE due to $FeCl_3$ not coordinating as strongly as $AlCl_3$ to oxygen atoms in the clay.

2.1.2.3 EPZ10

EPZ10 was said to have been prepared by depositing $ZnCl_2$ on acid activated montmorillonite K10 clay. EPZ10 is said to have good Lewis acidic properties.

2.2 Zeolites

Zeolites are three-dimensional, microporous, crystalline solids with well-defined structures that contain aluminium, silicon and oxygen in their regular framework. The silicon and aluminium atoms are tetrahedrally coordinated with each other through shared oxygen atoms. These four connected networks of atoms can form cages, cavities or channels (void space). These are of the right size to allow small molecules to enter, with the limiting pore sizes being approximately 3-10 Å in diameter. The size and shape of pores control access of certain molecules, allowing some to enter whilst excluding others.

Isomorphous substitution of Al^{3+} for Si^{4+} in the silicalite framework produces an overall negative charge on the zeolite structure, which is neutralised by metal cations. The porous structure of zeolites can accommodate a wide variety of cations such as Na^+, K^+, Ca^{2+} and Mg^{2+} and water. The loosely bound nature of the extra-framework metal ions means that they can be readily exchanged for other types of metal cations when in aqueous solution.

2.2.1 Zeolite-Y

Zeolite-Y exhibits the faujasite (FAU) structure of a three-dimensional pore structure with pores running perpendicular to each other in the x, y and z planes. The aperture

is defined by a 12-membered cavity of diameter 12 Å which is surrounded by ten sodalite cages (truncated octahedra) connected on their hexagonal faces (see Figure 1.7 in Chapter 1). The pore formed from the 12-membered ring has a relatively large diameter of 7.4 Å.

2.2.1.1 Rare-Earth Exchanged Zeolites

Rare-Earth exchanged zeolites are thought to exhibit improved thermal and chemical stabilities over the pure H-forms, whilst increasing the catalytic properties. Increase in catalytic activity has been linked to the formation of more Brønsted acid sites, due to the presence of several types of structural hydroxyl groups.

2.2.1.1.1 CeY

CeY was a cerium-exchanged Y-zeolite synthesised by a colleague at the University of Central Lancashire.[160] Y-zeolite pores are too small for large molecules to access, but the catalyst is thought to display good Brønsted and Lewis acidity.

2.2.1.1.2 LaY

LaY was a lanthanum-exchanged Y-zeolite synthesised by a colleague at the University of Central Lancashire.[160] LaY zeolite is thought to be able to coordinate small molecules and facilitate the rearrangement of alkenes in the pores. Previous experiments on the synthesised LaY zeolite gave a BET surface area of 471 m^2g^{-1} and Brønsted-acid sites and Lewis-acid sites of 49% and 51% respectively.[161]

2.2.2 ZSM-5

ZSM-5 (Zeolite Sieve of Molecular Porosity – 5) is a highly porous material composed of a two-dimensional pore structure formed from 10-membered oxygen rings. The first of these is straight and elliptical in cross section whilst the circular second pores intersect the straight pores at right angles. The structure is type MFI – Mordenite Framework Inverted – and is displayed in Figure 2.1.
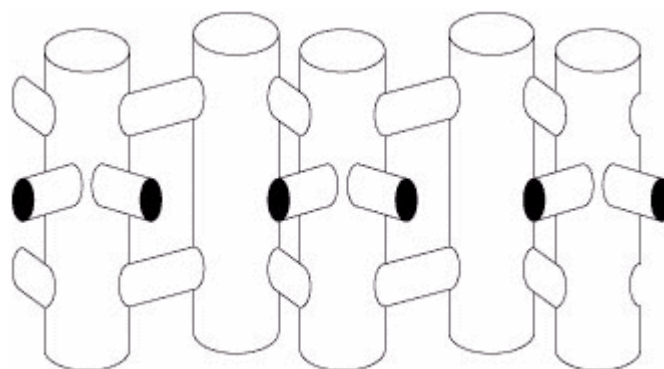
Figure 2.1: Schematic of the pore structure of ZSM-5

ZSM-5 is a zeolite with a high silica to alumina ratio. The substitution of an aluminium ion (3^+) for a silicon ion (4^+) requires the additional presence of a cation or a proton for neutrality. This zeolite is normally supplied as an ammonium salt that eliminates ammonia on heating, leaving a proton behind. This additional proton gives the zeolite a high level of acidity, which causes its activity. ZSM-5 has a larger pore than Y-zeolites and is therefore able to admit medium-sized molecules. ZSM-5 is known to be good at dehydrogenation and aromatisation of the molecules it admits into its pore cavities.

2.2.2.1 23z

23z was purchased from Zeolyst International and was supplied as the ammonium

form of ZSM-5. The surface area was given as 425 m^2g^{-1}.[162]

2.2.2.2 280z

280z was purchased from Zeolyst International and was supplied as the ammonium

form of ZSM-5. The surface area was given as 400 m^2g^{-1}.[162]

Table 2.1 lists the ten catalysts used in this study for the degradation of polymers.

Table 2.1: Catalysts used for the degradation of polymer samples

Name	Type	Catalyst Information
Fulacolor	Clay	Acid-activated montmorillonite, carbonless copy paper colour developer
Fulcat 435	Clay	Acid-activated montmorillonite, catalyst
Fulmont	Clay	Acid-activated montmorillonite, bleaching earth
EPZE	Clay	Acid-activated K10 montmorillonite-supported $ZnCl_2$ with deposited $AlCl_3$ microcrystals
EPZG	Clay	Acid-activated K10 montmorillonite-supported $FeCl_3$ with deposited $FeCl_3$microcrystals
EPZ10	Clay	Acid-activated K10 montmorillonite-supported $ZnCl_2$
CeY	Zeolite	Cerium-exchanged Y-zeolite
LaY	Zeolite	Lanthanum-exchanged Y-zeolite
23z	Zeolite	ZSM-5
280z	Zeolite	ZSM-5

In order to try to understand the effects that the catalysts were having on the decomposition of the various types of polymers, it was very important to characterise the zeolite and clay catalysts by a number of analytical techniques. By determining the elemental composition of the catalysts, their surface area, pore distribution and numbers of Brønsted- and Lewis-acid sites, the zeolites and clays, and their interaction with the degradation products of the plastics, could be better understood.

2.3 Scanning Electron Microscopy

In Scanning Electron Microscopy (SEM), the emissions of electrons from the elements in the upper layers of a sample are detected by a scintillator. Secondary electrons can escape from only a very thin layer of the surface as their energy is very low and most of them will be absorbed by the specimen itself,[163] but provide valuable information of opaque (solid) objects.[164] Irradiation of the sample also produces X-rays which may be emitted either by core scattering (producing a continuous spectrum of X-rays) or by inner-shell ionisation, which yields a characteristic X-ray spectrum. Typically, the transitions observed in X-ray spectra are K, L and M lines. Each shell comprises several energy levels, therefore the de-excitation process can produce complex transitions.

2.3.1 Materials and Methods

For this study, each powdered catalyst was pressed into a disk. Using the Quanta 200 SEM, five spectra were captured for each catalyst. Figure 2.2 displays an SEM-EDX spectrum for EPZ10 clay. The SEM-EDX spectra of all ten catalysts are displayed in Appendix B.
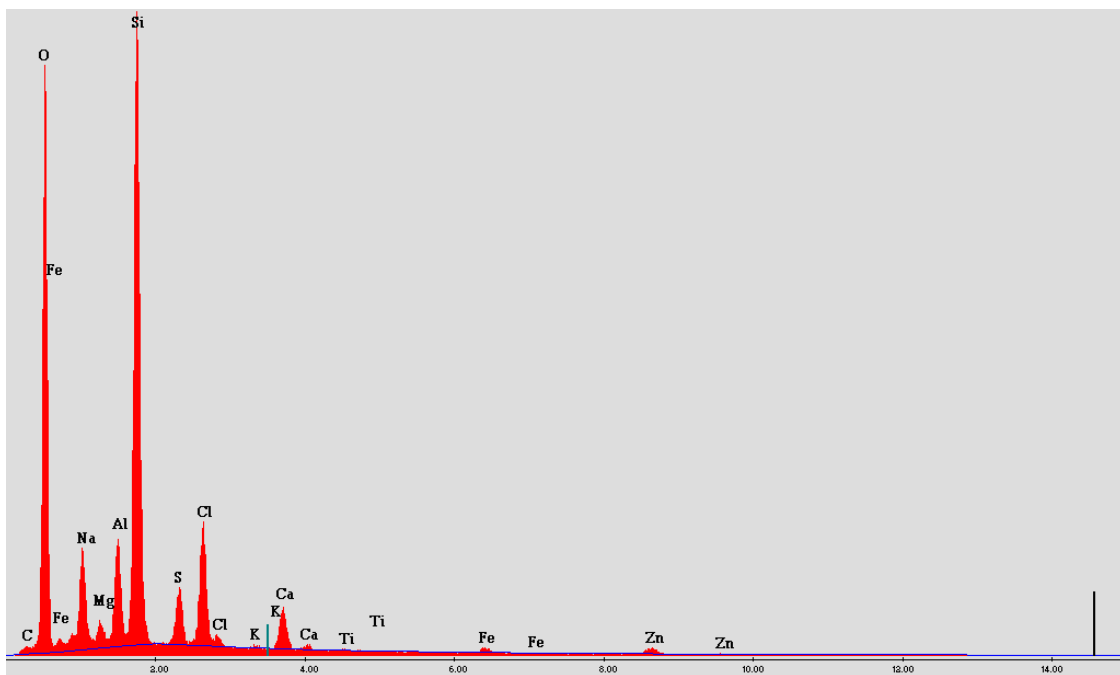
Figure 2.2: SEM-EDX spectrum of EPZ10 clay

An average Weight % and Atom % of each element in the catalyst sample was calculated by the instrument. Weight % is displayed in Appendix B, whilst Atom % is displayed in Table 2.2 below:

Table 2.2: Average Atomic % of catalyst elements

	Fulacolor	Fulcat	Fulmont	EPZE	EPZG	EPZ10	CeY	LaY	23-z	280-z
N							6.2	4.3		
O	64.9	65.4	64.2	63.2	63.4	58.5	65.5	65.8	64.1	62.4
Na	0.6	0.5	0.8	1.3	0.6	4.4	1.8	1.6		
Mg	1.6	1.9	1.5	1.2	1.0	1.2	0.5	0.2		
Al	5.3	5.9	4.6	4.1	6.0	3.7	7.1	8.0	3.0	0.6
Al_{tet}^{*}	1.3		1.9	0.8	0.7**	0.7				
Al_{oct}^{*}	4.0		2.7	3.3	5.3**	3.0				
Si	27.0	25.6	24.5	23.9	25.9	20.6	17.9	18.8	32.8	37.0
S			1.2	2.2		2.2				
Cl				0.7	1.1	4.4				
K			0.3	0.2	0.6					
Ca	0.3	0.2	1.0	1.8	0.1	2.0				
Ti			0.2	0.2		0.1				
Fe	0.4	0.5	1.6	0.7	1.3	0.6				
Zn				0.6		2.3				
Ce							1.0			
La								1.2		
Si/Al	5.1	4.3	5.3	5.8	4.3	5.6	2.5	2.4	10.9	61.7

* The proportions of tetrahedral (Al_{tet}) and octahedral (Al_{oct}) aluminium were determined using ^{27}Al MAS NMR measurements, see Section 2.4.
** It is assumed that any additional Al added to the K10 structure will be Al_{oct}.

2.3.2 SEM-EDX Results and Discussion

Silicon and oxygen were found to be the most common elements making up the catalysts, with aluminium also being prevalent. The commercially purchased ZSM-5 zeolites contained silicon and oxygen in the form of SiO_4 tetrahedra, with a very low amount of aluminium. No other elements were present, with the ammonium ions (NH_4^+) used to synthesise the zeolite likely to have volatilised from the catalyst under the high vacuum SEM conditions. The presence of nitrogen, chlorine and sulphur in some of the SEM-EDX spectra are likely to be due to anions left over from the

preparation of the catalysts. The presence of sulphur and hence residual sulphuric acid, could add to the effectiveness of the catalyst.

A clay contains SiO_2 with various amounts of aluminium in the form of aluminium oxide (Al_2O_3). From these compounds, for each silicon there are two oxygen atoms (SiO_2) and each aluminium atom is equivalent to one-and-a-half oxygen atoms. SEM-EDX analysis provides data on the amount of oxygen, silicon and aluminium in a sample; therefore it should be possible to validate the results for Si, Al and O using the above method. However, oxygen can be altered by the water content of a sample so these relationships can only be used as a reliable way of verifying the full formula of the mineral.

For true montmorillonite clays, the total amounts of sodium, potassium and half the calcium content should equal the amount of magnesium in the octahedral layer of the sample. From the SEM-EDX results, only Fulmont agreed with this. Fulacolor's magnesium content was twice that calculated from the other elements, whilst the magnesium present in Fulcat 435 was over three times greater. This suggests that the magnesium in Fulacolor and Fulcat is present both in the octahedral layer and as an exchange cation in the interlayer. In contrast, the K10 based EPZ catalysts all showed diminished levels of magnesium in comparison to the Na, K and (Ca/2) content, suggesting that a high proportion of layer charge may be due to Al_{tet}. EPZG contained only slightly less Mg than the other elements, EPZE had half of that expected, whilst EPZ10 contained less than a quarter of the magnesium expected from the sodium, potassium and half of the calcium content. These observations will have

to be revisited if striking differences in catalytic activity within this group of catalysts is observed.

All of the clays in this study were acid activated – a process which results in an increase in the relative amount of silicon present in the sample, and hence a decrease in the relative amount of aluminium. Therefore, higher Si/Al_{tot} ratios can be an indication as to the degree of acid activation of the catalyst. The purpose of acid activation is to increase the surface area of the clay and improve its effectiveness as a catalyst. Therefore, the Si/Al_{tot} ratios in Table 2.2 can be a useful indicator as to which catalysts may be the most beneficial to our study.

Using the ratio of silicon to the total aluminium in the sample, the HZSM-5 zeolites gave the highest Si/Al_{tot} ratio, with 23z and 280z containing about ten and sixty silicon atoms, respectively, to every aluminium atom. The clay samples had Si/Al_{tot} ratios varying from 4.3 to 5.8, with EPZE producing the highest of the six values, suggesting that extra aluminium cations had been added to the K10 in this case. In contrast, the CeY and LaY zeolites had the lowest Si/Al_{tot} ratios of 2.5 and 2.4 respectively, suggesting that these aluminosilicates have the highest exchange capacity of the catalysts examined.

However, unlike with the zeolites where virtually all the aluminium will be structural tetrahedral Al, the Al species for clays cannot be determined directly from the SEM-EDX results. The aluminium in clays can be present both in tetrahedral form in the silica layer and as octahedral Al either exchanged into the interlayer or as structural Al in the octahedral layer. Further experiments (*i.e.* solid state ^{27}Al NMR) were

carried out to gain insight into the speciation of the aluminium of the clay catalysts and these are reported in Section 2.4 below.

2.3.3   Conclusions of SEM-EDX Analysis

The Si/Al_{tot} ratios for the zeolites could be determined *via* SEM-EDX analysis. The CeY and LaY zeolites had the lowest Si/Al_{tot} ratios, suggesting that the high exchange capacity of these Y-zeolite based catalysts might give high catalytic activity. The low Al content of the HZSM-5 catalysts, 23z and 280z suggests that there will be fewer catalytic sites available in these zeolite catalysts.

The clay based catalysts fall into two groups; Lewis acid supported on the acid activated K10 clay and the acid activated montmorillonite series of Ful* catalysts. The highest Si/Al_{tot} ratios of these clays were seen for EPZE and EPZ10, with Fulcat 435 and EPZG having the lowest Si/Al_{tot} of this group.

However, the Si/Al_{tot} ratio of a catalyst is not the only criterion of a good catalyst. Catalytic sites must have high activity and be accessible to in coming molecules; thus knowledge of surface areas and pore sizes of the catalysts will help to give a greater insight into their effectiveness.

2.4 Adsorption Studies

The surface of a solid differs from the bulk due to differences in the co-ordination of ions. Sorption occurs at energies varying from weak van der Waals forces to those characteristic of chemical bonding. The amount of any species sorbed per unit area of surface depends on, *inter alia*, the nature of the species, the nature and texture of the surface and the partial pressure of the species in the gas phase.[165]

Physical adsorption (physisorption) is unselective and low energy. The extent of adsorption is related to the boiling point of the gas, not the nature of the solid surface. There is no breaking of molecular bonds and negligible changes in bond energies. *Associative chemical adsorption* is selective and depends strongly on both the gas and the composition of the solid surface, and involves higher energies of adsorption than those of physisorption. The bonds in the adsorbed molecules are changed in strength but not broken, *i.e.* the molecule is adsorbed whole. *Dissociative chemical adsorption* is selective and strongly dependent on both the gas and solid surface, and involves higher energies of adsorption than those of physisorption. The bonds in the adsorbed molecules are broken, *i.e.* the molecule is adsorbed as two or more molecular fragments. The above types of adsorption are displayed in Figure 2.3 below:
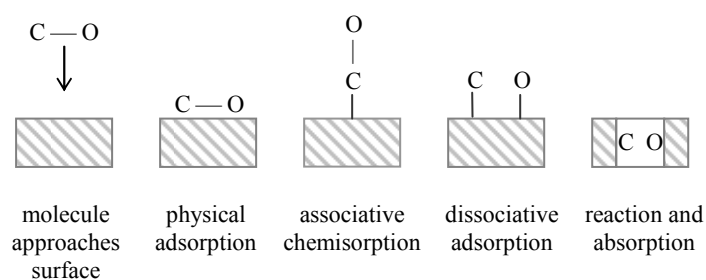
Figure 2.3: Increasing interaction of carbon monoxide on a solid surface[166]

68

2.4.1 Adsorption Isotherms

The process of adsorption is usually studied through an adsorption isotherm. The isotherm is a plot of the amount of gas adsorbed at equilibrium as a function of the partial pressure, p/p_0, and is expressed as the mass of gas (g) or the volume of gas reduced to standard temperature and pressure. For the measurement of an adsorption isotherm, a sample of solid material is placed in an evacuated space and kept at a fixed temperature as a known quantity of pure gas is admitted into the space surrounding the sample. The pressure within the space is recorded over time. The pressure falls rapidly from its initial value to a steady reading called the *equilibrium pressure*. A quantity of gas is effectively removed from the gas phase by the solid surface and the amount adsorbed is plotted against equilibrium pressure to form an adsorption isotherm. Gas atoms enter the pore space randomly and due to the dispersion forces or van der Waal's forces, spend more time near the surface. Therefore, the equilibrium distribution of gas atoms near the surface can be described as a function of pressure and the molecular properties of the components of the system.

In 1909, Freundlich produced the Freundlich Adsorption equation:[167]

$$\frac{x}{m} = kP^{\frac{1}{n}} \qquad \text{(Eq. 2.1)}$$

where x is the mass of the gas adsorbed on mass m of the adsorbent at pressure P. k and n are constants whose values depend upon the adsorbent and gas at a particular temperature. This equation established the relationship of adsorption with pressure correctly when P was low, but proved inaccurate at high pressure.

In 1916, Irving Langmuir proposed the Langmuir Adsorption Isotherm,[168] which was based on four assumptions:

1. The surface of the adsorbent is uniform (all adsorption sites are equivalent).

2. No interaction takes place between adsorbed molecules.

3. All adsorption occurs through the same mechanism.

4. At maximum adsorption only a monolayer is formed.

Based on this theory, the Langmuir Equation depicted a relationship between the number of active sites of the surface undergoing adsorption and pressure:

$$\theta = \frac{KP}{1 + KP}$$

(Eq. 2.2)

where θ = number of sites of the surface which are covered with gaseous molecules

P = pressure

K = equilibrium constant for distribution of adsorbate between the surface and the gas phase.

However, as with the Freundlich Isotherm, this theory was valid at low pressure only, where gaseous molecules would possess high thermal energy and high escape velocity, resulting in fewer gaseous molecules available near the surface of the adsorbate. At high pressure and low temperature the thermal energy of gaseous molecules decreases, with more gaseous molecules available per unit surface area. This leads to the formation of multilayers rather than the monolayer adsorption

proposed by Langmuir. This led to a theory by Brunauer, Emmett and Teller (BET) in which multilayer formation was explained.

2.4.1.1 BET Method

The standard method for measuring specific surface area is based on the physical adsorption of nitrogen on the solid surface, using the *BET method*. The BET isotherm accounts for multilayer adsorption and therefore gives a more accurate representation of physisorption than the Langmuir isotherm. Brunauer, Emmett and Teller[169] assumed that the rate of adsorption on the bare surface was equal to the rate of desorption from the monolayer and that the rate of adsorption onto the monolayer was equal to the rate of desorption from the second layer, and so on, giving the isotherm:

$$V = \frac{V_m c P}{(P_0 - P)(1 + \frac{(c-1)P}{P_0})}$$

(Eq. 2.3)

where c =   temperature dependent constant related to the enthalpies of
              adsorption of the first and higher layers

   P_0 =   normal (saturation) vapour pressure of the absorbing gas at the
              temperature of the experiment

   V =   volume of adsorbed gas

   V_m =   volume adsorbed to give a monolayer.

Five different types of isotherms which result from physical adsorption are displayed in Figure 2.4.
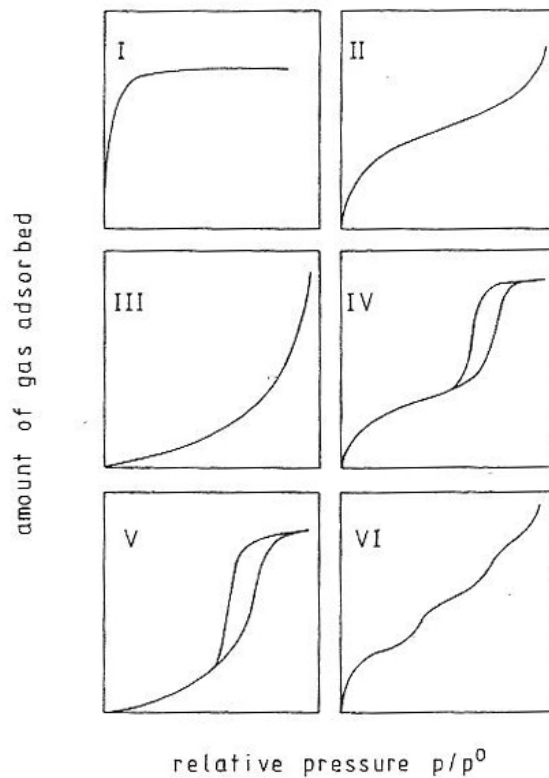
Figure 2.4: Five adsorption isotherms (I-V) and the stepped isotherm VI[170]

- Isotherm I: adsorption in micropores, *i.e.* for zeolites and activated carbons. This graph depicts monolayer adsorption and can be explained using the Langmuir Adsorption Isotherm.

- Isotherm II: multilayer physisorption on a flat surface, valid for many non-porous substances. This graph shows a large deviation from the Langmuir model of adsorption. The intermediate flat region in the isotherm corresponds to monolayer formation.

- Isotherm III: weak gas-solid interactions. This graph shows a large deviation from the Langmuir model of adsorption. This isotherm explains the formation of a multilayer. The absence of a flat region in the curve indicates no monolayer formation.

- Isotherm IV – multilayer adsorption accompanied by capillary condensation in mesopores. At lower pressure, the formation of a monolayer occurs (as for Isotherm II). This is then followed by multilayer formation at higher pressure.

- Isotherm V: weak gas-solid interactions. This graph also shows the phenomenon of capillary condensation of a gas.

- Isotherm VI: When the surface of a nonporous adsorbent is energetically uniform the isotherm may be stepped. This isotherm is said to be of theoretical interest only.

2.4.2 Pore Size Measurements

Individual pores in heterogeneous catalysts may vary greatly in both size and shape. Widths of micropores range from 0.3 nm to 2.0 nm, with mesoporous substances having pore sizes from 2 nm to 50 nm. Macropores range from widths of 50 nm to 10^5 nm. Porosity of a substance is given by:

$$P_r = \left(\frac{V_p}{V_{tot}}\right) \times 100\% \qquad \text{(Eq. 2.4)}$$

where V_p = pore volume ($cm^3 g^{-1}$)

V_{tot} = total volume of the porous substance ($cm^3 g^{-1}$).

Porosimetry is used to determine pore diameter and total pore volume of a material. Pore size can be determined based on the external pressure needed to force a non-wetting liquid (such as mercury) into a pore against the opposing force of the liquid's surface tension. For cylindrical pores, Washburn's Equation[171] can be used to calculate pore diameter, D_p:

$$P_L - P_G = \frac{4\sigma \cos\theta}{D_p}$$
(Eq. 2.5)

where P_L =   pressure of liquid

P_G =   pressure of gas

σ =   surface tension of liquid (the angle at which a liquid/vapour

interface meets a solid surface)

θ =   contact angle of intrusion liquid

D_P =   pore diameter.

2.4.3   Pore Size Distribution

Assuming that each pore acts independently, each pore size present contributes to the

total adsorption isotherm in proportion to the fraction of the total area of the sample

that it represents:

$$Q(p) = \int dH q(p,H) f(H)$$
(Eq. 2.6)

where $Q(p)$ =   experimental quantity adsorbed at pressure p

$q(p,H)$ =   quantity adsorbed per unit area at the pressure, p, in an ideal

pore size H

$f(H)$ =   total area of pores of size H in the sample.

2.4.4   Nitrogen Adsorption/Desorption

The nitrogen adsorption/desorption method is used to determine pore volume and size distribution of pores with pore radius in the range 10-300 Å. Nitrogen desorption involves filling the pores with liquid nitrogen. Gradually lowering the pressure results in desorption of measurable quantities of nitrogen, from which the pore volume and pore size distribution can be obtained. Nitrogen adsorption and the Kelvin Equation[172] (describing the change in vapour pressure due to a curved liquid/vapour interface with radius *r*) allow the correlation of pore size with the pressure at which condensation in the pore takes place. Use of the Kelvin Equation is accurate for large pore sizes, but becomes less accurate as the pore dimensions become less than a large multiple of molecular size.[173]

2.4.5   Materials and Methods

Nitrogen desorption of the ten powdered catalysts was undertaken using a Micromeritics ASAP 2010 Accelerated Surface Area and Porosimetry System (see Experimental Chapter). Repeat runs were carried out for each catalyst and erroneous results were discarded. The adsorption/desorption isotherm of Fulacolor clay is displayed in Figure 2.5. The graph plotted relative pressure (P/P_0) against the volume of nitrogen adsorbed. The ASAP system recorded both a BET surface area plot and a Langmuir surface area plot for each catalyst. Figure 2.6 and Figure 2.7 show the BET and Langmuir surface area plots for Fulacolor clay respectively.
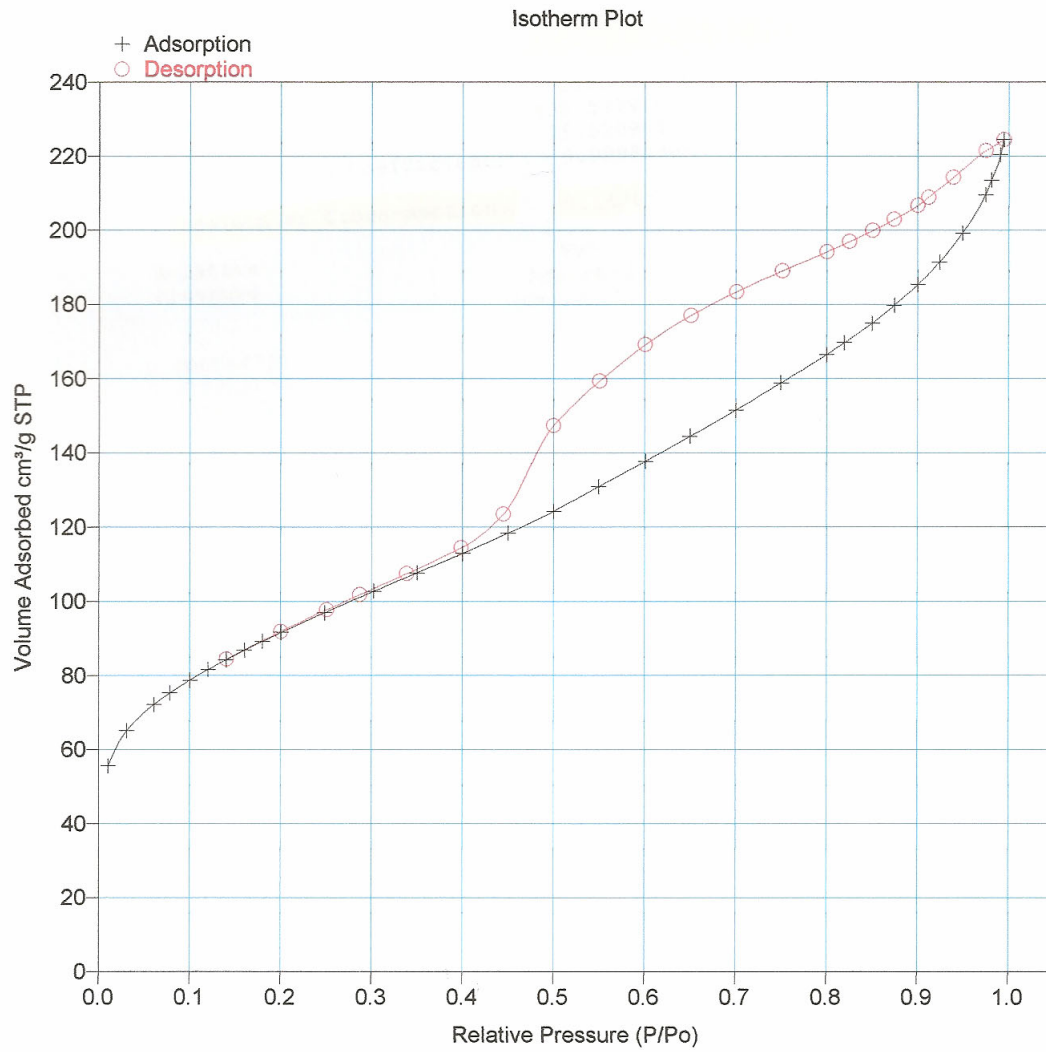
Figure 2.5: Nitrogen adsorption/desorption isotherm for Fulacolor clay.
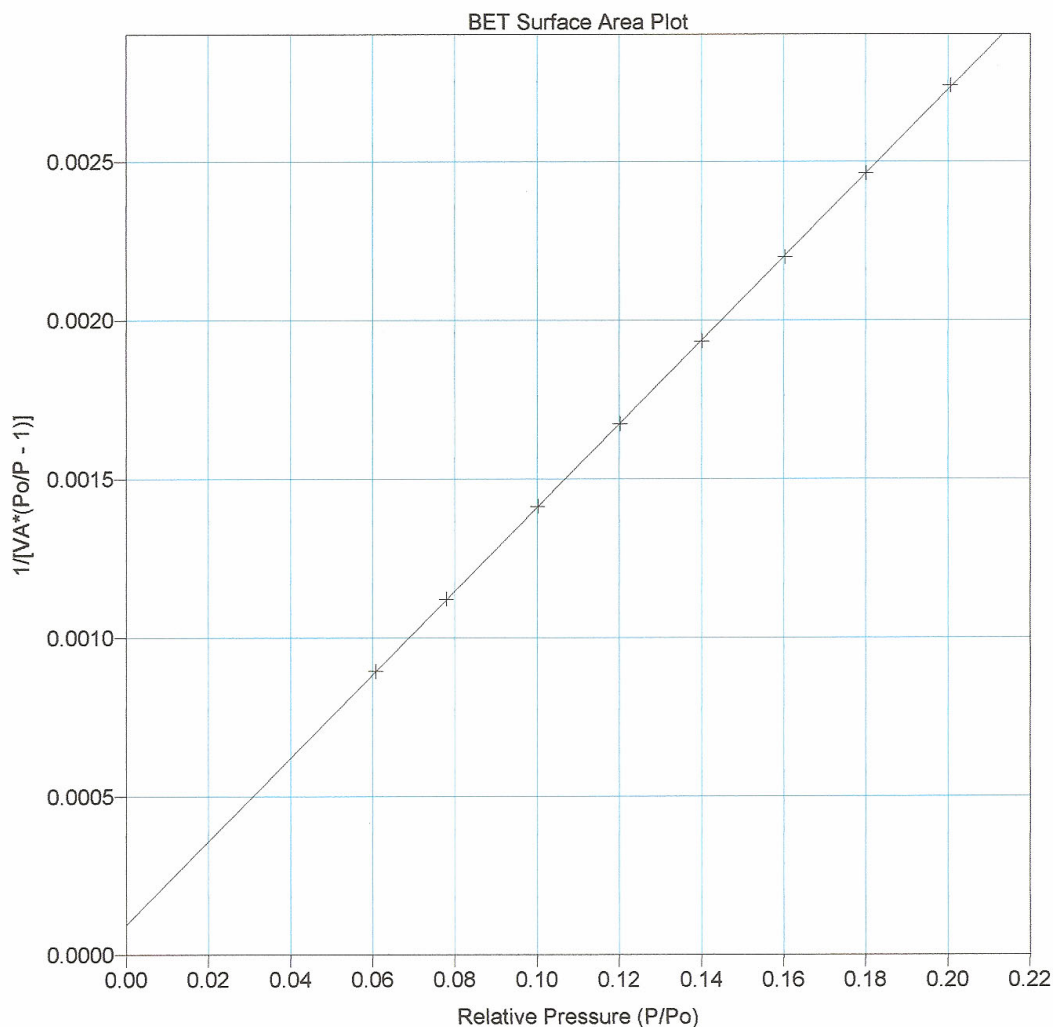
Figure 2.6: BET surface area plot for Fulacolor clay

The line of best fit in Figure 2.6 agrees extremely well with the BET surface area points recorded on the graph. This explains why the BET surface area results recorded in Table 2.3 have such low error margins. In comparison, the Langmuir surface area plot displayed in Figure 2.7 does not have the same level of agreement between the line of best fit and the recorded Langmuir surface area points on the graph. Therefore, the Langmuir surface area results reported in Table 2.3 have larger error margins.
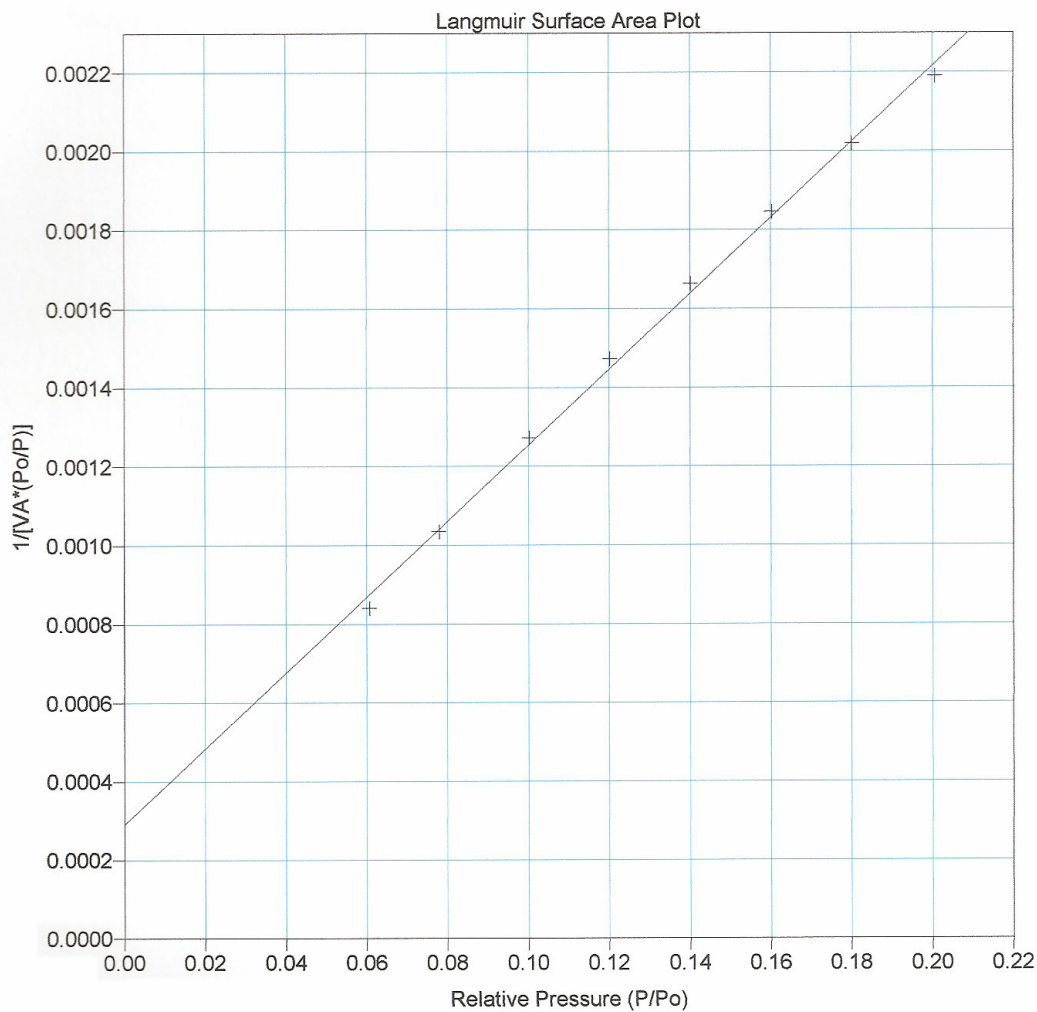
Figure 2.7: Langmuir surface area plot for Fulacolor clay

Table 2.3 displays the results of the nitrogen adsorption/desorption experiments for all ten catalysts.

Table 2.3: Results of Nitrogen adsorption/desorption experiments

Sample	BET Surface Area (m²/g)	Langmuir Surface Area (m²/g)	T-Plot Micropore Volume (cm³/g)	T-Plot Micropore Area (m²/g)	T-Plot External Surface Area (m²/g)	Single Point Surface Area at P/P_0 (m²/g)	Single Point Adsorption Total Pore Volume of Pores < 665 Å (cm³/g)	Adsorption Average Pore Diameter (Å)
Fulacolor	329 ± 1	452 ± 9	0.018	47	282	319	0.32	39
Fulcat 435	360 ± 1	493 ± 11	0.016	42	318	349	0.35	39
Fulmont	243 ± 1	334 ± 6	0.018	43	200	237	0.39	63
EPZE	287 ± 1	397 ± 8	0.007	22	266	277	0.4	56
EPZG	203 ± 1	282 ± 6	0.003	12	191	195	0.31	60
EPZ10	200 ± 4	280 ± 6	-0.003	-1	201	191	0.35	69
23z	301 ± 9	398 ± 13	0.130	278	27	314	0.14	19
280z	460 ± 8	630 ± 12	0.055	131	329	455	0.23	20
CeY	569 ± 7	751 ± 9	0.249	535	34	595	0.26	19
LaY	428 ± 16	566 ± 21	0.182	391	36	447	0.22	21

The BET and Langmuir surface area results for a catalyst were seen to differ greatly. This was due to the different equations used to calculate each result, which were based on different assumptions of the behaviour of the adsorption of nitrogen onto the catalyst surface (multilayer or monolayer). Due to the BET surface area plot (representing multilayer adsorption) having greater correlation between the points and line of best fit and hence a smaller error on each result, the BET surface areas were used for this study.

Appendix C displays the results obtained for the Surface Area (m^2/g), Total Pore Volume of Pores < 665 Å (cm^3/g) and Average Pore Diameter (Å) of each catalyst.

2.4.6 Nitrogen Desorption Results

Reddy *et al.*,[174] found the surface area of montmorillonite K10 to be 254.0 m^2g^{-1}. Arena, Dario and Parmaliana[175] calculated a BET surface area for K10 of 251 m^2g^-1. This study found the surface areas of EPZE, EPZG and EPZ10 as being 287 ± 1 m^2g^{-1}, 203 ± 1 m^2g^{-1} and 200 ± 4 m^2g^{-1} respectively. This suggests that EPZG and EPZ10 have larger crystals of metal salts deposited on their surface, producing a smaller surface area measurement, whereas EPZE is coated with smaller, powder-like crystals which increase the surface area of the clay vastly in comparison to the other K10 based clays.

In relation to Fulacolor, Fulcat 435 and Fulmont, the latter had a significantly smaller surface area (243 m^2g^{-1}), with Fulcat 435 having the largest (360 m^2g^{-1}) and Fulacolor lying in between (329 m^2g^{-1}). As mentioned previously, surface area can be related to acid activation, therefore, of all these clays, Fulcat 435 appears to be the most acid activated; an observation that is supported by it having the highest Si/Al_{tot} ratio of the

group. The calculated surface area value for Fulcat 435 (360 m^2g^{-1}) was in good agreement with the reported figure of 350 m^2g^{-1}.[158]

Selli and Forni[176] found the surface areas of five Y-zeolites to be between 579-750 m^2g^{-1}. Arena, Dario and Parmaliana[177] calculated a BET surface area for HY zeolite of 500 m^2g^{-1}. This study found the surface areas of CeY zeolite and LaY zeolite to be 569 ± 7 m^2g^{-1} and 428 ± 16 m^2g^{-1} respectively. The lower values found in this study in comparison to literature values for similar Y-zeolites could be related to the deposition of $CeCl_3$ and $LaCl_3$ into the pores, reducing the accessible surface area of the catalysts.

The previous BET values calculated by Dr. June Gardner at the University of Central Lancashire (2003) in relation to LaY zeolite were found to differ from the results of this study. The analysis undertaken in 2003 gave a surface area of 471 m^2g^{-1}, whereas this study gave a value of 428 m^2g^{-1}. This 10% decrease in surface area could be related to degradation of the powdered sample in some way over the years, or simply experimental variation.

In terms of the ZSM-5 catalysts, the BET surface area for 23z and 280z were found to be 301 ± 9 m^2g^{-1} and 460 ± 8 m^2g^{-1} respectively. Research by Uddin *et al*.,[178] and Sakata *et al*.,[179] found the surface area of their ZSM-5 catalyst as being 360 m^2g^{-1}, whilst Marcilla *et al*.,[180] calculated a value of 420 m^2g^{-1} for the HZSM-5 under investigation. As the ZSM-5 catalysts we investigated are in their ammonium forms and the 23z catalyst has the higher exchange capacity, the observed values are in accord with the ammonium ions blocking accessible surface sorption sites.

Clark *et al.*[181] found that K10 clay demonstrated significant porosity in the 50-150 Å pore diameter range, with a narrow distribution at approximately 65 Å. A specific surface area of 230 m^2g^{-1} and total pore volume of 0.36 cm^3g^{-1} were calculated. The results for this study appear to agree well with Clark *et al.*, with EPZE, EPZG and EPZ10 having a surface area of 200 – 287 m^2g^{-1}, a total pore volume of 0.31-0.40 cm^3g^{-1} and an average pore diameter of 56-59 Å. The slightly lower values of average pore diameter found for the K10 clays in this study could be related to the pores being clogged by the Lewis acids deposited on the catalysts.

2.4.7   Nitrogen Desorption Conclusions

In general, the zeolites were found to have a larger surface area, but smaller average pore diameter than the clay catalysts, suggesting that the zeolites should be more active for small molecules, but the clays could be more active for large ones. EPZ10 (acid-activated K10 montmorillonite-supported $ZnCl_2$) had the lowest surface area value of 200 $\pm$ 4 m^2g^{-1} and the largest average pore diameter (69 Å) of all the catalysts investigated. This could be due to the zinc chloride crystals blocking medium sized pores of the clay (giving a lower surface area), but producing large pores between the agglomerates of nanocrystals (higher values for pore diameter).

Fulcat 435 clay was found to have the largest surface area of all the clays (360 m^2g^{-1}), possibly suggesting a greater degree of acid activation than the other clay catalysts.

Up to this point, information in relation to the Si/Al_{tot} ratio, surface area and average pore size has been determined for each of the ten catalysts. However, surface acidity (Brønsted and Lewis) also plays a very important role in determining the effectiveness

of a catalyst. It is important to explore all properties that could have a positive or negative effect on the catalyst, therefore it was essential that analysis of the surface acidity of the zeolites and clays was determined.

2.5 Surface Acidity

The determination of surface acidity is of great importance when evaluating the catalytic action of solid acid catalysts. Elemental analysis, for example, cannot distinguish between Brønsted or Lewis acidic sites associated with aluminium incorporated in the different regions of the catalysts' framework or cationic aluminium or aluminium oxide deposited into the clays' interlayer region. However, Fourier Transform-Infra Red (FT-IR) spectrometry of adsorbed pyridine, allows an assessment of the number and strength of acidic active sites. Pyridine interacting as a Lewis base (LPy) has a distinctly different spectrum from that of pyridine acting as a Brønsted base (BPy).

Lewis and Brønsted acid sites can be differentiated by observing the changes in the 'ring' vibrations of pyridine and other bands in the region of 1700cm^{-1} to 1400cm^{-1}.[182] When pyridine is co-ordinately bonded, the 1583 cm^{-1} band shifts markedly. Larger shifts are said to indicate increasing hydrogen bond strength. The bands near 1540 cm^{-1}, 1640 cm^{-1} and at 1485 cm^{-1} are said to indicate proton acidity, whilst a band in the 1440-1465 cm^{-1} region gives an indication of aprotonic (Lewis) acidity. Chemisorbed BPy is characterised by bands at 3260 cm^{-1} and 3188 cm^{-1}, which are due to the NH^{+} stretching vibration, and by the bands at 1638 cm^{-1} and 1545 cm^{-1}, due to the combined C-C stretching and in-plane CH and NH bending modes. Chemisorbed LPy is characterised by the bands at 1452 cm^{-1} and 1577 cm^{-1}, which are due to the combined

C-C stretching and in-plane CH bending modes. Figure 2.8 displays protonated and bound amine at Brønsted and Lewis acid sites.
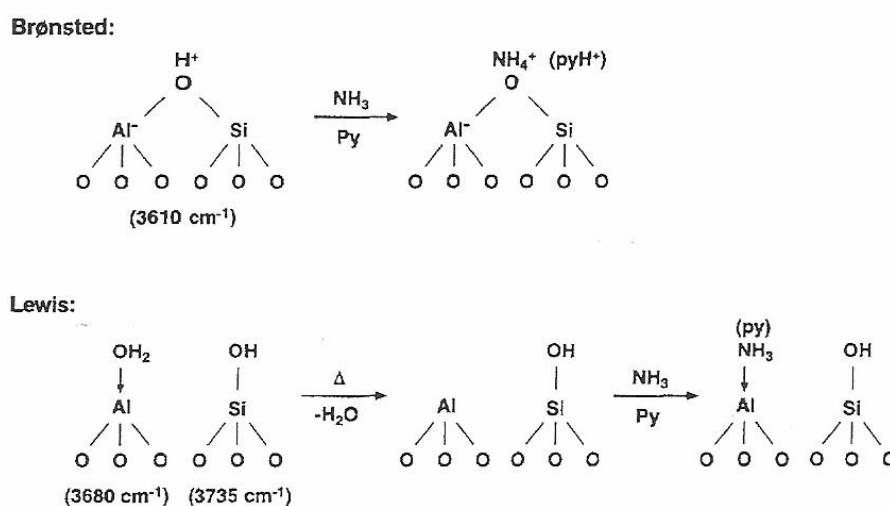
Figure 2.8: Protonated and bound amine at Brønsted and Lewis sites[184]

Emeis[183] recorded the IR spectra of five zeolites and two amorphous silica-aluminas as they were dosed with pyridine gas at 150°C. The Brønsted acid sites were found to produce a band at 1545 cm^{-1}, whilst the band at 1455 cm^{-1} was due to pyridine at a Lewis acid site.

Table 2.4 lists the infrared bands of pyridine on acid solids in the 1400-1700 cm^{-1} region.[185]

Table 2.4: Infrared bands of pyridine on acid solids in the 1400-1700 cm^{-1} region[185]

Hydrogen bonded pyridine	Coordinately bonded pyridine	Pyridinium ion
1440-1447 (v.s)	1447-1460 (v.s)	
1485-1490 (w)	1488-1503 (v)	1485-1500 (v.s)
		1540 (s)
1580-1600 (s)	1580 (v)	1620 (s)
	1600-1633 (s)	1640 (s)

(band intensities: v.s – very strong, s – strong, w – weak, v – variable)

Drago *et al*., undertook pyridine adsorption on H-ZSM-5 and found no evidence of Lewis acid sites, with neither the surface sites nor straight channels of the zeolite containing measurable quantities of Brønsted sites.[186] Misra *et al*., studied the acid sites of zeolite ZSM-5 at different temperatures and found H-ZSM-5 to have more intermediate-strength acid sites and very few sites of high acid strength. The total number of acid sites was said to be related to the SiO_2/Al_2O_3 ratio.[187]

Ward[188] found that, at a calcination temperature of 475°C, Y-zeolite was almost entirely in the Brønsted acid form. Increase of calcination temperature was said to have converted Brønsted acid sites into Lewis acid sites through elimination of hydroxyl groups and formation of tricoordinated aluminium atoms. Eberly[189] undertook infrared spectroscopy of pyridine adsorbed on various ion-exchanged faujasites at 100-260°C. The alkali-metal exchanged faujasites showed no pyridinium ions, indicating the surface acidity to be predominantly Lewis in nature. For Ca and Mg faujasites, the ability to form pyridinium ions was greatly enhanced by the addition of small amounts of water. Deka[190] studied the influence of exchanged cations on acidity and basicity of faujasite

zeolites. The Lewis acidity of the alkali-exchanged zeolites was found to decrease in the order $Li^+ > Na^+ > K^+$.

Aguiar et al.,[191] carried out FT-IR spectroscopy on rare-earth exchanged zeolites using pyridine adsorption. The intensity of the 1540 cm^{-1} band was found to be a function of the type of RE cation introduced. The higher the ionic radius of the RE cation, the higher the intensity of the band, indicating that zeolites containing lighter RE cations generate more acidic sites. Ballivet, Pichat and Barthomeuf[192] found that after calcination at high temperatures, the La zeolites exhibited fewer Lewis-acid sites than the unmodified zeolites. Maldonado et al.,[193] found the number of Lewis-acid sites decreased as the amount of rare-earth oxide (REO) applied to the zeolite increased.

2.5.1 Materials and Methods

The pressed-disk method is an extremely valuable technique for obtaining infrared spectra of solid materials. It requires reducing the particle size of the sample to below the shortest wavelength of light to be used and suspending the sample in a suitable matrix. The matrix material should have a refractive index similar to that of the sample. The pressed-disk method is based upon the fact that powdered alkali halides can be pressed into IR-transparent disks under pressure.

To determine the surface acidity of the clays and zeolites in this study, the catalysts were heated to 200ºC in order to remove any water present, then stored in an oven at 110ºC to prevent the absorption of water vapour from the atmosphere. Four anhydrous potassium bromide (KBr) disks were then made to a series of catalyst concentrations (0.8-1.2%) for each clay and zeolite. This was achieved by placing 20g of KBr in a

flask and heating it on a vacuum line for 30 minutes at 200ºC, then transferring the powder to an oven held at 110ºC. This ensured the KBr was free of any absorbed water. In order to make the disks of specific concentration, the amount of catalyst had to be weighed very accurately, then ground in a pestle and mortar with the correct amount of KBr to ensure homogeneity. The disks, weighing 100mg, were made by transferring the mixture of fine particles of KBr (~99%) and catalyst (~1%) to a press where a pressure of six tonnes was applied for twenty seconds.

The KBr disks of varying catalyst concentrations were then placed in an enclosed saturated atmosphere of pyridine vapour for seven days to ensure complete migration through the KBr pellet; previous work having shown that equilibrium was achieved within 3-4 days.

FT-IR analysis using a Perkin Elmer Spectrum RX1 instrument was then undertaken on all the disks (four per catalyst). A pure KBr disk was used as a background in order to reduce any effects that were not attributable to the catalysts. Each disk was measured four times, rotating by 90º each time, to improve the reproducibility of results by eliminating any directional effects of the pellet manufacture. The peak areas obtained from the IR absorbance spectra 470 cm^{-1} (Si-O) and 523 cm^{-1} (Al-O) were recorded for the four quarter rotations of each disk. A graph of average absorbance *vs.* catalyst concentration was plotted.

Equally, for the characteristic Brønsted frequency (1545 cm^{-1}) and Lewis frequency (1455 cm^{-1}) a plot of average absorbance *vs.* catalyst concentration for each catalyst at each of the frequencies was constructed. This allowed the average Brønsted site

concentration and average Lewis site concentration to be calculated *via* Equations 2.7 and 2.8 below. The multipliers of 1.88 and 1.42 were calculated from the integrated absorbance (peak area) of the Brønsted band and Lewis band respectively.

$$C_B = 1.88 \times IA(B) \times \left(\frac{R^2}{W} \right) \qquad \text{(Eq. 2.7)}$$

where C_B = amount of pyridine absorbed by catalyst (mmol/g)

   $IA(B)$ = integrated absorbance of B band (cm^{-1})

   R = radius of disk (cm)

   W = weight of disk (mg)

$$C_L = 1.42 \times IA(L) \times \left(\frac{R^2}{W} \right) \qquad \text{(Eq. 2.8)}$$

where C_L = amount of pyridine absorbed by catalyst (mmol/g)

   $IA(L)$ = integrated absorbance of L band (cm^{-1})

   R = radius of disk (cm)

   W = weight of disk (mg)

2.5.2   Results of Surface Acidity Experiments

Table 2.5 lists the concentrations of Brønsted and Lewis acid sites for each of the ten catalysts, and the corresponding Brønsted/Lewis ratio of sites.

Table 2.5: Concentrations of Brønsted and Lewis sites for each catalyst

Catalyst	Concentration of Sites (mmol/g)			Brønsted/Lewis Ratio
	Brønsted	Lewis	Total	
Fulacolor	0.3124	0.1128	**0.425**	2.77
Fulcat 435	0.1099	0.0421	**0.152**	2.61
Fulmont	0.2364	0.0926	**0.329**	2.55
EPZE	0.2943	0.1111	**0.405**	2.65
EPZG	0.2329	0.0889	**0.322**	2.62
EPZ10	0.0760	0.0236	**0.100**	3.22
CeY	0.0039	0.0030	**0.007**	1.32
LaY	0.0155	0.0079	**0.023**	1.97
23z	0.0085	0.0045	**0.013**	1.89
280z	0.0046	0.0024	**0.007**	1.89

2.5.3   Discussion of Results

Brown and Rhodes[194] compared the number of surface acid sites of a Fulcat clay (0.50 ± 0.1 mmol/g) and K10 montmorillonite (0.20 ± 0.1 mmol/g), and found that the Fulcat contained twice the number of acid sites of the K10. Fulcat 435 in this study was found to contain 0.1 mmol/g of Brønsted sites and 0.04 mmol/g of Lewis sites – very similar to EPZG, but far less than that for EPZE and far more than the concentration of sites on EPZ10. EPZE had a total surface acidity of 0.4 mmol/g, whilst the total Brønsted and Lewis acid sites for EPZG was 0.322 mmol/g. In contrast to these two K10 clays, EPZ10 revealed a much smaller number of surface acid sites (0.100 mmol/g) – a third of the amount of EPZG and a quarter of that on EPZE.

Selli and Forni[195] calculated the concentration of Brønsted and Lewis acid sites for a variety of Y-zeolites and found them to be in the region of 0.041 – 0.660 mmol/g and 0.007 – 0.556 mmol/g respectively. The results of the pyridine adsorption experiments in this study found CeY and LaY as having total surface acidities (Brønsted and Lewis) of 0.007 mmol/g and 0.023 mmol/g respectively. These values were small and may be due to the fact that both these catalysts had been prepared a few years earlier by a previous worker and further aging of the lanthanide species may have occurred.

The total numbers of surface acid sites for the ZSM-5 zeolites were 0.013 mmol/g (23z) and 0.007 mmol/g (280z). These values were the smallest of all the ten catalysts analysed.

The ratio of Brønsted-to-Lewis sites for each catalyst varied from 1.32 (CeY zeolite) to 3.22 (EPZ10 clay). Fulacolor, Fulcat 435 and Fulmont had similar Brønsted-to-Lewis ratios between 2.55 and 2.77. Two of the K10 clays (EPZE and EPZG) also had similar ratios to each other (2.65 and 2.62 respectively). Three zeolites: LaY, 23z and 280z, gave Brønsted-to-Lewis ratios of 1.97, 1.89 and 1.89 respectively.

The two remaining ratios, for CeY (1.32) and EPZ10 (3.22), did not appear to fit with the results obtained for the other catalysts in their groups. The remaining eight catalysts appeared to have 1.89-2.77 more Brønsted sites for every Lewis acid site present.

2.5.4 Surface Acidity Conclusions

Fulacolor clay was found to contain the largest number of Brønsted and Lewis acid sites- a result consistent with its use as a catalyst for colour forming on carbonless copy paper. The high acidity suggests that it should prove to be a very effective catalyst, but in truth, many factors must be taken into account (surface area, Si/Al ratio). EPZE displayed the second largest amount of Brønsted and Lewis sites, with Fulmont and EPZG having the third and fourth highest numbers of Lewis sites.

In general, the proportion of Lewis sites to Brønsted sites was much smaller than expected. The reduction in the number of Lewis sites for the clay catalysts was thought to have been due to the absorption of water onto their surfaces which would have given the appearance of a larger number of Brønsted acid sites by masking some of the Lewis acid sites. This masking of a proportion of the Lewis sites at room temperature was not of great concern as the catalysts would be used in the degradation of polymers up to temperatures of 500ºC; a temperature far above that required for the removal of water from the catalyst, so exposing the previously hidden Lewis acid sites.

2.6 MAS NMR Spectroscopy

2.6.1 ^{27}Al NMR Spectrometry

Nuclear Magnetic Resonance (NMR) spectroscopy is a technique involving the fact that transitions can be induced between magnetic spin energy levels of certain atomic nuclei in a magnetic field. Conventional NMR studies of solid silicates gave spectra with very broad lines. However, solid state NMR with sophisticated experimental techniques

such as Magic Angle Spinning (MAS), reduce the problem of line-broadening significantly. The most important isotopes used for multi-nuclear NMR spectroscopy of zeolites are ^{29}Si, ^{27}Al, ^{31}P, ^{11}B and ^{17}O incorporated in framework positions, ^{1}H in hydroxyl groups, ^{23}Na and ^{133}Cs on non-framework sites and ^{129}Xe, ^{31}P, ^{13}C and ^{15}N in probe atoms and probe molecules.[196]

An important application of ^{27}Al NMR is the detection and characterisation of non-framework aluminium species formed, *e.g* by various thermal or hydrothermal treatments applied in dealumination processes or the preparation of the acidic H-forms of zeolites. Well separated signals at approximately 60 ppm and 0 ppm appear in the ^{27}Al NMR spectra for four-coordinated framework Al and six coordinated non-framework Al respectively. The intensities of the signals, I_0 and I_{60} allow the relative proportions of framework and non-framework Al to be calculated.[197]

In naturally occurring zeolites, the Si/Al ratio is always less than about 5, but materials with much higher and lower Al contents can be prepared in the laboratory; e.g. ZSM-5 is said to have a Si/Al ratio of between 20 and 2000.[198] Hunger[199] found the Si/Al ratios of faujasite zeolites to be 2.6 and 3.5 and two HZSM-5 zeolites to be 15.0 and 26.0.

2.6.2   Materials and Methods

The ^{27}Al NMR spectra of the clay catalysts - Fulacolor, Fulmont, and K10 montmorillonite – were kindly obtained by Patric Cookson, NMR Technician at the University of Central Lancashire.

2.6.3 Results of ^{27}Al NMR Spectroscopy

The tetrahedral aluminium peak was found to occur at a displacement of approximately 59.38 from zero, with the octahedral Al peak occurring at a displacement of approximately 7.25. Because of the width of the octahedral peak, it was not possible to distinguish between the octahedral species (*i.e.* in the octahedral layer or exchanged into the interlayer). The ratio of Al_{tet}/Al_{oct} for three of the clay catalysts is displayed in Table 2.6.

Table 2.6: Ratio of tetrahedral to octahedral Al in the catalyst samples

Catalyst	Tetrahedral Al	Octahedral Al	Al_{tet}/Al_{oct}
Fulacolor	1.00	3.00	0.333
Fulmont	1.00	1.46	0.685
K10	1.00	4.26	0.235

Table 2.7 displays the estimated Si/Al ratios for five of the clay catalysts.

Table 2.7: Si/Al ratios estimated for clay catalysts

Catalyst	Fulacolor	Fulmont	EPZE	EPZG	EPZ10
Si/Al_{tot}	5.1	5.3	5.8	4.3	5.6
Si/Al_{tet}	20.8	12.9	29.9	37*	29.4
Si/Al_{oct}	6.8	9.1	7.2	4.9*	6.9

* These values are arrived at by assuming that the extra Al over the other K10 based catalysts will be octahedral.

2.6.4 Conclusions of MAS NMR Spectroscopy

The amount of Al_{tet} and Al_{oct} gives an insight into how the aluminium is incorporated into the clay. Acid activation of a clay can destroy the octahedral layer, suggesting that for a catalyst that has been acid activated, the amount of aluminium in the octahedral layer should be relatively low. However, as the solid state NMR cannot distinguish between the octahedral species, some of the aluminium from the octahedral layer may have become incorporated into the interlayer region, so the value of Al_{oct} will not be reduced as greatly as would have been expected.

2.7   Conclusions of Catalyst Characterisation Experiments

Undertaking SEM-EDX analysis, BET surface area experiments, surface acidity measurements and ^{27}Al NMR spectroscopy has produced valuable information that can be related to catalytic performance. It is important to look at all results as a whole, as although one catalyst may have a large surface area, it may contain smaller numbers of surface acid sites than other catalysts. Table 2.8 summarises the results of the catalyst characterisation experiments.

Table 2.8: Summary of catalyst characterisation results

Catalyst	BET Surface Area (m^2/g)	Total Pore Volume of Pores < 665 Å (cm^3/g)	Average Pore Diameter (Å)
Fulacolor	329 ± 1	0.32	39
Fulcat 435	360 ± 1	0.35	39
Fulmont	243 ± 1	0.39	63
EPZE	287 ± 1	0.4	56
EPZG	203 ± 1	0.31	60
EPZ10	200 ± 4	0.35	69
23z	301 ± 9	0.14	19
280z	460 ± 8	0.23	20
CeY	569 ± 7	0.26	19
LaY	428 ± 16	0.22	21

Catalyst	Brønsted Sites (mmol/g)	Lewis Sites (mmol/g)	Total Surface Acid Sites (mmol/g)	Si/Al$_{tot}$
Fulacolor	0.3124	0.1128	0.425	5.1
Fulcat 435	0.1099	0.0421	0.152	4.3
Fulmont	0.2364	0.0926	0.329	5.3
EPZE	0.2943	0.1111	0.405	5.8
EPZG	0.2329	0.0889	0.322	4.3
EPZ10	0.0760	0.0236	0.100	5.6
23z	0.0085	0.0045	0.013	10.9
280z	0.0046	0.0024	0.007	61.7
CeY	0.0039	0.0030	0.007	2.5
LaY	0.0155	0.0079	0.023	2.4

Fulacolor clay was found to contain the largest number of Brønsted and Lewis acid sites and the fifth largest surface area ($329 \, \mathrm{m^2g^{-1}}$) of the ten catalysts, suggesting that this clay could prove to be an effective catalyst. In general, the zeolites were found to have a larger surface area, but smaller average pore diameter than the clay catalysts and lower values for the total number of surface acid sites than the clays.

In order to establish the suitability of a particular catalyst, the clays and zeolites were rated on their performance in the catalyst characterisation experiments. Therefore, the catalyst that exhibited the largest BET surface area (enabling greater interaction between catalyst and polymer molecule), largest average pore diameter (allowing larger molecules to enter the active catalytic sites within the pores) and highest concentration of Brønsted- and Lewis-acid sites were assigned a score of 10 for that test. The catalyst performing the second greatest for any experiment was given a score of 9, and so on.

In terms of the Si/Al_{tot} ratios obtained *via* SEM-EDX analysis, it was difficult to determine which catalyst gave the best result as the aluminium present could exist either as structural octahedral or tetrahedral Al (both virtually inert except for when at the edge of a layer), exchanged octahedral Al in the acid activated clays or tetrahedral Al deposited on the clay surface (as for EPZE clay). The values of Si/Al_{oct} and Si/Al_{tet} were obtained for the clay catalysts using MAS NMR spectroscopy. EPZG was found to have the highest amount of structural octahedral Al, which was thought to provide low Lewis acidity. Fulmont had the largest amount of structural tetrahedral Al of all the clays, which was thought to give a good level of Lewis acidity to the catalyst. The largest Si/Al_{tot} value was obtained for EPZE, implying that this clay had retained the greatest amount of octahedral Al in the clay interlayer during deposition of the

ZnCl$_2$/AlCl$_3$ and therefore could also provide good Brønsted acidity. However, it must be noted that the removal of too much octahedral Al will lower the activity of a catalyst, whilst on the other hand, acid activation can improve Lewis acidity by exposing structural octahedral and tetrahedral Al. For zeolites, the lower the value of Si/Al$_{tot}$, the higher the exchange capacity and the higher the expected activity of the catalyst (Brønsted acidity). Due to the intricacies between the ratios for Si/Al$_{oct}$, Si/Al$_{tet}$ and the differences between zeolites and the acid activated clays, it was difficult to compare the Si/Al$_{tot}$ for the catalysts, therefore these values were not included in Table 2.9 below.

From the results of the nitrogen desorption experiments, and the calculations of the concentration of acid sites, a catalyst could score a maximum of 50 points. These results are displayed in Table 2.9.

Table 2.9: Ratings of catalyst performance in various characterisation tests

Catalyst	BET Surface Area	Ave. Pore Diameter	Conc. of Brønsted Sites	Conc. of Lewis Sites	Total (out of 40)
Fulacolor	6	6	10	10	32
Fulcat 435	7	6	6	6	25
Fulmont	3	9	8	8	28
EPZE	4	7	9	9	29
EPZG	2	8	7	7	24
EPZ10	1	10	5	5	21
CeY	10	2	1	2	15
LaY	8	4	4	4	20
23z	5	2	3	3	13
280z	9	3	2	1	15

Comparing the total score for each clay and zeolite (out of a possible 40), they could be ranked in terms of their potential as a successful catalyst. It must be remembered that the list in Table 2.10 below was based solely on the ratings from the catalyst characterisation experiments (without taking into account the results for Si/Al_{tot} ratios from SEM-EDX analysis). The decision on which catalysts would be used in subsequent experiments would also be dependent on their performance on the thermal degradation of various polymers reported in Chapter 4.

Table 2.10: Ranking of potential success of catalyst (1 being the greatest)

Ranking	Catalyst
1	Fulacolor
2	EPZE
3	Fulmont
4	Fulcat 435
5	EPZG
6	EPZ10
7	LaY
= 8	280z
= 8	CeY
10	23z

Fulacolor and EPZE clay were found to have exhibited the best characteristics to identify them as potentially successful catalysts. Fulmont and Fulcat 435 clays also appeared to perform very well in the catalyst characterisation experiments. In contrast, the rare-earth zeolites (CeY and LaY) and ZSM-5 zeolites (23z and 280z) did not exhibit the desired properties overall. CeY and LaY displayed the first and third largest

surface area measurements respectively, but received some of the lowest scores for pore diameter and concentration of acid sites in comparison to the other catalysts.

As mentioned previously, EPZE and the Ful* clays appear to have good all-round properties that could be extremely beneficial in the catalytic degradation of plastics. However, without conducting thermal analysis and pyrolysis-gas chromatography-mass spectrometry on the polymer-catalyst mixtures, it is not possible to determine which of the catalyst properties has the most influence in the effectiveness of the clays and zeolites. Additionally, the conditions under which the further experiments are conducted (temperature, polymer type and structure) will also play a part in how successful a catalyst is in the recycling of plastic waste into high grade fuel.

3   Waste Polymer Identification

Polymers can be simple or more complex, depending on the molecules they are made from.   Polyethylene, polypropylene and polystyrene contain only carbon and hydrogen atoms, but polystyrene differs in properties as it has a succession of bulky phenyl groups on alternate carbons that stiffen the main chain.   In addition to carbon and hydrogen, polyethylene terephthalate and polymethyl methacrylate contain oxygen, polyacrylonitrile contains nitrogen and polyamides and polyurethanes contain both nitrogen and oxygen.

It was important that this study represented the many different types of plastics found in everyday household waste and that the samples were identified correctly.   Infrared spectroscopy was selected as the analytical technique for determining the polymer types, based on the absorption of the radiation by functional groups within the sample and on the characteristic skeletal vibrations of the molecules (Fingerprint).

3.1   Materials and Methods

The infrared spectrum of a polyatomic molecule consists primarily of the fundamental vibrations of the infrared active bonds.   In the case of polymers, the various normal modes involving the carbon skeleton are complex, with the C-C stretching fundamentals occurring over a wide (1200-800 cm^{-1}) wavenumber range.   As the frequencies and intensities of these carbon-skeletal absorptions tend to be peculiar to each individual

compound, the portion of the spectrum from 1400 to 800 cm^{-1} is often referred to as the "fingerprint region". Attenuated Total Reflectance (ATR) spectrometry is a technique that enables the infrared spectra of solids or films to be obtained easily. To obtain ATR spectra of the solid polymers, a model FTIR-400 single-beam spectrometer with a Golden Gate^{TM} attachment was used. The FTIR-ATR spectra of waste polymer samples were identified by comparing their 'fingerprints' with a reference book of IR spectra.[200]

3.2   Results of ATR Spectrometry

When functional groups within a sample absorb infrared radiation, a decrease in beam energy is observed. This absorbance is defined as:

$$A = -\log\frac{I}{I_0} \qquad\qquad\qquad\text{(Eq. 3.1)}$$

where I = intensity of radiation transmitted by a sample

I$_0$ = intensity of radiation incident on the sample.

The ratio, I/I_0, is the fraction of radiation transmitted by the sample and is known as the transmittance, T. Absorbance and transmittance are related by the equation:

$$A = -\log\frac{I}{I_0} = -\log T \qquad\qquad\qquad\text{(Eq. 3.2)}$$

Infrared spectra obtained from the analyses of polymer samples in this study were reported as % transmittance *vs.* wavenumber. Six pure polymers were purchased from Sigma Aldrich: high-density polyethylene, low-density polyethylene, polystyrene,

polyethylene terephthalate and two isotactic polypropylene samples (A and B) of different molecular weights. PPA had a molecular weight of 12,000 and is commonly used to improve pigment dispersion in polypropylene films and fibres. Isotactic polypropylene B (molecular weight 190,000) is commonly used to make trays, containers and lids and more closely resembled a PP sample more commonly found in household waste. Infrared spectra of these pure plastics were then used as 'fingerprints' to identify the unknown polymer samples collected from everyday household waste.
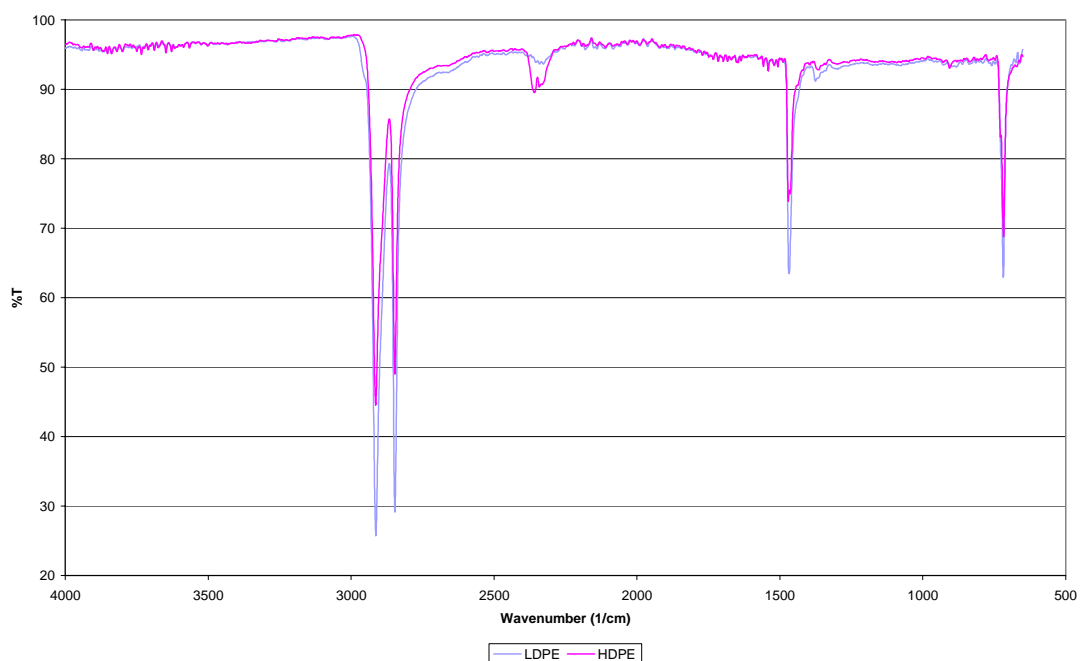
Figure 3.1: FTIR-ATR spectra of pure LDPE and HDPE

The two peaks appearing in the 2300cm^{-1} region of most spectra are due to carbon dioxide in air, and were present in all the FTIR-ATR spectra obtained.

The FTIR-ATR spectra of pure low-density polyethylene and high-density polyethylene (Figure 3.1) were found to display four characteristic peaks. The C-H stretches were found to occur at a wavenumber of 2915 cm^{-1} and 2848 cm^{-1}, whilst the methylene

deformations (C-H bends) occurred at 1469 cm^{-1} and 720 cm^{-1}. Seven different items of everyday household waste were identified as being made of polyethylene. Their spectra are displayed in Figure 3.2, with the peaks corresponding to C-H stretches and C-H bends being clearly recognisable.
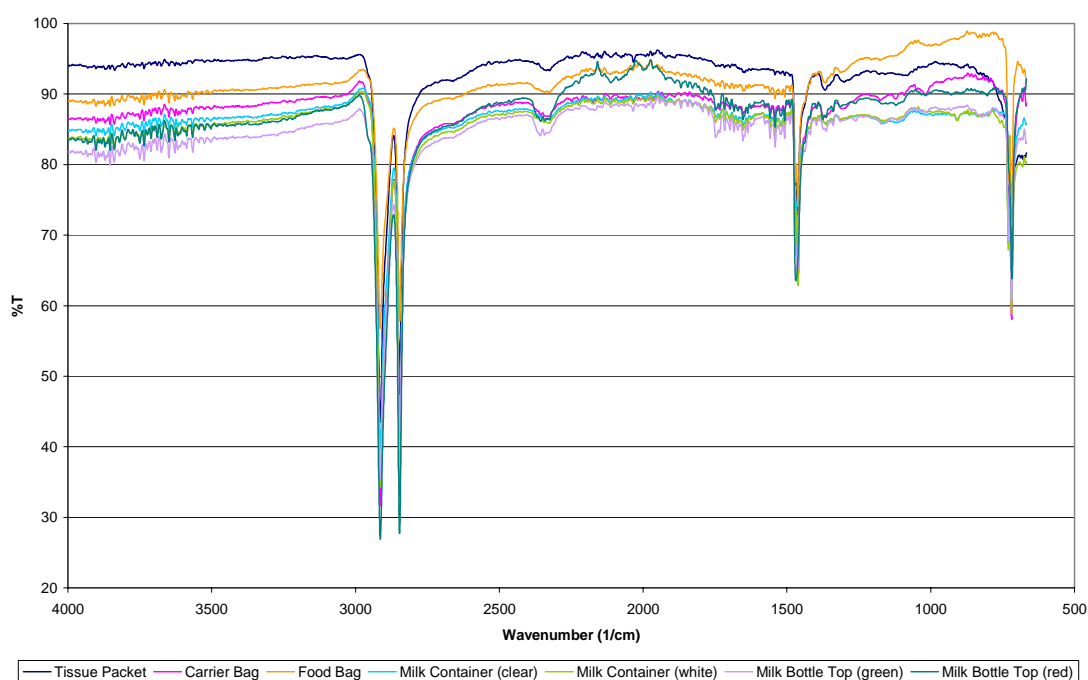
Figure 3.2: FTIR-ATR spectra of waste polyethylene samples

The infrared spectrum of pure polypropylene is displayed in Figure 3.3. Four peaks were found to correspond to C-H stretching vibrations (2950 cm^{-1}, 2917 cm^{-1}, 2870 cm^{-1} and 2838 cm^{-1}) whilst the peaks at 1457 cm^{-1} and 1376 cm^{-1} related to CH$_2$ and CH$_3$ bends respectively. Six different items of everyday household waste were identified as being made of polypropylene. Their spectra are displayed in Figure 3.4, with the peaks corresponding to C-H stretches and C-H bends being clearly recognisable.
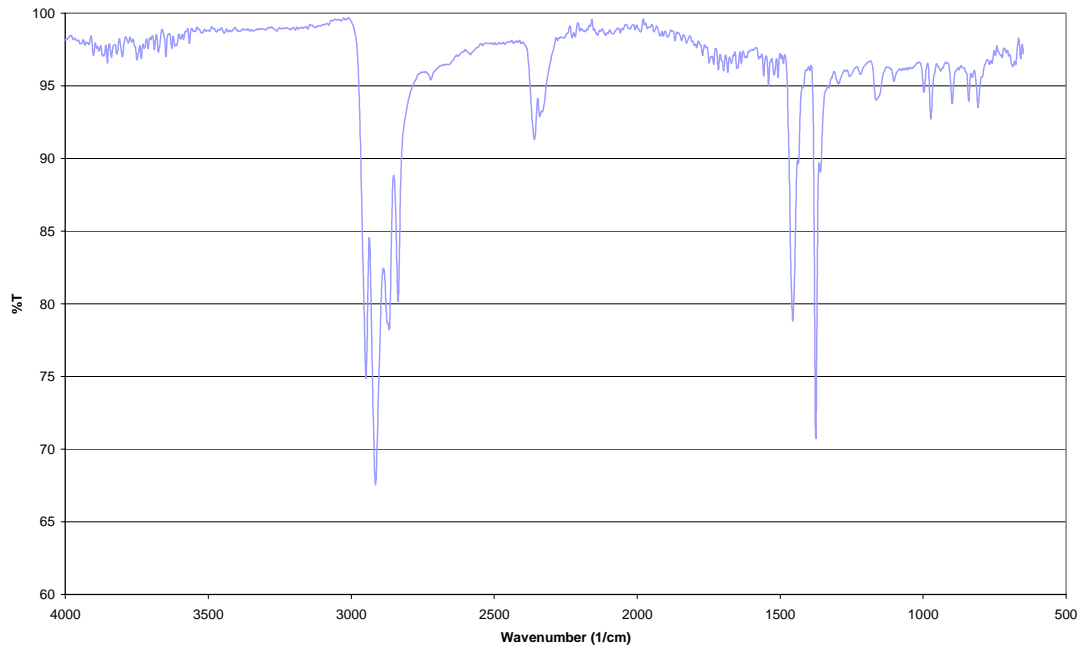
Figure 3.3: FTIR-ATR spectrum of pure polypropylene

Wrapping (clear) — Cellophane (clear) — Packaging (clear) — Spray Bottle Head (clear) — Spray Bottle Handle (orange) — Drinking Cup (clear)
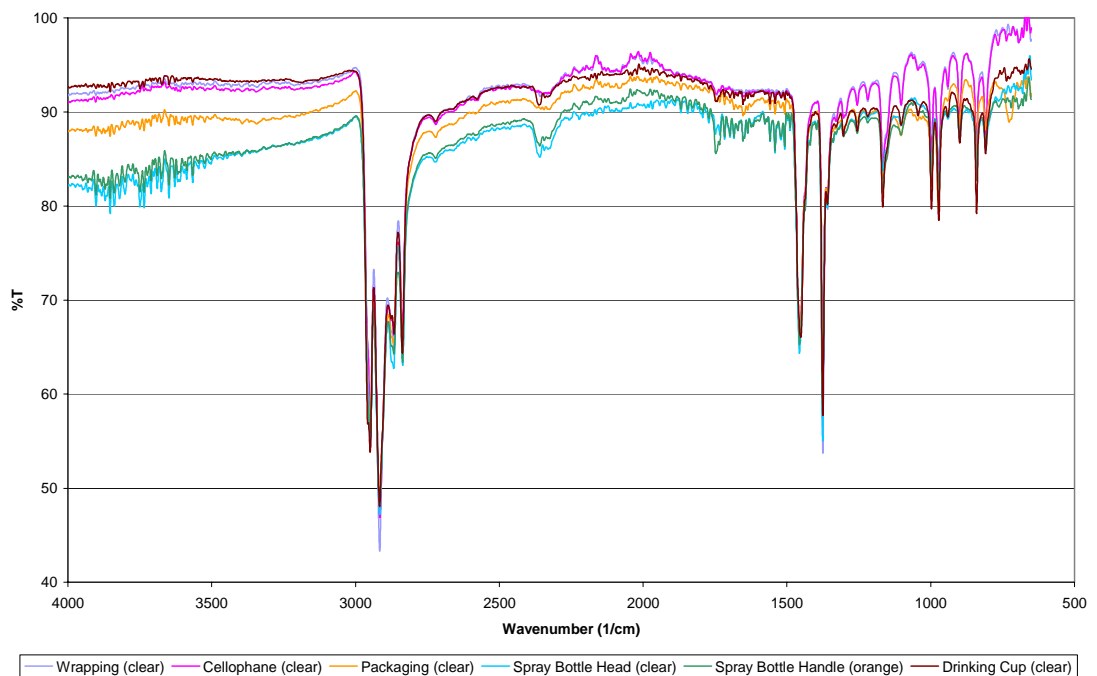
Figure 3.4: FTIR-ATR spectra of waste polypropylene samples

The infrared spectrum of pure polyethylene terephthalate is displayed in Figure 3.5. The PET spectrum was characterised by the carbonyl stretch (C=O) at 1716 cm^{-1}, the asymmetric C-C-O stretch involving the ester oxygen attached to the carbonyl bonded to the aromatic ring at 1240 cm^{-1} and the O-CH$_2$-CH$_2$- asymmetric stretch at 1094 cm^{-1}.
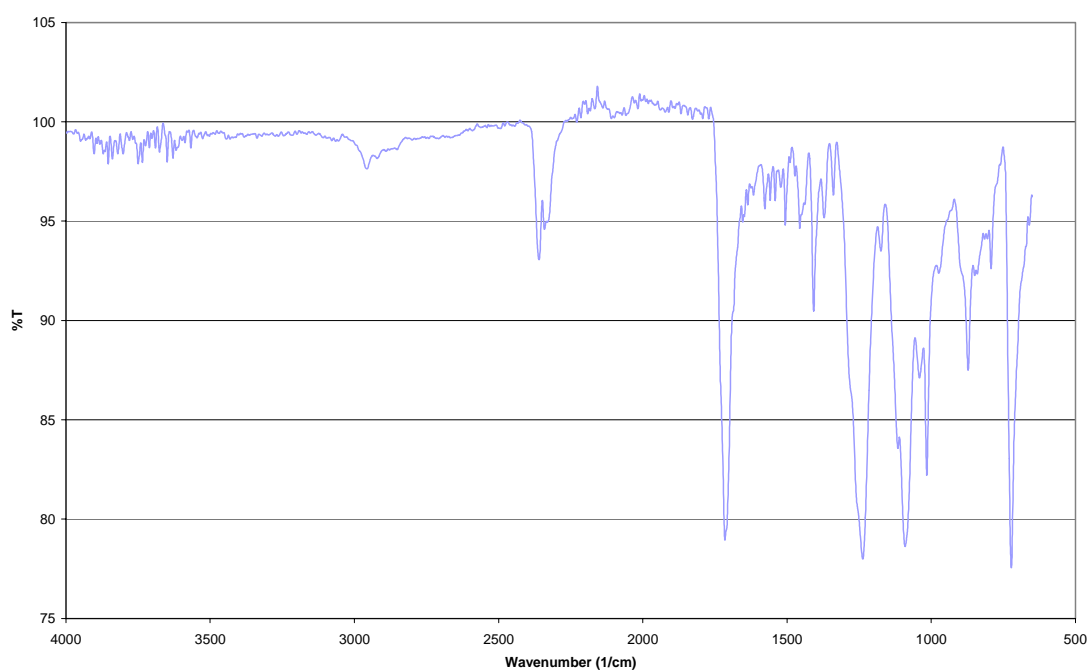
Figure 3.5: FTIR-ATR spectrum of pure polyethylene terephthalate

Six different items of everyday household waste were identified as being made of polyethylene terephthalate. Their spectra are displayed in Figure 3.6, with the peak corresponding to the C=O stretch and the peaks attributable to the C-O stretches being clearly recognisable.
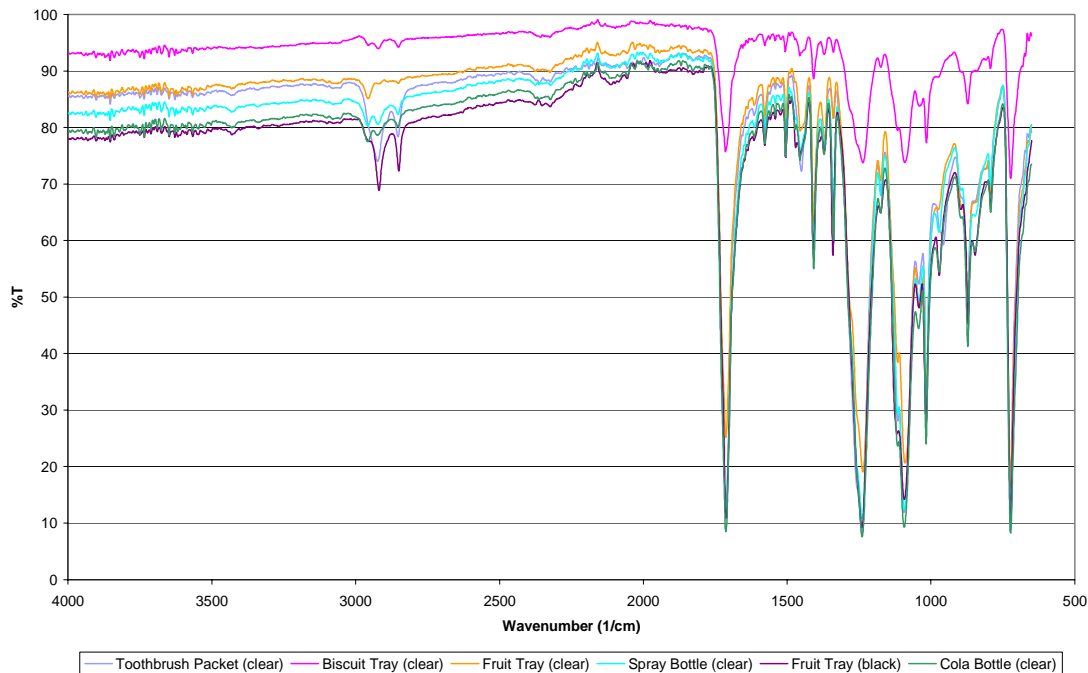
Figure 3.6: FTIR-ATR spectra of waste polyethylene terephthalate samples

The infrared spectrum of pure polystyrene is displayed in Figure 3.7. The PS spectrum was characterised by the aromatic C-H stretch at 3026 cm^{-1}, methylene stretches at 2921 cm^{-1} and 2851 cm^{-1}, aromatic ring breathing modes (1602 cm^{-1}, 1492 cm^{-1} and 1453 cm^{-1}) and out-of-plane C-H bends of the aromatic ring at 755 cm^{-1} and 696 cm^{-1}.

ATR spectra of seven different plastic samples were found to be characteristic of the infrared spectrum of polystyrene. Their spectra are displayed in Figure 3.8, with the aromatic ring breathing modes and out-of-plane C-H bends of the aromatic ring clearly recognisable.
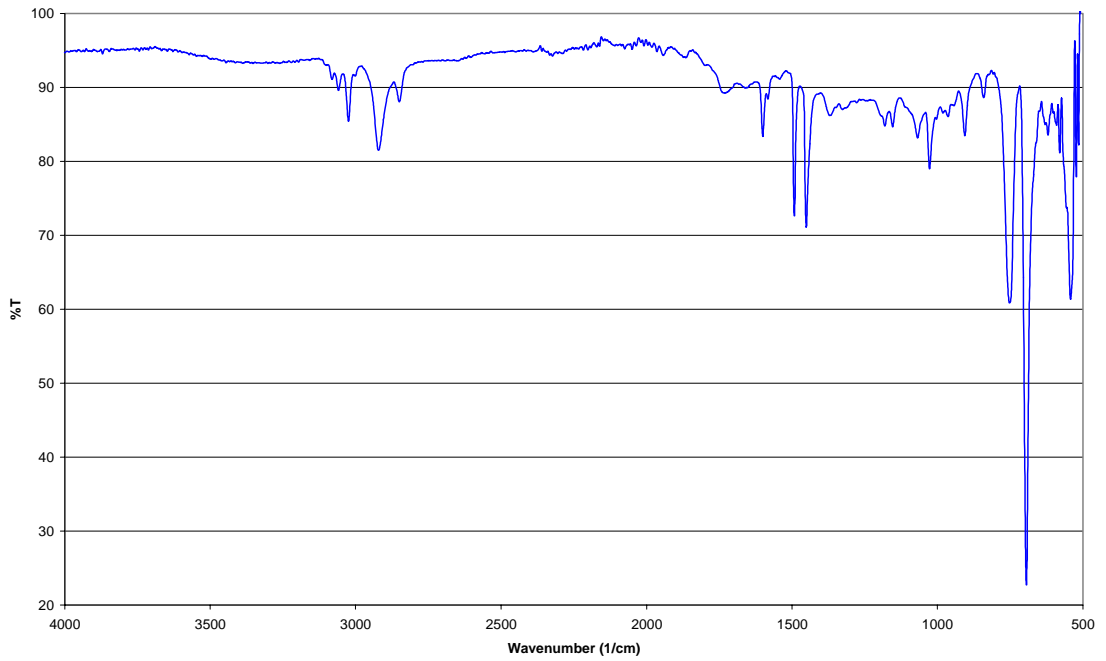
Figure 3.7: FTIR-ATR spectrum of pure polystyrene
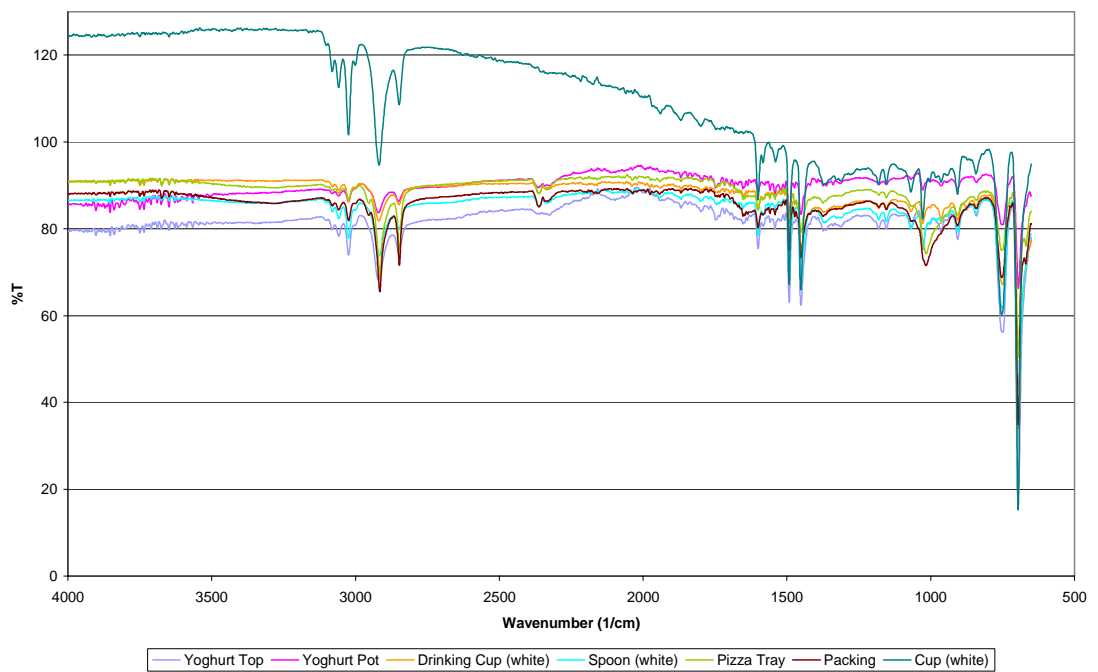
Figure 3.8: FTIR-ATR spectra of waste polystyrene samples

The FTIR-ATR spectrum of a pair of black tights (Figure 3.9) enabled the sample to be identified predominantly as a polyamide, due to the presence of the N-H stretch at 3303 cm^{-1}, the amide I band (C=O stretch) at 1655 cm^{-1} and the amide II band (N-H deformation) at 1535 cm^{-1}. The amide III band (OCONH) at 1276 cm^{-1} does not usually occur in the spectra of polyamides. However, the nylon tights contained a low percentage of Lycra® - a polyurethane-polyurea copolymer – which provides a degree of elasticity to the material. The presence of approximately 8% of elastane in the sample explains the appearance of the small amide III band in the spectrum.
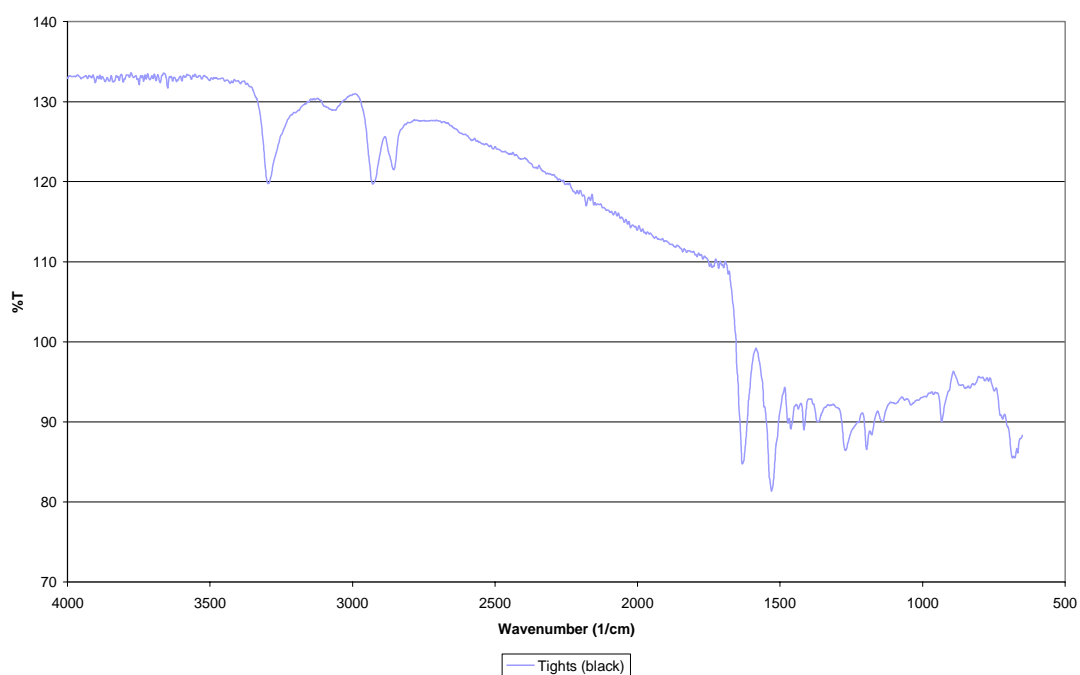
Figure 3.9: FTIR-ATR spectrum of waste polyamide

The FTIR-ATR spectra of two rubber bands (Figure 3.10) enabled the samples to be identified as polybutadiene. The characteristic spectra included methylene stretches at 2924 cm^{-1} and 2854 cm^{-1}, methylene bends at 1435 cm^{-1} and 1375 cm^{-1} and the C=C stretch at 1640 cm^{-1}. The alkene C-H out-of-plane bends at 1008 cm^{-1} and 669 cm^{-1} represent the *trans* and *cis* structures of polybutadiene.
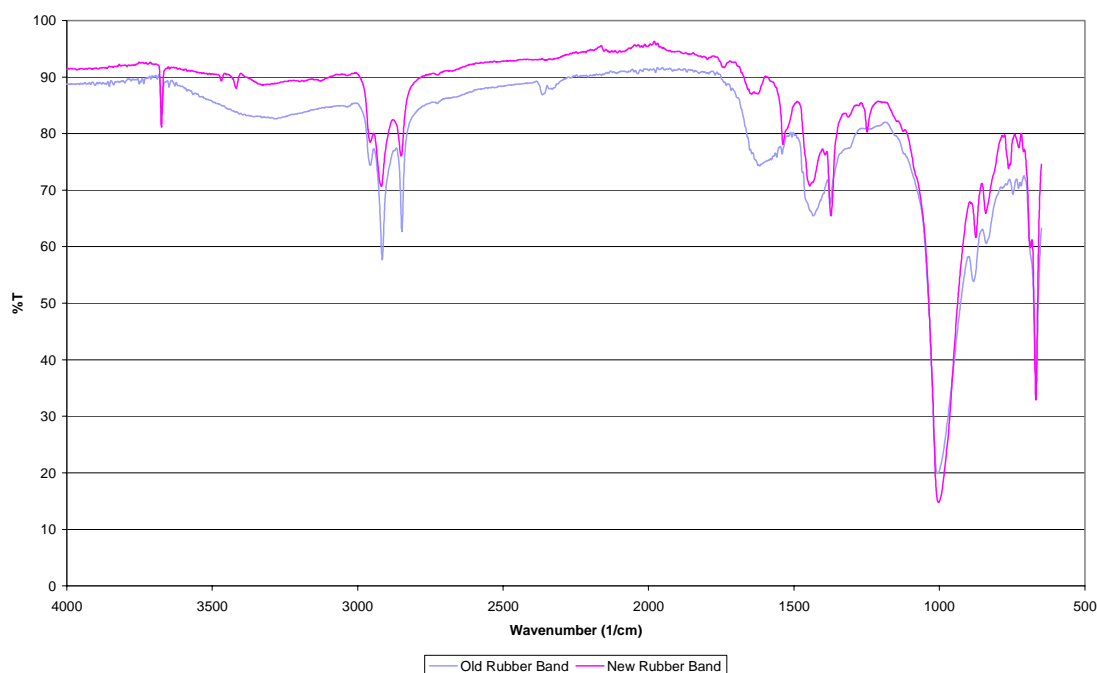
Figure 3.10: FTIR-ATR spectra of waste polybutadiene

Figure 3.11 displays the FTIR-ATR spectrum of electrical wire tubing, identified as being made of polyvinyl chloride. The methylene asymmetric stretch (2932 cm^{-1}) and the methylene deformation (1423 cm^{-1}) are the same absorption peaks as those seen for many other polymers (*i.e.* polyethylene, polypropylene). However, the feature at 1266 cm^{-1} is attributable to the CH$_2$ wagging seen when the adjacent carbon atom has a chlorine atom attached to it, whilst the peak at 873 cm^{-1} represents the C-Cl stretch.
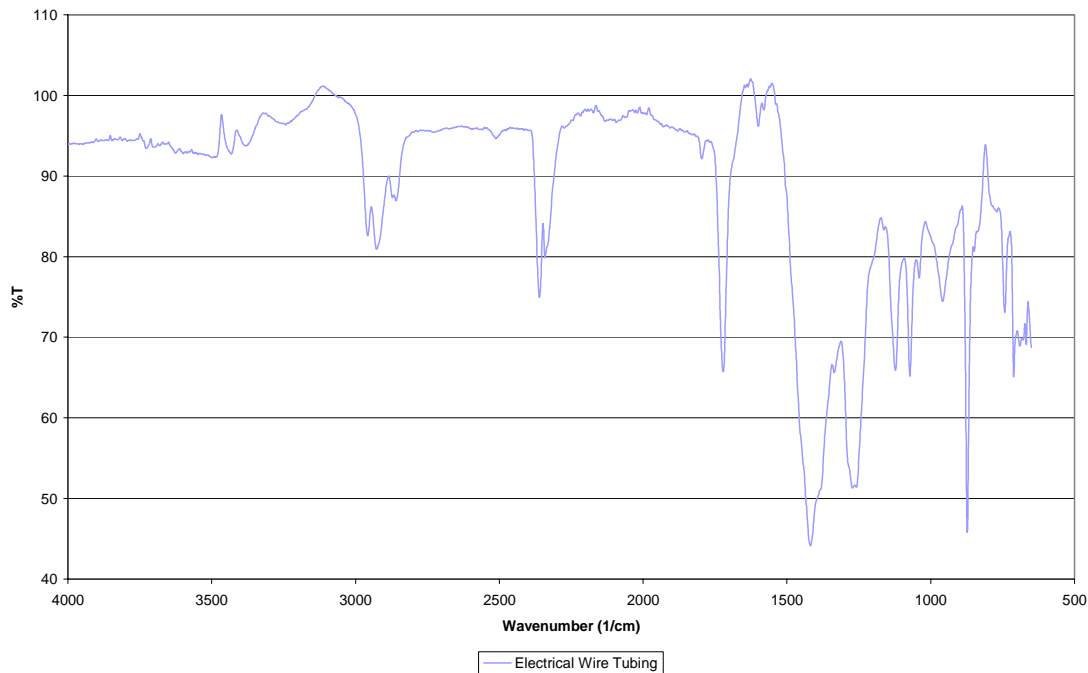
Figure 3.11: FTIR-ATR spectrum of waste polyvinyl chloride

A sample of flexible upholstery foam was identified as polyurethane. A second polyester polyurethane used in this study was synthesised by Dr Ralph van Calck at the University of Central Lancashire. Named RC35, the polyurethane was synthesised from 4,4'-methyl-di-(phenylisocyanate) and polycaprolactone at 90ºC. The FTIR-ATR spectra of the two polyurethanes are displayed in Figure 3.12. The small feature at 3286 cm^{-1} is attributable to the N-H stretch, whilst the peak at 1165 cm^{-1} is related to the stretching of the urethane C-O group. Along with the usual asymmetric C-H stretches at 2948 cm^{-1} and 2850 cm^{-1}, the amide I peak at 1726 cm^{-1} (C=O stretch), amide II peak at 1540 cm^{-1} (N-H deformation) and amide III peak at 1258 cm^{-1} (OCONH) were also present.
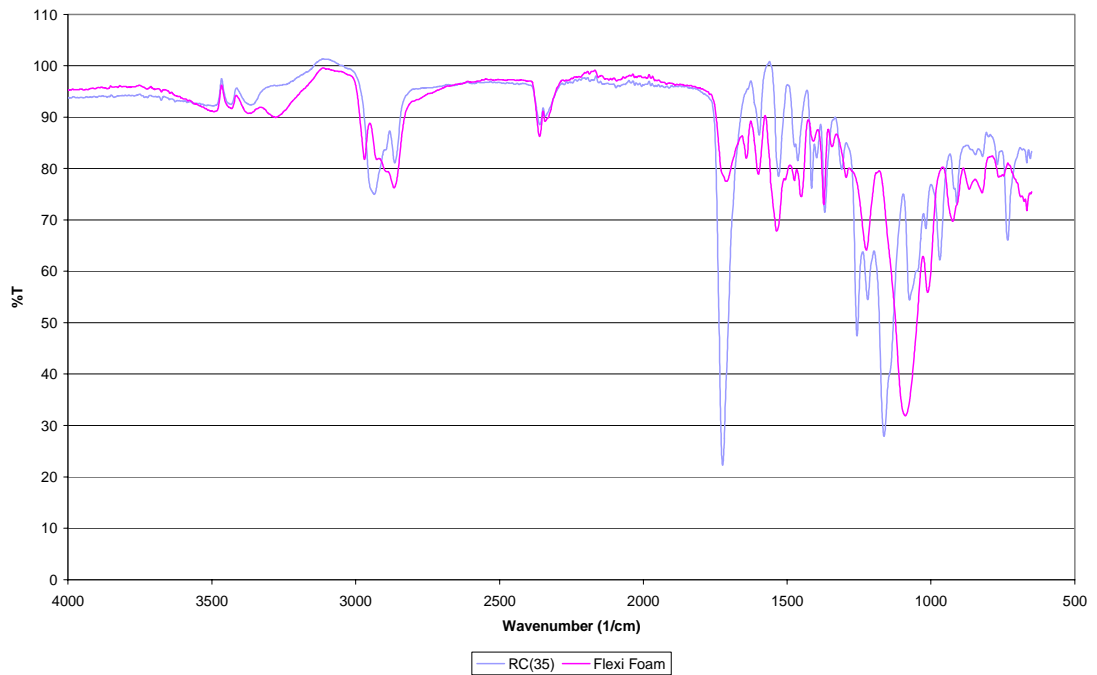
Figure 3.12: FTIR-ATR spectra of waste polyurethane

Figure 3.13 displays the FTIR-ATR spectrum of a Perspex block. The spectrum is of poor quality as it was very difficult to break a small section of PMMA from the block due to the brittleness of the polymer. This resulted in very tiny flakes of PMMA making poor contact with the ATR crystal when the infrared light was applied. However, the spectrum was of sufficient quality to identify certain characteristic absorption peaks and to identify the Perspex as polymethyl methacrylate. The feature at 1728 cm^{-1} represented the ester carbonyl stretching vibration, whilst the peak at 1148 cm^{-1} represented the C-O ester bond stretching vibration.
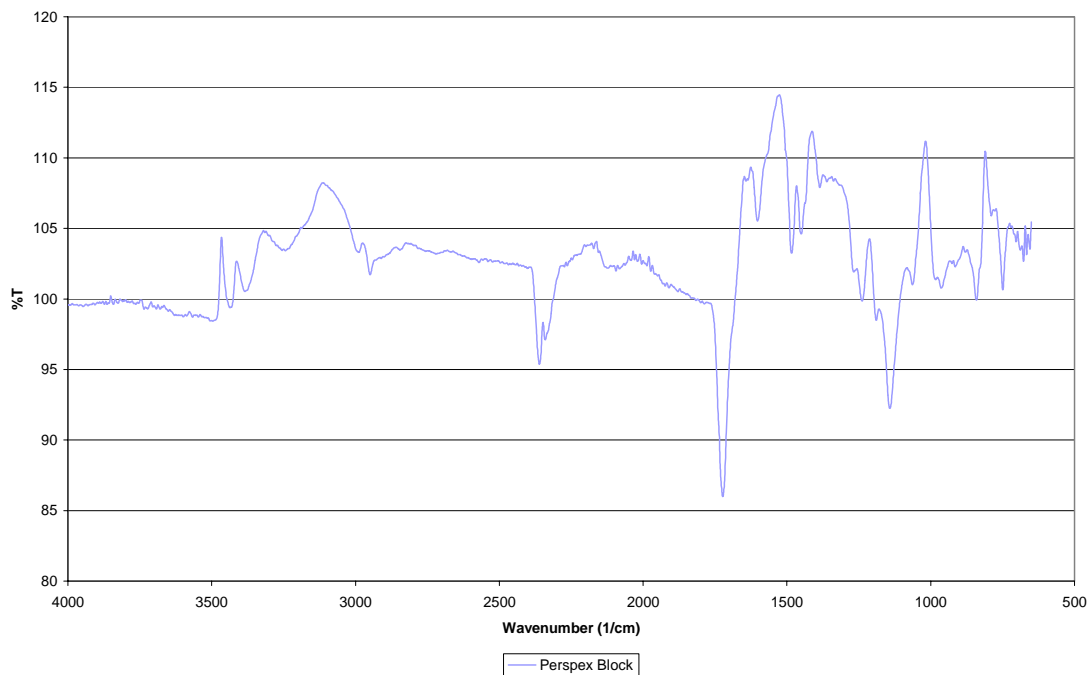
Figure 3.13: FTIR-ATR spectrum of waste polymethyl methacrylate

A black clothing garment with a label reading '100% polyester' was analysed *via* FTIR-ATR (Figure 3.14). The absorption peak corresponding to the carbonyl stretch was present at 1714 cm^{-1}, along with the asymmetric ester C-C-O stretch at 1244 cm^{-1} and the O-CH$_2$-CH$_2$ asymmetric stretch at 1097 cm^{-1}.

A second clothing garment with a label reading '100% acrylic' was also analysed *via* FTIR-ATR. Unfortunately, the spectrum was of poor quality. However, the sample was identified as polyacrylonitrile due to the presence of a nitrile peak at a wavenumber of 2243 cm^{-1}.
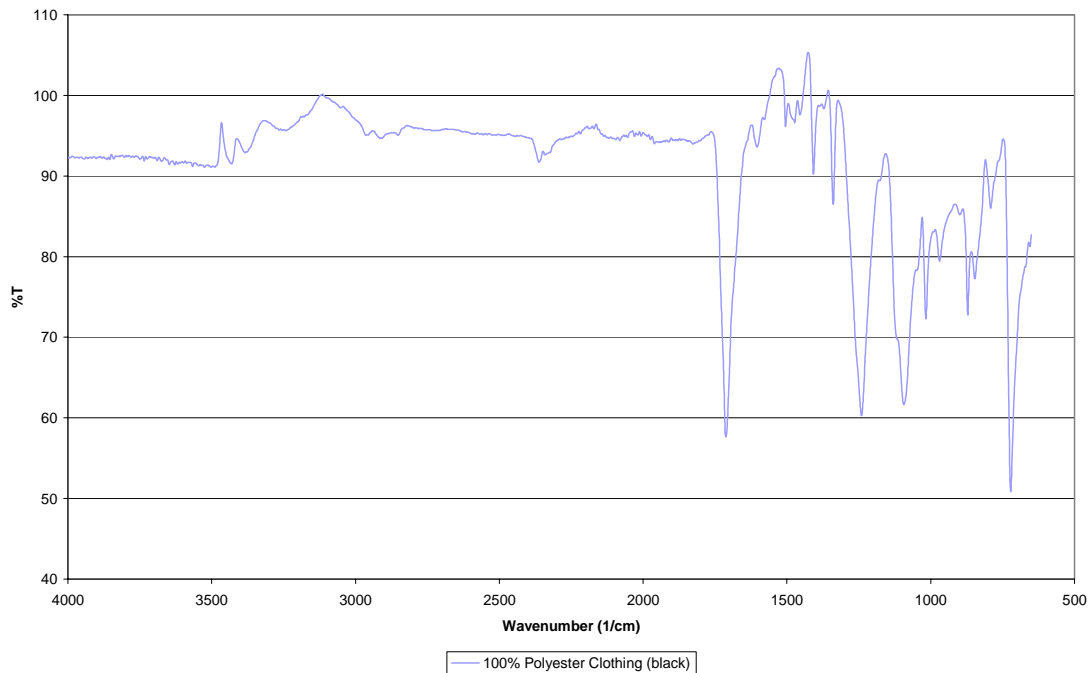
Figure 3.14: FTIR-ATR spectrum of waste polyester

3.3   Conclusions

The FTIR-ATR spectra for the waste polymers were obtained and the plastics identified. Table 3.1 displays the identification of the waste polymer sample, with ** symbolising the representative samples selected for further analysis in this study. From the samples collected, twelve polymers were selected as the waste plastics to be investigated in this research. A further polymer, a polyester polyurethane (RC35), synthesised by Dr Ralph van Calck at the University of Central Lancashire, was included in this study.

Table 3.1: Analysis and identification of waste polymer samples *via* FTIR-ATR

Identification	Waste Plastic Sample
Polyethylene	Tissue packet ** Carrier bag Food bag Milk container (clear) Milk container (white) Milk bottle top (green) Milk bottle top (red)
Polypropylene	Wrapping (clear) Cellophane (clear) Packaging (clear) Spray bottle head (clear) Spray bottle handle (orange) ** Drinking cup (clear)
Polyethylene Terephthalate	Toothbrush packet (clear) Biscuit tray (clear) Fruit tray (clear) Spray bottle (clear) Fruit tray (black) Cola bottle (clear) **
Polystyrene	Yoghurt top Yoghurt pot Drinking cup (white) Spoon (white) Pizza tray Packing Cup (white) **
Polyamide	Tights (black) **
Polybutadiene	Old rubber band ** New rubber band
Polyvinyl Chloride	Electrical wire tubing **
Polyurethane	RC35 ** Flexi Foam **
Polymethyl Methacrylate	Perspex block **
Polyester	100% Polyester clothing (black) **
Polyacrylonitrile	100% Acrylic clothing (green) **

Table 3.2 lists the final selection of six pure polymers and thirteen waste polymer samples to be investigated in this study. This wide range of samples was representative of the variety of plastics that we use and discard in our everyday lives. Pure polymers were selected in order to carry out identical experiments as those to be conducted on the corresponding waste plastic. It was hoped that this would give an insight as to whether the presence of additives and plasticisers had a significant effect on the degradation properties of a polymer.

Table 3.2: Final selection of polymer samples for use in this study

Polymer	Sample	Acronym
Pure		
Low-Density Polyethylene	Pellet of LDPE	PLDPE
High-Density Polyethylene	Pellet of HDPE	PHDPE
Polypropylene A	Pellet of PPA	PPPA
Polypropylene B	Pellet of PPB	PPPB
Polyethylene Terephthalate	Pellet of PET	PPET
Polystyrene	Pellet of PS	PPS
Waste		
Low-Density Polyethylene	Tissue Packet	LDPE
High-Density Polyethylene	Clear Milk Container	HDPE
Polypropylene	Orange Spray Bottle Head	PP
Polyethylene Terephthalate	Clear Cola Bottle	PET
Polystyrene	White Cup	PS
Polyamide	Black Tights	PA
Polybutadiene	Rubber Band	PB
Polyvinyl Chloride	Electrical Wire Tubing	PVC
Polyurethane	Synthesised RC35	PU(RC35)
Polyurethane	Flexi Foam	PU(foam)
Polymethyl Methacrylate	Perspex Block	PMMA
Polyester	Black 100% Polyester Clothing	PE
Polyacrylonitrile	Green 100% Acrylic Clothing	PAN

Chapter 4

Thermal Analysis of Polymer Degradation

4 Thermogravimetric Analysis

In order to investigate the thermal and catalytic degradation of waste polymers as a function of increasing temperature, a technique needed to be employed with which the heating of the samples could be controlled and the onset temperatures of decomposition recorded accurately. Thermogravimetric analysis was the ideal choice.

4.1 Thermogravimetry

Thermogravimetry (TG) is defined as a technique whereby the weight of a substance, in an environment heated or cooled at a controlled rate, is recorded as a function of time or temperature.[201] Thermogravimetry involves the continuous measurements of the sample temperature and the sample weight, whilst the temperature of the sample is raised at a uniform rate. This is known as dynamic or non-isothermal thermogravimetry. The resulting graph of weight *vs.* temperature is termed the *thermogravimetric curve*. Alternatively, isothermal measurements can be undertaken, where the physical properties of the sample are determined by analysis at a constant temperature. The thermobalance is an instrument that allows the continuous weighing of a sample as a function of temperature. A modern thermobalance generally consists of a recording balance, furnace, furnace temperature programmer or controller and recorder.[202]

4.1.1 Recording Balances

Ideally, a recording balance should have accuracy, precision, sensitivity, resistance to corrosion and insensitivity to ambient temperature changes. The balance should be able to respond rapidly to changes in mass and be relatively unaffected by vibration. Recording balances can be divided into three general classifications based on their mode of operation: deflection-type instruments, null-type instruments and those based on changes in a resonance frequency. The latter type is highly sensitive but very specialised in its application. Null-type balances use a sensing element that detects a deviation of the balance beam from its null position, a restoring force is then applied, restoring the beam to the full position. Deflection-type balances involve the conversion of balance-beam deflections into mass-change curves. The Shimadzu TGA-50 used in the thermogravimetric analysis of polymers utilised a taut band as the deflection device. For this type of instrument, the sample is suspended from a lever or beam rigidly attached to a horizontal torsion wire. The sample weight is opposed by the torque generated on twisting the torsion wire and is proportional to the angle of twist (see Figure 4.1). Therefore, the deflections measured are proportional to the changes in mass and the torsional characteristics of the wire.
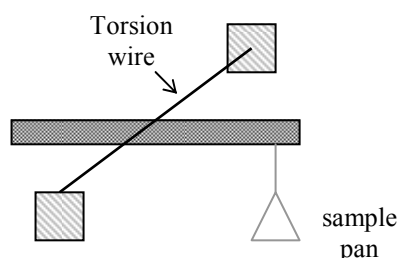
Figure 4.1: Torsion balance

4.1.2 Furnace and Furnace Temperature Programmers

The furnace should have a uniform hot-zone of a reasonable size to accommodate the sample and crucible, to allow the sample to be held at a constant uniform temperature, and should be capable of reaching 100-200°C above the maximum desired working temperature.[203] Ideally, the furnace should reach the desired starting temperature as quickly as possible (*i.e.* have a low heat capacity) and not affect the balance mechanism through radiation or convection. Heating of the sample is *via* conduction, through solid or gas, with inevitable large temperature gradients, especially when dealing with samples of low conductivity such as polymers. The rate of temperature increase or decrease is controlled by a furnace temperature programmer, with the most common heating rates employed in thermogravimetry being between 5-10°C/min. Figure 4.2 displays the arrangement of the furnace and balance mechanism in the Shimadzu TGA-50 used in this study.
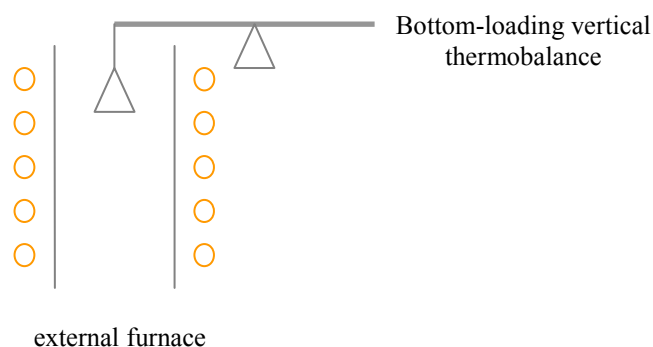
Figure 4.2: Furnace and balance mechanism in the Shimadzu TGA-50

4.1.3 The Atmosphere

The environmental atmosphere around the sample can cause drastic changes in the TG results obtained. A flowing atmosphere has advantages in that it reduces condensation

of reaction products on cooler parts of the weighing mechanism, flushes out corrosive products, reduces secondary reactions and acts as a coolant for the balance mechanism.[204]

4.1.4 Factors Affecting Weight-Loss Results

4.1.4.1 Sample Size and Geometry

Structural differences in a solid, such as defect content, porosity and surface properties can have an effect on the solid's behaviour on heating. As the amount of sample increases, the temperature of the sample becomes non-uniform through slow heat transfer and self-heating or self-cooling as the reaction occurs. Additionally, the sample size can affect the degree of diffusion of the product gas through the void space around the solid particles. Ideally, the use of as small a weight of sample as possible, within the limits of the sensitivity of the balance, is preferred. Most thermogravimetric studies have been carried out on powdered samples and it was found that the smaller the particle size, the greater the extent to which equilibrium is reached, and at any given temperature, the extent of decomposition was found to be greater.[205] Grain size, grain size distribution and closeness of the size fraction all have effects on the thermogravimetric curve obtained.[206]

4.1.4.2 Atmospheric Effects

For thermogravimetric analysis carried out under flowing gas conditions, draughting, buoyancy and convection effects can influence the weight changes recorded dramatically.[207] Draughting effects arise directly as a result of operating the thermobalance under a flowing gas atmosphere, where a stream of gas molecules flows unidirectionally past the sample container.[208] This '*buoyancy effect*' has been found to

decrease with an increase in the furnace temperature. Convection currents, turbulence and the flow of the atmosphere can give rise to a high-frequency aerodynamic noise which increases slightly in amplitude with temperature. However, a constant gas flow will produce a constant error, and therefore can be neglected.

4.1.4.3   Heating Rate Effects

If a fast heating rate is employed, a polymer decomposing in one step will appear to have an initial temperature of decomposition higher than its true initial temperature.[209] This effect is a result of the finite time required to cause a detectable weight change.[210] At any given temperature, the extent of decomposition is greater at a slow rate of heating than for a similar sample heated at a fast rate.

4.2   Thermogravimetric Curves

The thermogravimetric curve obtained from the constant heating of a sample can give direct information in relation to the number of decomposition stages and the fractional weight-loss of each stage. Chemical reactions are temperature-dependent rate processes; therefore weight-losses occur over a range of temperatures. Since rate of weight-loss and heating rate are dynamic processes, weight-loss curves will shift along the temperature axis when obtained at different constant heating rates.[211] On a thermogravimetric curve, the following features may be identified:

i.   A horizontal portion or plateau, indicative of constant weight.

ii. A curved portion, the steepness of which is indicative of the rate of weight-loss and will pass through a maximum giving an inflection with *dw/dt* as a maximum.

iii.   An inflection at which *dw/dt* is a minimum, but not zero (a trough on the differential thermogravimetric curve), which may imply the formation of an intermediate compound.

The shape of a thermogravimetric curve is influenced by many factors, such as design of the crucible, heating rate, sample form and sample weight. Variations in technique and apparatus can lead to considerable discrepancies in the values of the decomposition temperature and range reported for the same material by different workers. As these measured values depend on which thermal analytical procedure has been selected and the procedural variables chosen, the temperatures of decomposition are referred to as 'procedural decomposition temperatures' or *pdt*'s. For similar materials under identical conditions, the TG curves may be compared on the basis of shape and procedural decomposition temperatures.

In many polymer pyrolyses, the TG curve follows a relatively simple sigmoidal path with the sample weight decreasing slowly as the reaction begins and then decreasing rapidly over a comparatively narrow temperature range before levelling off when the reactant becomes spent. The shape of the curve depends primarily upon the reaction order (*n*), frequency factor (*A*) and activation energy (*E*). If two or more inflection points are observed, the separate sigmoidal traces are analysed individually for *E*, *n* and *A*.

The resolution of complex TG curves can be facilitated by recording the corresponding differential or derivative thermogravimetric (dTG) curve. A dTG curve consists of a series of peaks corresponding to the various stages in the decomposition, with the peak

maximum being equivalent to the point of inflection of the TG curve and the peak area being proportional to the fractional weight-loss at each particular stage. The curve returns to the baseline when the sample weight reaches a plateau. However, if the weight does not become constant, due, for example, to the overlapping of two reactions, the minimum will not reach the baseline, therefore the resolution of overlapping curves is greater on dTG curves than for TG curves.

4.2.1 Method of Thermogravimetric Analysis

The thermogravimetric analysis of six polymers and thirteen waste polymers was undertaken with a Shimadzu TGA-50 instrument. The experiments were conducted in a nitrogen atmosphere at a heating rate of 10ºC/min up to 550ºC (see Experimental Chapter). These plastic samples were then analysed in the presence of each of the ten catalysts (at a polymer-to-catalyst weight ratio of 2:1). Sample preparation was kept to a minimum and involved no grinding or shredding of the plastic into small fragments. The catalyst powder was placed in the bottom of the aluminium sample pan and a small piece of untreated polymer (<10 mg) was placed directly on top of the catalyst. No mixing of the polymer and catalyst was undertaken in order to simulate how plastics could be recycled in the future with next to no initial preparation. The effects on the onset temperatures and activation energies of the decomposition steps of the polymers were recorded and compared.

4.2.2 Onset Temperature of Decomposition

A thermogravimetric curve of the thermal degradation of waste high-density polyethylene is shown in Figure 4.3. The *x*-axis of the thermogram represents the temperature in degrees Celsius (which can be easily converted to a time scale due to the

constant temperature ramp of 10ºC/min).   The *y*-axis represents the percentage mass change of the polymer as the temperature was increased at a steady rate.   Figure 4.3 shows that HDPE underwent a single degradation step.
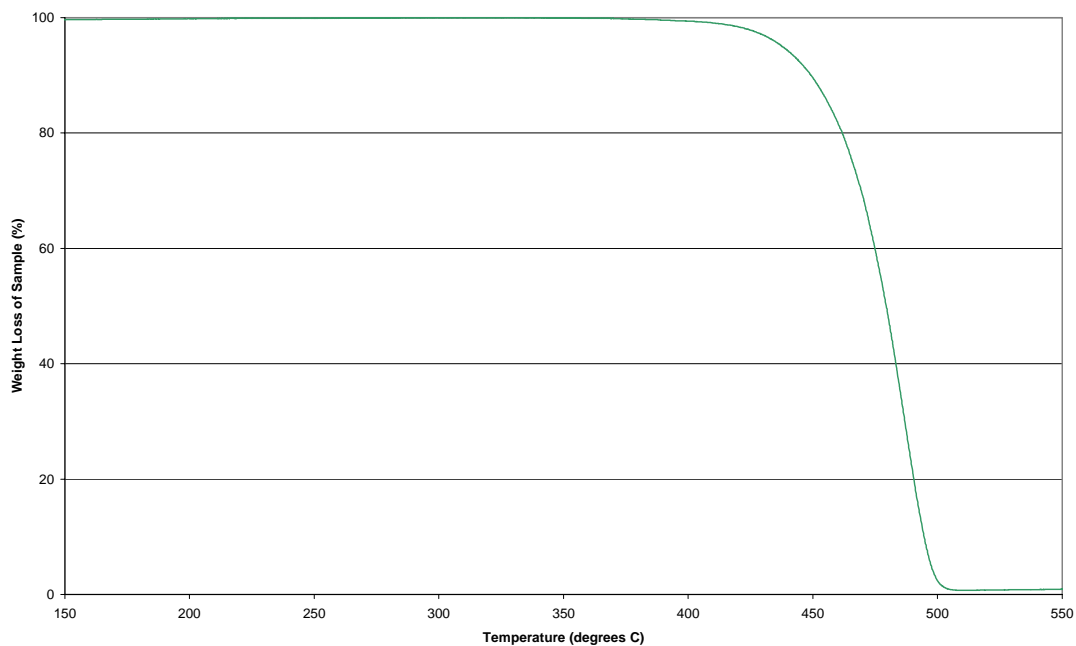
Figure 4.3: TG curve for the thermal degradation of waste HDPE

Figure 4.4 below shows the differential thermogravimetric curve of the degradation of waste HDPE. A peak maximum on a dTG curve is equivalent to a point of inflection on the TG curve, whilst peak area is proportional to the fractional weight-loss.
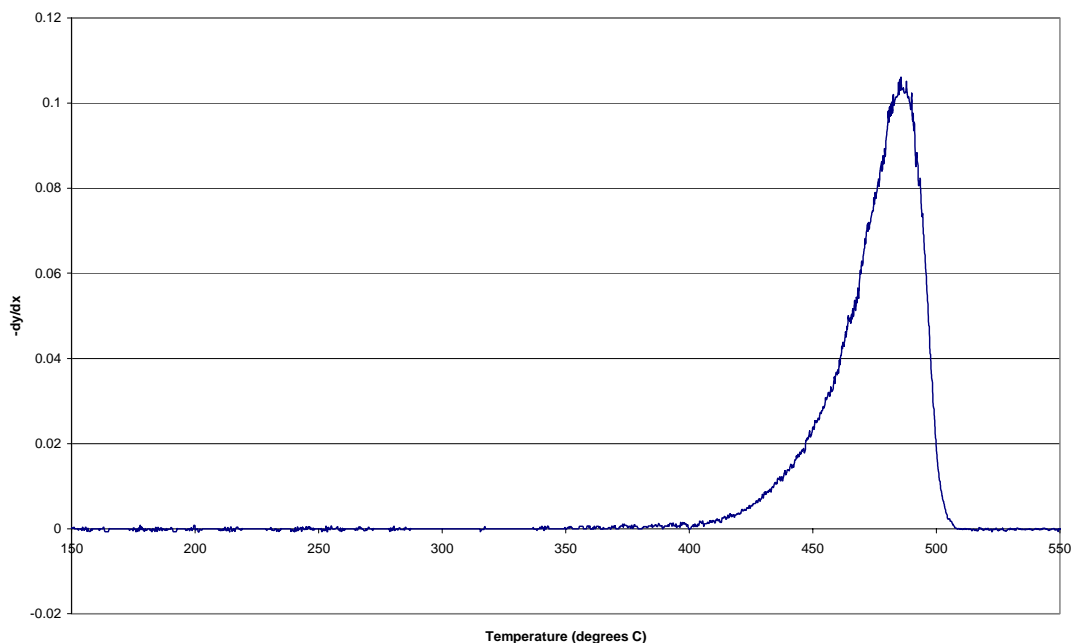
Figure 4.4: dTG curve for the thermal degradation of waste HDPE

The *onset temperature* for a particular degradation step of a polymer sample was calculated by the Shimadzu TGA-50 software by placing a cursor at the plateau before the weight-loss step and a second cursor at the plateau after the weight-loss had stabilised. For waste high-density polyethylene, an onset temperature of 455ºC was quoted. To verify this value, T_{onset} was calculated manually from the TG curve, dTG curve and point of inflection. From the dTG curve of the thermal degradation of waste HDPE (Figure 4.4), the temperature at which *dw/dt* was a minimum (greatest rate of change on the weight loss curve) was named the 'point of inflection' and was found to be 485ºC. A tangent was drawn from this inflection point on the TG curve and joined with an extrapolation of the previous plateau of constant weight. The point on the *x*-axis where the two lines met was the onset temperature of degradation and was found to be 460ºC (Figure 4.5).
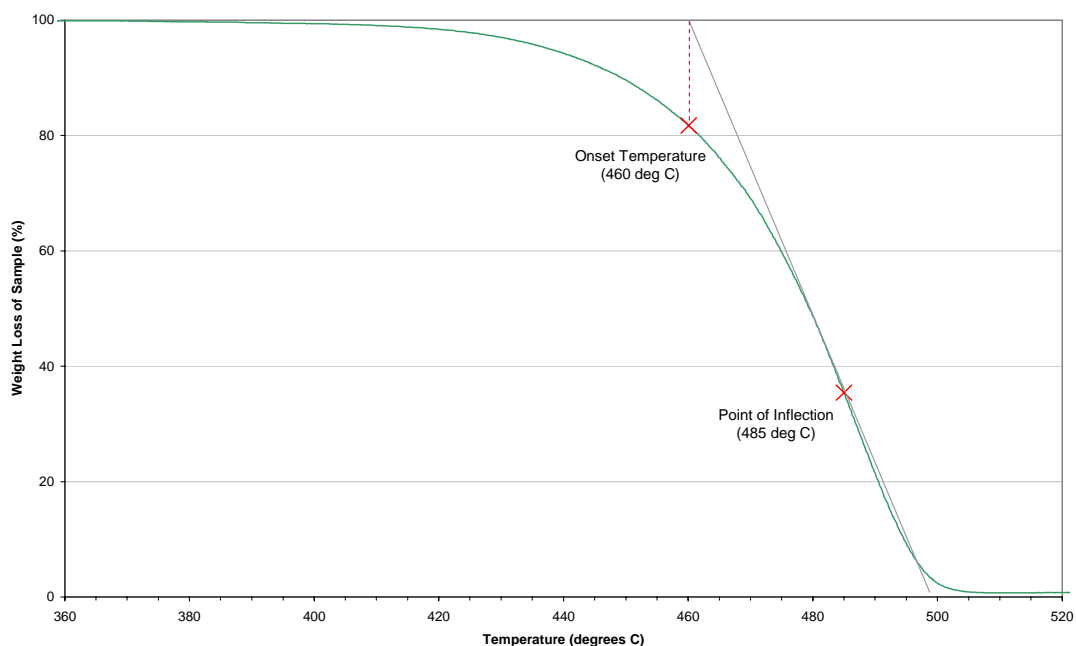
Figure 4.5: Manual calculation of T_{onset} for waste HDPE

The thermal degradation of waste HDPE was found to occur over the temperature range 380-510ºC. The manual calculation of the onset temperature of decomposition was found to differ from the value given by the Shimadzu TGA-50 software by 5ºC. This corresponds to a 4% error between the two temperatures over the 130ºC degradation range. Slight deviations of 2-3ºC in onset temperature were found when repeating the thermal degradation of a polymer multiple times. This was likely to have been related to the small variation in sample size, which had a slight effect on the TG curve. Combining these two errors gave a reasonable assumption that the onset temperatures quoted in this study had a ± 5ºC error associated with the values.

4.2.3   Kinetic Analysis of Thermogravimetric Data

In order for a reaction to occur between stable molecules, a certain amount of energy must be absorbed to weaken the bonds holding the reactant molecules together. The *activation energy*, E_a, represents the energy required to bring the reactants to the point where they can rearrange to form products and is the difference in energy between the activated complex and the reactant molecules. The rate of a chemical change is proportional to the concentrations of the reacting substances, therefore the *order of reaction* is the number of atoms or molecules whose concentrations determine the rate or kinetics of the process.

The probability that a molecule will possess energy in excess of an amount E per mole, at temperature T, is related to the Boltzmann factor, $e^{-E/RT}$ where R is the molar gas constant.[212]   If the *frequency factor, A,* represents the total frequency of encounters between two reactant molecules, irrespective of whether they possess sufficient energy or not, the reaction rate will be dependent on the product of A and $e^{-E/RT}$. Hence, the specific reaction rate is represented by:

$$k = Ae^{\frac{-E_a}{RT}}$$ (Eq. 4.1)

Equation 4.1, known as the *Arrhenius Equation*, expresses the influence of temperature on reaction velocity. The definition of a rate constant, k, and an activation energy, E_a, for solid state reactions in comparison with reactions occurring in gases or solutions gives rise to several difficulties. In gases or solutions, the rate constant is the proportionality factor between the reaction velocity and the concentration of the starting products, thus it can be defined as the velocity for unit concentrations. In solid state

reactions, the concepts of concentrations and order of reaction generally have no significance and, consequently, a rate constant can not be defined in the same way as for reactions in gases or solutions.

In solid state reactions governed by logarithmic laws, the rate constant and activation energy can only be defined clearly when a suitable hypothesis for the mechanism of the given reaction is available. If the rate constant is derived from the experimental relation between the quantity of product formed and time, it is difficult to predict whether it will show an exponential dependence on temperature.[213]

A number of methods have been developed for obtaining kinetic parameters from thermogravimetric curves of solid state reactions. Doyle[214] derived a procedure for obtaining preliminary kinetic data from a thermogram, but the theory was known to have limitations. Freeman and Carroll derived equations for a non-reversing reaction, so that the rate dependent parameters such as energy of activation and order of reaction could be calculated from a single thermogravimetric curve.[215] Coats and Redfern derived a method to determine the activation energy and order of reaction, but stated that the method suffered from a number of disadvantages.[216] Sharp and Wentworth evaluated the method used by Coats and Redfern and concluded that it could lead to satisfactory kinetic analyses, but was not a method to be recommended.[217]

Coats and Redfern developed a method for estimating E_a by use of an integrated form of the rate equation. The graph of:

$$\log \frac{1-(1-\alpha)^{1-n}}{(1-n)T^2} \qquad vs. \qquad \frac{1}{T}$$

127

was said to be a straight line of slope $-E_a/2.3R$ (where α = fraction decomposed). The order of reaction can not be attributed as for gas reactions, but mathematical models of solid systems have led to orders of reaction of 0, ½, 2/3 and 1. The correct value of n was said to give the best linear plot from which E_a was determined. The dependence of an n value in order to calculate the activation energy for the solid state reaction of polymer degradation was a disadvantage of the Coats and Redfern method.

Horowitz and Metzger[218] characterised the decomposition of polymers on pyrolysis. The sample weight was said to have dropped slowly as pyrolysis begins, then to have dropped precipitously over a narrow temperature range and finally to have resumed a zero slope as the reactant is exhausted. The shape of the curve was said to have been determined by the kinetic parameters of pyrolysis. Assuming a reaction in which all evolution products were gases, Horowitz and Metzger derived an expression to calculate the activation energy. This method is still used to analyse the thermodegradative behaviour of polymers[219] and was used to analyse the thermogravimetric data obtained in this thesis.

4.2.3.1 Method of Horowitz and Metzger

It was assumed that no intermediates were formed throughout the pyrolysis and that all products were gaseous and escaped immediately. The method of Horowitz and Metzger is based on a combination of the reaction rate dependence on concentration (Equation 4.2) and on temperature (Arrhenius Equation 4.1 above). The reaction rate dependence on concentration is given by:

$$\frac{dC}{dt} = -kC^n \qquad\qquad\qquad \text{(Eq. 4.2)}$$

where C = concentration (mole fraction or amount of reactant)

k = specific rate constant

n = order of reaction

t = time

Equation 4.2 shows that the rate of disappearance of reactant, per unit volume or per unit total weight or per unit total moles, is a power function of the concentration of reactant:

$$\frac{dW}{W_t dt} = -kC^n$$ (Eq. 4.3)

where W = volume, weight or number of moles of reactant

W_t = total at any time

For pyrolysis, the total change in concentration is due to the decrease of W as well as the change in total weight due to the loss of reactant and accumulation of products. By assuming all gaseous products escape immediately, it can be said that the concentration is constant throughout the pyrolysis (C = 1 on a weight or mole fraction basis). Combining Equation 4.3 with the Arrhenius Equation gives:

$$\frac{dW}{W_t dt} = -Ae^{\frac{-E_a}{RT}}C^n$$ (Eq. 4.4)

As order of reaction in solid state reactions generally has no significance and C = 1, Equation 4.4 becomes:

129

$$\frac{dW}{W_t dt} = -Ae^{\frac{-E_a}{RT}}$$
(Eq. 4.5)

where $W = W_t$ = sample weight.

If q is defined as the rate of temperature rise ($dT/dt = q$), then:

$$\ln\frac{W}{W_0} = \int_0^T \frac{A}{q} e^{\frac{-E_a}{RT}} dT$$
(Eq. 4.6)

where W_0 = initial weight. As most pyrolyses occur over a narrow temperature range at a relatively high absolute temperature, a reference temperature, T_s, can be defined, such that at T_s, $W/W_0 = 1/e$.

Defining θ such that $T = T_s + \theta$, then:

$$\frac{1}{T} = \frac{1}{T_s + \theta} = \frac{1}{T_s\left(1 + \dfrac{\theta}{T_s}\right)}$$
(Eq. 4.7)

Since $\theta/T_s \ll 1$:

$$\frac{1}{T} \cong \frac{1 - \dfrac{\theta}{T_s}}{T_s}$$
(Eq. 4.8)

Substituting Equation 4.8 into Equation 4.6 and then integrating gives:

$$\ln \frac{W}{W_0} = -\frac{A}{q} \frac{RT_s^2}{E_a} \exp\left[\frac{-E_a}{RT_s}\left(1 - \frac{\theta}{T_s}\right)\right] \qquad \text{(Eq. 4.9)}$$

When $T = T_s$, $\theta = 0$, $W/W_0 = 1/e$ and $ln\ W/W_0 = -1$. Thus, when $\theta = 0$, Equation 4.9 becomes:

$$-1 = \frac{-A}{q} \frac{RT_s^2}{E_a} e^{\frac{-E_a}{RT_s}} \qquad \text{(Eq. 4.10)}$$

Substituting Equation 4.10 for the corresponding part of Equation 4.9:

$$\ln \frac{W}{W_0} = -e^{\frac{E_a \theta}{RT_s^2}} \qquad \text{(Eq. 4.11)}$$

or

$$\ln \ln \frac{W_0}{W} = \frac{E_a \theta}{RT_s^2} \qquad \text{(Eq. 4.12)}$$

Thus, for any single-reaction pyrolysis which yields only gaseous products, a plot of *ln ln* W_0/W against θ gives a straight line with a slope of E_a/RT_s^2. The relationship in Equation 4.12 duplicates the characteristic shape of the thermogravimetric traces, that is, a gradual weight loss followed by a sharp drop, followed by a turning toward zero slope when the pyrolysis is complete. For the cases where there appear to be two or three degradation steps, T_s and θ are defined for each.

4.2.3.2   Application of the Method of Horowitz and Metzger

From the thermogravimetric curves of polymer degradation and the application of the method of Horowitz and Metzger, the activation energy of degradation was established for each experiment. Below are some examples of the processes undertaken to calculate the values of E_a for different types of TG curves.

4.2.3.2.1   One Degradation Step

For a thermogravimetric curve of one degradation step it was expected that only one value for the activation energy of decomposition would be calculated. This proved to be the case for waste high-density polyethylene degraded in the presence of EPZE clay catalyst.   Figure 4.6 displays (a) the TG curve and (b) the dTG graph for the decomposition reaction.

a

b
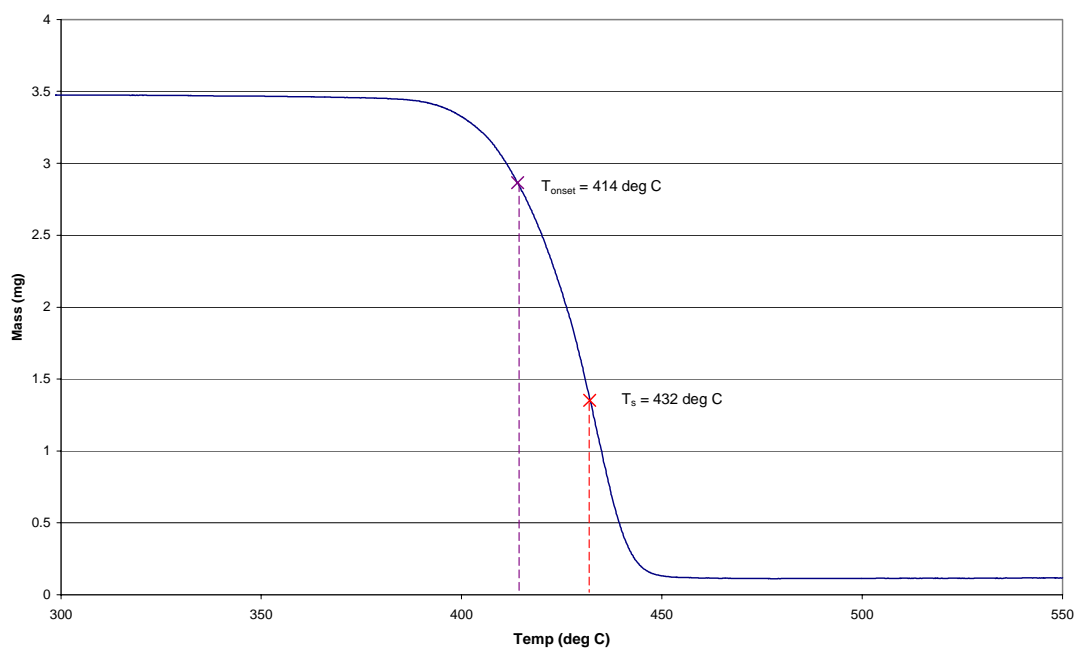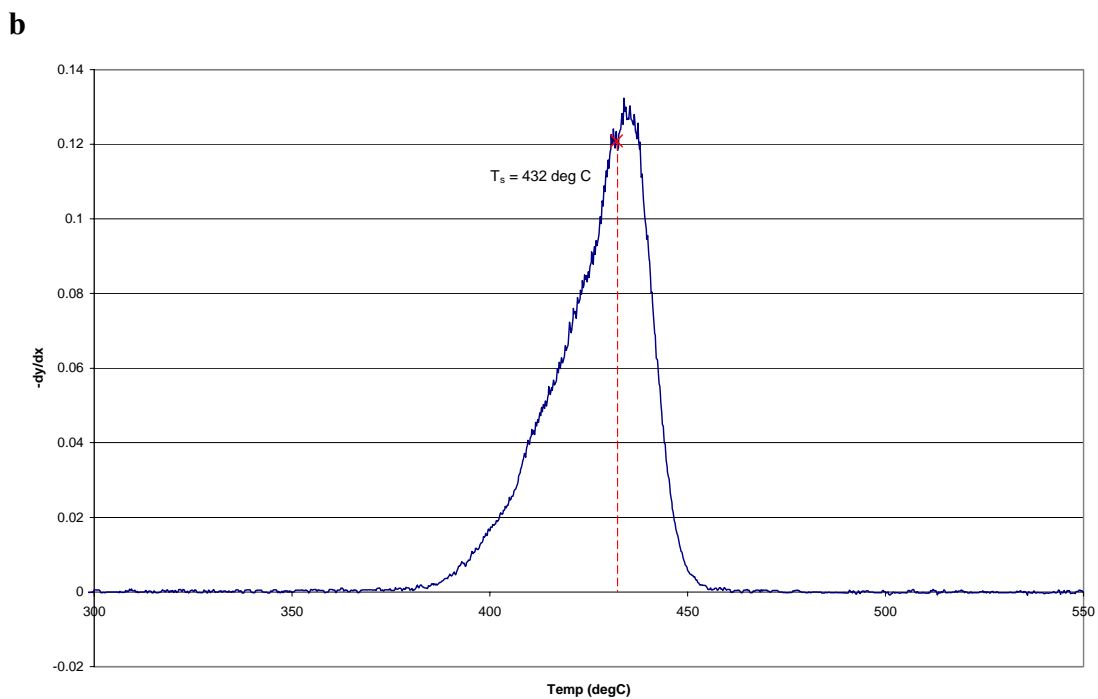
Figure 4.6: (a) TG and (b) dTG graphs for waste HDPE and EPZE clay

The degradation of the polymer occurred over the temperature range 380-460ºC. From the method of Horowitz and Metzger, the reference temperature was defined as 432ºC. Over the 380-460ºC decomposition temperature range, the values of θ ranged from -29 to +11. The plot of *ln ln W_0/W* against θ is displayed in Figure 4.7.

$$y = 0.0964x + 0.0443$$
$$R^2 = 0.9986$$
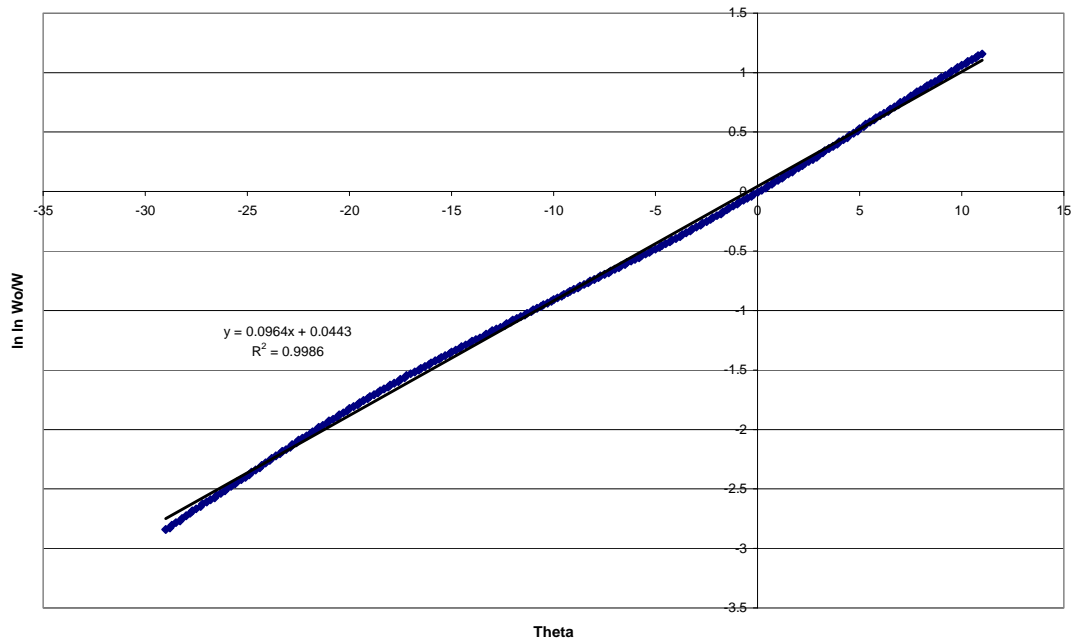
Figure 4.7: Plot of *ln ln W₀/W* against θ for HDPE degraded with EPZE clay

It can be seen that the line-of-best-fit in Figure 4.7 above has one gradient and the equation of the line has a high R^2 value of 0.9986. From the $y = mx + c$ equation, the value of E_a was established as 398 kJ/mol.

4.2.3.2.2 Two Degradation Steps

For the degradation of polybutadiene, polyurethane and polyacrylonitrile, a two-step weight-loss was observed. In these cases, the method of Horowitz and Metzger was applied over two separate temperature ranges. An example of two-step weight-loss was the degradation of waste polyurethane foam in the presence of 23z zeolite. Figure 4.8 displays (a) the TG and (b) the dTG curves for the polymer decomposition.
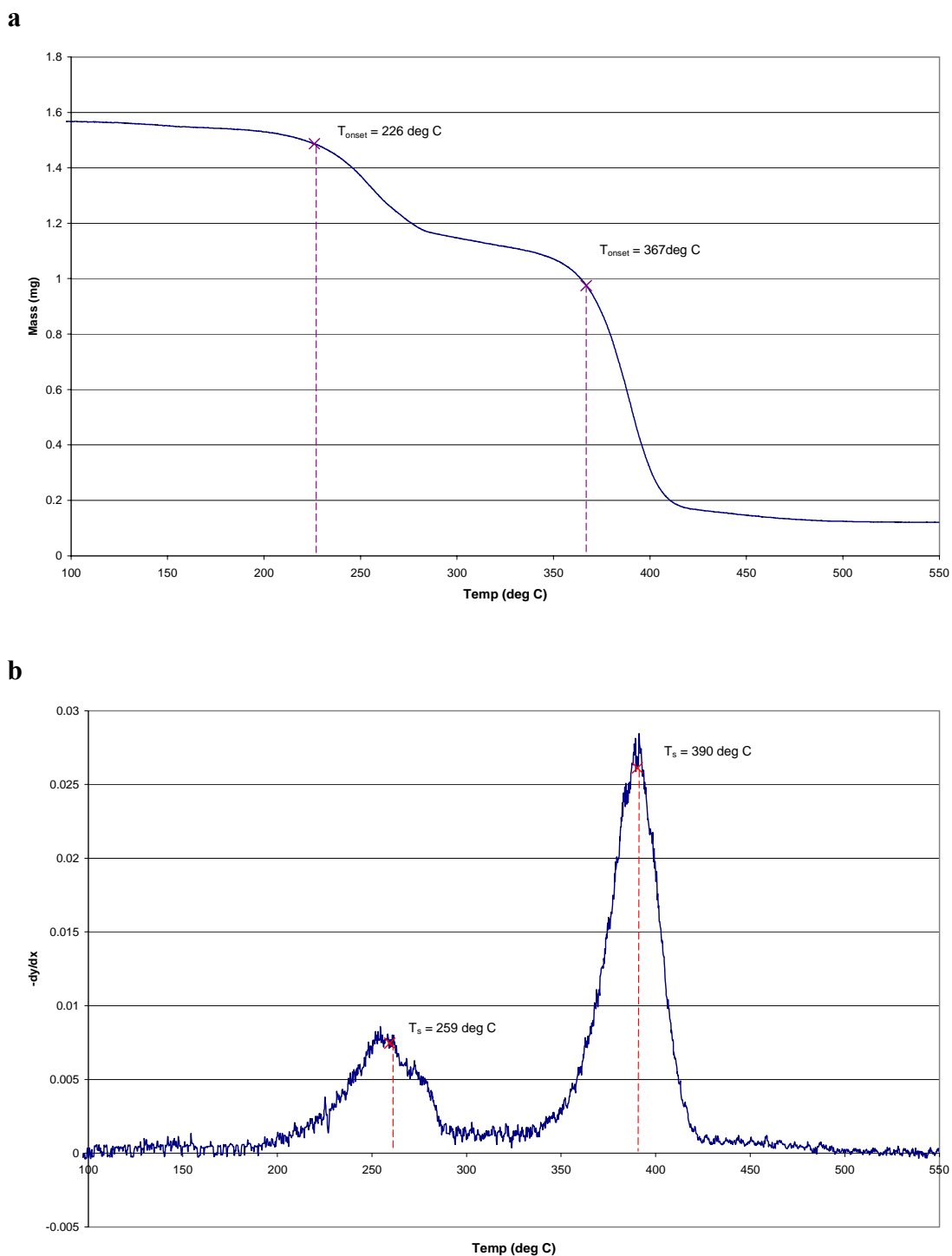
Figure 4.8: (a) TG and (b) dTG graphs for waste PU(foam) and 23z zeolite

The degradation of the polymer occurred over two separate temperature ranges; (a) 190-290ºC and (b) 290-430ºC. These two distinct weight-loss steps were analysed individually. Step one corresponded to a T_s value of 259ºC and θ values in the range

-40 to +12. Step two corresponded to a T_s value of 390ºC and θ values between -20 and
+19. The plots of *ln ln W_0/W* against θ are displayed in Figure 4.9.

a

b
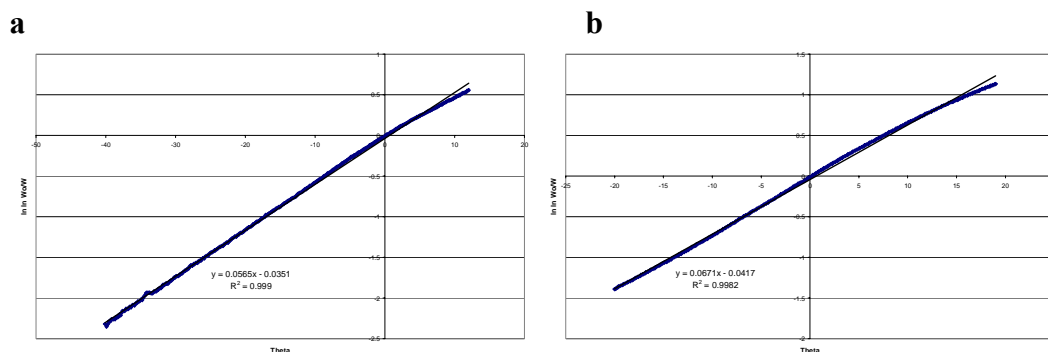
Figure 4.9: Two plots of *ln ln W_0/W* against θ for PU(foam) degraded with 23z

The equations of the two gradients in Figure 4.9 above corresponded to activation
energies of: (a) 133 kJ/mol and (b) 246 kJ/mol respectively.

4.2.3.2.3   Three Degradation Steps

For the degradation of polyvinyl chloride and polymethyl methacrylate, a three-step
weight-loss was observed. In these cases, the method of Horowitz and Metzger was
applied over three separate temperature ranges. Figure 4.10 displays (a) the TG and (b)
the dTG curves for the degradation of waste PVC.

a

b
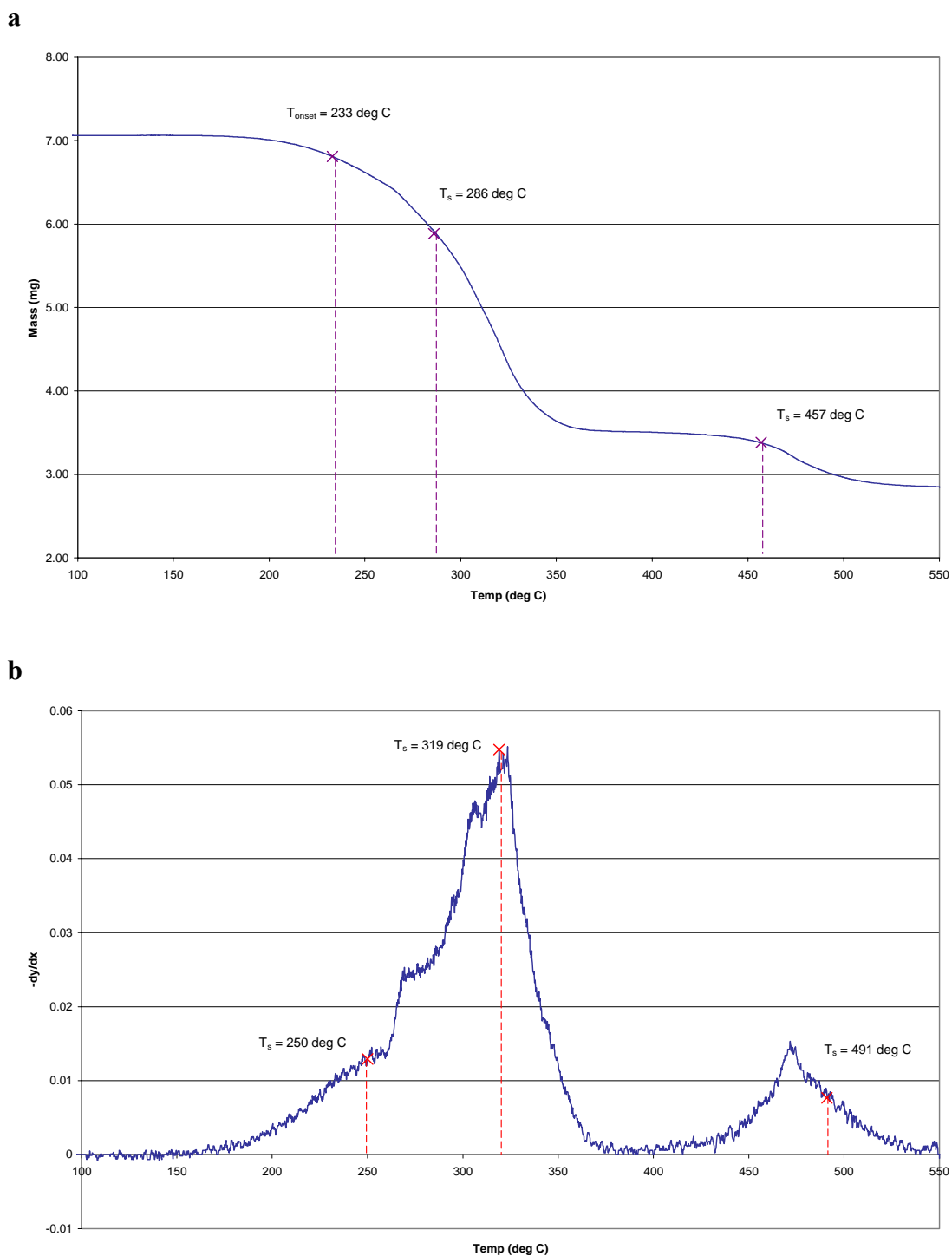
Figure 4.10: (a) TG and (b) dTG graphs for waste PVC and 280z zeolite

The degradation of the polymer occurred over three separate temperature ranges; (a) 242-254ºC, (b) 312-323ºC and (c) 488-495ºC. These distinct weight loss steps were analysed individually. Step one corresponded to a T_s value of 250ºC and θ values in the

range -8 to +4. Step two corresponded to a T_s value of 319ºC and θ values between -7 and +4. Step three corresponded to a T_s value of 491ºC and θ values in the range -2 to +4. The three plots of *ln ln W_0/W* against θ are displayed in Figure 4.11.

a

b

c
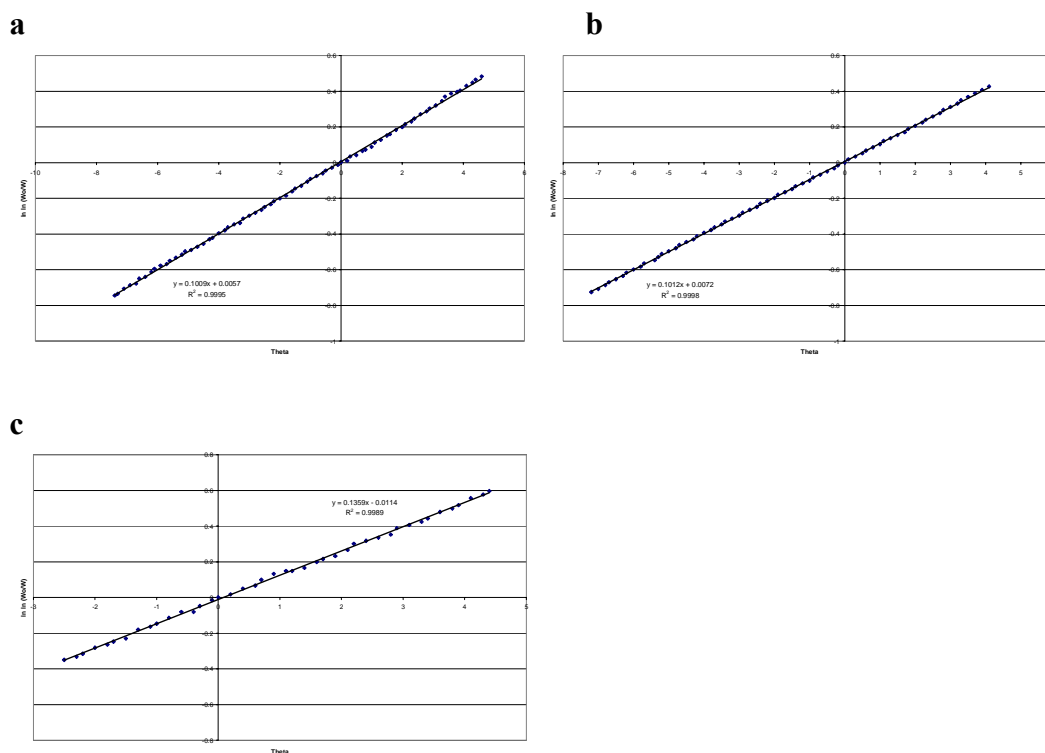
Figure 4.11: Three plots of *ln ln W_0/W* against θ for waste PVC

The equations of the three gradients in Figure 4.11 above corresponded to activation energies of (a) 230 kJ/mol, (b) 295 kJ/mol and (c) 660 kJ/mol respectively.

4.2.3.2.4 Two Activation Energy Values from a Single Degradation Step

In some cases, the analysis of a thermogravimetric curve showing a single degradation step revealed two activation energies when applying the method of Horowitz and Metzger. Figure 4.6 displays the degradation of waste HDPE in the presence of EPZE. This single decomposition step was accompanied by a dTG curve with a single smooth

peak. In comparison, although the thermogravimetric curve of the degradation of pure LDPE in the presence of Fulacolor clay appears as a single weight-loss step, the corresponding dTG graph is not a single peak but is composed of two overlapping peaks (see Figure 4.12 below). This suggests that two distinct reactions are occurring during the decomposition of the polymer, but the degradation is too complex for these to be resolved into two separate events.

a

b
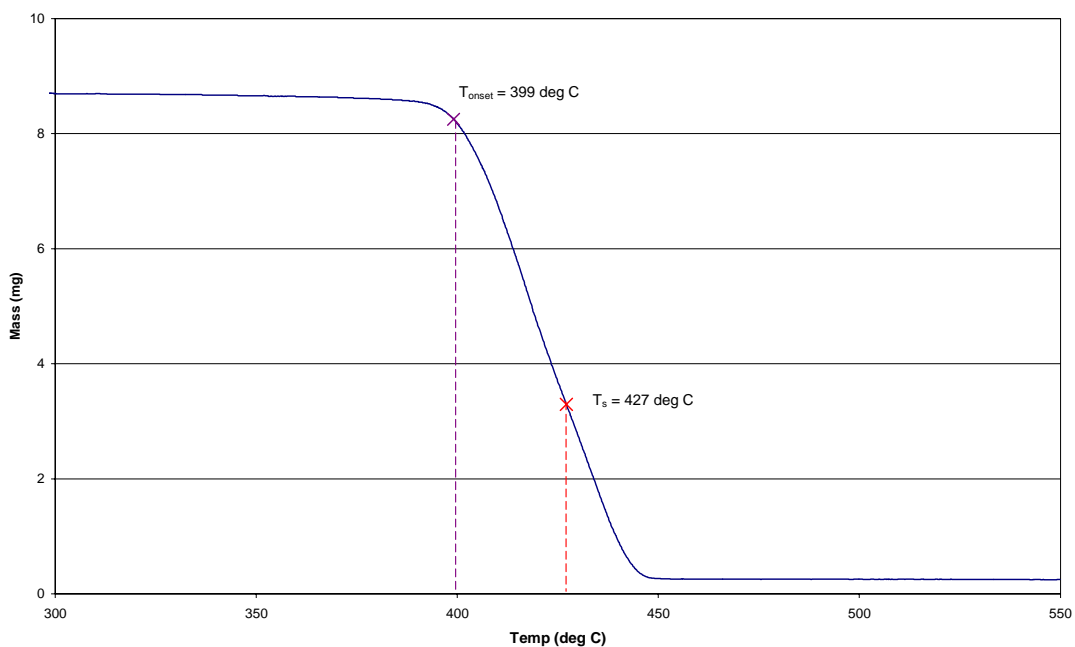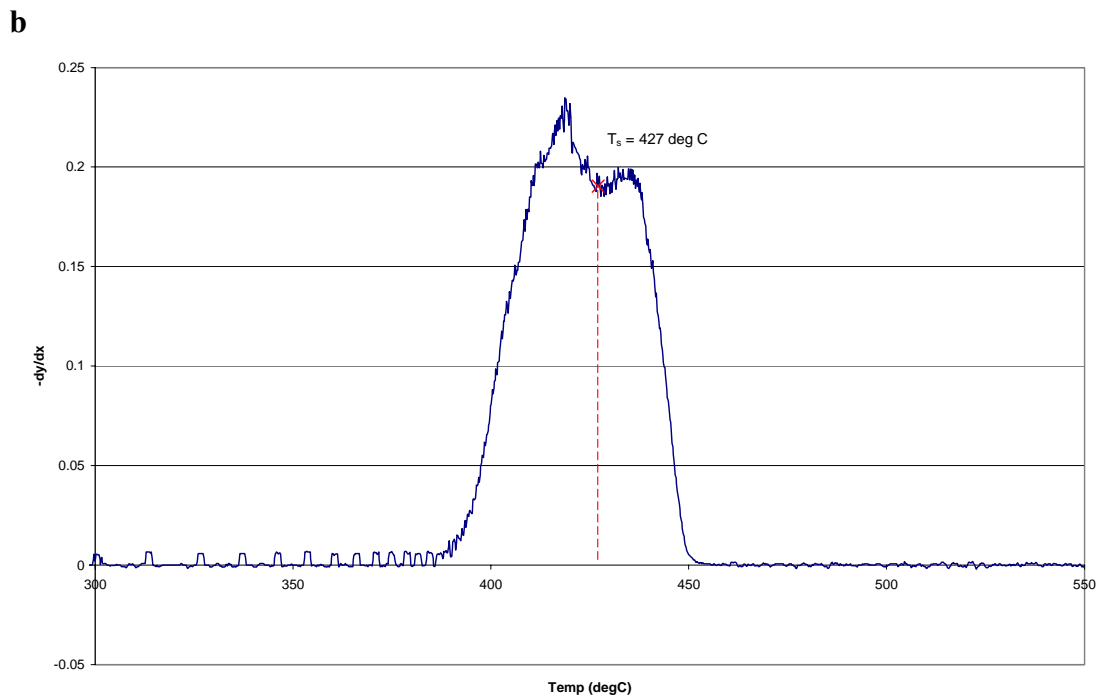
Figure 4.12: (a) TG and (b) dTG graphs for pure LDPE and Fulacolor clay

Using the Horowitz and Metzger method, in this example, only one reference temperature was defined ($T_s = 427$ºC). Therefore, this produced an *ln ln (W_o/W)* against θ graph of two gradients. These are displayed in Figure 4.13.
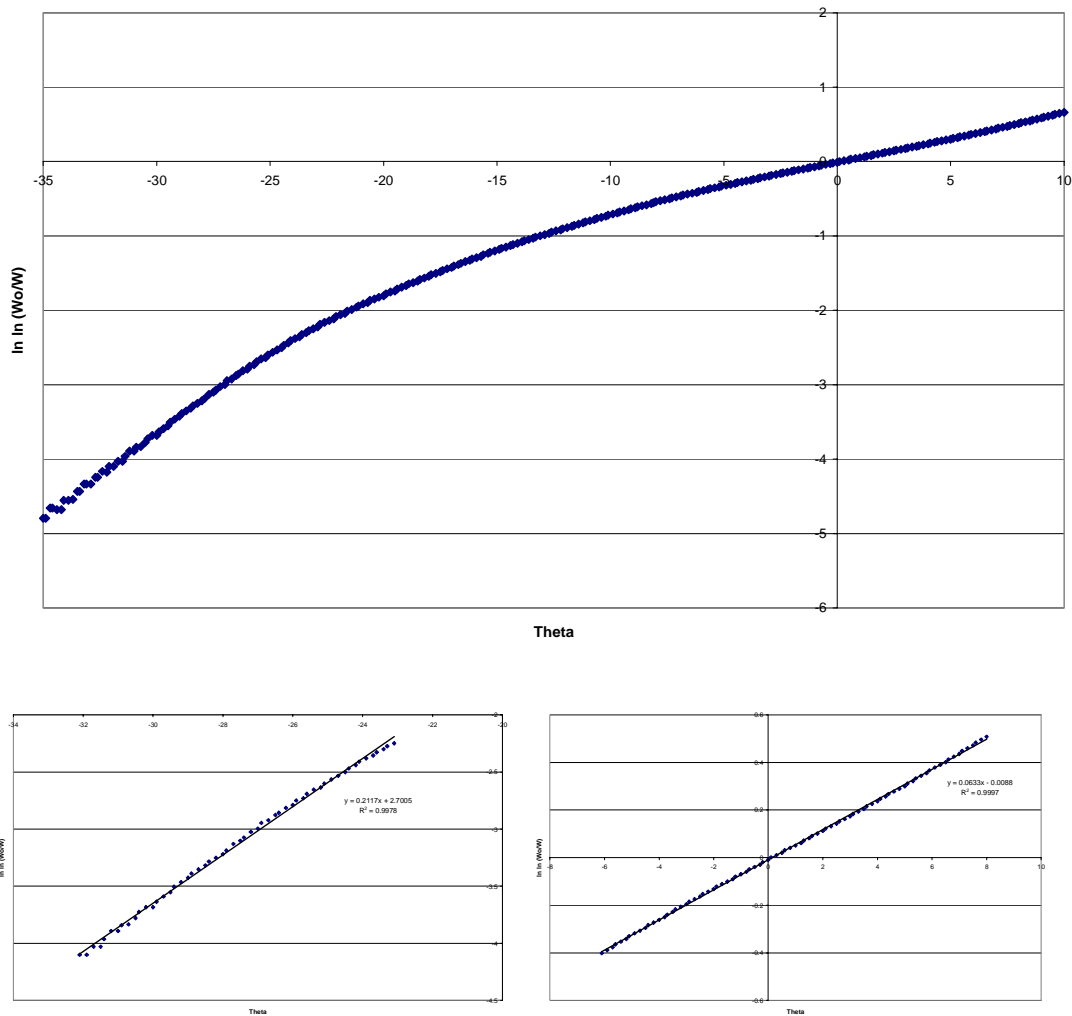
Figure 4.13: Plots of *ln ln W₀/W* against θ for pure LDPE and Fulacolor

From the single degradation step of pure LDPE and Fulacolor, two activation energies were calculated as 862 kJ/mol (from 394-403ºC) and 258 kJ/mol (from 420-434ºC).

The value of T_s calculated from the method of Horowitz and Metzger appears to be within the temperature range of the second calculated activation energy for both degradations (with and without catalyst). This suggests that the value of Ea_2 will be of significantly greater accuracy than Ea_1. The first activation energy uses the reference temperature that corresponds to the overlapping *dy/dx* peak at a higher temperature.

The Horowitz and Metzger method uses the assumption that most pyrolyses occur over a narrow temperature range at a relatively high temperature. However, polymer degradation in the presence of a catalyst may dramatically reduce the temperature of decomposition, possibly by more than 100ºC. From the relationship of E_a/RT_s^2, it can be seen that temperature has an inverse-squared relationship with activation energy, therefore if the value of T_s is inaccurate, at lower temperatures the error on the value of E_a could be very significant. The error in T_s originates from the presence of overlapping peaks in the *dy/dx* graph. If the polymer had degraded with two obvious weight-loss steps, two distinct peaks would have been noticeable in the differential thermogravimetric curve and two separate T_s values would have been used to calculate two separate activation energies. However, overlapping peaks in the *dy/dx* graph led to only one reference temperature being defined and hence an initial activation energy that did not obey the laws of thermodynamics (*i.e.* the presence of a catalyst reducing the activation energy of the reaction). In these cases, 'Origin 8' multi-curve fitting analysis was undertaken in order to separate the multiple peaks into two or more distinct features. For example, using the method of Horowitz and Metzger, the degradation of pure low-density polyethylene in the presence of EPZ10 clay gave one value for T_s (441ºC) and two gradients for the *ln ln W_0/W* against θ graph (hence two separate activation energies for the polymer decomposition). However, Figure 4.14 below displays the differential thermogravimetric curve of pure LDPE degradation with EPZ10, with the dTG curve clearly being the combination of two distinct thermal events. By using the 'Origin 8' software package, the raw data was deconvoluted in order to obtain a value of T_s for each of the two peaks, therefore improving the accuracy of the activation energy calculations.
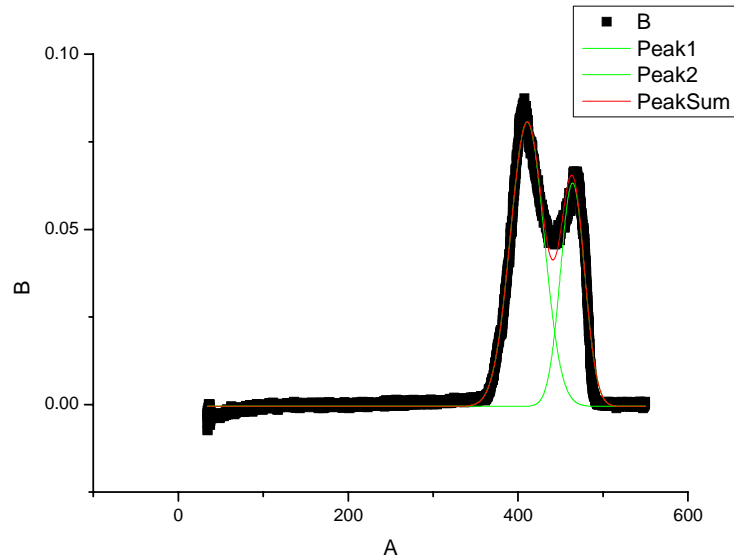
Figure 4.14: dTG curve for the degradation of pure LDPE with EPZ10

After the multi-curve fitting analysis procedure, the singular value of T_s (441ºC) was found to be the combination of two separate peaks at 411ºC and 464ºC. By relating each value of T_s to its corresponding $ln\ ln\ W_0/W$ against θ gradient, the first activation energy changed from 369 kJ/mol to 339 kJ/mol (30 kJ/mol reduction), whilst the second activation energy changed from 92 kJ/mol to 98 kJ/mol (6 kJ/mol increase). Applying this analysis to all thermogravimetric experiments that displayed overlapping dTG peaks, the largest alteration to an activation energy was found to be a 7% change.

4.2.3.3 Factors Affecting E_a

Bockhorn *et al.*[220] stated that recent studies concerning the pyrolysis of polystyrene revealed large discrepancies between parameters derived from isothermal and dynamic experiments, with each yielding an overall activation energy (E_a) of 172 kJ/mol and 322.8 kJ/mol respectively. Carniti, Gervasini and Bernardelli[221] found the activation energy for pure thermal degradation of polystyrene to be 185 kJ/mol (isothermal measurement). However, from modelling isothermal and dynamic pyrolysis, Bockhorn

found that a combination of heating rates below 10°C/min and sample masses below 50 mg were sufficient to keep the deviations below 10 kJ/mol.

From the *ln ln W_0/W* against θ plots determined from the Horowitz and Metzger method of analysis of the thermogravimetric curves, all R^2 values for the equations of the lines used to calculate the activation energies were extremely close to 1 (0.99 and above). The R-squared value (from 0 to 1) gives an indication of how closely the estimated values for the trendline correspond to the actual thermogravimetric data (with the line of best fit being most reliable when $R^2 = 1$). Therefore, the 0.99 and above values for R^2 obtained using the method of Horowitz and Metzger gives good confidence as to the accuracy of the calculations.

However, it must be remembered that, in order to evaluate the thermogravimetric data, certain assumptions had to be made which were not altogether realistic, *i.e.* all products from the polymer degradation were gaseous and escaped immediately. This simplistic approach means that it is likely that the decomposition rates are higher than those recorded, and consequently, the associated activation energies will be slightly lower than those determined in this study. Pérez-Maqueda, Sánchez-Jiménez and Criado[222] calculated the relative errors in the activation energies determined by a number of approximated integral methods and found that the Horowitz and Metzger method gave an error in E_a of 5.2%. Combining this error with the slight variations in the experimental procedure for each run (such as particle size of sample) and weighing the effects with the data analysis techniques used to make the calculations of E_a as accurate as possible - such as removal of catalyst effects from the TG curve and deconvolution of

overlapping dTG peaks – it is reasonable that an error of ± 5% be applied to the activation energies calculated in this study.

4.2.4 Thermogravimetric Results

All thermogravimetric experiments were conducted with the pure and waste polymers alone or with each of the catalysts, with a polymer-to-catalyst ratio of 2:1. For the TG curves of the polymer decomposition in the presence of each catalyst, the catalyst weight was subtracted from the experimental thermograms, along with the weight loss of the catalyst (mainly due to the loss of water as it was heated to 550ºC), in order to obtain thermograms relevant only to the polymer. From the weight loss curves and the application of the method of Horowitz and Metzger, the kinetics of polymer decomposition were calculated. The onset temperatures (T_{onset}) of degradation are displayed for each polymer and polymer-catalyst run. For the majority of plastics, single-step decomposition with only one T_{onset} was observed, whilst for polymers such as polybutadiene, polyurethane and polyacrylonitrile, two defined stages of degradation were seen. In the cases of polymethyl methacrylate and polyvinyl chloride, three separate stages of weight loss were evident from the thermogravimetric curve, giving rise to three values of onset temperature. The application of the method of Horowitz and Metzger to the raw data obtained from the TG runs allowed the activation energy for each degradation step to be determined. Figure 4.15 displays the thermogravimetric curves for the degradation of pure low-density polyethylene without catalyst and in the presence of each of the ten catalysts.
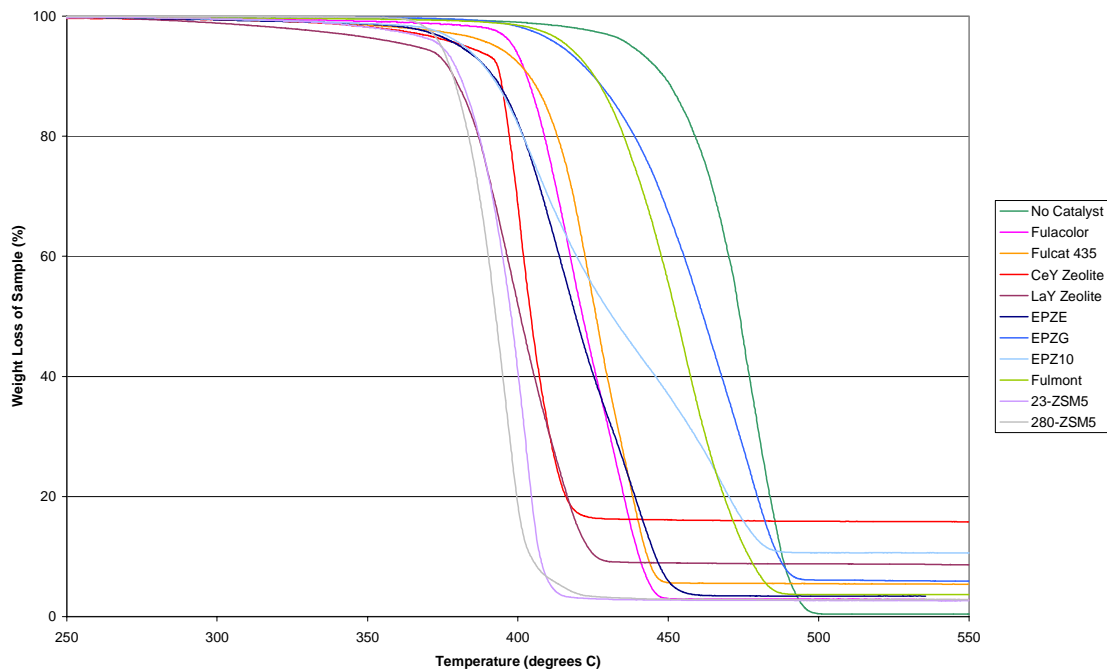
Figure 4.15: TG curves for non-catalytic and catalytic degradation of pure LDPE

The thermogravimetric curves for the decomposition of all pure and waste polymer samples are collected in Appendix D. These graphs represent how the presence of either a clay or zeolite catalyst can have an affect on the onset temperature of degradation, the number of decomposition steps, the gradient of the TG curve and the amount of residue left after heating.

4.2.4.1 No Catalyst
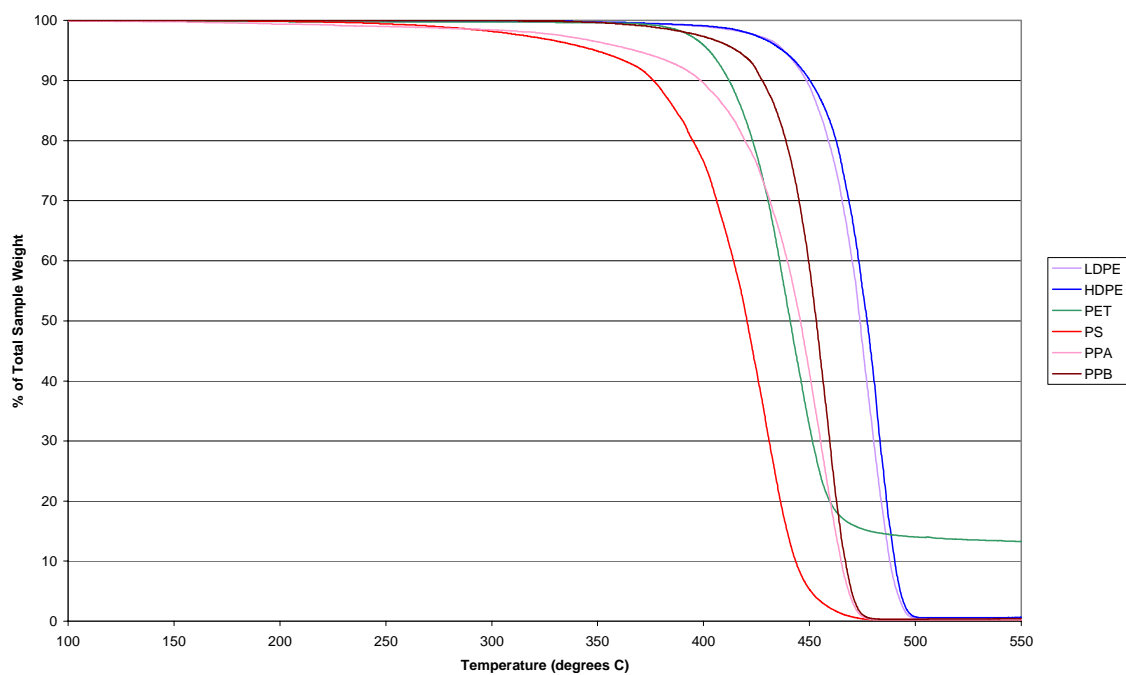
Figure 4.16: TG curves for the thermal degradation of pure polymers

Table 4.1 displays the onset temperatures of degradation of all six pure polymers when no catalyst was present.

Table 4.1: T_{onset} of degradation of pure polymers (no catalyst) (^{o}C)

Polymer	T_1
LDPE	451
HDPE	460
PET	416
PS	397
PPA	420
PPB	437

For the pure polyethylenes, no significant difference was found between the onset temperatures of degradation of LDPE and HDPE. The low-molecular weight polypropylene PPA (MW = 12,000) had a lower onset temperature than PPB (MW =190,000) with the 17ºC reduction suggesting that the variation in molecular weight has an effect on the onset temperature of degradation.

Figure 4.17 displays the non-catalytic thermogravimetric curves for the degradation of the thirteen waste polymers. It can clearly be seen which plastics decompose *via* a single step or with multiple weight-loss steps. The variation in the amount of residue left after degradation is also apparent.
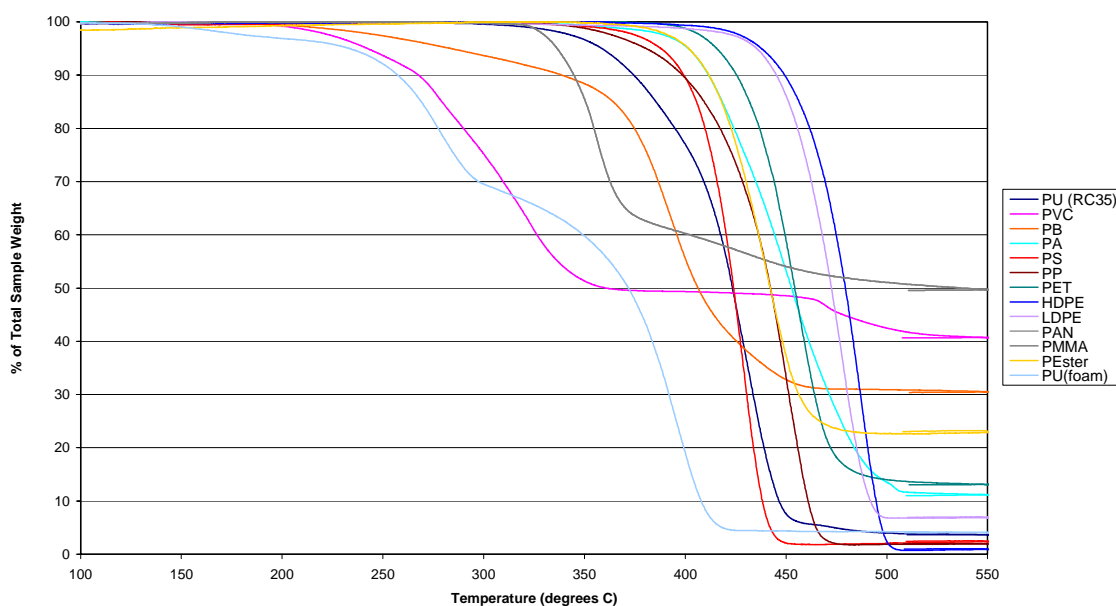
Figure 4.17: TG curves for the thermal degradation of waste polymers

The onset temperatures for each weight-loss step of the non-catalytic degradation of waste polymers are displayed in Table 4.2. Comparing the onset temperatures of degradation for pure polymers with their corresponding waste polymer, the difference in

148

T_{onset} was within 10ºC, with some showing a reduction in temperature and others an increase in T_{onset}. This suggests that this small difference may be due to slight differences in purity of the polymer or polymer length. Waste polyethylene and polypropylene have a slightly lower onset temperature, suggesting that the presence of additive impurities in the waste samples may decompose first and help in the degradation mechanism of the polymer. In contrast, waste PET and polystyrene showed an increase in onset temperature of degradation, which could possibly be due to the samples being of a higher molecular weight than their pure counterparts.

Table 4.2: T_{onset} of degradation of waste polymers (no catalyst) (ºC)

Polymer	T_1	T_2	T_3
LDPE	449		
HDPE	455		
PET	425		
PP	414		
PS	405		
PA	410		
PE	414		
PVC	233	286	457
PMMA	215	290	362
PB	283	372	
PU(RC35)	366	411	
PU(foam)	246	362	
PAN	337	383	

From the weight-loss curves of waste polymers, polyvinyl chloride and polyacrylonitrile appear to form a large amount of residue on decomposition. Thermogravimetric data showed PVC and PAN to lose only 60% and 50% of their original mass respectively. From the molecular weights of carbon, hydrogen and chlorine, the ratio of hydrogen chloride to the CH_2CHCl monomer of PVC were compared and showed that, if only HCl gas was evolved during the decomposition of PVC, the sample would experience a weight loss of 58.4%. The TG curve for PVC showed the polymer losing half of its weight by 350ºC and then a total of 60% by 550ºC, suggesting that the evolution of HCl occurs in two stages and the polymer undergoes negligible further weight loss in its conversion to coke.

Applying the same method to polyacrylonitrile, from the molecular weights of carbon, hydrogen and nitrogen, the ratio of hydrogen cyanide to the CH_2CHCN monomer of PAN were compared. This showed that, if only HCN gas was evolved during the decomposition of PAN, the sample would experience a weight loss of 50.9%. The TG curve for PAN showed this polymer also losing 50% of its total weight by 550ºC, suggesting that evolution of HCN and conversion of the polymer to coke are the main reactions.

In relation to the activation energies of decomposition, applying the method of Horowitz and Metzger to the thermogravimetric data obtained in the degradation of pure polymers, two values of E_a were discovered for each plastic. These are displayed in Table 4.3, along with the temperature range over which the activation energy applies.

Table 4.3: E_a for the decomposition of pure polymers (no catalyst) (kJ/mol)

Polymer	T of Ea_1 (ºC)	Ea_1	T of Ea_2 (ºC)	Ea_2
LDPE	418-432	332 ± 17	438-496	376 ± 19
HDPE	432-459	305 ± 16	471-495	433 ± 22
PET	396-411	378 ± 19	416-445	280 ± 14
PS	317-368	100 ± 5	402-443	208 ± 11
PPA	359-392	122 ± 7	402-437	182 ± 9
PPB	397-419	234 ± 12	441-473	385 ± 20

Bockhorn, Hornung and Hornung[223] found the apparent energy of activation of the thermal degradation of pure powdered polyethylene to be 268 ± 3 kJ/mol, using a fourth order Runge-Kutta[224] method to calculate the kinetic parameters. Our study found the degradation of polyethylene to occur *via* two activation energies, as shown in Table 4.3. Albano and de Freitas[225] analysed the thermodegradative behaviour of polypropylene, and using the method of Horowitz and Metzger, the activation energy of pure PP was found to be 259 kJ/mol, which was said to be related to a combination of both gas reactions that occur *via* free radicals, and a chain reaction. This figure appears comparable to the first activation energy of PPB (397º-419ºC), calculated using the same method (234 ± 12 kJ/mol).

The activation energies of the non-catalytic degradation of the waste polymer samples are displayed in Table 4.4.

Table 4.4: E_a for the decomposition of waste polymers (no catalyst)

Polymer	T of Ea$_1$ (ºC)	Ea$_1$ (kJ/mol)	T of Ea$_2$ (ºC)	Ea$_2$ (kJ/mol)	T of Ea$_3$ (ºC)	Ea$_3$ (kJ/mol)
LDPE	428-447	428 ± 22	448-462	354 ± 18		
HDPE	414-430	460 ± 23	438-485	309 ± 15		
PP	435-457	297 ± 15				
PET	427-452	306 ± 16				
PE	418-439	312 ± 16				
PS	409-435	338 ± 17				
PA	424-443	213 ± 11	451-459	161 ± 8		
PVC	242-254	230 ± 12	312-3323	295 ± 15	488-495	660 ± 33
PMMA	243-249	329 ± 17	336-346	309 ± 16	376-388	357 ± 18
PB	283-299	156 ± 8	387-395	515 ± 26		
PU(RC35)	388-395	529 ± 27	427-436	618 ± 31		
PU(foam)	275-282	420 ± 21	394-399	576 ± 29		
PAN	354-358	1014 ± 51	425-441	307 ± 16		

Bockhorn, Hornung and Hornung[226] found the activation energies of polystyrene and polyamide degradation to be 329 kJ/mol and 211 kJ/mol respectively. These activation energies appear to be in general agreement with those calculated in this study. However, the activation energy of polypropylene calculated by Bockhorn *et al*., (224 kJ/mol) is a lower E_a than the 297 ± 15 kJ/mol determined from our thermogravimetric analysis.

Straus and Madorsky[227] found the activation energy of polybutadiene to be 62 kcal/mol (259 kJ/mol). This study found PB as having two distinct energies of activation; 156 ± 8 kJ/mol (283-299ºC) and 515 ± 26 kJ/mol (387-395ºC) respectively.

4.2.4.2 'No Catalyst' Conclusions

In contrast to the onset temperatures of degradation, waste LDPE, HDPE and polystyrene were found to have significantly higher first energies of activation than their corresponding pure polymer, implying that, although the degradation of the polymer occurred at a similar temperature, the presence of additives and plasticisers may result in a greater amount of energy being required to begin thermal decomposition.

Additionally, all pure polymers were found to have two distinct activation energy steps, whereas the degradation of waste polypropylene, PET and polystyrene could not be separated into two values for E_a. Combining Ea_1 and Ea_2 for pure polypropylene A, the total activation energy of decomposition was found to be 304 ± 16 kJ/mol, almost exactly that for the single E_a of waste PP (297 ± 15 kJ/mol). Combining the two activation energies of pure polystyrene (308 ± 16 kJ/mol) and comparing the total E_a to the single value for the degradation of waste polystyrene (338 ± 17 kJ/mol) gave a result 20 kJ/mol lower. This difference in activation energy may be related to the presence of additives and plasticisers in the waste polymer, resulting in a greater amount of energy being required to begin thermal decomposition. Combining the two activation energies of pure PET (658 ± 33 kJ/mol) gave a significantly higher total activation energy than that seen for the waste sample (306 ± 16 kJ/mol). The temperature range ($427\text{-}452\,^{\circ}\text{C}$) over which the E_a of waste PET was calculated, corresponded to the second energy step of pure PET (280 kJ/mol at $416\text{-}445\,^{\circ}\text{C}$). The energies of 306 ± 16 kJ/mol and 280 ± 14 kJ/mol appear more comparable than for the total combined energy of 658 kJ/mol.

4.2.4.3   Catalytic Degradation

4.2.4.3.1   Single Degradation Step

All the six pure polymer samples analysed were found to decompose thermally in a single degradation step. An example of the thermogravimetric curves obtained for the degradation of a pure polymer with each of the ten catalysts compared to non-catalytic decomposition is displayed in Figure 4.18.

The thermogravimetric curves for many of the polymers show how catalytic degradation results in the decomposition reaction completing fully at a temperature lower than the onset temperature of degradation when no catalyst is present (see Appendix D). The TG curves also demonstrate possible changes in the rate of decomposition, with very steep curves symbolising the reaction occurring over a narrow temperature range, and changes in the gradient of the curve suggesting possible changes in the reaction mechanism of degradation.
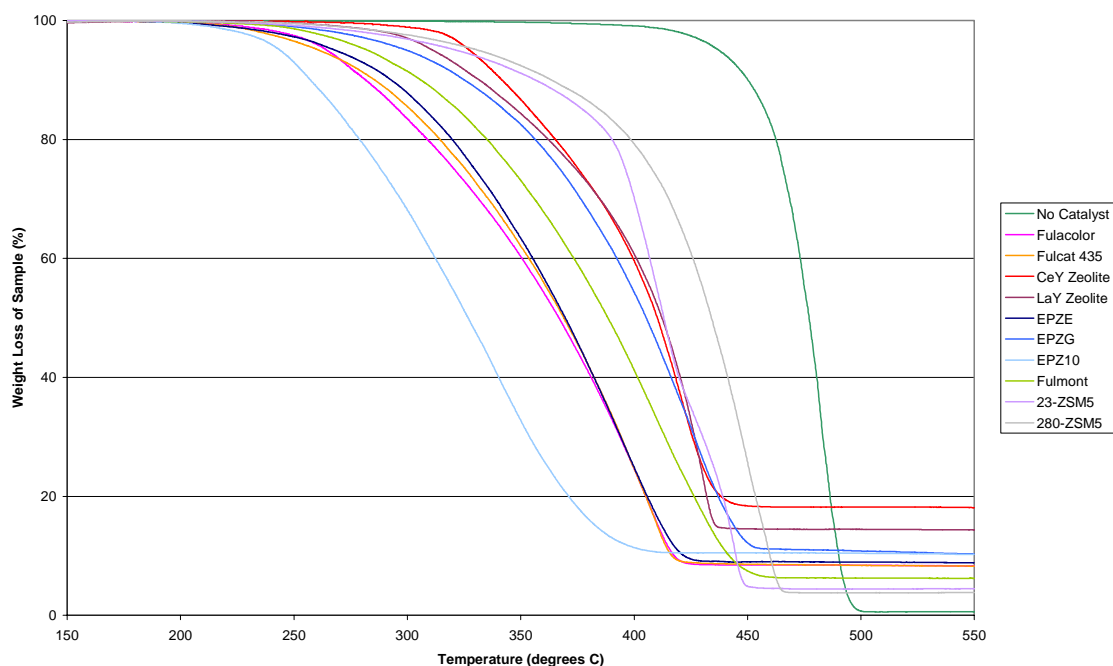
Figure 4.18: TG curves for the catalytic degradation of pure polystyrene

Tests were also carried out with celite (an inert fine white powder) to ensure that any changes to polymer decomposition were not related to the presence of the catalyst as a fine powder. The celite was found to not alter the degradation characteristics of the plastics, therefore the differences seen when the polymers degraded in the presence of the clays and zeolites could be attributed purely to catalytic effects.

Table 4.5 lists the onset temperatures of degradation of the six pure polymers alone and in the presence of the ten catalysts. Figure 4.19 displays these results graphically.

Table 4.5: T_{onset} of degradation of pure polymers and catalysts (ºC)

Catalyst / Polymer	None	Fulacolor	Fulcat	Fulmont	EPZE	EPZG	EPZ10	CeY	LaY	23z	280z
LDPE	451	399	406	426	389	431	385	389	376	381	374
HDPE	460	414	403	446	413	435	430	405	400	397	395
PET	416	406	393	412	406	400	393	413	404	412	410
PS	397	312	321	327	312	356	261	373	384	397	406
PPA	420	242	232	291	249	299	242	298	281	364	376
PPB	437	348	338	393	340	368	331	342	340	358	367
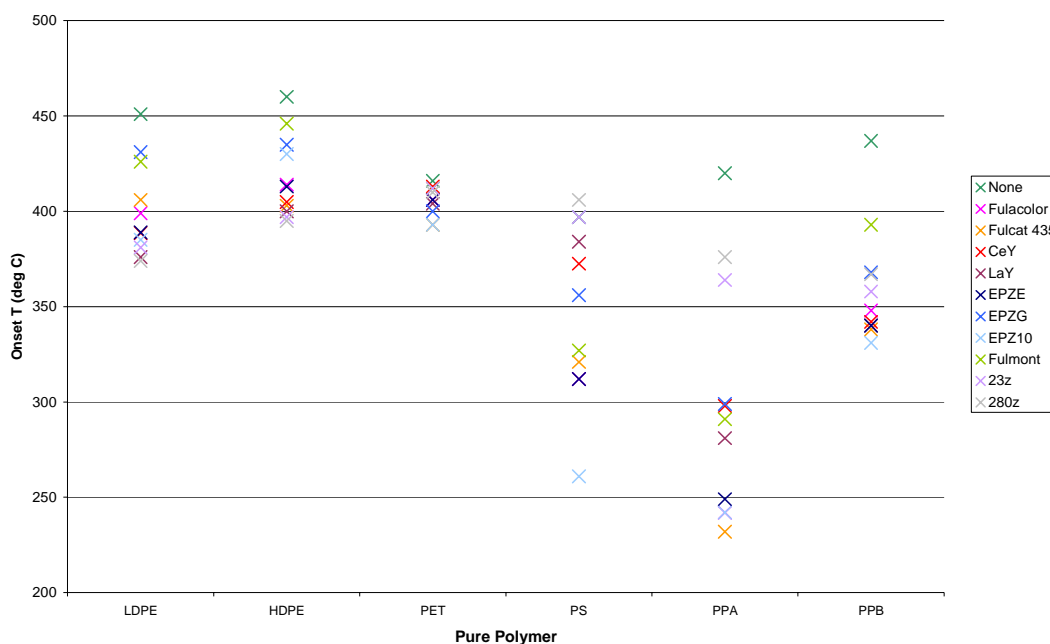
Figure 4.19: T_{onset} of degradation of pure polymers and catalysts (ºC)

Of the thirteen waste polymer samples analysed, seven were found to decompose thermally in a single degradation step. These plastics were low-density polyethylene, high-density polyethylene, polyethylene terephthalate, polypropylene, polystyrene, polyamide and polyester. Table 4.6 displays the onset temperatures of these in ºC.

Table 4.6: T_{onset} of one-step degradation of waste polymers and catalysts (°C)

Catalyst /Polymer	None	Fulacolor	Fulcat	Fulmont	EPZE	EPZG	EPZ10	CeY	LaY	23z	280z
LDPE	449	424	371	456	434	455	430	396	395	407	402
HDPE	455	406	415	440	414	431	401	402	400	405	404
PET	425	413	394	413	404	413	400	414	410	411	407
PP	414	357	361	398	367	394	371	326	347	347	401
PS	405	397	391	397	389	398	394	392	391	392	393
PA	410	403	406	392	393	390	402	397	393	396	391
PE	414	411	413	405	406	400	399	410	409	406	405
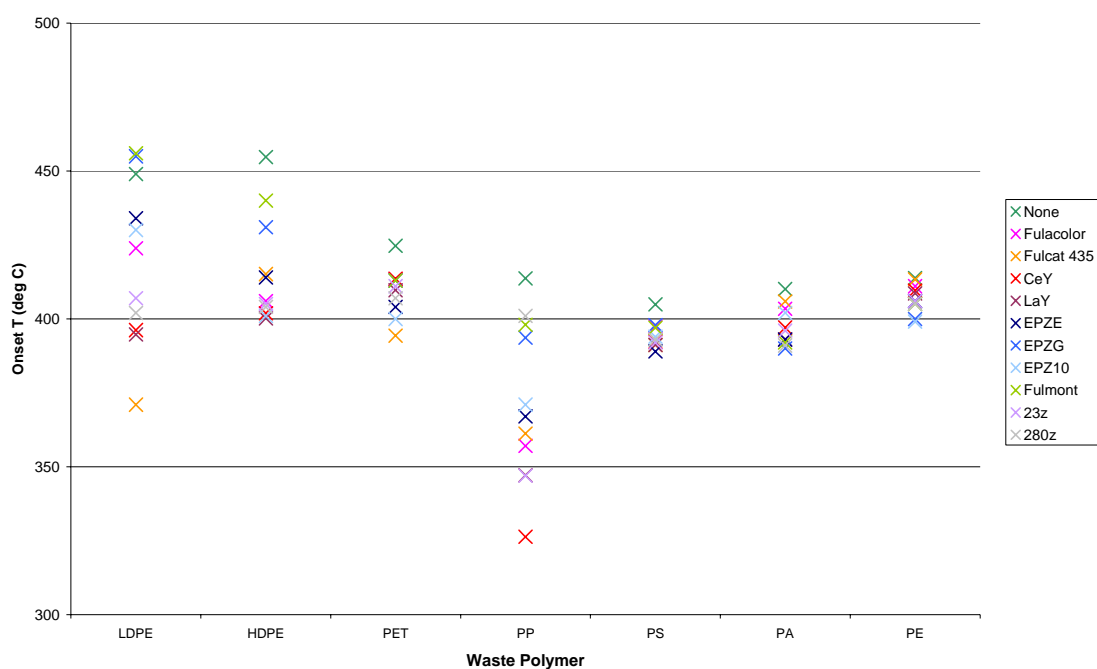
Figure 4.20: T_{onset} of one-step degradation of waste polymers and catalysts (°C)

4.2.4.3.2 Multiple Degradation Steps

The thermogravimetric analysis of four of the waste polymers – polybutadiene, polyester polyurethane (RC35), polyurethane foam and polyacrylonitrile – produced two distinct degradation steps (see Table 4.7 and Figure 4.21). Polyvinyl chloride and

polymethyl methacrylate displayed three separate weight-loss curves on heating (see
Table 4.8 and Figure 4.22).

Table 4.7: T_{onset} of two-step degradation of waste polymers and catalysts (^oC)

Catalyst	Onset T	PB	PU(RC35)	PU(foam)	PAN
None	T_1	283	366	246	337
	T_2	372	411	362	383
Fulacolor	T_1	259	344	231	334
	T_2	362	392	371	385
Fulcat	T_1	246	347	245	331
	T_2	359	389	338	374
Fulmont	T_1	261	344	233	320
	T_2	354	386	360	355
EPZE	T_1	213	359	229	320
	T_2	353	-	323	361
EPZG	T_1	251	349	224	321
	T_2	352	-	355	358
EPZ10	T_1	263	331	225	317
	T_2	354	379	330	360
CeY	T_1	232	315	225	322
	T_2	351	384	367	354
LaY	T_1	239	335	233	324
	T_2	354	387	363	367
23z	T_1	248	292	226	322
	T_2	354	387	367	360
280z	T_1	211	334	234	323
	T_2	354	386	370	346

The multiple decomposition steps in Figure 4.21 and Figure 4.22 below are represented
by X, O and Δ for the 1st, 2nd and 3rd stages of degradation respectively.
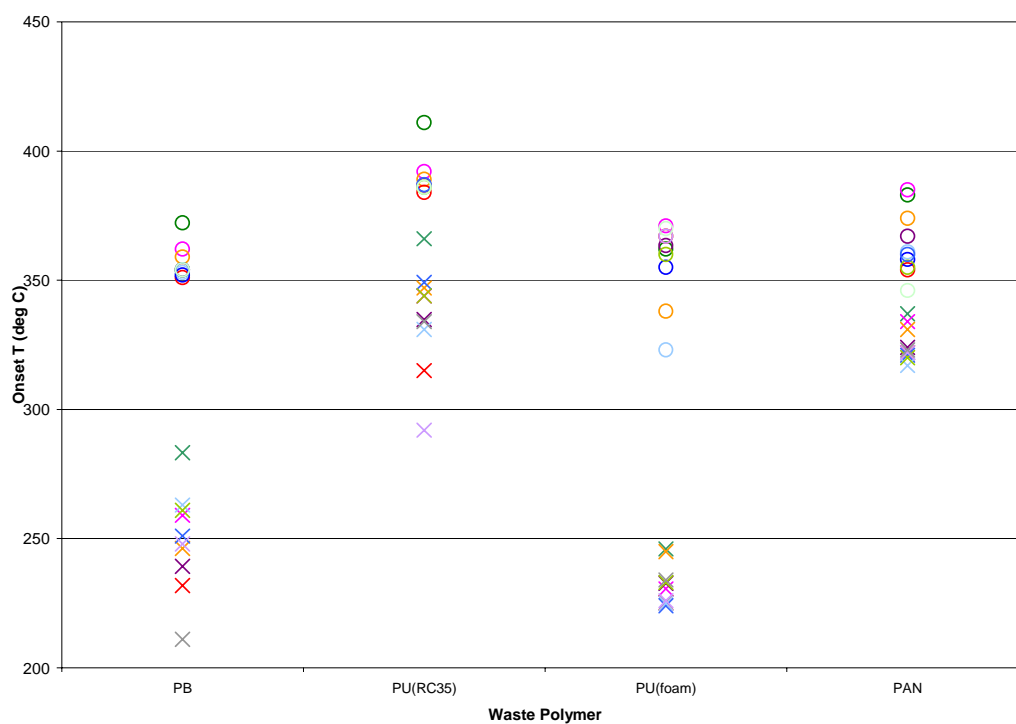
Figure 4.21: T$_{onset}$ of two-step degradation of waste polymers and catalysts (°C)

For polybutadiene, the first degradation step is said to be almost exclusively due to volatile depolymerisation products, whilst the second is attributed to degradation of a residue due to cyclised and cross-linked butadiene rubber.[228]

Table 4.8: T_{onset} of three-step degradation of waste polymers and catalysts (ºC)

	Onset T	PVC	PMMA
None	T_1	233	215
	T_2	286	290
	T_3	457	362
Fulacolor	T_1	196	191
	T_2	274	264
	T_3	458	345
Fulcat	T_1	192	186
	T_2	263	287
	T_3	451	345
Fulmont	T_1	195	189
	T_2	273	263
	T_3	436	345
EPZE	T_1	186	192
	T_2	250	283
	T_3	430	351
EPZG	T_1	183	187
	T_2	254	262
	T_3	437	341
EPZ10	T_1	185	185
	T_2	257	289
	T_3	431	344
CeY	T_1	204	210
	T_2	276	278
	T_3	454	348
LaY	T_1	206	199
	T_2	269	298
	T_3	445	351
23z	T_1	190	213
	T_2	253	295
	T_3	434	348
280z	T_1	204	189
	T_2	262	279
	T_3	436	343
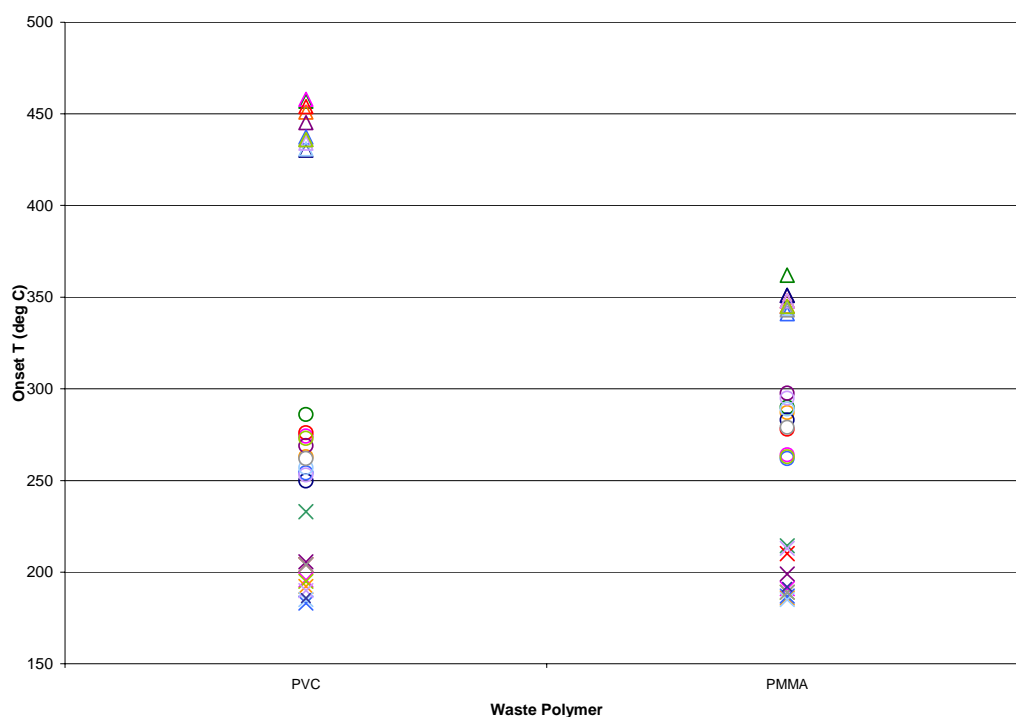
Figure 4.22: T_{onset} of three-step degradation of waste polymers and catalysts (^{o}C)

Bockhorn, Hornung and Hornung stated that PVC decomposed in two steps: dehydrochlorination between 220°C and 350°C, and formation of a mixture of hydrocarbons (mainly aromatic compounds) between 400°C and 550°C. Dehydrochlorination was said to be accompanied by benzene formation. Dehydrochlorination was said to occur *via* a free radical mechanism, with initiation proceeding with the formation of a chlorine radical, followed by hydrogen abstraction and HCl formation. The radical site in the polymer chain was said to form a chlorine radical *via* an elimination reaction, giving polyene structures (endothermic process).[229] In comparison to these previous studies, this study found the degradation of PVC to involve three distinct weight loss steps.

The weight loss exhibited during the thermal degradation of PMMA is said to be the result of a complex process, consisting of chain initiation reactions, depropagation reactions, termination reactions and the transport of the decomposition products through softened PMMA (by bubbles and diffusion) from the inside of the sample to the outside. Since there are no tertiary hydrogens in the PMMA structure, intermolecular chain transfer is said to be neglected in the depolymerisation process. Hirata, Kashiwagi and Brown[230] undertook thermogravimetric analysis of PMMA under a nitrogen atmosphere. Two reaction stages of weight loss were determined. The first was said to have been the result of the chemical process of degradation, with end initiation beginning at around 160°C, with an activation energy of 31 kJ/mol (determined by isothermal heating). The second reaction stage, the random scission initiation, was found to have an activation energy of 233 kJ/mol.

4.2.4.4 Discussion of T_{onset} Results

The onset temperatures of degradation of the six pure polymers and thirteen waste polymers have been reduced in the presence of a catalyst. Fulcat 435 clay was found to have reduced the T_{onset} of low molecular weight polypropylene (PPA) by nearly 200°C. The best improvement in onset temperature for pure LDPE and HDPE (both with 280z zeolite) reduced the uncatalysed values by approximately 80°C. The simple polyethylene molecules were obviously of sufficiently small size to access the active pores of the ZSM-5 zeolite. The onset temperatures of PET and PAN were found to have not been altered significantly by the presence of catalysts. This may have been due to the large PET or PAN molecules being too 'bulky' to enter the active pores of the catalysts.

One noticeable result occurred for the laboratory synthesised polyester polyurethane RC35. Without a catalyst, the polymer degraded in two steps. In the presence of eight catalysts, PU(RC35) still decomposed *via* two distinct onset temperatures. However, in the presence of EPZE and EPZG clays, the degradation occurred in a single step.

Without a catalyst, the degradation of polymers occurs *via* a radical mechanism, which requires a large amount of energy to begin breaking the bonds. This explains why the onset temperature of degradation of plastics occurs at a higher temperature when catalysts are not present. In the presence of a catalyst, T_{onset} is reduced and the degradation reaction is completed at a lower temperature.

Using the method of Horowitz and Metzger, the activation energies of decomposition were then compared to those obtained from the catalytic degradation of each polymer sample. Recent research has been undertaken into the activation energies of thermal and catalytic cracking reactions of various hydrocarbons.

For zeolites, the formation of carbonium ions from the reaction of a proton with alkanes requires the breaking of the zeolitic hydroxyl groups to generate the protons. Lercher, van Santen and Vinek (1994) studied carbonium ion formation in zeolite catalysis, based on data of *n*-butane conversion over HZSM5. The energies involved in the heterolytic breaking of the OH bond of SiOHAl groups were found to be in the region of 1300 kJ/mol, with a large proportion of this energy provided by the formation of the carbonium ion and its hydrogen bonding to the zeolite lattice.[231] Theoretical calculations by Lercher *et al*. suggested that the strong interactions between the hydrocarbons and the zeolite walls at the SiOHAl site and the close distance between

the *n*-alkane carbon atom and the zeolite oxygens did not allow the formation of stable carbonium ions. It was thought that carbonium ion formation in zeolites was likely to be a transition state rather than a stable high energy intermediate.

Kazansky (1999) used quantum chemical calculations to study the adsorbed carbenium and carbonium ion active intermediates of acid catalysed transformations of hydrocarbons on zeolites. The activation energy for the protolytic cracking and dehydrogenation of *iso*butane were found to be 241 kJ/mol and 279 kJ/mol respectively.[232] The activation energy of the hydride transfer reaction was calculated as 203 kJ/mol.

Milas and Nascimento (2003) simulated the Brønsted acid site and the cavity of a HZSM-5 zeolite and calculated the energies of activation of dehydrogenation and cracking of *iso*butane as being 194 kJ/mol and 198 kJ/mol respectively.[233]

Zheng and Blowers (2005) used the Complete Basis Set Composite Energy method to calculate activation energy barriers for ethane conversion reactions on zeolites. The cracking reaction was said to consist of the C-C bond cleavage of ethane by the zeolite Brønsted acid proton, where the proton attaches to one methyl group of the ethane reactant and forms methane and a surface oxide.[234] For ethane cracking, the activation energy was calculated as 299 kJ/mol. The activation energy of the hydrogen exchange reaction was calculated as 131 kJ/mol. The dehydrogenation reaction consisting of the cleavage of a C-H bond by the zeolite Brønsted acid proton gave an activation energy of 318 kJ/mol.

A further computational study was undertaken by Zheng and Blowers (2006) into methane catalytic reactions on zeolites. The activation barrier of dehydrogenation and hydrogen exchange were found to be 368 kJ/mol and 136 kJ/mol respectively.[235] For both studies, Zheng and Blowers calculated the deprotonation energy for the breaking of the bond between the acidic hydrogen and its oxygen neighbour for zeolites as 1236 kJ/mol.

Macht, Carr and Iglesia (2009) estimated the deprotonation energy for solid Brønsted acid catalysts and found the values to be in the region of 1110-1120 kJ/mol.[236] The OH groups remaining after dehydroxylation of the catalysts were found to be stronger acid sites due to a decrease in electron density in the conjugate anion and the formation of Brønsted-Lewis acid conjugate pairs.

4.2.4.5   Activation Energy

By comparing the temperature ranges over which the activation energies of decomposition apply, information into the reaction mechanisms for thermally and catalytically degraded polymers can be ascertained. For example, the first activation energy (Ea_1) of the thermal (non-catalytic) degradation of pure low-density polyethylene applied to a temperature range of 418-432ºC, with Ea_2 applying to the temperature range 438-496ºC. A catalytic reaction has a lower rate-limiting free energy of activation in comparison to the corresponding uncatalysed reaction. In relation to the values obtained in this thermogravimetric study, the E_a observed is mainly the activation energy of the rate determining step (slowest reaction) of the sequence of reactions occurring at that temperature range.

For thermal degradation, the first activation energy, $E_a\bullet$, is thought to represent the energy required to begin the decomposition of the polymer *via* a free radical mechanism and is controlled by the amount of energy required to break the weakest bond. The second activation energy, $E_a\cdot\bullet$, represents the energy required for rearrangement and β-scission of the radical intermediates/molecules at a higher temperature as the polymer degradation proceeds. For catalytic degradation in this study, over some temperature ranges, large activation energies were seen. This was thought to correspond to a Si-OH protonation (B, Brønsted) of the polymer, and these values were placed in the $\mathbf{E_a^{C+B}}$ columns of the following Tables. For other catalysed reactions, lower activation energies were observed. These were thought to represent Lewis-acid removal of hydride (H⁻) from the polymer, and were placed in the $\mathbf{E_a^{C+L}}$ columns. It must be noted that in a few instances, the temperature order of the process is not sequential from column to column in the Tables (these have been highlighted with a * symbol). The "second" activation energy observed for catalytic degradation of the plastics was compared to $E_a\bullet$ and $E_a\cdot\bullet$ for the radical decomposition processes.

From the calculations of Pérez-Maqueda *et al.*,[222] and the slight variations in experimental procedure for each run (such as particle size of sample), whilst also considerng the data analysis techniques used to make the calculations of E_a as accurate as possible (removal of catalyst effects from the TG curve, deconvolution of overlapping dTG peaks), an error of ± 5% was assigned to the activation energies calculated in this study (see Section 4.2.3.3).

4.2.4.5.1 Pure Polymers and Catalysts

Table 4.9 and Table 4.10 display the activation energies calculated for the degradation of pure LDPE and HDPE alone and in the presence of each of the ten catalysts.

Table 4.9: Activation energies of pure LDPE and catalysts (kJ/mol)

LDPE	E_a^{C+B}	T of E_a^{C+B}	E_a^{C+L}	T of E_a^{C+L}	$E_a\bullet$	T of $E_a\bullet$	$E_a\bullet$	T of $E_a\bullet$
No Catalyst					332 ± 17	418-432	376 ± 19	438-496
Fulacolor	862 ± 43	394-403					258 ± 13	420-434
Fulcat 435			375 ± 19	404-430				
Fulmont			465 ± 24	404-425			279 ± 14	440-463
EPZE					323 ± 17	382-414		
EPZG							231 ± 12	432-474
EPZ10			339 ± 17	381-402			98 ± 5	431-454
CeY			400 ± 20	405-418*	185 ± 10	373-391*		
LaY			246 ± 13	395-419*	99 ± 5	334-365*		
23z			441 ± 22	359-373	218 ± 11	373-401		
280z	743 ± 37	370-380	468 ± 24	383-400				

* N.B. Temperature ranges not sequential.

For pure LDPE, degradation in the presence of Fulacolor and 280z was thought to have been initiated by a Si-OH protonation of the polymer. For Fulacolor clay, this could be attributed to the catalyst displaying the highest concentration of Brønsted-acid sites of all the catalysts. In comparison, 280z exhibited the second-lowest number of Brønsted sites and a high Si/Al_{tot} ratio, suggesting low overall Brønsted acidity. Therefore, the high energy value relating to deprotonation energy observed for 280z is a surprise and may in fact be due to another process entirely; *i.e.* one that leads to aromatic compound formation, a reaction sequence which is well known with this type of catalyst. LDPE decomposition with Fulcat 435, Fulmont and EPZ10 clays, and CeY, LaY, 23z and 280z zeolites was thought to have occurred *via* Lewis-acid removal of hydride ions. The lowest activation energy of these seven catalysts was seen for LaY zeolite – a

surprising result considering the catalyst was fourth out of the six in relation to the concentration of Lewis-acid sites. One possible explanation is that, on heating of the catalyst, the removal of water exposed the previously hidden Lewis sites of the zeolite (the Y-zeolites were found to have a greater amount of adsorbed water at room temperature than the other catalysts).

The second activation energy seen for CeY, LaY and 23z zeolites corresponded to the initiation of the free radical degradation mechanism ($E_a\bullet$). The value of $E_a\bullet$ was found to be reduced in all cases, with LaY showing the greatest reduction of 233 kJ/mol. The second activation energy seen for Fulacolor, Fulmont and EPZ10 clay appear to correspond to rearrangement reactions of the free radical degradation mechanism (based on the corresponding temperature ranges over which the energies were calculated).

Simply from the E_a and T range data it appears that EPZE does not initiate a Brønsted- or Lewis-catalysed degradation mechanism, but is just reducing the activation energy of the free radical decomposition and subsequent rearrangement reactions by 53 ± 3 kJ/mol. This is a slightly surprising result, especially as the catalyst appeared to display some very promising characteristics, such as the second largest concentrations of Brønsted- and Lewis-acid sites. It may be that we are observing a Lewis-acid catalysed mechanism replacing the radical mechanism, but with the data available this is not certain.

The non-catalytic degradation of pure LDPE was found to produce only 1% residue, whilst in the presence of 23z and 280z zeolites the amount of residue increased slightly to 3%. However, for CeY and EPZ10, after decomposition the residue was found to be

17% and 12% respectively of the initial total mass of the polymer, showing that these catalysts were also initiating char formation (graphitisation) of the intermediate molecules.

Table 4.10: Activation energies of pure HDPE and catalysts (kJ/mol)

HDPE	E_a^{C+B}	T of E_a^{C+B}	E_a^{C+L}	T of E_a^{C+L}	$E_a\bullet$	T of $E_a\bullet$	$E_a\bullet$	T of $E_a\bullet$
No Catalyst					305 ± 16	432-459	433 ± 22	471-495
Fulacolor	522 ± 26	421-435						
Fulcat 435			308 ± 16	387-415*	186 ± 10	352-375*		
Fulmont			360 ± 18	448-485				
EPZE			447 ± 23	419-431				
EPZG			252 ± 13	450-472				
EPZ10	745 ± 38	389-402					139 ± 7	432-459
CeY	832 ± 42	403-413	423 ± 22	420-435				
LaY			247 ± 13	418-436				
23z	548 ± 28	395-415*	301 ± 15	373-385*				
280z	551 ± 28	402-422						

* N.B. Temperature ranges not sequential.

For pure HDPE, degradation in the presence of Fulacolor, EPZ10, CeY, 23z and 280z was thought to have been initiated by a Si-OH protonation of the polymer. The lack of branches in the HDPE raises the temperature at which the reaction begins with Fulacolor (by about 30°C) compared to LDPE, which does have branches where reaction initiation is easier. This raising of temperature may also explain the lowering of the E_a^{C+B} with HDPE.

Of the four remaining catalysts, the ZSM-5 zeolites were far more successful in reducing the deprotonation energy by a half (from approximately 1100 kJ/mol to around 550 kJ/mol), suggesting that they were more powerful Brønsted acids. HDPE decomposition with Fulcat 435, Fulmont, EPZE, EPZG, CeY, LaY and 23z was thought

to have occurred *via* Lewis-acid removal of hydride ions. The lowest activation energy of these carbocation reactions was seen for LaY zeolite – in accordance with the results from the degradation of pure LDPE. EPZG also gave one of the lowest activation energies in this group. The success of EPZG could be due to a combination of the catalyst displaying the third largest pore diameter in relation to the other clays and zeolites (allowing access of the polymer molecules to the active sites) and the fourth highest concentrations of Brønsted- and Lewis-acid sites.

The second activation energy seen for Fulcat 435 corresponded to the initiation of the free radical degradation mechanism ($E_a\bullet$), and was found to be reduced by 119 ± 6 kJ/mol and to occur at a far lower temperature (80ºC less). The second activation energy seen for EPZ10 clay corresponded to rearrangement reactions of the free radical degradation mechanism (based on the corresponding temperature ranges over which the energies were calculated). This value was reduced by 294 ± 15 kJ/mol.

For pure HDPE, the presence of all ten catalysts appeared to initiate either a Brønsted or Lewis reaction that may have required more energy but appears to have occurred at a lower temperature than thermal degradation of the polymer, but at higher temperatures than with LDPE, in the majority of cases.

The non-catalytic degradation of pure HDPE was found to produce only 1% residue, whilst in the presence of 23z and 280z zeolites the amount of residue increased to 5%. However, for CeY, LaY and EPZ10, after decomposition the residue was found to be 17%, 13% and 12% respectively of the initial total mass of the polymer. Again, these catalysts are initiating unwanted char formation.

From the literature, the gasification of PE over zeolite CaX was said to have proceeded through a carbocation ion mechanism, with an apparent activation energy of 32.5 kcal/mol (136 kJ/mol). This lower value of E_a than expected was explained by the isomerisation of carbocations being an exothermic process and cancelling out the endothermic decomposition of the carbocations partially.[237] The activation energies for different alkane and alkene fractions were reported as: *1-alkene* − C_6-C_{11}: 265 kJ/mol, C_{12}-C_{16}: 157 kJ/mol, C_{17}-C_{20}: 183 kJ/mol, *n-alkane* - C_6-C_{11}: 247 kJ/mol, C_{12}-C_{16}: 138 kJ/mol, C_{17}-C_{20}: 57 kJ/mol.[238] Kinetic analysis of TGA data from the thermolysis of HDPE beads, LDPE powder and waste PE gave activation energies of 56.7 kcal/mol (237 kJ/mol), 60.3 kcal/mol (252 kJ/mol) and 66.6 kcal/mol (278 kJ/mol) respectively. LDPE was found to exhibit the fastest thermolysis rates, due to the tertiary carbon-carbon bonds at the branch points being more susceptible to thermolysis than linear C-C sigma bonds in the PE chain.

Ballice[239] degraded powdered LDPE and HDPE under non-isothermal conditions. The activation energies for 1-olefin production from LDPE and HDPE were found to be 118.7 kJ/mol and 124.7 kJ/mol respectively. The activation energies for *n*-paraffin production from LDPE and HDPE were 35.6 kJ/mol and 41.6 kJ/mol respectively.

Garforth *et al.*,[240] found the average activation energy for the thermal degradation of HDPE to be 255 kJ/mol, whilst catalytic degradation was found to reduce the energy of activation (77-201 kJ/mol) significantly. Incorporation of aluminium into the frameworks of the catalysts were said to generate both Brønsted- and Lewis-acid sites, leading to a notable reduction in the activation energy. Lin *et al.*,[241] heated HDPE in the presence of zeolite US-Y up to 500°C and found activation energies of degradation of

87-115 kJ/mol, with a mean value of 101 kJ/mol. In relation to the results obtained in our study, these low activation energy values would appear to correspond with reduction in the energy of a free radical mechanism, rather than to deprotonation energy or the initiation of a Lewis-acid catalysed reaction.

Tables 4.11-4.12 display the activation energies of the degradation of pure PPA (MW = 12,000) and PPB (MW = 190,000) respectively, whilst Tables 4.13-4.14 display the activation energies calculated for pure PET and PS.

Table 4.11: Activation energies of pure PPA and catalysts (kJ/mol)

PPA	E_a^{C+B}	T of E_a^{C+B}	E_a^{C+L}	T of E_a^{C+L}	$E_a\bullet$	T of $E_a\bullet$	$E_a\cdot\bullet$	T of $E_a\cdot\bullet$
No Catalyst					122 ± 6	359-392	182 ± 10	402-437
Fulacolor			169 ± 9	202-258	85 ± 5	287-344		
Fulcat 435					73 ± 4	264-324		
Fulmont			142 ± 7	248-281	88 ± 5	284-340		
EPZE			173 ± 9	225-252	85 ± 5	275-319		
EPZG					89 ± 5	299-392		
EPZ10			212 ± 11	205-232	93 ± 5	259-305		
CeY			320 ± 16	233-249	143 ± 8	261-287		
LaY					53 ± 3	257-321		
23z			$201 \pm 10?$	310-384	$201 \pm 10?$	310-384		
280z			$144 \pm 8?$	328-403	$144 \pm 8?$	328-403		

For pure polypropylene A (MW = 12,000), degradation in the presence of Fulacolor, Fulmont, EPZE and EPZ10 clays and CeY zeolite was seen to have occurred *via* a Lewis-acid catalysed reaction. Fulmont clay required the least energy of the five catalysts to initiate this type of reaction, which is consistent with it displaying one of the largest concentrations of Lewis-acid sites of the catalysts tested (third out of the ten catalysts). EPZE also required one of the lowest amounts of energy to initiate the

carbocation degradation mechanism. This also corresponds with the clay exhibiting the second highest concentration of Lewis-acid sites of all the catalysts.

The second activation energy seen for the five catalysts corresponded to the initiation of the free radical degradation mechanism ($E_a\bullet$) which occurred at higher temperatures than the carbocation mechanism. The value of $E_a\bullet$ was found to be reduced in the presence of the four clay catalysts, whereas for CeY zeolite, the activation energy for free radical degradation appeared to increase by 21 ± 1 kJ/mol (which could be attributed to experimental error).

Fulcat 435, EPZG, LaY, 23z and 280z were found to not initiate a carbocation degradation mechanism. Fulcat 435, EPZG and LaY were successful in reducing the activation energy of free radical decomposition, with the largest reduction of 69 ± 2 kJ/mol occurring for LaY zeolite. However, the values of E_a for the ZSM-5 zeolites (23z and 280z) are difficult to assign. As no distinct value for $E_a\cdot\bullet$ was evident for these two zeolites from the analysis of the TGA curves, it is possible that the larger values found for E_a are in fact combined activation energies of the initiation of the free radical mechanism and the subsequent rearrangement and β-scission as the reaction proceeds (especially at the higher end of the temperature range over which the energies applied). It may be that this is not an $E_a\bullet$ value, but an $\mathbf{E_a}^{\mathbf{C+L}}$ value. However, there is insufficient evidence from the data available to make a confident assignment.

The non-catalytic degradation of pure PPA was found to produce only 1% residue, whilst in the presence of Fulacolor clay the amount of residue increased to 3%. Most

other catalysts produced 3-7% residue with the exception of LaY (12% residue) and CeY (14% residue).

Table 4.12: Activation energies of pure PPB and catalysts (kJ/mol)

PPB	E_a^{C+B}	T of E_a^{C+B}	E_a^{C+L}	T of E_a^{C+L}	$E_a\bullet$	T of $E_a\bullet$	$E_a\cdot\bullet$	T of $E_a\cdot\bullet$
No Catalyst					234 ± 12	397-419	385 ± 20	441-473
Fulacolor			143 ± 8	283-311				
Fulcat 435			91 ± 5	284-324				
Fulmont			290 ± 15	359-403				
EPZE			106 ± 6	283-316	228 ± 12	355-375		
EPZG	973 ± 49	337-345	189 ± 10	359-390				
EPZ10			145 ± 8	278-324	181 ± 9	343-376		
CeY			141 ± 8	309-346	224 ± 12	369-394		
LaY			175 ± 9	291-322	208 ± 11	335-389		
23z			262 ± 13	353-385				
280z			233 ± 12	351-415				

For pure polypropylene B (MW = 190,000), degradation in the presence of EPZG was found to have been initiated by a Si-OH protonation of the polymer. The clay had been found to exhibit the fourth largest concentration of Brønsted-acid sites of the ten catalysts, but did not appear successful in reducing the deprotonation energy significantly. PPB decomposed with all ten catalysts was thought to have occurred *via* Lewis-acid removal of hydride ions. The lowest activation energy of these Lewis-acid catalysed reactions was seen for Fulcat 435 clay. The success of Fulcat 435 in initiating a carbocation degradation mechanism of very low activation energy (91 ± 5 kJ/mol) may be attributed to its good surface area and surface acidity properties. EPZE also required one of the lowest amounts of energy to initiate the carbocation degradation mechanism (106 ± 6 kJ/mol). This also corresponds with the clay exhibiting the second highest concentration of Lewis-acid sites of all the catalysts.

The second activation energy seen for EPZE, EPZ10, CeY and LaY corresponded to the initiation of the free radical degradation mechanism ($E_a\bullet$) which occurred at higher temperatures than the carbocation mechanism. The value of $E_a\bullet$ was found to be reduced in the presence of the four catalysts, with the greatest reduction occurring for EPZ10 clay (reduced by 53 ± 3 kJ/mol).

The non-catalytic degradation of pure PPB was found to produce only 1% residue, whilst in the presence of Fulcat 435 clay the amount of residue increased to 3%. Most other catalysts produced 3-7% residue with the exception of LaY (11% residue) and CeY (13% residue).

Table 4.13: Activation energies of pure PET and catalysts (kJ/mol)

PET	E_a^{C+B}	T of E_a^{C+B}	E_a^{C+L}	T of E_a^{C+L}	$E_a\bullet$	T of $E_a\bullet$	$E_a\bullet$	T of $E_a\bullet$
No Catalyst					378 ± 19	396-411	280 ± 14	416-445
Fulacolor					242 ± 12	416-451		
Fulcat 435					171 ± 9	393-450		
Fulmont	575 ± 29	389-401			289 ± 15	414-448		
EPZE					237 ± 12	400-449		
EPZG					242 ± 12	405-443		
EPZ10					191 ± 10	375-441		
CeY					314 ± 16	409-447		
LaY					268 ± 14	420-450		
23z	569 ± 29	388-406			269 ± 14	415-451		
280z					270 ± 14	415-451		

For pure polyethylene terephthalate, degradation in the presence of Fulmont clay and 23z zeolite was found to have been initiated by a Si-OH protonation of the polymer. The clay had been found to exhibit the fourth largest concentration of Brønsted-acid sites of the ten catalysts. In comparison, 23z exhibited the third-lowest number of

Brønsted sites and a high Si/Al$_{tot}$ ratio, suggesting low overall Brønsted acidity. Therefore, the energy value relating to deprotonation energy observed for 23z is a surprise. However, both Fulmont and 23z appeared successful in reducing the deprotonation energy by approximately a half (1100 kJ/mol to around 550 kJ/mol). The second activation energy seen for these two catalysts corresponded to the free radical degradation mechanism which occurred at higher temperatures.

Degradation of pure PET in the presence of all ten catalysts resulted in the reduction of the activation energies associated with a free radical mechanism and all subsequent rearrangement reactions (due to the large temperature ranges over which the activation energies applied). The reductions in activation energy for PET do not appear to be as significant as those seen for the less complex polymers such as polyethylene. This could be related to the 'bulky' PET molecule having difficulty accessing the active sites of the catalysts, especially for zeolites which have a rigid structure of specific pore dimensions. The degradation of pure PET in the presence of Fulcat 435 clay produced the greatest reduction in the activation energy of a free radical mechanism. The success of Fulcat 435 in reducing the energy by 207 ± 11 kJ/mol may be attributed to its good surface area and surface acidity properties.

The non-catalytic degradation of pure PET was found to produce 13% residue, which increased when the polymer was heated in the presence of the catalysts. The amount of residue increased to 16-17% with 23z and 280z zeolites, with the largest amount of residue being produced in the presence of CeY (25% residue) and EPZG (26% residue). The production of 26% residue when PET was decomposed with EPZG (FeCl$_3$ deposited on K10 clay) is an unusual result and could be related to the presence of

Fe(III) which could oxidise hydrogen to water at the temperatures used, so increasing aromatisation, graphitisation and coke formation.

Table 4.14: Activation energies of pure PS and catalysts (kJ/mol)

PS	E_a^{C+B}	T of E_a^{C+B}	E_a^{C+L}	T of E_a^{C+L}	$E_a\bullet$	T of $E_a\bullet$	$E_{a'}\bullet$	T of $E_{a'}\bullet$
No Catalyst					100 ± 5	317-368	208 ± 11	402-443
Fulacolor			207 ± 11	241-272	71 ± 4	313-376		
Fulcat 435			109 ± 6	256-302	76 ± 4	317-384		
Fulmont					110 ± 6	290-333	83 ± 5	333-401
EPZE			117 ± 6	257-304	83 ± 5	321-367		
EPZG					111 ± 6	288-334	99 ± 5	336-405
EPZ10			191 ± 10	222-253	73 ± 4	276-393		
CeY					91 ± 5	361-396	221 ± 11	418-439
LaY			280 ± 14	283-312	90 ± 5	343-403		
23z					96 ± 5	310-384		
280z					102 ± 5	328-403		

For pure polystyrene, degradation in the presence of Fulacolor, Fulcat 435, EPZE and EPZ10 clays and LaY zeolite was seen to have occurred *via* a Lewis-catalysed reaction. Of these five catalysts, Fulcat 435 and EPZE clays required the lowest energies to initiate the carbocation mechanism (109 ± 5 and 117 ± 6 kJ/mol respectively). Their success may correspond with the clays exhibiting some of the higher concentration of Lewis-acid sites of the catalysts tested. The second activation energy seen for the five catalysts corresponded to the free radical degradation mechanism and subsequent rearrangement reactions (based on the large temperature range over which the activation energies applied). The value of $E_a\bullet$ was found to be reduced in all these cases.

Fulmont, EPZG, CeY, 23z and 280z were found to not initiate a carbocation degradation mechanism. Four of the five catalysts were successful in reducing the total

activation energy associated with free radical decomposition and the subsequent rearrangement reactions ($E_a\bullet + E_{a'}\bullet$). The only exception occurred for CeY zeolite, where the total energy was increased by 4 kJ/mol. This may be attributed to experimental error.

The non-catalytic degradation of pure PS was found to produce only 1% residue (as for polyethylene and polypropylene), which increased when the polymer was heated in the presence of the catalysts. The amount of residue increased to 4-5% with 23z and 280z zeolites, with the largest amount of residue being produced in the presence of LaY (15% residue) and CeY (18% residue).

From the literature, the thermal degradation of polypropylene was found to be 220 ± 5 kJ/mol, whilst under dynamic conditions, E_a = 223.7 ± 3 kJ/mol.[242] Ciliz, Ekinci and Snape[243] pyrolysed mixtures of PE:PP and PS:PP plastic wastes. Virgin and waste PP were said to give E_a values of 167 kJ/mol and 181 kJ/mol respectively, with the thermogravimetric onset temperature found to be slightly lower for the virgin plastic. Chan and Balke[244] applied first-order kinetics to temperatures less than 421°C (said to be attributed to scission of 'weak links' in the polymer) and found an average value of the activation energy of 98.3 ± 3.1 kJ/mol (23.0 ± 0.7 kcal/mol). This was thought to be associated with the decomposition to free radicals of various oxidised functionalities (e.g. –OOH, -CO-, -CHO, -COOH, *etc.*) added to commercial polypropylene through processing and drying. Additionally, the isotactic, atactic and syndiotactic triads were said to add to the 'weak link' theory in this lower temperature region. The higher activation energy of 327.9 ± 8.6 kJ/mol (78.4 ± 2.0 kcal/mol) was said to be characterised by large weight losses, associated with high temperatures and high

degrees of chain scission. As the value of E_a was found to be similar to the carbon-carbon bond dissociation energy of 320-350 kJ/mol, it was thought that this was associated with random scission throughout the polymer. The activation energy for non-catalytic degradation was said to be 114 kJ/mol – lower than activation energy values reported previously, since the sample powder contained no additives, stabilisers, *etc*. This value of E_a was reduced to 51.2 kJ/mol in the presence of MOR, 59.2 kJ/mol with BEA and 98.2 kJ/mol and 62.2 kJ/mol for two types of ZSM-5. Although MOR was found not to lower degradation temperatures compared to the other catalysts, it decreased the activation energy of PP degradation, suggesting that the scission of C-C bonds begin at higher temperature with smaller segments easily diffusing into MOR pores.[245]

Peterson, Vyazovkin and Wight[246] carried out thermogravimetric analysis on PS, PP and PE, yielding activation energies of 200 kJ/mol, 150-250 kJ/mol and 150-240 kJ/mol respectively. The constancy of the activation energy of PS was said to suggest that the degradation kinetics were limited by a single reaction step, initiated by random scission. The observed variations in the activation energies of PP and PE were said to imply that the degradation kinetics were governed by different processes at the initial and final stages, with the lower values being associated with initiation processes at weak links and the higher values due to degradation initiated by random scission.

From the literature, the activation energy of polystyrene heated from 335-355°C was found to be approximately 20 kcal/mol (84 kJ/mol).[247] Our study found the onset temperature of degradation of pure polystyrene to be 397ºC (without the presence of a catalyst), corresponding to an initial activation energy of 100 ± 5 kJ/mol, followed by

208 ± 11 kJ/mol for subsequent rearrangement reactions. Onset temperature of waste polystyrene was found to be 405ºC, with a total activation energy of 338 ± 17 kJ/mol. The low activation energy value from the literature suggests that the value of E_a was not related to the decomposition of the polymer.

4.2.4.5.2 Waste Polymers and Catalysts

Tables 4.15-4.21 display the activation energies of the waste polymers that decompose in a single degradation step. As well as LDPE, HDPE, PP, PET and PS, the waste plastics of polyamide and polyester also degraded in one step.

Table 4.15: Activation energies of waste LDPE and catalysts (kJ/mol)

LDPE	E_a^{C+B}	T of E_a^{C+B}	E_a^{C+L}	T of E_a^{C+L}	$E_a\bullet$	T of $E_a\bullet$	$E_{a'}\bullet$	T of $E_{a'}\bullet$
No Catalyst					428 ± 22	428-447	354 ± 18	448-462
Fulacolor	721 ± 36	413-425	375 ± 19	430-448				
Fulcat 435	575 ± 29	403-418	274 ± 14	436-473				
Fulmont			417 ± 21	443-493				
EPZE	649 ± 33	413-425	299 ± 15	435-476				
EPZG	670 ± 34	446-459			399 ± 20	465-490		
EPZ10	608 ± 31	426-439			268 ± 14	449-475		
CeY			205 ± 11	436-450				
LaY	808 ± 41	389-403	174 ± 9	410-432				
23z	539 ± 27	394-430						
280z	606 ± 31	391-414	405 ± 21	413-426				

For waste LDPE, degradation in the presence of all catalysts – with the exception of Fulmont clay and CeY zeolite - was thought to have been initiated by a Si-OH protonation of the polymer. The result for CeY is unsurprising due to the low concentration of Brønsted-acid sites exhibited by the polymer. The change of the rate determining reaction to a Brønsted acid catalysed process with waste LDPE and most of

the catalysts may be attributed to the influence of plasticisers on the activity of Lewis acid sites. However, Fulmont clay displayed the third greatest concentration of Brønsted-acid sites, therefore the absence of a Brønsted-acid catalysed reaction at this lower temperature is a surprise. Fulcat 435 and 23z were the most successful in reducing the deprotonation energy by a half (from approximately 1100 kJ/mol to around 550 kJ/mol). LDPE decomposition with Fulacolor, Fulcat 435, Fulmont and EPZE clays, and CeY, LaY and 23z zeolites was thought to have occurred *via* Lewis-acid removal of hydride ions. The lowest activation energy of these seven catalysts was seen for LaY zeolite (as in accordance with pure LDPE) – a surprising result considering the catalyst was fifth out of the seven in relation to the concentration of Lewis-acid sites. One possible explanation is that, on heating of the catalyst, the removal of water exposed the previously hidden Lewis sites, allowing the carbocation mechanism to occur.

The second activation energy seen for EPZG and EPZ10 corresponded to the initiation and subsequent rearrangement reactions of a free radical degradation mechanism (based on the large temperature range over which the activation energies applied). The energy value was reduced in both cases.

The non-catalytic degradation of waste LDPE was found to produce 7% residue, compared to 1% reside for pure LDPE. This decrease in total conversion of the polymer to gaseous products during heating may be attributed to the presence of additives and plasticisers in the waste LDPE which could have hindered the decomposition. In the presence of CeY and LaY zeolites, the residue was found to be 18% of the initial total

mass of the polymer. Once again these were found to be poor in respect of char formation.

Table 4.16: Activation energies of waste HDPE and catalysts (kJ/mol)

HDPE	E_a^{C+B}	T of E_a^{C+B}	E_a^{C+L}	T of E_a^{C+L}	$E_a\bullet$	T of $E_a\bullet$	$E_a,\bullet$	T of $E_a,\bullet$
No Catalyst					460 ± 23	414-430	309 ± 16	438-485
Fulacolor	711 ± 36	391-404	297 ± 15	420-439				
Fulcat 435	1121 ± 56	407-415	512 ± 26	424-445				
Fulmont			513 ± 26	414-437	332 ± 17	450-479		
EPZE			393 ± 20	403-443				
EPZG	630 ± 32	414-436			279 ± 14	450-469		
EPZ10	612 ± 31	389-406	135 ± 7	424-453				
CeY			316 ± 16	409-431				
LaY	727 ± 37	398-410						
23z	991 ± 50	402-410	536 ± 27	410-429				
280z	672 ± 34	409-422						

For waste HDPE, degradation in the presence of all catalysts − with the exception of Fulmont, EPZE and CeY - was thought to have been initiated by a Si-OH protonation of the polymer. The result for CeY is unsurprising due to the low concentration of Brønsted-acid sites exhibited by the polymer. The change of the rate determining reaction to a Brønsted acid catalysed process with waste HDPE and most of the catalysts may be attributed to the influence of plasticisers on the activity of Lewis acid sites. However, EPZE and Fulmont clays displayed the second and third greatest concentration of Brønsted-acid sites respectively, therefore the absence of a Brønsted-acid catalysed reaction at this lower temperature is a surprise. Additionally, Fulcat 435 failed to reduce the deprotonation energy significantly. This is very surprising, considering many other results in which the clay has been a successful reducer of the activation energies of both Brønsted- and Lewis-catalysed reactions.

HDPE decomposition with Fulacolor, Fulcat 435, Fulmont, EPZE and EPZ10 clays, and CeY and 23z zeolites was thought to have occurred *via* Lewis-acid removal of hydride ions. By far the lowest activation energy of these seven catalysts was seen for EPZ10 (135 ± 7 kJ/mol). The success of EPZ10 could be related to its large average pore diameter and average surface acidity properties.

The second activation energy seen for Fulmont and EPZG clays corresponded to the initiation and subsequent rearrangement reactions of a free radical degradation mechanism (based on the large temperature range over which the activation energies applied). The energy value was reduced in both cases.

The non-catalytic degradation of waste HDPE was found to produce only 1% residue (as for pure HDPE), whilst in the presence of most of the catalysts the amount of residue increased 3-7%. Decomposition of HDPE with EPZ10 gave 9% residue, whilst in the presence of CeY and LaY, 15% and 14% respectively of the initial total mass of the polymer remained.

Table 4.17: Activation energies of waste PP and catalysts (kJ/mol)

PP	E_a^{C+B}	T of E_a^{C+B}	E_a^{C+L}	T of E_a^{C+L}	$E_a\bullet$	T of $E_a\bullet$	$E_a\cdot\bullet$	T of $E_a\cdot\bullet$
No Catalyst					288 ± 15	435-457		
Fulacolor			166 ± 9	321-340	212 ± 11	351-390		
Fulcat 435			107 ± 6	299-328	222 ± 11	367-389		
Fulmont			294 ± 15	368-427				
EPZE			309 ± 16	326-342	174 ± 9	357-382		
EPZG	563 ± 29	384-410						
EPZ10			246 ± 13	333-354	137 ± 7	364-385	206 ± 11	387-414
CeY			207 ± 11	306-324	186 ± 10	332-369		
LaY					175 ± 9	308-355		
23z					229 ± 12	341-379		
280z			345 ± 18	355-380			182 ± 9	400-459

For waste polypropylene, degradation in the presence of EPZG was found to have been initiated by a Si-OH protonation of the polymer. EPZG clay had been found to exhibit the fourth largest concentration of Brønsted-acid sites of the ten catalysts and appeared successful in reducing the deprotonation energy by a half (from approximately 1100 kJ/mol to around 550 kJ/mol). Comparing the results of waste PP with pure polypropylene B, the deprotonation energy for PPB when degraded with EPZG was found to be 973 ± 49 kJ/mol, in comparison to 563 ± 29 kJ/mol for the waste polymer. This large difference in energy could be attributed to the temperature range over which the energies applied. The higher energy seen for PPB corresponded to a temperature of 337-345ºC, whilst the lower deprotonation energy for waste PP corresponded to 384-410ºC. It would be expected that at a 50ºC lower temperature, the Brønsted-catalysed reaction would require markedly more energy to initiate.

PP decomposition with Fulacolor, Fulcat 435, Fulmont, EPZE and EPZ10 clays, and CeY and 280z zeolites was thought to have occurred *via* Lewis-acid removal of hydride

ions. The lowest activation energy of these Lewis-acid catalysed reactions was seen for Fulcat 435 clay. The success of Fulcat 435 in initiating a carbocation degradation mechanism of very low activation energy (107 ± 6 kJ/mol) may be attributed to its good surface area and surface acidity properties. Fulacolor also required one of the lowest amounts of energy to initiate the carbocation degradation mechanism (166 ± 9 kJ/mol). This also corresponds with the clay exhibiting the highest concentration of Lewis-acid sites of all the catalysts.

The second activation energy seen for Fulacolor, Fulcat 435, EPZE, EPZ10 and CeY corresponded to the initiation of the free radical degradation mechanism ($E_a\bullet$) which occurred at higher temperatures than the carbocation mechanism. The value of $E_a\bullet$ was found to be reduced in the presence of the five catalysts, with the greatest reduction occurring for EPZ10 clay (reduced by 151 ± 8 kJ/mol).

The non-catalytic degradation of waste PP was found to produce only 1% residue, which did not increase in the presence of EPZG clay. Heating polypropylene in the presence of Fulcat 435 and EPZ10 clays produced residues of 8% and 12% respectively. The largest amount of residue occurred when PP was degraded with CeY (17% residue) and LaY (14% residue) respectively.

Table 4.18: Activation energies of waste PET and catalysts (kJ/mol)

PET	E_a^{C+B}	T of E_a^{C+B}	E_a^{C+L}	T of E_a^{C+L}	$E_a\bullet$	T of $E_a\bullet$	$E_a\cdot\bullet$	T of $E_a\cdot\bullet$
No Catalyst					306 ± 16	427-452		
Fulacolor	644 ± 33	391-408			260 ± 13	417-443		
Fulcat 435					180 ± 9	397-452		
Fulmont					298 ± 15	412-448		
EPZE	467 ± 24	374-392			249 ± 13	400-443		
EPZG	535 ± 27	380-398			287 ± 15	407-444		
EPZ10			338 ± 17	381-403	219 ± 11	411-446		
CeY					302 ± 15	410-447		
LaY					255 ± 13	416-456		
23z					279 ± 14	402-454		
280z	741 ± 37	388-400			257 ± 13	412-450		

For waste polyethylene terephthalate, degradation in the presence of Fulacolor, EPZE, EPZG and 280z was found to have been initiated by a Si-OH protonation of the polymer. Fulacolor, EPZE and EPZG clays had been found to exhibit some of the largest concentration of Brønsted-acid sites of the ten catalysts (first, second and fourth greatest respectively). In comparison, 280z exhibited the second-lowest number of Brønsted sites and a high Si/Al_{tot} ratio, suggesting low overall Brønsted acidity. Therefore, the energy value relating to deprotonation energy observed for 280z is a surprise. The second activation energy seen for these four catalysts corresponded to the free radical degradation mechanism which occurred at higher temperatures.

PET decomposition with EPZ10 clay was thought to have occurred *via* Lewis-acid removal of hydride ions. The success of EPZ10 could be related to its large average pore diameter gifting access to the bulky PET molecules and allowing the carbocation mechanism to occur.

Degradation of waste PET in the presence of all ten catalysts resulted in the reduction of the activation energies associated with a free radical mechanism and all subsequent rearrangement reactions (due to the large temperature ranges over which the activation energies applied). The reductions in activation energy for PET do not appear to be as significant as those seen for the less complex polymers such as polyethylene. This could be related to the 'bulky' PET molecule having difficulty accessing the active sites of the catalysts, especially for zeolites which have a rigid structure of specific pore dimensions. The greatest reduction in activation energy was seen with Fulcat 435 – consistent with the results for the degradation of pure PET. The success of Fulcat 435 clay in reducing the energy by 126 ± 7 kJ/mol (waste PET) and 207 ± 11 kJ/mol (pure PET) may be attributed to its good surface area and surface acidity properties. The presence of plasticisers in the waste polymer was likely to have inhibited the effectiveness of the catalyst in reducing the activation energy of the free radical mechanism, so explaining the differences between the two values above.

The non-catalytic degradation of waste PET was found to produce 13% residue (as for pure PET), which increased when the polymer was heated in the presence of the catalysts. The amount of residue increased to 18% with EPZE, EPZ10, 23z and 280z, with the largest amount of residue being produced in the presence of CeY (26% residue) and Fulcat 435 (26% residue).

Table 4.19: Activation energies of waste PS and catalysts (kJ/mol)

PS	E_a^{C+B}	T of E_a^{C+B}	E_a^{C+L}	T of E_a^{C+L}	$E_a\bullet$	T of $E_a\bullet$	$E_a{}'\bullet$	T of $E_a{}'\bullet$
No Catalyst					338 ± 17	409-435		
Fulacolor			194 ± 10	343-438				
Fulcat 435			177 ± 9	360-441				
Fulmont			340 ± 17	372-421				
EPZE			278 ± 14	363-427				
EPZG			321 ± 16	376-420				
EPZ10			304 ± 16	364-395	380 ± 19	403-423		
CeY			167 ± 9	371-414				
LaY			263 ± 14	367-425				
23z			367 ± 19	372-415				
280z			320 ± 16	376-418				

For waste polystyrene, degradation in the presence of all ten catalysts was thought to have occurred *via* Lewis-acid removal of hydride ions. The lowest activation energies of these Lewis-acid catalysed reactions were seen for CeY zeolite and Fulcat 435 clay. The success of Fulcat 435 in initiating a carbocation degradation mechanism of low activation energy (177 ± 9 kJ/mol) may be attributed to its good surface area and surface acidity properties. However, the success of CeY is surprising, in that the zeolite displayed the second-lowest concentration of Lewis-acid sited of all the catalysts. The positive result could be attributed to the exposure of 'hidden' Lewis sites at a higher temperature, and the high surface area of the catalyst allowing access to the bulky phenyl groups on alternate carbon atoms of the polymer.

The second activation energy seen for EPZ10 corresponded to the free radical degradation mechanism and subsequent rearrangement reactions (based on the large temperature range over which the activation energies applied).

The non-catalytic degradation of waste PS was found to produce 3% residue (slightly more than the 1% residue seen for pure PS). The amount of residue increased significantly in the presence of LaY and CeY (17% and 22% residue respectively).

Table 4.20: Activation energies of waste PA and catalysts (kJ/mol)

PA	E_a^{C+B}	T of E_a^{C+B}	E_a^{C+L}	T of E_a^{C+L}	$E_a\bullet$	T of $E_a\bullet$	$E_a\bullet$	T of $E_a\bullet$
No Catalyst					213 ± 11	424-443	161 ± 8	451-459
Fulacolor			272 ± 14	383-411	197 ± 10	413-454		
Fulcat 435			450 ± 23	390-407	176 ± 9	423-465		
Fulmont			379 ± 19	371-401	217 ± 11	411-432		
EPZE			351 ± 18	373-407				
EPZG			356 ± 18	372-403	181 ± 9	416-436		
EPZ10			382 ± 19	372-395	159 ± 8	420-445		
CeY			449 ± 23	370-390	181 ± 9	411-448		
LaY			369 ± 19	377-403	155 ± 8	421-460		
23z			401 ± 20	377-399	226 ± 12	411-435		
280z			429 ± 22	376-398	194 ± 10	417-439		

For waste polyamide, degradation in the presence of all ten catalysts was thought to have occurred *via* Lewis-acid removal of hydride ions. The lowest activation energy for the carbocation mechanism was seen for Fulacolor clay (272 ± 14 kJ/mol). The success of Fulacolor could be attributed to the clay displaying the highest concentration of Lewis-acid sites in relation to the other ten catalysts. The second activation energy seen for nine of these catalysts, corresponded to the free radical mechanism and all subsequent rearrangement reactions (due to the large temperature ranges over which the activation energies applied). The energy values were found to be reduced in seven of the cases by up to 58 ± 3 kJ/mol (in the presence of LaY zeolite), whilst Fulmont and 23z were found to slightly increase $E_a\bullet$ (by up to 13 ± 1 kJ/mol), which could be attributed to experimental error.

The non-catalytic degradation of waste PA was found to produce 13% residue which decreased slightly in the presence of 280z and Fulmont. All other catalysts increased the amount of residue, with the largest amount of residue being produced in the presence of LaY (22% residue) and CeY (26% residue).

Table 4.21: Activation energies of waste PE and catalysts (kJ/mol)

PE	E_a^{C+B}	T of E_a^{C+B}	E_a^{C+L}	T of E_a^{C+L}	$E_a\cdot$	T of $E_a\cdot$	$E_a\cdot\cdot$	T of $E_a\cdot\cdot$
No Catalyst					312 ± 16	418-439		
Fulacolor			358 ± 18	392-432				
Fulcat 435			486 ± 25	390-410	272 ± 14	419-456		
Fulmont			287 ± 15	379-442				
EPZE			278 ± 14	381-439				
EPZG			266 ± 14	379-434				
EPZ10			274 ± 14	382-427				
CeY					328 ± 17	409-440		
LaY					299 ± 15	405-445		
23z			276 ± 14	386-445				
280z			276 ± 14	391-442				

For waste polyester, degradation in the presence of eight catalysts was thought to have occurred *via* Lewis-acid removal of hydride ions. The lowest activation energy for the carbocation mechanism was seen for the ZSM-5 zeolites (23z and 280z). This could possibly be due to the increase in Lewis acidity of the catalysts on heating (by removal of water that had been obscuring Lewis-acid sites during surface acidity measurements). The second activation energy seen for Fulcat 435 corresponded to the free radical mechanism and all subsequent rearrangement reactions (due to the large temperature ranges over which the activation energy applied). The energy value was found to be reduced by 40 ± 2 kJ/mol.

For CeY zeolite, the activation energy corresponding to a free radical mechanism appeared to increase slightly (up by 16 ± 1 kJ/mol). This could be attributed to experimental error.

The non-catalytic degradation of waste polyester was found to produce 17% residue, which increased to 22-28% in the presence of eight of the ten catalysts. The least amount of residue occurred for EPZ10 clay (18% residue), whilst the greatest amount of remaining material occurred for CeY zeolite (31% residue).

This study found that polybutadiene, polyurethane RC35, polyurethane foam and polyacrylonitrile decomposed *via* two steps. No carbocation degradation mechanism appeared to be found during the thermogravimetric analysis of these polymers. However, in all cases, the presence of a catalyst was seen to reduce the activation energies of each of the degradation steps (Ea_1 and Ea_2).

Table 4.22: Activation energies of waste PB and catalysts (kJ/mol)

PB	Ea_1	T of Ea_1	Ea_2	T of Ea_2
No Catalyst	156 ± 8	283-299	515 ± 26	387-395
Fulacolor	74 ± 4	279-301	311 ± 16	355-383
Fulcat 435	82 ± 4	297-320	285 ± 15	358-377
Fulmont	90 ± 5	266-308	239 ± 12	353-382
EPZE	68 ± 4	263-313	262 ± 13	346-373
EPZG	76 ± 4	259-307	301 ± 15	342-367
EPZ10	71 ± 4	262-213	267 ± 14	349-372
CeY	96 ± 5	244-306	265 ± 13	347-376
LaY	238 ± 12	352-382	100 ± 5	395-440
23z	85 ± 5	261-316	261 ± 13	361-382
280z	79 ± 4	273-315	257 ± 13	349-379

Straus and Madorsky[227] found the activation energy for non-catalytic degradation of polybutadiene as being 62 kcal/mol (259 kJ/mol). In this study, all catalysts were very successful in reducing the activation energy of the initiation step of the free radical mechanism (Ea_1) by 60-88 kJ/mol. The second activation energy was reduced by 204-276 kJ/mol. LaY appears to be different from the other catalysts as the Ea_1 for the first reaction has increased, signifying that a mechanistic change (probably Brønsted acid catalysis), has occurred. No particular clay or zeolite appeared to stand out as the best performer in aiding the degradation of polybutadiene. All TGA runs of PB decomposition were found to produce 30-42% residue.

Table 4.23 and Table 4.24 display the activation energies of degradation of two polyurethane samples. Day, Cooney and MacKinnon[248] found the activation energies at 10% weight loss for the first and second stages of degradation of polyurethane to be 122.0 kJ/mol and 181.6 kJ/mol respectively. Polyurethane contaminated with dirt gave activation energies of 124.1 kJ/mol and 159.5 kJ/mol, and reduced the weight loss temperature from 263°C to 255.5°C. Our study gave non-catalytic activation energies for Ea_2 of PU(RC35) and PU(foam) of 618 ± 31 kJ/mol and 576 ± 29 kJ/mol respectively. These values appear far larger than those reported, but correspond to full degradation of the polymer, rather than the first 10% weight loss.

Table 4.23: Activation energies of waste PU(RC35) and catalysts (kJ/mol)

PU(RC35)	Ea$_1$	T of Ea$_1$	Ea$_2$	T of Ea$_2$
No Catalyst	529 ± 27	388-395	618 ± 31	427-436
Fulacolor	199 ± 10	310-349	262 ± 14	383-422
Fulcat 435	173 ± 9	316-351	198 ± 10	396-425
Fulmont	291 ± 15	327-345	151 ± 8	353-387
EPZE	191 ± 10	326-376		
EPZG	265 ± 14	309-356		
EPZ10	207 ± 11	305-330	234 ± 12	342-371
CeY	210 ± 10	317-346	276 ± 14	377-422
LaY	210 ± 10	335-361	280 ± 14	388-420
23z	255 ± 13	321-354	211 ± 11	396-427
280z	320 ± 16	321-431	187 ± 10	397-426

For PU(RC35), all catalysts were very successful in reducing the activation energy of the initiation step of the free radical mechanism (Ea$_1$) by 209-356 kJ/mol. The second activation energy was reduced by 338-467 kJ/mol.

The non-catalytic degradation of waste PU(RC35) was found to produce 4% residue, which decreased to 3% in the presence of EPZG clay. Degradation of the polymer in the presence of eight of the catalysts produced residue from 7-16% of the initial weight of the plastic, with CeY zeolite producing the most residue of 20%.

Table 4.24: Activation energies of waste PU(foam) and catalysts (kJ/mol)

PU(foam)	Ea_1	T of Ea_1	Ea_2	T of Ea_2
No Catalyst	420 ± 21	275-282	576 ± 29	394-399
Fulacolor	125 ± 7	230-285	280 ± 14	356-397
Fulcat 435	144 ± 8	229-285	174 ± 9	335-369
Fulmont	128 ± 7	214-274	272 ± 14	366-394
EPZE	150 ± 8	238-264	183 ± 10	320-342
EPZG	125 ± 7	212-267	272 ± 14	364-389
EPZ10	133 ± 7	219-275	150 ± 8	328-358
CeY	144 ± 8	225-259	294 ± 15	363-400
LaY	141 ± 7	220-276	262 ± 13	352-406
23z	133 ± 7	219-271	246 ± 13	370-409
280z	152 ± 8	226-270	262 ± 13	344-369

For PU(foam), all catalysts were very successful in reducing the activation energy of the initiation step of the free radical mechanism (Ea_1) by 268-295 kJ/mol. The second activation energy was reduced by 282-426 kJ/mol. EPZ10 and Fulcat 435 clays appeared to perform the best. EPZ10 was found to exhibit the largest average pore diameter of all the catalysts which may have allowed the bulkier polyurethane molecules to access the catalyst's active sites. The success of Fulcat 435 may be attributed to its good surface area and surface acidity properties.

The catalytic degradation of PU(foam) was found to increase the production of residue from 5% to up to 20% of the initial mass of the polymer. CeY zeolite produced the greatest amount of remaining material, whilst 280z was the only catalyst that did not increase residue formation above 5%.

Table 4.25: Activation energies of waste PAN and catalysts (kJ/mol)

PAN	Ea$_1$	T of Ea$_1$	Ea$_2$	T of Ea$_2$
No Catalyst	1014 ± 51	354-358	307 ± 16	425-441
Fulacolor	608 ± 31	330-341	88 ± 5	389-431
Fulcat 435	662 ± 33	328-340	76 ± 4	391-459
Fulmont	589 ± 30	321-330	90 ± 5	378-451
EPZE	648 ± 33	320-329	120 ± 6	388-437
EPZG	523 ± 27	314-330	104 ± 6	401-440
EPZ10	428 ± 22	317-325	227 ± 12	330-351
CeY	700 ± 35	320-330	84 ± 5	370-410
LaY	642 ± 32	325-333	328 ± 17	335-344
23z	733 ± 37	316-332	79 ± 4	383-457
280z	823 ± 42	318-328	90 ± 5	378-451

For polyacrylonitrile, all catalysts were very successful in reducing the activation energy of the initiation step of the free radical mechanism (Ea$_1$) by 191-586 kJ/mol. The second activation energy was reduced by up to 231 ± 12 kJ/mol. EPZ10 was found to be the greatest reducer of the free radical initiation step (1014 ± 51 kJ/mol reduced to 428 ± 22 kJ/mol) which could be related to the large pore sizes admitting the bulky PAN molecules to the active sites. Fulcat 435 was found to reduce Ea$_2$ by the greatest amount, which could be related to the good surface area and surface acidity characteristics of the clay.

All TGA runs of PAN decomposition were found to produce 45-60% residue (with 50% residue for non-catalytic degradation as mentioned in Section 4.2.4.1). Less residue was observed in the presence of 280z, 23z and EPZE, whilst the greatest amount of residue occurred with LaY and CeY zeolites.

195

This study found that polyvinyl chloride and polymethyl methacrylate decomposed *via* three steps. No carbocation degradation mechanism appeared to be found during the thermogravimetric analysis of these polymers. However, in all cases, the presence of a catalyst was seen to reduce the activation energies of each of the degradation steps (Ea_1, Ea_2 and Ea_3).

Table 4.26 displays the activation energies of degradation of waste polyvinyl chloride. Day, Cooney and MacKinnon[248] found the activation energy at 10% weight loss of PVC to be 141.8 kJ/mol. This study found the activation energy of the first degradation step of PVC as being 230 ± 12 kJ/mol (without a catalyst), over the temperature range 242-254ºC.

Table 4.26: Activation energies of waste PVC and catalysts (kJ/mol)

PVC	Ea_1	T of Ea_1	Ea_2	T of Ea_2	Ea_3	T of Ea_3
No Catalyst	230 ± 12	242-254	295 ± 15	312-323	660 ± 33	488-495
Fulacolor	97 ± 5	220-248	105 ± 6	284-311	414 ± 21	464-481
Fulcat 435	93 ± 5	215-246	100 ± 5	289-311	379 ± 19	465-481
Fulmont	119 ± 6	215-239	102 ± 5	278-302	277 ± 14	455-475
EPZE	95 ± 5	210-238	102 ± 5	279-302	120 ± 6	460-489
EPZG	105 ± 6	202-238	100 ± 5	273-296	361 ± 18	437-454
EPZ10	99 ± 5	211-235	105 ± 6	272-298	248 ± 13	451-469
CeY	110 ± 6	211-239	105 ± 6	305-328	454 ± 23	450-461
LaY	94 ± 5	235-266	119 ± 6	281-320	357 ± 18	445-470
23z	167 ± 9	196-214	99 ± 5	297-345	220 ± 11	436-469
280z	133 ± 7	211-236	94 ± 5	279-304	287 ± 15	448-469

For polyvinyl chloride, all catalysts were very successful in reducing the activation energy of the initiation step of the free radical mechanism (Ea_1) by 63-137 kJ/mol. The

second activation energy was reduced by 176-201 kJ/mol, whilst Ea_3 was reduced by 206-540 kJ/mol. EPZE appeared to stand out as the greatest overall reducer of activation energy, which may be related to the clay exhibiting the second highest number of Brønsted and Lewis acid sites compared to the other catalysts.

All TGA runs of PVC decomposition were found to produce 37-50% residue (with 50% residue for non-catalytic degradation as mentioned in Section 4.2.4.1). The least amount of residue was observed with EPZE clay.

Table 4.27 displays the activation energies of the degradation of waste polymethyl methacrylate. Jellinek and Luh studied the thermal degradation of isotactic and syndiotactic PMMA over a range of temperatures from 300-400°C. For atactic PMMA, the overall activation energy was found to be around 36 kcal/mol (150 kJ/mol). For the syndiotactic polymer, the overall energy of activation was given by $E_a \cong E_i$.[249] Barlow, Lehrle and Robb found the activation energy for degradation of a thin film of PMMA was 25 kcal/mol (104 kJ/mol).[250] In comparison, this study found three distinct activation energies of 329 ± 17 kJ/mol, 309 ± 16 kJ/mol and 357 ± 18 kJ/mol, corresponding to three weight loss steps.

Table 4.27: Activation energies of waste PMMA and catalysts (kJ/mol)

PMMA	Ea_1	T of Ea_1	Ea_2	T of Ea_2	Ea_3	T of Ea_3
No Catalyst	329 ± 17	243-249	309 ± 16	336-346	357 ± 18	376-388
Fulacolor	112 ± 6	199-244	125 ± 7	273-317	185 ± 10	358-401
Fulcat 435	103 ± 6	210-238	145 ± 8	270-304	185 ± 10	353-397
Fulmont	132 ± 7	201-230	147 ± 8	280-314	221 ± 11	350-382
EPZE	113 ± 6	215-232	133 ± 7	280-304	192 ± 10	343-398
EPZG	151 ± 8	192-216	116 ± 6	256-300	191 ± 10	346-383
EPZ10	123 ± 7	200-228	154 ± 8	290-320	180 ± 9	363-387
CeY	150 ± 8	221-237	148 ± 8	296-316	224 ± 12	352-380
LaY	206 ± 11	255-274	168 ± 9	298-314	204 ± 11	356-380
23z	138 ± 7	221-250	120 ± 6	295-319	211 ± 11	351-379
280z	128 ± 7	205-231	126 ± 7	263-302	192 ± 10	349-383

For polymethyl methacrylate, all catalysts were very successful in reducing the activation energy of the initiation step of the free radical mechanism (Ea_1) by 123-226 kJ/mol. The second activation energy was reduced by 141-193 kJ/mol, whilst Ea_3 was reduced by 133-177 kJ/mol. The clay catalysts appeared to perform slightly better than the zeolites. All TGA runs of PMMA decomposition were found to produce les than 10% residue, with the exception of CeY and LaY zeolites (17% and 23% residue respectively).

4.3 Thermogravimetric Conclusions

Catalytic degradation of the polymer samples resulted in a decrease in the onset temperature of decomposition in comparison to the corresponding thermal (non-catalytic) degradation. A significant decrease in the activation energy of the free radical degradation mechanism was also found in most cases. However, with some catalysts and polymers, two further activation energies were found to occur at a lower temperature than the initiation of the free radical mechanism (E_a•). The first was

thought to be related to the Si-OH protonation (B, Brønsted) of the polymer at uncatalysed energies of approximately 1100 kJ/mol, whilst the second was thought to represent Lewis-acid removal of hydride ions (H⁻) from the polymer. The deprotonation energy and Lewis-acid catalysed reaction energy were termed E_a^{C+B} and E_a^{C+L} respectively.

Waste polymers PB, PVC, PAN, PU(RC35), PU(foam) and PMMA, were all found to decompose *via* two or three separate weight-loss steps. The presence of the clay or zeolite reduced the activation energy of the free radical degradation process and may even have changed the mechanism to an acid catalysed process.

The success of each catalyst in reducing the onset temperatures and activation energies of the plastics was found to be very much dependent on both the structure of the catalyst and the polymer molecule. Limitations can often arise with zeolites, due to their rigid pore structure allowing only small molecules to enter the internal active sites. However, if accessible, zeolites have the capability to reduce T_{onset} significantly and also increase the rate of degradation. Due to the differences in the structures of the polymer samples – from simple molecules such as high-density polyethylene to more complex molecules such as polyethylene terephthalate – and the way each plastic interacts with the clay or zeolite, it was difficult to select one individual catalyst as the most successful for polymer recycling. Table 4.28 displays the polymer and catalyst pairs that were thought to have altered the mechanism of polymer decomposition from a free radical process to either a Brønsted- or Lewis-acid catalysed mechanism. By combining these results with the pairings that produced the largest reductions in onset temperature of decomposition, a select group of plastic and catalyst samples were chosen for further analysis.

Table 4.28: Polymer and catalyst pairs showing a change in degradation mechanism

Polymer	Fulacolor	Fulcat	Fulmont	EPZE	EPZG	EPZ10	CeY	LaY	23z	280z
Pure										
LDPE	X	X	X			X	X	X	X	X
HDPE	X	X	X	X	X	X	X	X	X	X
PPA	X		X	X		X	X			
PPB	X	X	X	X	X	X	X	X	X	X
PET			X						X	
PS	X	X		X		X		X		
Waste										
LDPE	X	X	X	X	X	X	X	X	X	X
HDPE	X	X	X	X	X	X	X	X	X	X
PP	X	X	X	X	X	X	X			X
PET	X			X	X	X				X
PS	X	X	X	X	X	X	X	X	X	X
PA	X	X	X	X	X	X	X	X	X	X
PE	X	X	X	X	X	X			X	X

Fulacolor and EPZ10 clay were found to be the most successful of the catalysts in changing the mechanism of polymer degradation from a free radical process to a Brønsted- or Lewis-acid catalysed reaction. These were closely followed by Fulcat 435 and Fulmont clays and 280z zeolite. From the catalyst characterisation experiments in Chapter 2, Fulacolor clay had been found to exhibit overall the most promising properties (see Table 2.10), including the highest concentration of Brønsted- and Lewis-acid sites. This explains Fulacolor's good performance in the thermogravimetric runs. Surprisingly, EPZ10 clay was seen to initiate a carbocation degradation mechanism on many occasions, despite coming only sixth out of ten catalysts when rating overall catalyst performance. EPZ10 displayed the highest average pore diameter of all catalysts tested, suggesting that this particular characteristic may be more significant (by

allowing the polymer molecules access to active sites) than other properties. However, for 280z zeolite which also initiated carbocation degradation mechanisms (and was ranked as the joint eighth best performer of the ten catalysts), the large surface area measurement appeared very significant in its success as a catalyst.

From Table 4.28, CeY and LaY were found to be the two least successful zeolites in initiating a carbocation degradation mechanism. Combining this with the high content of residue formed after each polymer decomposition, these rare-earth Y-zeolites were not investigated further.

From analysing all the thermogravimetric results, Fulcat 435 clay and 23z and 280z zeolites were chosen for further study. Although Fulacolor clay appeared to be slightly more successful than Fulcat 435 in initiating a carbocation degradation mechanism, Fulcat 435 was found to be one of the greatest reducers of the onset temperature of decomposition of plastics – an important result when trying to create the most energetically sound method of polymer recycling. Low-density polyethylene and polypropylene, common plastics found in everyday household waste, were selected as the polymers for further analysis. Coupling a furnace to a mass spectrometer (MS) will allow the products of decomposition to be obtained as a function of temperature. By selecting certain temperatures from the TGA degradation curve and analysing the products formed on heating the polymer/catalyst samples at these temperatures, it will be possible to determine which catalysts and polymers produce optimum results under which operating conditions. Pyrolysis-Gas Chromatography / Mass Spectrometry (Py-GC/MS) will also allow the determination of decomposition products. These experiments are discussed in Chapter 5.

4.4 Differential Thermal Analysis

Knowledge of the energy input required to crack a polymer is an important consideration in deciding whether a catalytic degradation process will be viable for commercialisation, i.e. there must be much more energy available in the products than that required to make them. Differential Thermal Analysis (DTA) is a technique for recording the difference in temperature between a substance and a reference material as a function of either time or temperature. The two specimens are subjected to identical temperature regimes in an environment heated or cooled at a controlled rate, therefore any physical or chemical change occurring in the test sample which involves the evolution of heat will be measured. The resultant DTA curve is not a true *differential* curve, but simply a straightforward *difference* curve. All transformations or reactions involving energy changes in the sample are reflected in the DTA curve.

The modern differential thermal analyser consists of seven basic components: (a) temperature programmer, (b) heating-cooling system, (c) differential temperature-measuring circuit, (d) sample temperature-measuring circuit, (e) sample and/or reference container, (f) recorder and (g) atmosphere control.[251] The heating rate affects peak height, peak width and, for decomposition reactions, peak temperature on the DTA curve. Rates of 8-12°C/min produce peaks of satisfactory size with minimal overlap of neighbouring peaks.

The Shimadzu DTA used in this study had a sample and reference container set-up the same as that displayed in Figure 4.23. The sample is placed in a small cup or crucible which is placed on the small circular disk containing the thermojunction. The individual thermally conducting bases provide a single good path for heat loss from the

sample. However, the temperatures recorded are not those of the sample and the reference, but those of their containers. This system responds more slowly and tends to average out thermal effects, but does allow more accurate quantitative measurement of heats of transition from peak areas.
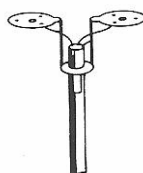
Figure 4.23: DTA sample container[252]

Organic compounds can be examined in either an oxidising atmosphere to enable the burning characteristics to be determined, or in an inert atmosphere to suppress oxidation and so permit melting points, boiling points and phase changes to be observed.[253] A flowing inert atmosphere is desirable for the removal of evolved decomposition products, which would otherwise retard the reaction. Shallow open pans allow good contact between the sample and the atmosphere; hence, better resolution is obtained, giving sharper and well-separated peaks. Additionally, evolved reaction products are removed before they are able to undergo secondary reactions.

The amount of sample, physical nature of the sample and the way that it is packed into the sample container are very important variables. However, In the case of decomposition reactions which proceed *via* a mechanism other than diffusion control, the effect of particle size is generally minimal. The ideal sample would be an infinitely small sphere around the thermocouple junction.

The chosen reference material should match the sample as closely as possible in thermal properties (specific heat, conductivity *etc*.) and should be thermally inert over the whole temperature range. The weight and method of packing of the reference material should be identical to that of the sample to reduce spurious effects. In many calorimetric DTA measurements, an empty metal pan (matched to the sample pan) is used as a reference, the net measured effect then being that of the sample alone. The 'empty pan' approach was used for the DTA experiments in this study.

4.4.1 Interpretation of the DTA Curve

The peaks on a DTA curve arise from both physical and chemical changes. A thermal event in the sample is detected by the deviation of the ΔT signal from the baseline. Key features are signal displacement and peak area which enable heat capacity and enthalpy to be calculated respectively.[254] The area under a DTA peak is defined as the area enclosed between the peak and the interpolated baseline. This area is directly proportional to the total enthalpy change and is not affected by the heat capacity of the sample or the heating rate, provided this is uniform.[255,256] However, the peak area is said to depend on the conductivities of the test sample and the other materials in the furnace and on the conductance between the surface of the specimen-holder block and the furnace wall.[257]

Changes in the slope and sharp changes in the position of the baseline are normally associated with *second-order transitions* (*i.e.* the glass transition), which are accompanied by a change in specific heat, but no change in enthalpy ($\Delta H = 0$). Hence, no peak appears on the DTA curve, but the heat-flow and temperature gradient within the sample are changed by the transition, producing a discontinuity in the baseline.[258]

Variables relating to the heat absorbed or evolved by the sample must be taken into account when evaluating the DTA curve. Slightly before or during a phase transformation or decomposition, a change in sample heat capacity, ΔC_p, occurs, resulting in a change in the temperature difference ΔT. Additionally, loss of products during decomposition results in the sample being cooled. Baseline deviation, especially at the beginning of a run, is a common occurrence, due to an imbalance in heat capacities between the sample and reference thermocouples which is affected by symmetry, particle size and packaging.[259] Table 4.29 displays a number of processes which produce either an exotherm or endotherm in differential thermal analysis.

Table 4.29: Processes giving enthalpic peaks[260]

Process	Exotherm	Endotherm
Solid-solid transition	x	x
Crystallisation	x	
Melting		x
Vapourisation		x
Sublimation		x
Adsorption	x	
Desorption		x
Desolvation (drying)		x
Decomposition	x	x
Solid-solid reaction	x	x
Solid-liquid reaction	x	x
Solid-gas reaction	x	x
Curing	x	
Polymerisation	x	
Catalytic reactions	x	

The shape of the DTA curve is little altered by variations in the activation energy, E_a, or pre-exponential factor, A, but the position and size of the peak do change. Changing the order of reaction, n, causes a drastic change in the shape of the curve. The effects of kinetic parameters on the appearance of a DTA peak are shown in Table 4.30.

Table 4.30: Effect of kinetic parameters on the appearance of a DTA peak[261]

Increase	Effect on Peak		
	Position	Size	Shape
A	Moves to lower T	Increases	Little change
E	Moves to higher T	Decreases	Little change
n	Little change	Decreases	Drastic change

4.4.2 Reaction Kinetics

When a reaction occurs in differential thermal analysis, the change in heat content is indicated by a peak on the DTA curve. If the reaction proceeds at a rate varying with temperature, *i.e.* possesses an activation energy, the position of the peak varies with the heating rate, if other experimental conditions remain fixed. Several factors are said to influence the kinetics and reaction order of simple decomposition reactions, but it has been found that the dominant factor controlling the shape and position of the DTA peak is the nature of the reaction itself.[262] Kinetic parameters for the reaction giving rise to the DTA curve can be accurately determined by an analysis of the shape (slope, area, height) of the curve.[263] The change in state from solid to liquid involves latent heat of fusion. A polymer may consist of amorphous and crystalline regions. The size and degree of the crystallites will affect the broadness of the endotherm melting peak, as smaller crystallites will melt at a lower temperature.[264]

Enthalpy is the measure of the total energy of a thermodynamic system, but cannot be measured directly. Thus, change in enthalpy, ΔH, is often used instead. Enthalpy change is the difference between the enthalpy of the products and the initial enthalpy of the system, and can be positive (endothermic reactions) or negative (exothermic reactions). The definition of enthalpy is:

$$H = U + pV \qquad \text{(Eq. 4.13)}$$

where H = enthalpy of the system

U = internal energy of the system

p = pressure at the boundary of the system and its environment

V = volume of the system

Differentiating Equation 4.13 gives:

$$dH = dU + pdV + Vdp \qquad \text{(Eq.4.14)}$$

For quasi-static (infinitely slow) processes under constant pressure, ΔH is equal to the change in the internal energy of the system (ΔU), plus the work that the system has done on its surroundings. Therefore, the change in enthalpy under such conditions is the heat absorbed (endothermic) or released (exothermic) by a chemical reaction.

The area under the DTA peak is the enthalpy change observed as the polymer undergoes decomposition. Hence, by undertaking differential thermal analysis of the degradation

of plastics in the presence of different catalysts, it is possible to gain insight into the enthalpy of the products formed.

4.4.3   Method of Differential Thermal Analysis

The differential thermal analysis of each of the six pure polymers in the presence of the ten catalysts (polymer-to-catalyst ratio 2:1) was undertaken with a Shimadzu DTA-50 instrument. The experiments were conducted in a nitrogen atmosphere at a heating rate of 10ºC/min up to 550ºC (see Experimental Chapter). The effects on the shape and energy of the decomposition endotherms were recorded and compared.

Sample preparation was kept to a minimum and involved no grinding or shredding of the plastic into small fragments. The catalyst powder was placed in the bottom of the aluminium sample pan and a small piece of untreated polymer (<10 mg) was placed directly on top of the catalyst. No mixing of the polymer and catalyst was undertaken in order to simulate how plastics could be recycled in the future with next to no initial preparation.

4.4.4   Results of Differential Thermal Analysis

Figure 4.24 to Figure 4.29 display the differential thermal analysis of each of the six pure polymers degraded in the presence of the ten catalysts.
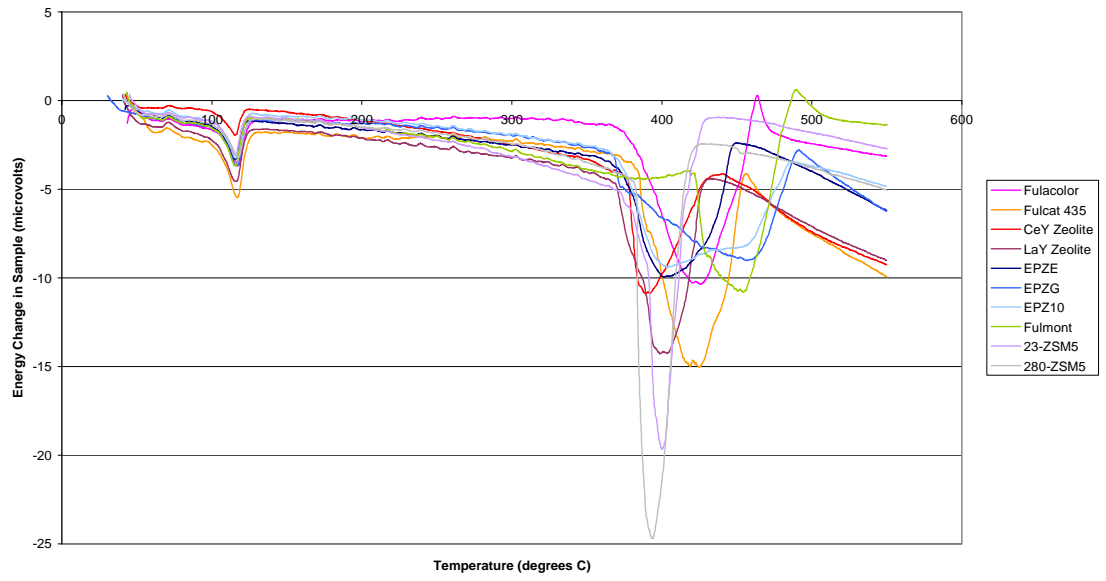
Figure 4.24: DTA of pure LDPE and catalysts
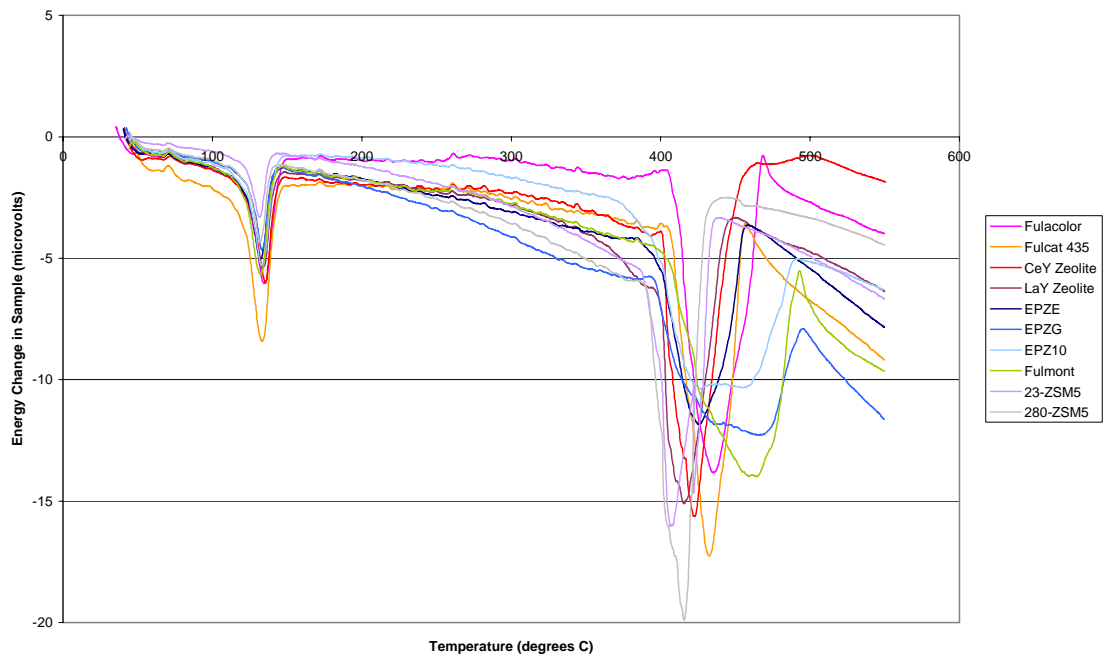
Figure 4.25: DTA of pure HDPE and catalysts

209
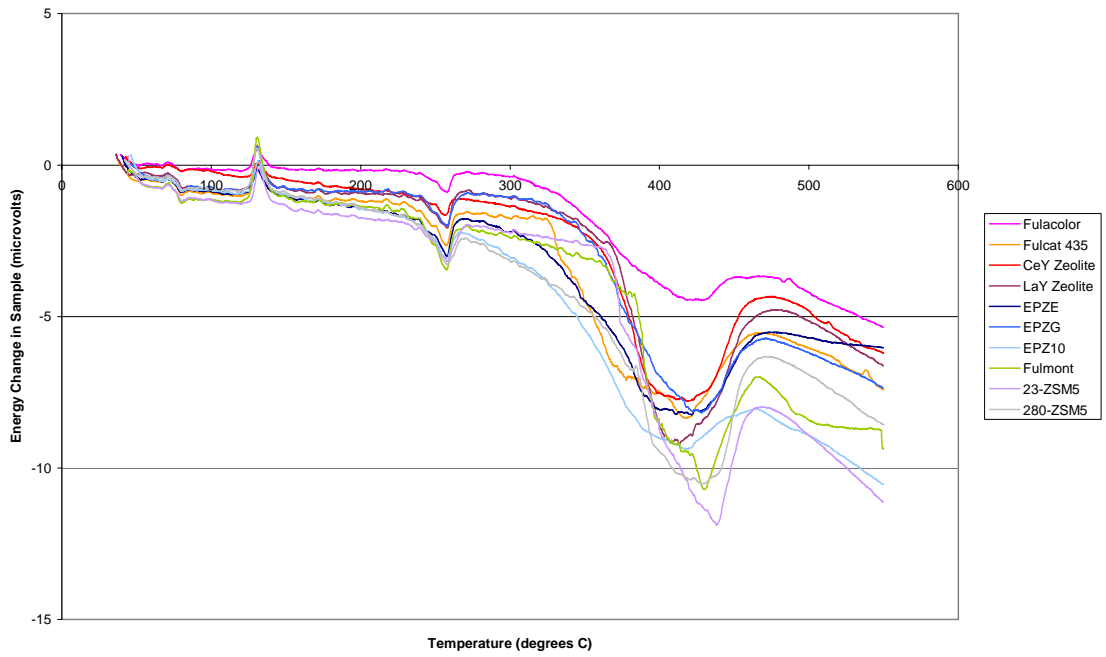
Figure 4.26: DTA of pure PET and catalysts
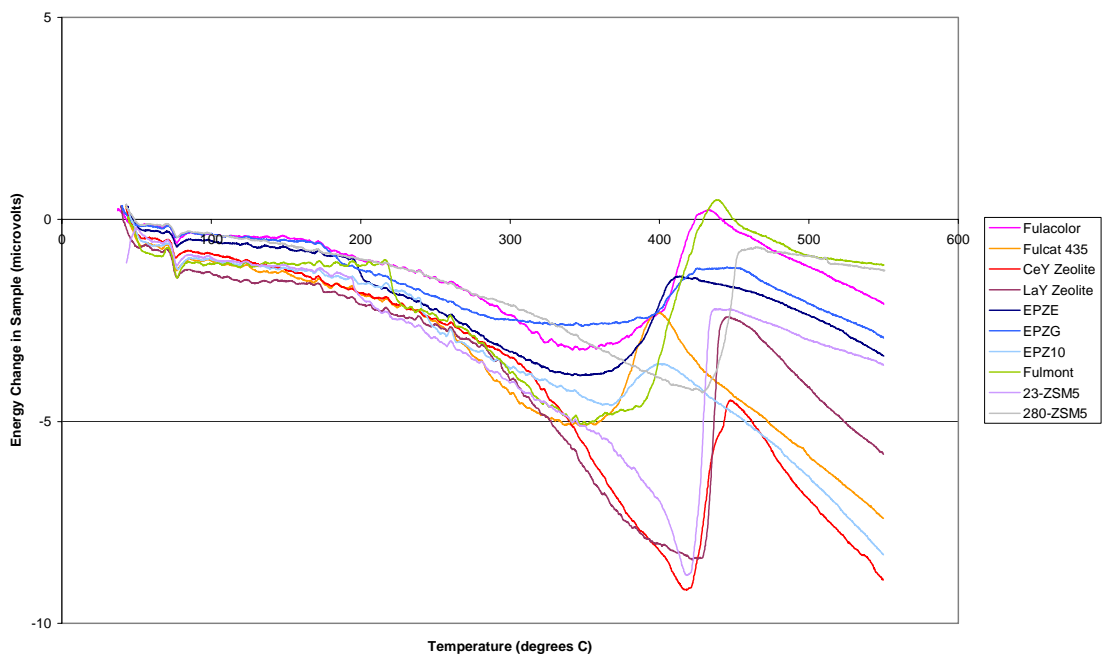
Figure 4.27: DTA of pure PS and catalysts
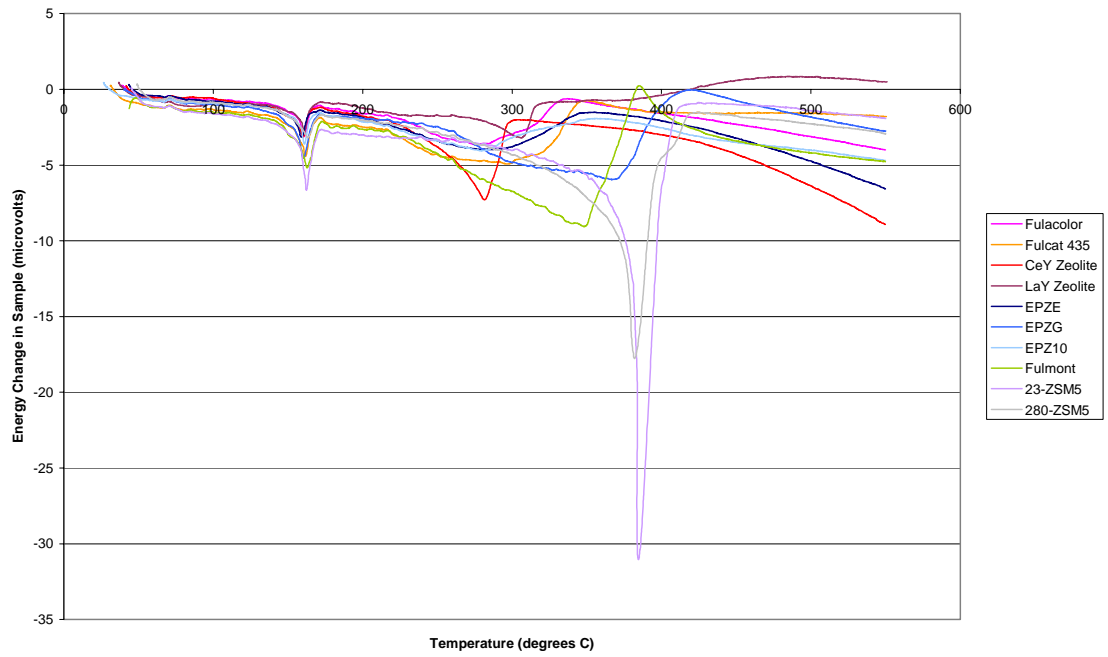
Figure 4.28: DTA of pure PPA and catalysts
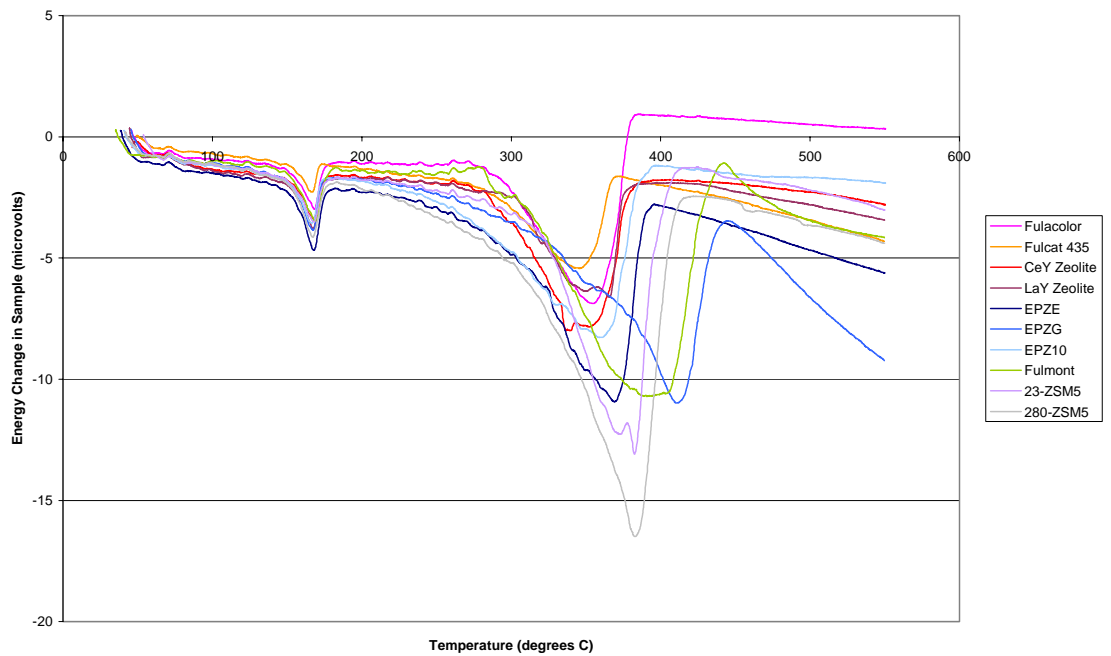
Figure 4.29: DTA of pure PPB and catalysts

211

The differential thermal analysis of waste polyethylene (LDPE, HDPE), polypropylene, polyester, polyvinyl chloride, polystyrene, polyamide, polyurethane and polybutadiene was also undertaken. Figure 4.30 displays the varying DTA curves obtained from the decompositions of these polymers.
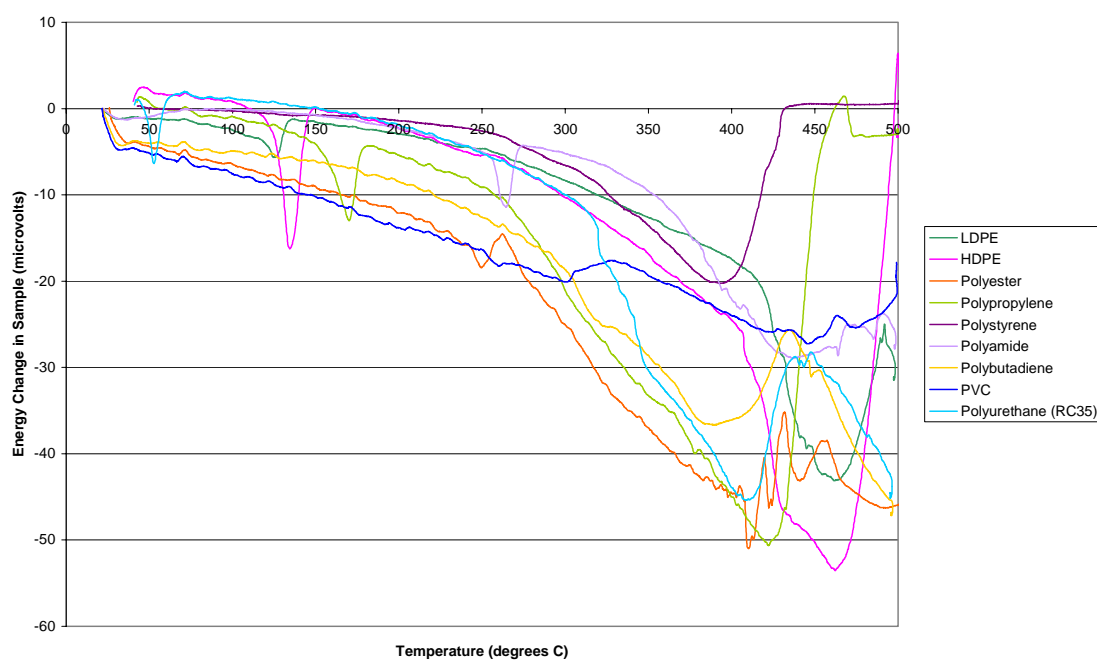
Figure 4.30: DTA of a variety of waste plastic samples

The area of the degradation endotherms for each pure polymer gave an insight into the enthalpy change of decomposition. The polyethylene samples (LDPE, HDPE) were evaluated between 165ºC and 500ºC, whilst the degradation peaks of pure PS, PET, PPA and PPB were calculated over the temperature ranges 165-470ºC, 275-480ºC, 180-430ºC and 190-450ºC respectively. Table 4.31 displays the energies of decomposition for the six pure polymers. Although the differential thermal analyser was calibrated by recording the heat of fusion of indium and zinc standards (see Experimental Chapter),

the energies varied slightly, therefore an error of ±10% should be applied to the experimental results in Table 4.31.

Table 4.31: Energies of decomposition of pure polymers and catalysts (J/g)

	LDPE	HDPE	PET	PS	PPA	PPB
Fulacolor	-851	-869	-516	-506	-497	-437
Fulcat 435	-1558	-1420	-1036	-1039	-711	-656
CeY	-1271	-1134	-848	-1345	-751	-827
LaY	-1599	-1407	-886	-1333	-312	-737
EPZE	-1203	-1382	-1078	-726	-645	-1228
EPZG	-1244	-1955	-883	-575	-821	-1226
EPZ10	-1255	-1257	-1334	-1022	-682	-944
Fulmont	-1207	-1663	-1117	-776	-1123	-1135
23z	-1182	-1361	-1195	-1199	-1297	-1086
280z	-1322	-1469	-1291	-687	-1188	-1551

Figure 4.31 below compares the energies of the degradation peak for each pure polymer and catalyst mixture. Large differences can be seen for the energies of degradation, with 23z and 280z zeolites often requiring a greater amount of energy for decomposition of the polymer to occur, whilst Fulacolor clay appears the most successful in reducing the amount of energy required to degrade the polymer in all but one case.
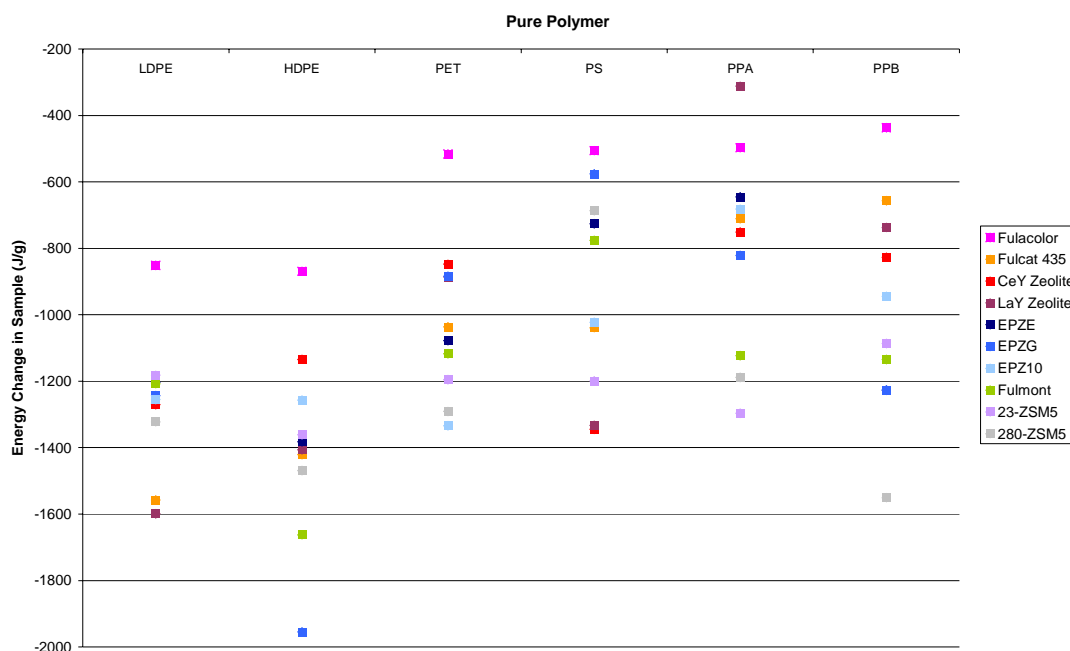
Figure 4.31: Energies of degradation for pure polymers and catalysts

Table 4.32 compares the energies of degradation of the six polymers in the presence of the ten catalysts and ranks the results in the order 1-10, with 1 being the catalyst for which the least energy was required for polymer decomposition and 10 being the clay or zeolite which caused the polymer to require the largest intake of energy to degrade. Table 4.32 gives an indication as to the catalyst/polymer combinations for which the enthalpy of the products formed are greatest or lowest in comparison to the other pairings. In the case of Fulacolor clay, the degradation of five of the pure polymers (LDPE, HDPE, PET, PS and PPB) required the least energy to occur and, hence, the products formed with these combinations required the least energy to be formed. In contrast, the polymer/catalyst combinations requiring the largest amounts of energy to degrade the polymer, and hence creating products of the largest enthalpies, appear to be distributed amongst the clays and zeolites with no obvious catalyst standing out.

214

Table 4.32: Comparison of the energies of degradation (1 being the lowest energy)

	LDPE	HDPE	PET	PS	PPA	PPB
Fulacolor	1	1	1	1	2	1
Fulcat 435	9	7	5	7	5	2
Fulmont	4	9	7	5	8	7
EPZE	3	5	6	4	3	9
EPZG	5	10	3	2	7	8
EPZ10	6	3	10	6	4	5
CeY	7	2	2	10	6	4
LaY	10	6	4	9	1	3
23z	2	4	8	8	10	6
280z	8	8	9	3	9	10

4.5   Conclusions of Differential Thermal Analysis

This DTA study suggests that the presence of certain catalysts affects the energy profile of degradation greatly. It is likely that this could be related to the type of products being formed on degradation of the polymer in the presence of a particular type of catalyst. For example, a branched product stores more energy than its straight-chain counterpart, whilst the presence of C=C double bonds in relation to C-C single bonds is also of a greater energy. The ZSM-5 zeolites (23z and 280z) were often found to give some of the highest energies of degradation of all the catalysts. Previous studies have shown that the degradation of plastics in the presence of ZSM-5 zeolites produce a higher proportion of aromatics than catalysts such as clays. The presence of aromatic products during the polymer decomposition could explain the high energy of degradation seen for 23z and 280z.

The total energy required for the decomposition of the pure polymers (melting and decomposition peaks) will be compared to bomb calorimetry results of the energy

expelled on combustion of the polymer. By comparing the J/g values of these endothermic and exothermic processes, it will be possible to gain insight as to whether the catalytic degradation of various polymers is viable energetically.

4.6 Bomb Calorimetry

Bomb calorimetry is used to determine the heat change associated with the combustion of a compound. The combustion reaction occurs in a closed container under constant volume ('bomb') and a sample of known weight is placed in contact with an ignition wire inside the bomb, which is then pressurised with excess oxygen, sealed and submerged under a known volume of water. An electric current is passed through the wire to initiate the combustion of the sample. The bomb (sample and oxygen) forms a closed system, therefore by recording the temperature change of the calorimeter and surrounding water, the heat evolved during the reaction can be determined. A diagram of bomb calorimetry apparatus is displayed in Figure 4.32.
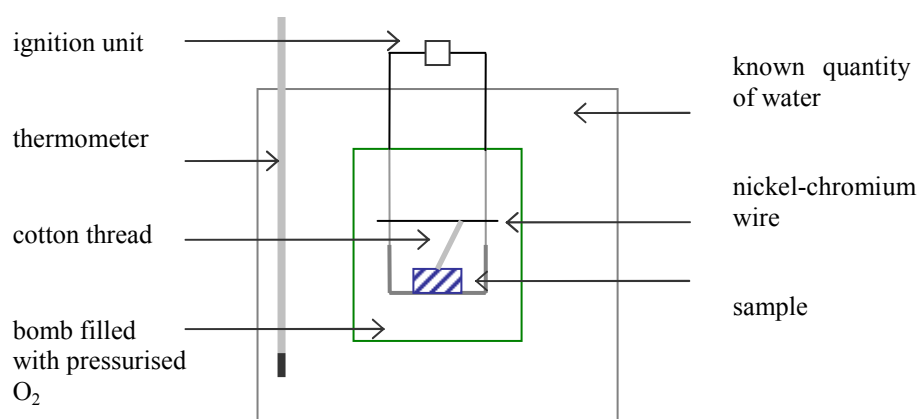
Figure 4.32: Bomb calorimetry apparatus

216

4.6.1 Internal Energy of Combustion

From the first law of thermodynamics, a change in internal energy depends on heat transfer between the system and the surroundings and work done by/on the system. The calorimeter can be thought of as completely isolated; therefore the reactants (sample and oxygen) can be defined as the *system* and the bomb and water as the *surroundings*. The change in internal energy of the reactants upon combustion can be calculated from:

$$dU_{tot} = dU_{sys} + dU_{surr} = 0 \qquad \text{(Eq. 4.15)}$$

$$dU_{sys} = -dU_{surr} = -\left[\left(\frac{\partial U}{\partial T} \right)_V dT + \left(\frac{\partial U}{\partial V} \right)_T dV \right] \qquad \text{(Eq. 4.16)}$$

As the volume remains constant, $dV = 0$ and

$$dU_{sys} = -C_v dT \qquad \text{(Eq. 4.17)}$$

where C_v is the heat capacity. Assuming C_v is independent of T over small temperature ranges, integration of Eq. 4.17 gives:

$$\Delta U = -C_v \Delta T \qquad \text{(Eq. 4.18)}$$

where C_v is the heat capacity of the surroundings.

4.6.2 Calibration of the Calorimeter System

For accurate results, it is necessary to determine the heat capacity of the calorimeter (C_{cal}). C_{cal} is the number of J/g or calories/g necessary to raise the temperature of the entire calorimeter system by one degree Celsius and is found by burning a sample of material of known heat of combustion (dU). The Gallenkamp Autobomb Calorimeter CBA-305 used in this study was calibrated by recording the temperature rise (in °C) produced in 2000 ml of distilled water (accurately measured by weighing 2 kg of distilled H_2O on a set of scales) by the combustion of a benzoic acid standard. Benzoic acid was selected as it burns completely (*i.e.* 100% combustion releasing all its energy as heat) and has a known heat of combustion (-26.43 kJ/g).

$$q_{cal} = (C_{cal} + C_{water})\Delta T \qquad \text{(Eq. 4.19)}$$

where q_{cal} =   amount of heat adsorbed by calorimeter

ΔT =   change in temperature, T_{final} - $T_{initial}$

C_{cal} =   heat capacity of the calorimeter

C_{water} =   heat capacity of water

As the specific heat capacity of water is 4.186 J/g °C, from Equation 4.19, the heat capacity of the calorimeter can be determined:

$$C_{cal} = \frac{q_{cal}}{\Delta T} - (weight of water) x 4.186 \qquad \text{(Eq. 4.20)}$$

For the Gallenkamp Autobomb Calorimeter CBA-305 used in this study, the heat capacity of the system was found to be 10.17 kJ/g °C. The heat released from ignition

of the cotton thread and the nickel chromium wire was also calculated. These corrections were found to be negligible.

4.6.3   Results of Bomb Calorimetry

The average heat of combustion (kJ/g) for the polymer samples was calculated from the temperature change recorded, the percentage of plastic consumed during combustion and the heat capacity of the calorimeter system. The results are shown in Table 4.33. Bomb calorimetry assumes 100% combustion of the sample in question. From Table 4.33, it can be seen that all but one of the pure polymers were completely burnt (over 99%) in the calorimeter. Pure polyethylene terephthalate left almost 8% residue, and although the heats of combustion were calculated by taking into account the amount of material combusted in the run, the corrected energy value will not be as accurate as for those polymers which were fully combusted. For the waste polymer samples, PET underwent 91% combustion (similar to the 92% for pure PET), whilst PAN and PU(foam) left approximately 11% and 8% of residue after combustion respectively. However, polybutadiene and the synthesised polyurethane RC35 produced around 20% residue, whilst the combustion of polyvinyl chloride was unsuccessful and consumed only 67% of the polymer. The presence of a proportion of residue may be the result of the formation of a layer of char on combustion of the polymer, which would prevent the final amount of polymer from having access to the oxygen in the bomb. This would leave a certain percentage of the sample unburnt.

From repeating the experiments of the almost fully combusted polymers, the variation in results was found to be 1-5%, therefore an error of 5% was given to these heat of combustion values. For the polymer samples in which noticeable residue remained in

219

the crucible, the repeated runs were not within 5% of each other. Although the heat of

combustion values were corrected for the percentage of polymer burnt, a 10-30% error

was applied to these experiments.

Table 4.33: Results of the bomb calorimetry of pure and waste plastics

Polymer	% Consumed	Heats of Combustion* (kJ/g)	Energy of Combustion (kJ/g)[6,7]
Pure			
LDPE	100.00	47.65 ± 1.20	42-46
HDPE	100.00	49.14 ± 1.23	42-46
PS	99.04	44.34 ± 1.11	42-45
PET	92.19	27.23 ± 2.05	
PPB	99.90	53.22 ± 1.34	46
Waste			
LDPE	95.60	52.60 ± 1.32	
HDPE	99.95	47.63 ± 1.20	
PS	99.73	46.54 ± 1.17	
PET	91.30	25.90 ± 1.95	
PP	99.37	53.19 ± 1.33	
PA	99.18	42.46 ± 1.07	30-35
PB	79.10	44.33 ± 4.44	
PVC	67.26	13.20 ± 1.98	19-22
PU(RC35)	82.00	60.36 ± 6.04	
PU(foam)	91.85	29.85 ± 1.50	23
PMMA	96.74	57.13 ± 1.43	33
PE	97.64	29.48 ± 0.74	30
PAN	89.10	36.20 ± 2.72	

 * **measured at constant volume**

Comparing the average heats of combustion of the polymers in Table 4.33 to the calorific values of waste materials and fuels in Table 1.1,[6,7] it can be seen that the experimental results from the bomb calorimetry of polyethylene and polystyrene are in good agreement with the literature. The experimental value of heat of combustion of polypropylene (53 ± 2 kJ/mol) appears 15% higher than the literature value (46 kJ/mol). The experimental results for the bomb calorimetry of waste polymers do not appear to correspond as well with the literature values (with the exception of polyester which is in very good agreement). This may be in part due to the varying presence of additives and plasticisers contained in the waste polymers of this study and the polymers tested in the literature.

In relation to polyethylene terephthalate, the heat of combustion from the bomb calorimetry experiments (27 ± 2 kJ/mol) appears to be in general agreement with the literature value[265] (23 kJ/mol), which also found PET to release approximately half the energy than polyethylene. This could be related to the presence of oxygen in the PET molecule, which lowers the overall carbon and hydrogen content and thus the energy available. This can be explained by a C—C bond, C—H bond and C=C bond of a polyalkene having energies of 347 kJ/mol, 414 kJ/mol and 610 kJ/mol respectively. In comparison, the C—O bond of PET has an energy of 357 kJ/mol, less than that of C—H and C=C bonds. However, the C=O bond for polyethylene terephthalate has an energy of 748 kJ/mol, which is much greater than the bond energies seen in polyethylene and polypropylene.

Polypropylene was seen to have a higher heat of combustion than polyethylene. Although both polymers contain just carbon and hydrogen atoms, the presence of

regular branching in polypropylene gives a structure of higher potential energy and therefore releases a greater energy on combustion than an unbranched polymer. However, bomb calorimetry of pure LDPE released 3% less energy than pure HDPE, which should not have been the case due to the presence of branches in the LDPE. This slight discrepancy is likely to be experimental error as combustion of waste LDPE produced 5 kJ/g more energy from the branched polyethylene than for waste HDPE, as would be expected.

4.7   Conclusions of Energy Analysis

Comparing the heats of combustion of the pure polymer samples with the energies of melting and decomposition obtained from the DTA curves, it is possible to ascertain whether the degradation of a polymer in the presence of a catalyst is an energetically viable process. Although the amount of waste plastics in our society is an ever-growing problem, it is important to discover solutions that do not result in more energy being taken in by the process than that given out. The degradation of the plastic waste must be exothermic or mildly endothermic and environmentally sound.

Table 4.34: Total energy of degradation of pure polymers and catalysts (J/g)

	LDPE	HDPE	PET	PS	PPA	PPB
Fulacolor	-913	-820	-517	-1317	-609	-909
Fulcat	-703	-640	-604	-427	-660	-977
Fulmont	-912	-1180	-291	-1062	-1057	-1131
EPZE	-900	-880	-796	-1205	-1102	-812
EPZG	-1054	-1360	-577	-1363	-833	-953
EPZ10	-1154	-1140	-637	-275	-517	-1415
CeY Zeolite	-1025	-730	-1486	-915	-602	-869
LaY Zeolite	-662	-980	-953	-933	-504	-515
23-ZSM5	-1160	-1052	-660	-1204	-783	-1043
280-ZSM5	-1084	-1280	-422	-1683	-1690	-1357

Table 4.34 shows the combined energies of the melting and decomposition endotherms. The largest energy value is found to occur for the degradation of low molecular weight polypropylene in the presence of 280z zeolite. All other energies of degradation are below this energy value of -1,690 J/g. Relating this to the heats of combustion, the lowest energy value was found to be 27.23 kJ/g, or 27,230 J/g. It can be seen that correcting the smallest exothermic value of combustion with the largest endothermic value of degradation, energy of +25 kJ/g still remains. Although this calculation is crude, it gives a first approximation of the maximum energy obtainable from the polymer cracking products and implies that the degradation of these polymers in the presence of catalysts is energetically viable. Please see the Conclusions section for an improvement to this validation method.

Chapter 5

Pyrolysis-GC-MS Analysis of Polymer Degradation

5   Py-GC-MS of Polymer Degradation

5.1   Mass Spectrometry

A mass spectrometer is designed to vapourise compounds of widely varying volatility, produce ions from the resulting gas-phase molecules and separate the ions according to their mass-to-charge ratios (*m/e*).   The most common technique for generating a characteristic positive ion spectrum of a molecule is electron impact-mass spectrometry, where the sample vapour is introduced into the ion source at a pressure between 10^{-5} and 10^{-7} mmHg and is bombarded by an electron beam of energy 10-100 eV. *Molecular ions* are produced at 10-15 eV, where an electron has been removed from the sample, forming a positive ion.   Increasing the energy results in decomposition of the molecular ions to *fragment ions*, which are characteristic of the molecular structure. Figure 5.1 displays the ionisation and possible fragmentation sequences of a molecule being analysed in a mass spectrometer, whilst Figure 5.2 represents a typical mass spectrum.
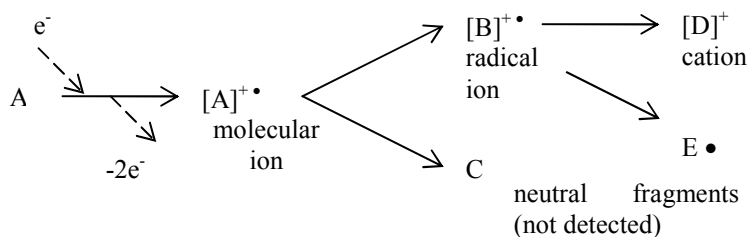
Figure 5.1: Ionisation and possible fragmentation sequences[266]
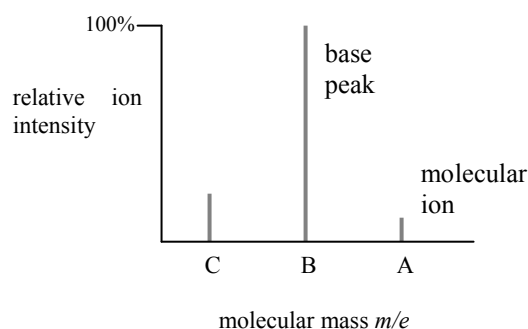
Figure 5.2: Representation of a mass spectrum

In the mass spectrometer, the ions are sorted *via* a magnetic sensor analyser, in which ions with different values of *m/e* follow different paths under the influence of a magnetic field. The acceleration of an ion charge, *e*, in an electrostatic field of voltage *V*, imparts a kinetic energy ½*mv²*, where *m* and *v* are the ion's mass and final velocity respectively. The potential energy, *eV*, of the ion before acceleration equals the kinetic energy, hence:

$$eV = \frac{1}{2}mv^2 \qquad\qquad \text{(Eq. 5.1)}$$

On entering the magnetic field, *H*, the ion is subjected to a centripetal force, *HeV*. This is balanced by a centrifugal force, *mv²/r*, where *r* is the radius of the ion's path.

If
$$HeV = \frac{mv^2}{r} \qquad\qquad \text{(Eq. 5.2)}$$

then
$$\frac{m}{e} = \frac{H^2 r^2}{2V} \qquad\qquad \text{(Eq. 5.3)}$$

From Equation 5.3, a mass spectrometer separates ions according to their mass-to-charge ratios, *m/e*.[267]

5.1.1 Determination of Molecular Formulae

The molecular ion is formed by the loss of one electron from the molecule:

$$M: + e \rightarrow M^{\cdot +} + 2e$$
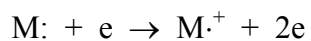
The stability of the molecular ion and consequently the intensity of the molecular ion peak is related to molecular structure. The approximate order for increasing probability of fragmentation is displayed in Figure 5.3:

Aromatic compounds

Conjugated alkenes

Alicyclic compounds

Sulphides

Straight-chain hydrocarbons

Thiols

Ketones

Amines

Esters

Ethers

Carboxylic acids

Branched hydrocarbons

Alcohols

increasing probability
of fragmentation
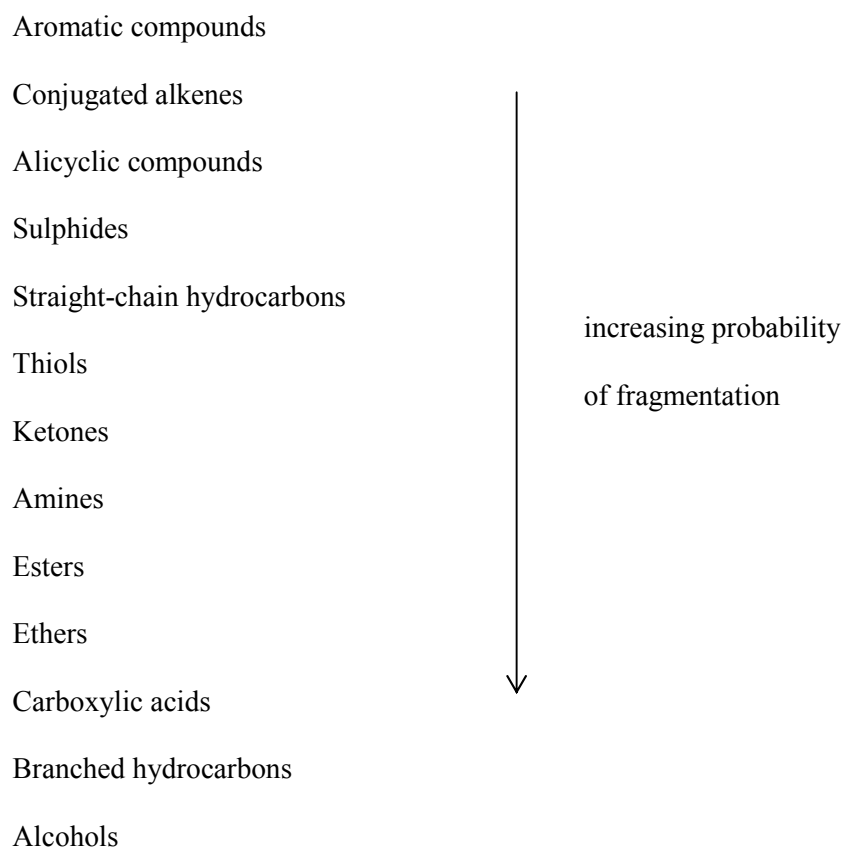
Figure 5.3: Approximate order for increasing probability of fragmentation[268]

Absence of molecular ions is characteristic of highly branched molecules, alcohols and molecules with long alkyl chains. In hydrocarbons, the fragments lost appear as multiples of (CH_2) units. Due to the low pressure in the ion source, collisions between ions and molecules are rare. When they do occur, an ion-molecule reaction may result (the commonest being hydrogen abstraction by the molecular ion), giving rise to a peak at *m/e* M+1.

Mass Spectrometry could be a very useful technique in investigating the decomposition products of various polymer samples. From past research of the thermal degradation of plastic, it is known that alkanes, alkenes, cycloalkanes and aromatic hydrocarbons are among some of the decomposition products.

For **alkanes**, the molecular ion will normally be seen in their mass spectra, but its intensity decreases with increased size and branching of the chain. Branched-chain alkanes rupture predominantly at the branching points, with the largest group attached to this branching point being expelled as a radical. **Cycloalkanes** are said to undergo complex fragmentations, such as loss of alkenes or splitting off of the side-chains at a branching point. For **alkenes,** the molecular ion will normally be seen in their mass spectra. The most common fragmentation in alkene groups involves the rupture of the allylic bond (β to the double bond), forming a stable allylic cation. Unfortunately, most alkene spectra represent a homologous series of fragments separated by 14 mass units, equivalent to the difference of a CH_2 unit between subsequent fragments and are not easily distinguishable by mass spectrometry alone, due to the migration of double bonds and the tendency of *cis-trans* isomers to interconvert during fragmentation. In the case of **cycloalkenes**, the double bond and presence of acyclic alkanes determine the allylic

rupture. The molecular ions of **aromatic hydrocarbons** are abundant, with $M^{\cdot+}$ as the base peak and *M+1* and *M+2* peaks clearly present.

In relation to the mass spectra of other types of plastic, **esters, -COOR,** produce weak molecular ion peaks with their spectra being characterised by the loss of the -OR group and of the COOR group. Primary aliphatic **amides**, $RCONH_2$, form $R\cdot$ and $CONH_2^+$ at *m/e* 44. For **nitriles**, the molecular ion peaks are usually weak or absent, although an M-1 ion ($R-CH=C=N^+$) may be seen. M-27, corresponding to M-HCN is also present.

The above information will be very helpful when coming to interpret the mass spectra obtained from the degradation of our polymer samples.

5.1.2 Methods of Mass Spectrometry

Following the extensive thermal analysis carried out on pure and waste polymers in the presence of clay and zeolite catalysts, the particular plastic and catalyst pairings which produced the most significant changes in the onset temperature and activation energy of decomposition were selected for further testing (see Table 4.28).

5.1.2.1 U-Tube Furnace

The first set of mass spectrometry investigations were carried out using a Hiden Mass Spectrometer and the experimental set-up in Figure 5.4. Initial experiments involved the use of a U-shaped stainless steel tube of ¼" diameter. The polymer (with or without catalyst) was heated to 550ºC and any condensate collected in the cold trap was extracted for analysis. A more detailed description of the method is presented in the Experimental Chapter (Chapter 7).

Sample preparation was kept to a minimum and involved no grinding or shredding of the plastic into small fragments. The catalyst powder (0.25 g) was placed first in the tube and allowed to settle at the bottom of the U-bend. Then, 0.5 g of untreated polymer (pellets for pure polymers, small pieces of waste polymer) were placed directly on top of the catalyst. No mixing of the polymer and catalyst was undertaken in order to simulate how plastics could be recycled in the future with next to no initial preparation.
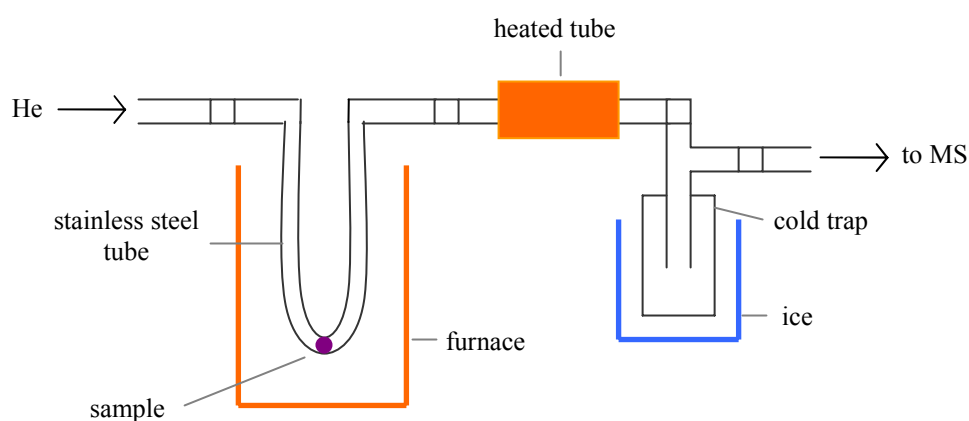
Figure 5.4: U-tube furnace set-up

The mass spectrometer required manual programming of the components it was to be detecting. From researching previous literature into the degradation of plastics, specific information for eighteen gases was input into the spectrometer, in order for the detector to reliably identify the components. For example, when programming the MS for the detection of 'ethane, C_2H_6' (molecular mass 30), the information in Table 5.1 was used.

Table 5.1: Molecular mass data for ethane

Molecular Mass	28	27	30	26	29	15	25	14	24	13
Relative Intensity	99.9	33.2	26.2	23.2	21.5	4.4	3.5	3.0	0.5	1.0

The range of molecular masses and the corresponding relative abundance of these masses allowed the MS to identify ethane correctly. By programming a range of molecular masses with their relative abundances for each component, the MS was able to distinguish between certain gases of the same molecular weight (*i.e.* methylbutene and 1-pentene, both of molecular mass 70). The eighteen initial gaseous components programmed into the mass spectrometer, along with their molecular formulae and molecular mass are listed in Table 5.2. A large number of runs were carried out with this initial furnace method. This allowed basic comparisons to be made in relation to the evolution of specific decomposition products when the plastics were heated in the presence of a catalyst or degraded alone.

Table 5.2: Table of gaseous components programmed into Hiden MS

Gaseous Component	Molecular Formula	Molecular Mass
Butene	C_4H_8	56
Ethene	C_2H_4	28
Methane	CH_4	16
n-butane	C_4H_{10}	58
Propane	C_3H_8	44
Propene	C_3H_6	42
3-methylbut-1-ene	C_5H_{10}	70
Ethane	C_2H_6	30
2-methylbut-2-ene	C_5H_{10}	70
2-methylbut-1-ene	C_5H_{10}	70
Pentane	C_5H_{12}	72
Methylbutene	C_5H_{10}	70
1-pentene	C_5H_{10}	70
(Z)-2-pentene	C_5H_{10}	70
*Iso*butene	C_4H_8	56
2-methylbutane	C_5H_{12}	72
2,2-dimethylpropane	C_5H_{12}	72

5.1.2.2   Results of U-Tube Experiments

The data obtained from this set of experiments was used purely as a comparative tool to determine the relative amounts of gaseous products from the degradation of a plastic in the presence of a catalyst. The amount of each component formed in a particular experiment was not compared to the amount from another experiment as it was evident that the quantitative data was not of sufficient accuracy for this. Examples of the gases emitted for a polymer degraded alone and then in the presence of a catalyst are shown below in Figure 5.5 and Figure 5.6. The graphs demonstrate how the profile of the emission gases changes when the polymer is heated in the presence of a catalyst.

For the U-Tube furnace experiments, fourteen successful runs with pure LDPE, HDPE and polypropylene A and B, along with a variety of catalysts, were achieved. These are listed in Table 5.3. From the emission data, the area under each respective gas curve allowed the amounts of gases to be compared, in isolation, for each run. The results of the ten most common gaseous products for each run are shown in Appendix E.

Table 5.3: Experiments carried out using the U-tube furnace

PLDPE	PHDPE	PPPA	PPPB
PLDPE-Fulcat	PHDPE-Fulcat	PPPA-Fulcat	PPPB-Fulcat
	PHDPE-EPZ10		PPPB-EPZG
	PHDPE-CeY		PPPB-EPZ10
	PHDPE-23z		
	PHDPE-280z		

1-Butene was found to be the greatest decomposition product, except for when pure HDPE was decomposed in the presence of EPZ10, CeY and 280z. In these cases, 1-pentene was the most common gas, which was more usually found as the 11th most abundant product. Additionally, the zeolites 23z and 280z produced a greater amount of methane (an increase from 18th place to 10th and 9th place respectively). No significant condensate was collected in the cold trap for any of these experiments.
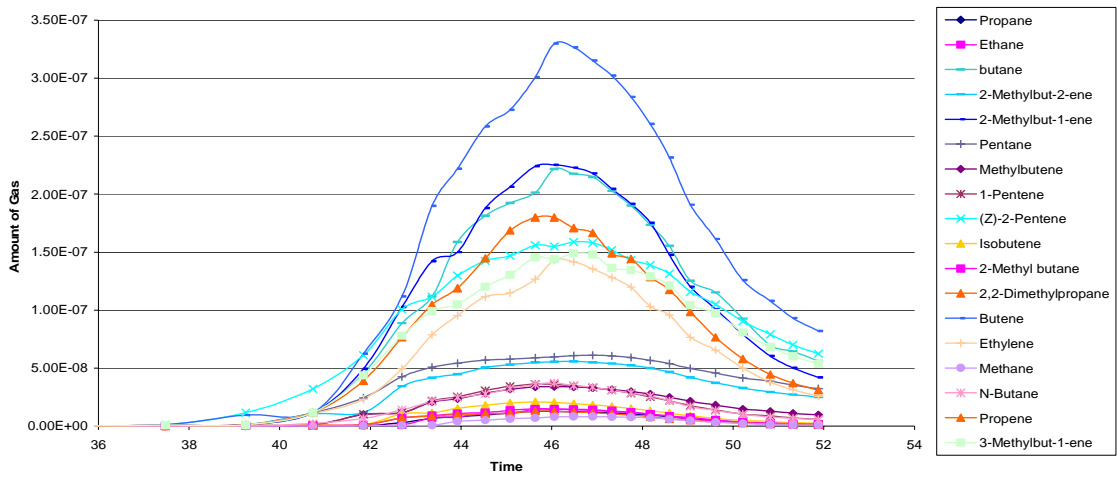
Figure 5.5: Emission of gases from the degradation of pure HDPE
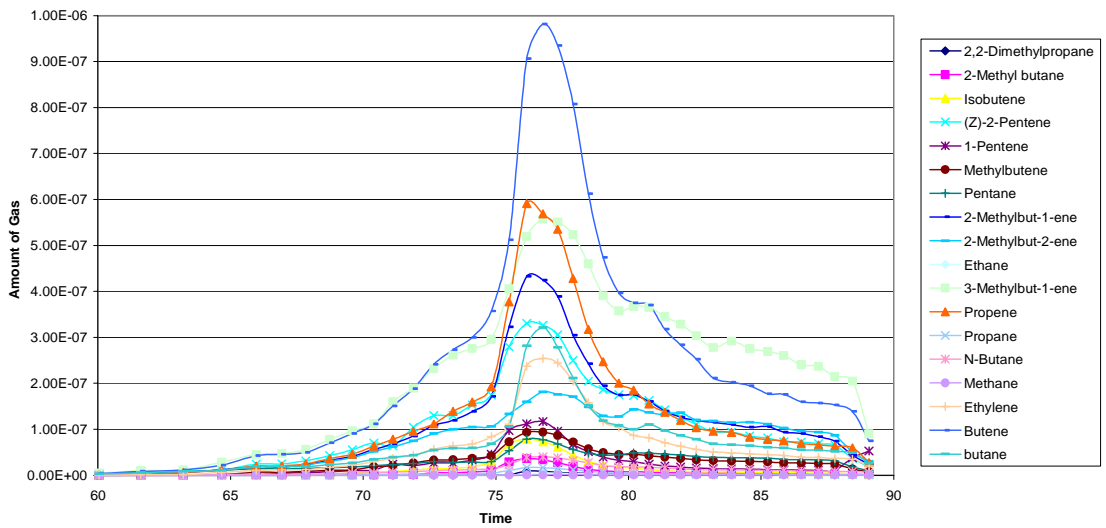
Figure 5.6: Emission of gases from the degradation of pure HDPE and Fulcat

233

5.1.2.3   Straight-Tube Furnace

To improve the rearrangement of decomposition products into lighter and more-branched gaseous components, the experimental set-up was modified. The ½" stainless steel U-tube was replaced with a ¾" straight tube. By positioning only the bottom half of the tube into the heated furnace, the top section of the steel tube remained at a lower temperature. Any heavier decomposition products, instead of passing straight out of the tube and across the heated line and into the cold trap, would reach the cooler section of the sample tube and reflux back down into the furnace for further decomposition and possible rearrangement into branched products by the catalyst (see Figure 5.7).
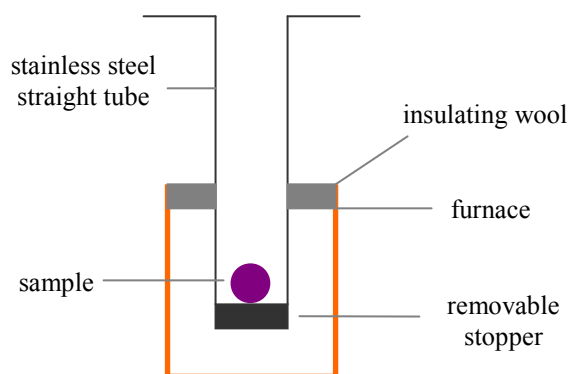
Figure 5.7: Straight tube furnace set-up

In order for the mass spectrometer to detect these more-branched products, the database was modified. Butene and methylbutene values were removed and the following components in Table 5.4 were added:

Table 5.4: Table of gaseous components programmed into Hiden MS

Gaseous Component	Molecular Formula	Molecular Mass
*iso*butane	C_4H_{10}	58
1-butene	C_4H_8	56
trans-2-butene	C_4H_8	56
cis-2-butene	C_4H_8	56
o-xylene	C_8H_{10}	56
m-xylene	C_8H_{10}	106
p-xylene	C_8H_{10}	106
ethylbenzene	C_8H_{10}	106

5.1.2.4 Results of Straight-Tube Experiments

Experiments were carried out using the ¾" straight tube set-up which was thought to allow a greater degree of reflux, and hence rearrangement, of the decomposition products as they were able to interact further with the catalyst. Pure low-density polyethylene was degraded alone and then in the presence of six different catalysts (Fulcat, EPZE, EPZG, EPZ10, LaY and 280z). Pure polypropylene B was heated alone and then in the presence of eight catalysts (Fulacolor, Fulcat, Fulmont, EPZE, EPZG, EPZ10, 23z and 280z). The results of the ten most common gases are presented in Appendix E. In all cases, propene was the commonest of all products, with *cis*-2-butene being the second most common. The degradation of pure LDPE in the presence of EPZ10 clay was undertaken a second time, using the same catalyst and adding more polymer before the start of the run. The re-use of the EPZ10 did not produce any significant change in the decomposition products.

5.1.2.4.1 Analysis of Condensate

For the degradation in the ¾" straight tube furnace of pure LDPE and PPB in the presence of catalysts, traces of condensate were sometimes collected in the cold trap. It was important to analyse this condensate in order to ascertain the liquid component produced from the polymer decomposition. This was achieved *via* gas chromatography coupled to a mass spectrometer.

Gas chromatography – the means of separating and analysing a range of gaseous samples, liquid solutions and volatile solids – involves the partitioning of analytes between a stationary phase and a gaseous mobile phase. Fundamentally, the greater the affinity of the compound for the stationary phase, the more the compound will be retained by the column and the longer it will be before it is eluted from the gas chromatograph and detected. The characteristic time taken for a component to be eluted is known as the retention time, R_t, and can be used to aid in the identification of the constituents of a sample.

The condensate collected from the degradation of pure LDPE and PPB in the presence of catalysts was injected into a GC-MS and identified as small amounts of toluene and ethylbenzene.

Waste high-density polyethylene was degraded in the straight-tube furnace, along with Fulcat, EPZ10 and 23z (see Appendix E). A significant amount of condensate was collected for waste HDPE heated with 23z, which was identified *via* GC-MS as benzene (R.T = 1.55), toluene (R.T = 2.21), ethylbenzene (R.T = 2.94), 1,3-dimethylbenzene (R.T = 3.05), *o*-xylene (R.T = 3.23), 1-ethyl-3-methylbenzene (R.T = 3.80) and 1,2,3-

trimethylbenzene (R.T = 4.10). The chromatogram of the liquid degradation products

of waste HDPE in the presence of 23z is displayed in Figure 5.8 below.
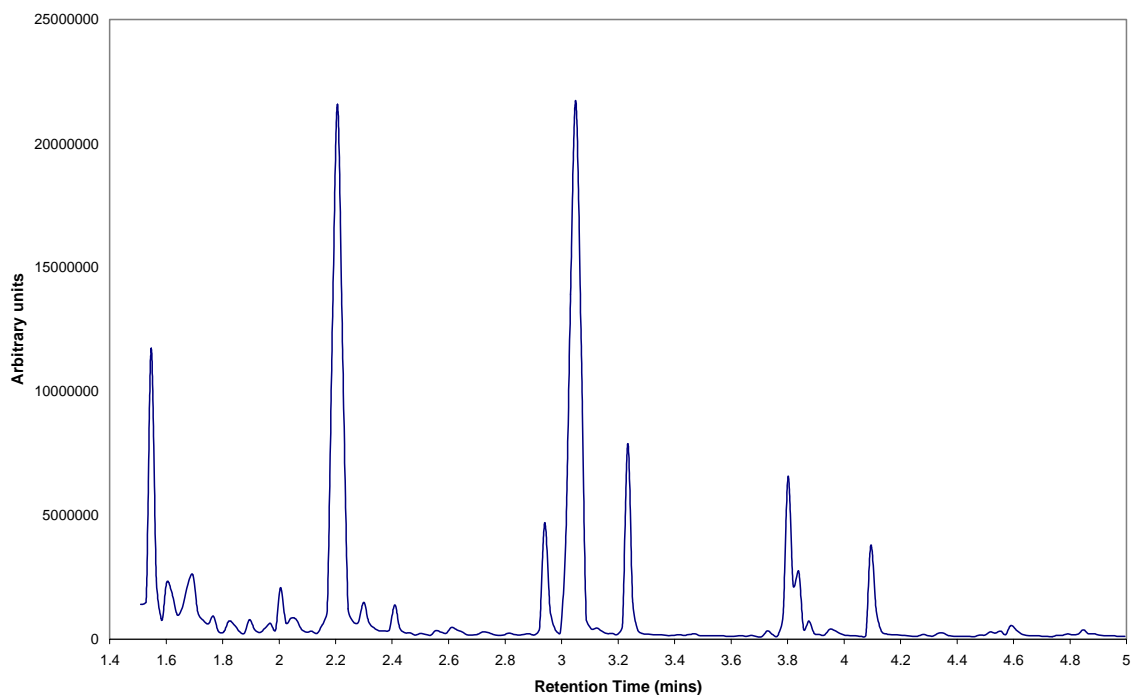
Figure 5.8: Chromatogram of the liquid degradation products of waste HDPE with 23z

Waste polyethylene terephthalate was heated alone and in the presence of Fulacolor,

Fulcat, EPZE, EPZG, EPZ10 and 280z. For all runs, *iso*butene and ethane were the first

and second most significant products.

5.1.2.4.2 Degradation of Mixed Plastics

Mixtures of plastics were also degraded in the straight-tube furnace in order to simulate everyday household waste for recycling and to determine whether there were any synergistic effects with the polymers. The total plastic-to-catalyst weight ratio was fixed at 2:1, but the relative ratios of the polymers in each mixture were varied. Pure LDPE and pure PPB at a weight ratio 2:1 were degraded with 280z. Waste HDPE and pure PPB (ratio 1:1) were heated with 23z. Pure LDPE, waste HDPE and pure PPB (ratio 2:1:1) were degraded with 23z and then the same ratio mix was heated with Fulcat. The top two gaseous products were propene and *cis*-2-butene respectively. Pentane, 2-methylbut-1-ene and 3-methylbut-1-ene were also amongst the most common decomposition gases. From the results of these experiments, degrading a mixture of plastics (LDPE, HDPE and polypropylene) in the presence of catalysts did not appear to have a significant effect on the degradation products formed in comparison to heating the polymers individually with the catalyst.

GC-MS analysis of the condensate collected from the degradation of waste HDPE+PPB+23z identified *m*-xylene as the main liquid product (R.T = 3.05), with smaller amounts of toluene R.T = 2.19), *o*-xylene (R.T = 3.23), ethyl benzene (R.T = 2.94), 1-methylethyl benzene (R.T = 3.84) and 1-ethyl-2-methyl benzene (R.T = 4.10). The chromatogram of the degradation of waste HDPE and polypropylene B in the presence of 23z zeolite is displayed in Figure 5.9 below.
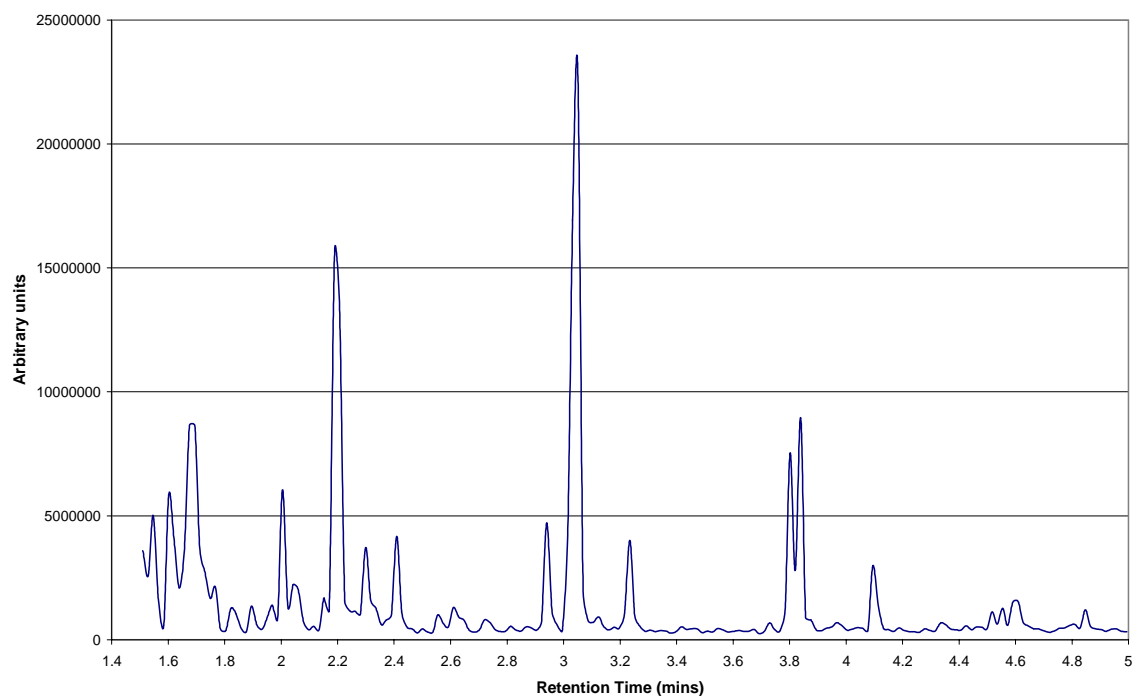
Figure 5.9: Chromatogram of the liquid degradation products of waste HDPE+PPB with 23z

5.1.3   Mass Spectrometry Conclusions

The straight-tube furnace was found to be a very useful method for determining the gaseous decomposition products of the plastics in the presence of various catalysts. Therefore, it was decided to link this furnace set-up to a mass spectrometer that was coupled to a gas chromatograph in order to analyse the polymer degradation products in greater detail.

5.2 Pyrolysis-Gas Chromatography (Py-GC)

Gas Chromatography is essentially a technique for analysing volatile samples, but can be applied to involatile materials if a reliable method of converting these substances to a volatile form can be found. The main method for this is the *pyrolysis* process, where large molecules are broken down by heat to numerous smaller, more volatile fragments without causing their thermal degradation. Rapid heating decomposes the sample into fragments characteristic of the original solid, therefore by identifying and quantifying these smaller fragments, much information regarding the structure and bonding of the initial larger molecule can be established. When the pyrolysis products, or *pyrolysates*, are injected into the gas chromatograph for analysis, they interact uniquely with the stationary phase in the column. Pyrolysates of different compounds yield different chromatograms, or *pyrograms*, which serve as a basis for their identification.

5.2.1 Previous Analysis of Polymers using GC

Neumann and Nadeau[269] pyrolysed polyethylene, producing methane, ethylene, ethane, combined propylene and propane, *iso*butane, 1-butene, *n*-butane, *trans*-2-butene, *cis*-2-butene, 2-methylbutane and *n*-pentane. Gröten[270] carried out pyrolysis-gas chromatography on polymers, including polyethylene, polystyrene, polypropylene of varying stereoregularity (isotactic, atactic), nylon 6, nylon 66, nylon 610 and polyurethane. Py-GC was said to be suitable for the identification of polymers similar in composition, *i.e.* polyolefins. The nylon samples were found to give roughly similar chromatograms. In the case of polyurethane, ester pyrolysis resulted in the formation of acid and olefinic products. Haller[271] pyrolysed a styrene homopolymer and a methyl methacrylate homopolymer. Both were said to yield around 90% monomer. Secondary

reactions were said to occur during pyrolysis, due to the diffusion of fragments through the degrading polymer. Cox and Ellis[272] carried out Py-GC on a variety of polymeric materials. Different chromatograms were produced for low-density polyethylene and high-density polyethylene. Hydrocarbon peaks were evident for the pyrolysis of PVC, due to the elimination of hydrogen chloride from the polymer.

5.2.2   Pyrolysis-Mass Spectrometry and Py-GC-MS

The heating of polymers in a furnace attached to a mass spectrometer allows identification of residual gases, solvents or monomers that are driven off. Direct coupling between the mass spectrometer and the furnace allows the identification of gases evolved from a polymer as the sample is heated under controlled conditions. The real time data enables assessment of the temperatures at which various components evolve and eliminates the problems inherent in trapping or collecting fractions for subsequent analysis, such as secondary reactions and/or contamination of products from more than one reaction.[273] Commonly, gas chromatography combined with mass spectrometry is used to characterise pyrolysates and is particularly useful as the pyrolysis products are separated prior to the mass determination.

Bart[274] compared the techniques of Py-GC, Py-MS and Py-GC-MS in the analysis of polymer additives. The limiting factor of Py-GC was said to be the chromatographic time needed to resolve all the pyrolysis products. The method also allowed only the determination of volatile products of pyrolysis, with the composition of the products, depending on the specific pyrolysis conditions (temperature, duration, sample size, carrier gas flow rate *etc*.). Py-MS experiments, in which a pyrolysis device was coupled directly or indirectly *via* a chromatographic interface to a mass spectrometer, was

performed in a few minutes. Py-MS eliminated some of the problems associated with the transfer of pyrolysis products from an external pyrolyser to a gas chromatograph. Py-GC-MS involved the separation of fragments in the gas chromatograph, before detection in the mass spectrometer. For the analysis of polymers, Py-GC-MS was said to have many advantages, such as the direct analysis of complex mixtures and high information content. However, the inclusion of the gas chromatograph increased the sampling time and made the technique unsuitable for very polar and high molecular weight pyrolysis products.

Tsuge and Ohtani[275] stated that the Py-MS of polymers resulted in complicated mass spectra, due to overlapping of fragment ion peaks from the ionisation process of the complex degradation products. In the case of Py-GC-MS, the column provided a separation of the complex pyrolysates, yielding a specific program of which individual peak components can be identified based on their mass spectra. The Py-GC-MS of high-density polyethylene produced serial triplets, corresponding to α, ω-alkadiene, α-alkenes and *n*-alkanes up to C_{30}. Singlet peaks were observed up to C_{64}. The pyrogram of polystyrene at 600°C showed the styrene monomer (80% intensity), dimer (6%) and trimer (5%). The polymethyl methacrylate pyrogram showed two dimer peaks at 16 minutes and 18 minutes, and a trimer peak at 33 minutes.

5.2.3   Method of Py-GC-MS

5.2.3.1   Non-isothermal Heating

The ¾" stainless steel straight tube was used as the sample reactor and, on heating, the gaseous polymer degradation products were passed to a Thermo Scientific DSQIIXL Mass Spectrometer coupled to a Focus GC (see Experimental Chapter). The pure

plastics and catalysts chosen for investigation were those that had produced the most interesting results from the thermal analysis and from the previous furnace experiments.

Pure low-density polyethylene and pure polypropylene B (molecular weight 190,000) were selected for investigation. These two polymers were analysed without a catalyst and in the presence of a clay (Fulcat 435) and a zeolite (23z or 280z). Using the Xcalibur Qual Browser software program, the peaks could be identified by consulting the National Institute of Standards and Technology (NIST) library. From the area under the peak, the relative amount of each decomposition product formed could be discovered.

5.2.3.2 Isothermal Heating

A second type of Py-GC-MS experiment was carried out with pure LDPE and pure polypropylene B. The polymer and catalyst were held at 400ºC or 450ºC for 340 minutes, with gas chromatograms being recorded every ten minutes. This allowed the changes in decomposition products of the sample to be investigated for a period of over five hours.

5.2.3.3 Analysis of Cold Trap Products

For all furnace experiments (U-tube and straight tube), any condensate collected in the cold trap during the run was analysed using a Perkin Elmer AutoSystem XL Gas Chromatograph with a Turbomass mass spectrometer as the detector. In most cases, there did not appear to be any condensate collected in the cold trap, but in the experiments where it appeared as though a trace of condensate had been formed, the

cold trap was rinsed with dichloromethane (DCM) and the total amount of liquid was transferred to a sampling tube where it was injected into the GC-MS.

5.2.3.4 Pyroprobe Studies

Towards the end of my research, the University of Central Lancashire purchased a CDS Analytical Pyroprobe 5200 that could be coupled to the Perkin Elmer AutoSystem XL Gas Chromatograph with Turbomass mass spectrometer. The use of a pyroprobe had several advantages over the use of a Curie-point wire. Firstly, the sample holder was a quartz tube within which a small amount of polymer and catalyst (< 1mg) could be placed and easily held in position with glass wool at either end of the tube. Additionally, the volatile organic compounds were purged to a trap where they were concentrated and then thermally desorbed for transfer to the GC-MS.

5.2.4 Results of Py-GC-MS

5.2.4.1 Calibration

In order to interpret the GC-MS data correctly, several calibration steps were carried out. A liquid calibration sample containing nineteen potential decomposition products of the polymers (see Appendix F) was run through the GC-MS. Each calibration peak was identified and then matched to the corresponding component on the manufacturer's calibration data sheet. The amount of each hydrocarbon in the calibration sample was known and the amount of each compound detected by the GC-MS was determined from the peak area. The size of a spectral peak is proportional to the amount of the substance that reaches the detector in the GC instrument. Therefore molar response factors (RF) were plotted against carbon number for the straight-chain alkanes, single-branched

alkanes, a double-branched alkane and aromatics present in the calibration sample (Figure 5.10).
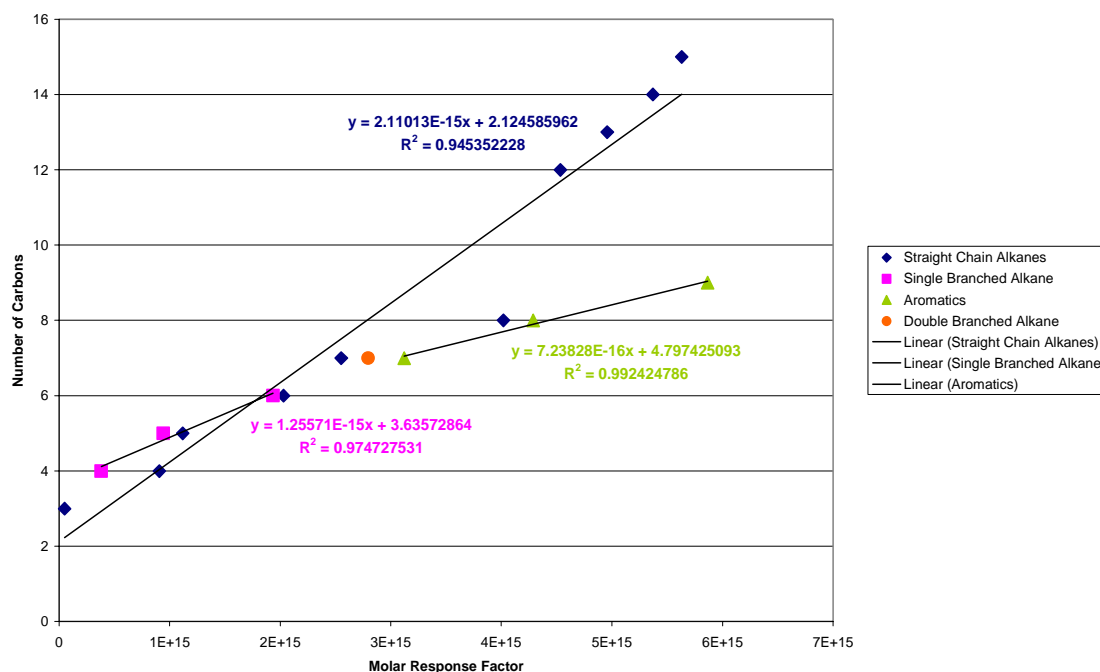
Figure 5.10: Molar Response Factors *vs*. no. of carbons for alkanes and aromatics

Using the line equation, $y = mx + c$, for a straight chain alkane, single-branched alkane and aromatic, a response factor (*x*-value) could be determined for any carbon number (*y*-value). Only one double-branched alkane was present in the calibration sample and was found to give a response that was 17% less than that of a single-branched alkane of the same carbon number. Therefore, a multiplier of 0.831 was applied to any response factors calculated for the double-branched products. This will introduce obvious inaccuracies, but the overall error will be small as few double branched alkanes were observed.

Further assumptions, which should have similar low impact on the overall value of the results, were made to reduce the increasing number of variables. These included: dienes being treated as alkenes, and compounds with two or more single branches being treated as single branched compounds. To improve the fit of the data to the trendlines, the occasional compounds that were obvious outliers (probably due to special molecular structural circumstances, *e.g.* decane and butylbenzene) were given individual RF's and removed from the RF calculations for that molecular group, thus improving the R^2 values dramatically.

The calibration sample did not contain any alkenes; therefore it was important to determine reasonable molar response factors for these components as they appeared readily as decomposition products of the plastics. In order to determine a reasonable comparison between the molar response factors of an alkane and the corresponding alkenes, GC-MS data was obtained from the NIST mass spectrometric database for a variety of alkane-alkene pairs (*e.g.* pentane / 1-pentene and pentane / 2-pentene), As m/z 57 and m/z 55 were usually major peaks in the mass spectra of the alkane and alkene respectively, the intensity of the 57-peak for the alkane was divided by the sum of the intensities, I_{tot}, of the alkane and the 55-peak of the alkene was divided by the I_{tot} for the alkene, for each data set. This 57/55 ratio was then plotted on the *x*-axis against carbon number, which allowed a reasonable prediction of the molar response factor of an alkene from that of the corresponding alkane in our standards, for each specific carbon number. Different graphs were plotted for 1-alkenes, 2-alkenes and 3-alkenes, as the position of the double bond was found to produce a different response factor in relation to other alkenes of the same carbon number. Interestingly, a definite 'odd-even' effect for carbon number was seen for 1-alkenes, therefore two separate graphs

were constructed displaying the 57/55 ratio for odd carbon numbers and the 55/57 ratios for even carbon numbers. The data points on the two 1-alkene graphs and the 2-alkene graph appeared to follow a second-order polynomial line-of-best fit, therefore a quadratic function, $y = ax^2 + bx + c$, was used to calculate a multiplier per carbon number that could be related to the alkane response factor equations determined from the calibration samples at the start.

It was also important to obtain an accurate correction factor for propene (carbon number 3) as this appeared as one of the polymer decomposition products. As there can be no 55 peak from propene (MW 42), it was not possible to calculate this from the 57/55 ratios used for alkenes of carbon number 4 and above. Therefore, GC-MS data was obtained for propane and 1-propene and the 43-alkane peak was compared with the 41-alkene peak in the same method as used previously. This correction factor was then used as the specific propene multiplier for the alkane responses for products with a carbon number of 3. The 43/41 peak ratios were also calculated for butane *vs.* 1-butene and pentane *vs.* 1-pentene to help validate the propene result. All alkene calibration curves are presented in Figure 5.11.
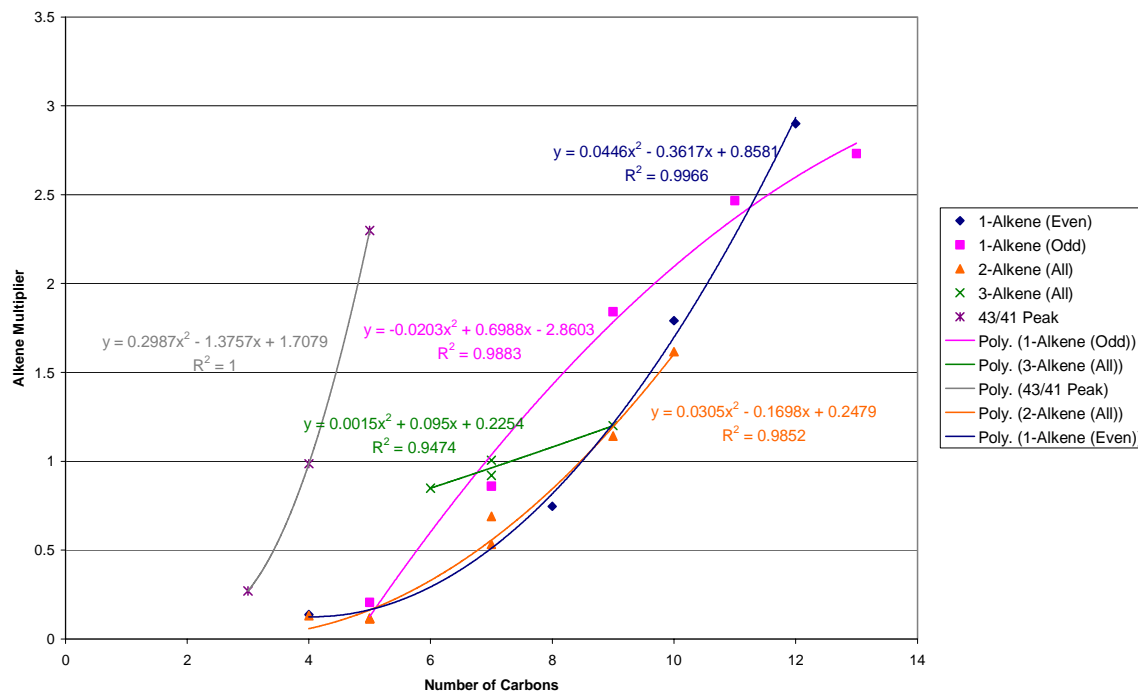
Figure 5.11: Calibration curves for various alkene types

Once this comprehensive list of response factors had been determined, it was possible to apply the specific correction factor to the decomposition products of the GC-MS experiments, which had been identified using the same NIST MS database used in the calculation of the alkene RF's. The degradation components were classified as: straight-chain alkane, single-branched (SB) alkane, double-branched (DB) alkane, straight-chain alkene, single-branched (SB) alkene, double-branched (DB) alkene or aromatic. Sub-classes depending on positions 1-, 2- or 3- of the double bond on the alkene were also added and the response factors (per number of carbons in the product) were applied. A list of the polymer degradation components obtained in the GC-MS analysis is listed in Table 5.5.

For each run, peak areas less than 0.5% of the total were not included in the analysis. The remaining peaks were normalised to be a percentage of the total area left and were then corrected with the corresponding response factor. No C_1-C_2 components were detected, or any products of carbon number greater than C_9, therefore the results tables and corresponding bar graphs were divided into categories of C_3-C_5, C_6-C_7 and C_8-C_9 for the straight, single-branched or double-branched alkanes or alkenes. Aromatics were not divided into groups by carbon number and were grouped simply as 'aromatics'.

Obviously, this approach does not give absolute accuracy, but it does give a substantial improvement in the estimates for un-calibrated components in the complex mixtures produced.

Table 5.5: Identification of peaks

R.T (mins)	Component	Family	MW	Carbon No.
1.80	propene	Straight	42.08	3
1.83	1-butene	Straight	56.11	4
1.85	(Z)-2-butene	Straight	56.11	4
1.90	*iso*-pentane	SB	72.15	5
1.92	2-methyl-1-butene	SB	70.13	5
1.93	1-pentene	Straight	70.13	5
1.97	2-methyl-2-butene	SB	70.13	5
2.02	1,3-pentadiene	Straight	68.12	5
2.08	*iso*-hexane	SB	86.18	6
2.12	3-methylpentane	SB	86.18	6
2.15	1-hexene	Straight	84.16	6
2.18	*n*-hexane	Straight	86.18	6
2.21	3-methyl-2-pentene	Straight	84.16	6
2.26	3-methylene-1-pentene	SB	82.16	6
2.28	2,4-dimethylpentane	SB	100.20	7
2.34	methylcyclopentane	SB	84.16	6
2.42	1-methyl-1,3-cyclopentadiene	SB	80.13	6
2.48	3-methylcyclopentene	SB	82.14	6
2.54	2-methylhexane	SB	100.20	7
2.58	benzene	Aromatic	78.11	6
2.61	3-methylhexane	SB	100.20	7
2.64	5-methyl-1,3-cyclopentadiene	SB	80.13	6
2.72	*trans*-1,3-dimethylcyclopentane	SB	98.19	7
2.77	1-heptene	Straight	98.19	7
2.83	*n*-heptane	Straight	100.20	7
2.87	(Z)-3-methyl-3-hexene	SB	98.19	7
2.92	3-heptene	Straight	98.19	7
2.96	(Z)-3-methyl-2-hexene	SB	98.19	7
3.12	1-methylene-2-methylcyclopentane	SB	112.00	7
3.17	2,5-dimethylhexane	SB	114.23	8
3.30	ethylcyclopentane	SB	98.16	7

R.T (mins)	Component	Family	MW	Carbon No.
3.56	3,5-dimethyl-1-cyclopentene	SB	96.00	7
3.63	4-methylheptane	SB	114.23	8
3.73	2-methylheptane	SB	114.23	8
3.88	3-methylheptane	SB	114.23	8
3.95	toluene	Aromatic	92.14	7
4.27	2-ethyl-1-hexene	SB	112.24	8
4.33	1-octene	Straight	112.21	8
4.41	1,2,3-trimethylcyclopentane	Straight	112.21	8
4.51	*n*-octane	Straight	114.23	8
4.57	2-methyl-2-heptene	SB	112.21	8
4.76	trans-1,3-dimethylcyclohexane	SB	112.22	8
5.37	2-methyl-methylenecyclohexane	SB	110.20	8
5.53	3,5-dimethylheptane	SB	128.26	9
5.64	ethylcyclohexane	SB	128.26	8
6.37	1,2,4-trimethyl-cyclohexane	SB	126.24	9
6.71	4-methyloctane	SB	128.26	9
6.91	ethylbenzene	Aromatics	106.17	8
7.12	3-ethylheptane	SB	128.26	9
7.42	*o*-xylene	Aromatics	106.17	8
7.46	*m*-xylene	Aromatics	106.17	8
7.97	4-ethyl-3-heptene	SB	126.24	9
8.65	*p*-xylene	Aromatics	106.17	8
8.79	n-nonane	Straight	128.26	9

5.2.4.2 Non-Isothermal Results

Two polymers (LDPE and PPB) and three catalysts (Fulcat 435, 23z and 280z) were chosen for this part of the study as they had given some of the best results in the TGA experiments. The results were displayed for thermal degradation and for degradation in the presence of each of the catalysts. Fulcat 435 had been used as a catalyst with pure LDPE (400ºC, 450ºC, 500ºC) and pure polypropylene B (500ºC). 280z had been heated

with pure LDPE (400ºC, 450ºC, 500ºC), whilst 23z had been used as a catalyst with pure PPB (450ºC, 500ºC). Pure LDPE and pure PPB had also been degraded without the presence of a catalyst for comparison purposes.

Two graphs for each run were prepared: % of Total Moles and % of Total Mass, with the former illustrating information relating to the mechanisms of the reactions and the latter useful for interpreting the potential RON and calorific values of the products. The discussion for each run is represented in terms of % of Total Mass.

5.2.4.2.1 No Catalyst

	Alkane			Alkene			Aromatics
	Straight	SB	DB	Straight	SB	DB	Aromatics
				PLDPE			
■ C8 - C9	1.9%	4.9%	0.0%	0.0%	2.0%	0.0%	0.0%
■ C6 - C7	29.1%	21.4%	0.0%	16.0%	8.3%	0.0%	0.0%
■ C3 - C5	0.0%	6.9%	0.0%	7.3%	1.2%	0.0%	0.0%
■ Aromatics	0.0%	0.0%	0.0%	0.0%	0.0%	0.0%	1.0%
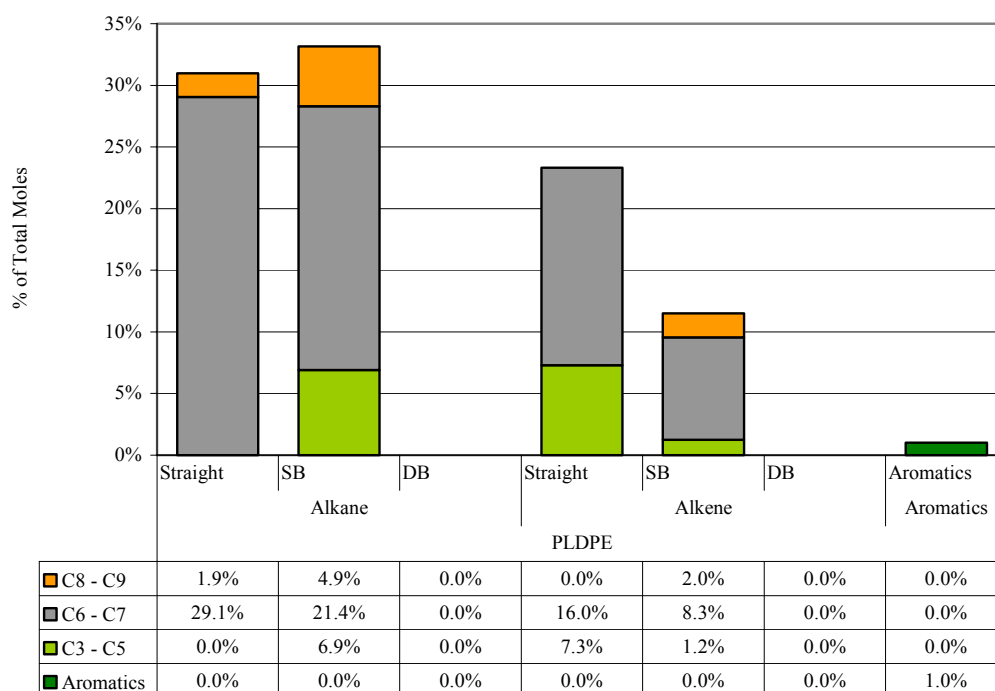
Figure 5.12: Degradation products of pure LDPE at 450ºC (% of Total Moles)

252

	Straight	SB	DB	Straight	SB	DB	Aromatics
		Alkane			Alkene		Aromatics
				PLDPE			
■ C8 - C9	2.5%	6.2%	0.0%	0.0%	2.5%	0.0%	0.0%
■ C6 - C7	29.8%	21.7%	0.0%	17.0%	8.2%	0.0%	0.0%
■ C3 - C5	0.0%	5.6%	0.0%	4.6%	1.0%	0.0%	0.0%
■ Aromatics	0.0%	0.0%	0.0%	0.0%	0.0%	0.0%	0.9%
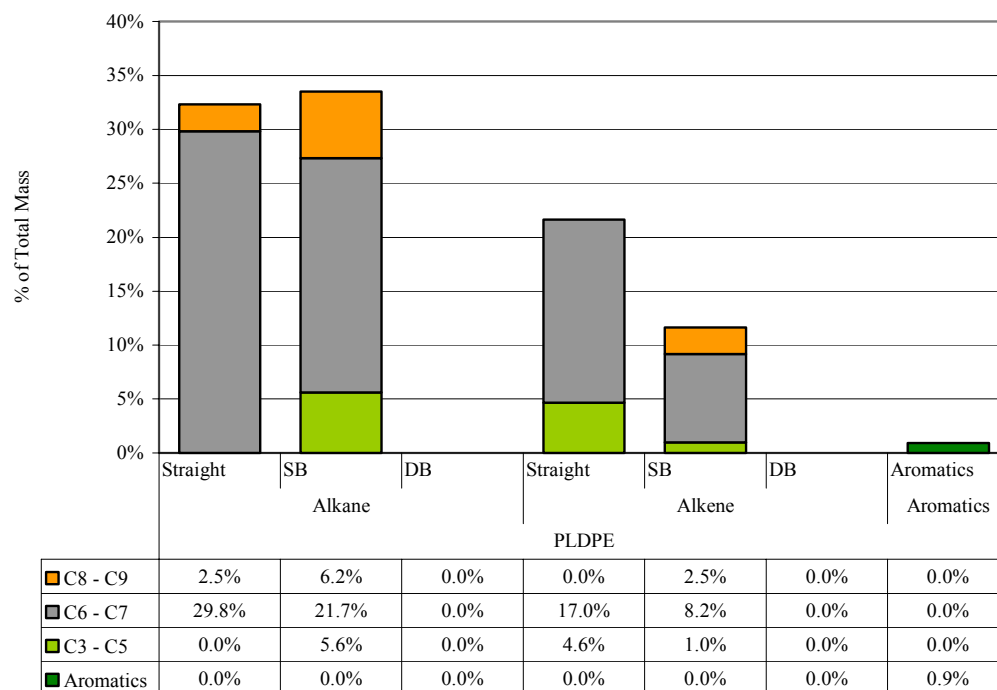
Figure 5.13: Degradation products of pure LDPE at 450ºC (% of Total Mass)

As shown in Figure 5.13, the degradation of pure low-density polyethylene at 450ºC (no catalyst) produced a large number of C_6-C_7 alkanes (65% of total mass), with 32% being straight-chain and 33% being single-branched alkanes. 33% of the total mass of the products were alkenes, with only a small number of C_8-C_9 alkenes (2.5%) in comparison to nearly 9% C_8-C_9 alkanes. No double-branched alkanes or alkenes were formed. The yield of aromatics (1%) was very low.

		Alkane			Alkene		Aromatics
	Straight	SB	DB	Straight	SB	DB	Aromatics
				PLDPE			
☐ C8 - C9	7.8%	10.4%	0.0%	5.5%	3.1%	0.0%	0.0%
☐ C6 - C7	25.0%	13.0%	0.0%	17.6%	7.7%	0.0%	0.0%
☐ C3 - C5	0.0%	0.0%	0.0%	5.8%	0.4%	0.0%	0.0%
☐ Aromatics	0.0%	0.0%	0.0%	0.0%	0.0%	0.0%	3.7%
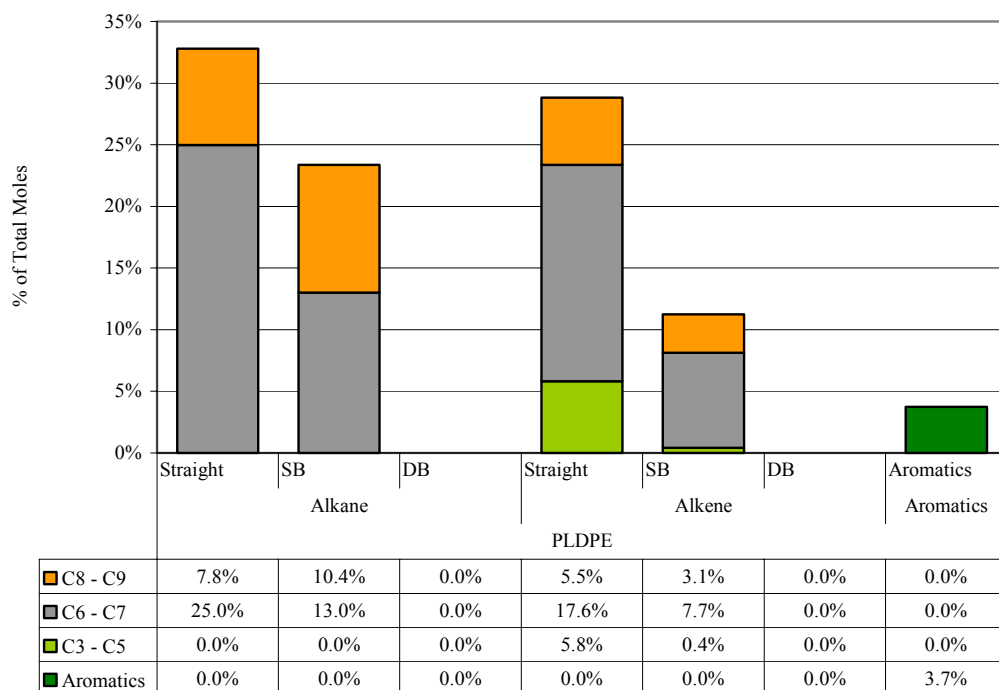
Figure 5.14: Degradation products of pure LDPE at 500ºC (% of Total Moles)

		Alkane			Alkene		Aromatics
	Straight	SB	DB	Straight	SB	DB	Aromatics
				PLDPE			
☐ C8 - C9	9.3%	12.2%	0.0%	6.4%	3.6%	0.0%	0.0%
☐ C6 - C7	24.1%	12.6%	0.0%	17.4%	7.2%	0.0%	0.0%
☐ C3 - C5	0.0%	0.0%	0.0%	3.3%	0.3%	0.0%	0.0%
☐ Aromatics	0.0%	0.0%	0.0%	0.0%	0.0%	0.0%	3.6%
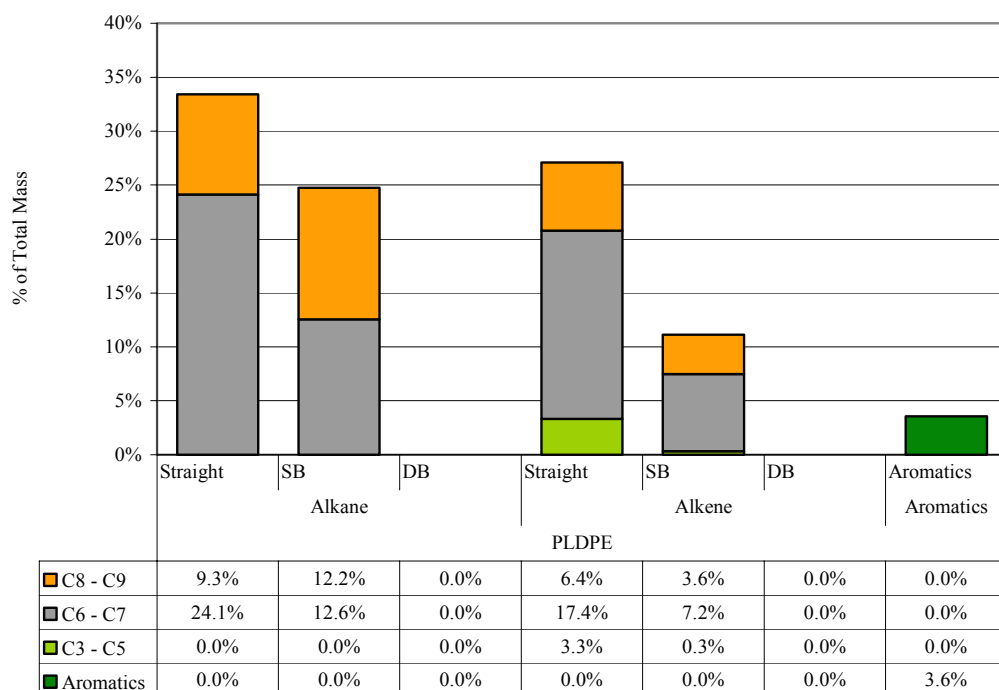
Figure 5.15: Degradation products of pure LDPE at 500ºC (% of Total Mass)

From Figure 5.15, the degradation of pure low-density polyethylene at 500ºC (no catalyst) produced a greater amount of C_8-C_9 products, up to 28% of the total mass, (alkanes and alkenes, both straight chain and single-branched) than that seen at a temperature of 450ºC. This was unusual, as we would have expected the amount of larger alkanes to be reduced at a higher temperature. The C_3-C_5 products were reduced from 15% at 450ºC to 3% at 500ºC. Overall, the C_6-C_7 alkane and alkene components were the most abundant at 61% of the total mass. No double-branched products were formed. The aromatic content quadrupled from 450ºC to 500ºC, but still remained low at 3.6%.

	Straight	SB	DB	Straight	SB	DB	Aromatics
		Alkane			Alkene		Aromatics
				PPB			
C8 - C9	1.7%	39.5%	0.0%	0.0%	0.0%	0.0%	0.0%
C6 - C7	0.0%	14.3%	0.0%	8.8%	18.1%	0.0%	0.0%
C3 - C5	0.0%	0.8%	0.0%	10.2%	0.6%	0.0%	0.0%
Aromatics	0.0%	0.0%	0.0%	0.0%	0.0%	0.0%	6.1%
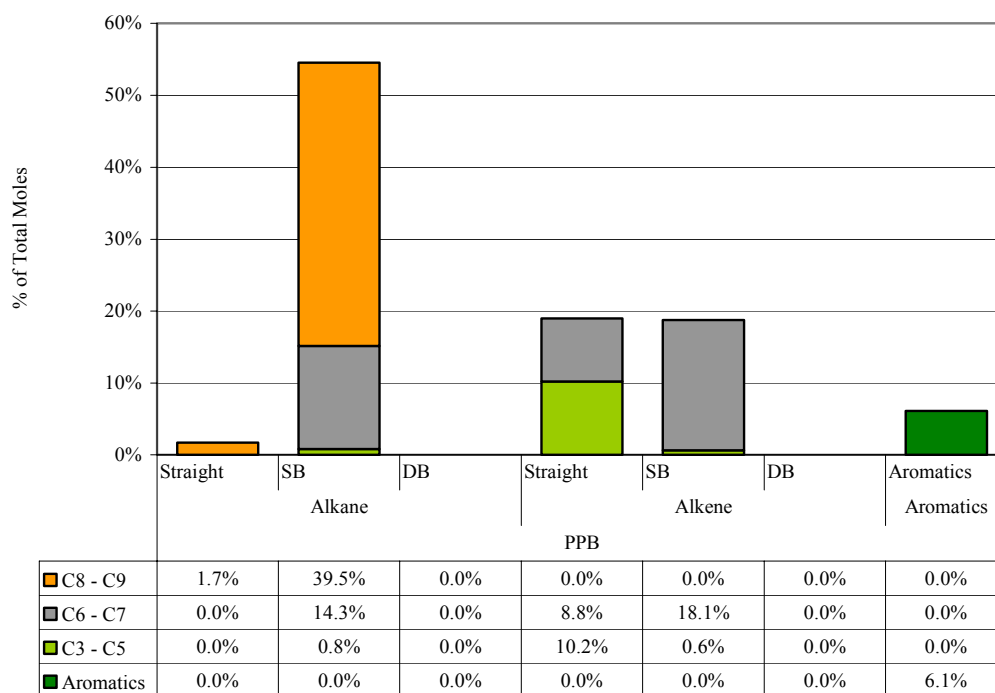
Figure 5.16: Degradation products of pure PPB at 500ºC (% of Total Moles)

	Straight	SB	DB	Straight	SB	DB	Aromatics
		Alkane			Alkene		Aromatics
				PPB			
■ C8 - C9	1.9%	47.9%	0.0%	0.0%	0.0%	0.0%	0.0%
■ C6 - C7	0.0%	13.2%	0.0%	7.6%	16.9%	0.0%	0.0%
■ C3 - C5	0.0%	0.6%	0.0%	5.6%	0.5%	0.0%	0.0%
■ Aromatics	0.0%	0.0%	0.0%	0.0%	0.0%	0.0%	5.8%
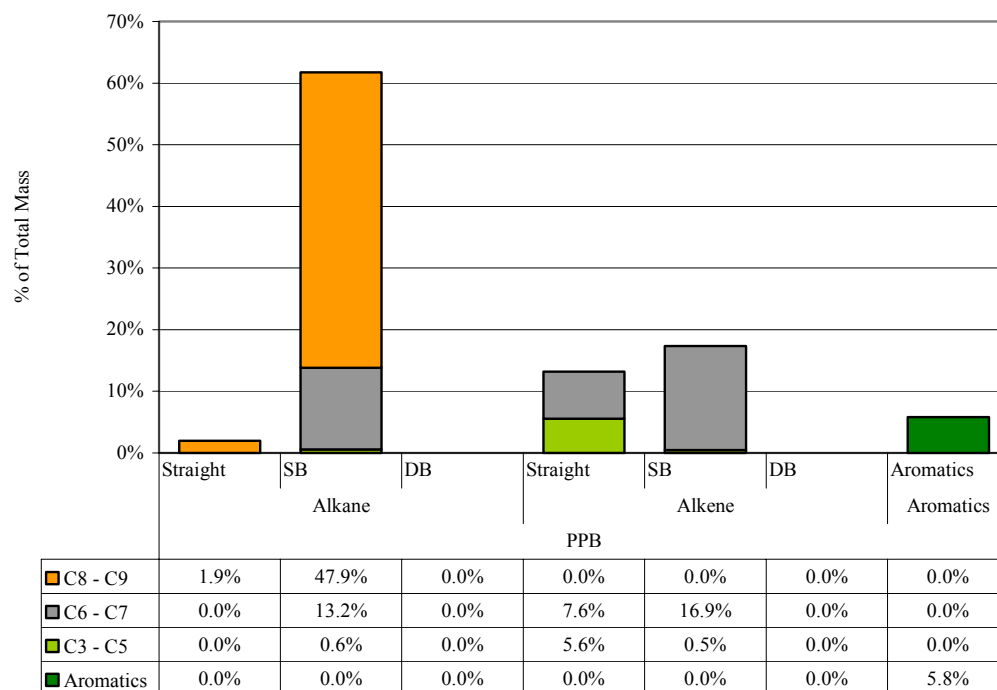
Figure 5.17: Degradation products of pure PPB at 500ºC (% of Total Mass)

The non-catalytic degradation of pure polypropylene B at 500ºC (Figure 5.17) was very different to that for LDPE (Figure 5.15). Very few straight chain alkanes were produced (a reduction from 33% to 2%), and the amount of single-branched alkanes increased from 25% to 61%, with 48% of them being C_8-C_9 length. A reduction in the straight-chain alkenes was observed from 27% to 13%, whilst no C_8-C_9 single-branched alkenes were formed, so increasing the C_6-C_7 content of single-branched alkenes from 7% to 17%. The aromatic content increased to 6% of the total mass.

It was hoped that LDPE and polypropylene would yield higher-grade products (branched products and aromatics, with a reduction in straight-chain alkanes) when the polymers are degraded in the presence of a catalyst.

5.2.4.2.2 Fulcat 435

	Alkane			Alkene			Aromatics
PLDPE	Straight	SB	DB	Straight	SB	DB	Aromatics
■ C8 - C9	0.0%	16.3%	0.0%	0.0%	0.0%	0.0%	0.0%
■ C6 - C7	2.0%	58.3%	0.0%	0.0%	0.0%	0.0%	0.0%
■ C3 - C5	0.0%	10.1%	0.0%	2.6%	0.1%	0.0%	0.0%
■ Aromatics	0.0%	0.0%	0.0%	0.0%	0.0%	0.0%	10.6%
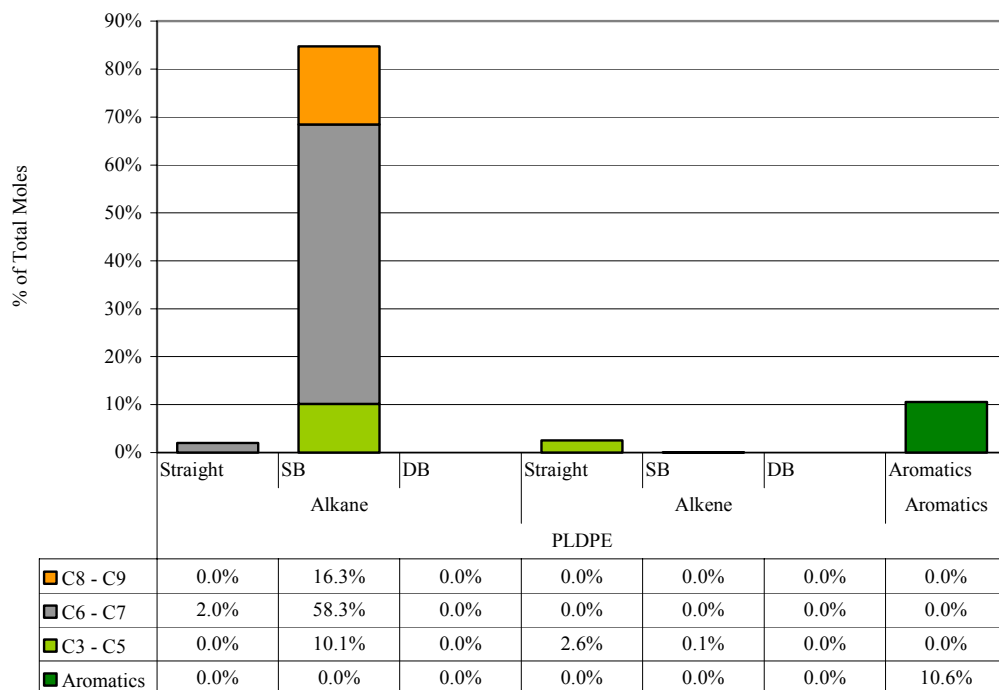
Figure 5.18: Degradation products of pure LDPE and Fulcat 435 at 400ºC (% of Total Moles)

	Alkane			Alkene			Aromatics
PLDPE	Straight	SB	DB	Straight	SB	DB	Aromatics
■ C8 - C9	0.0%	20.2%	0.0%	0.0%	0.0%	0.0%	0.0%
■ C6 - C7	2.0%	58.3%	0.0%	0.0%	0.0%	0.0%	0.0%
■ C3 - C5	0.0%	7.8%	0.0%	1.4%	0.1%	0.0%	0.0%
■ Aromatics	0.0%	0.0%	0.0%	0.0%	0.0%	0.0%	10.2%
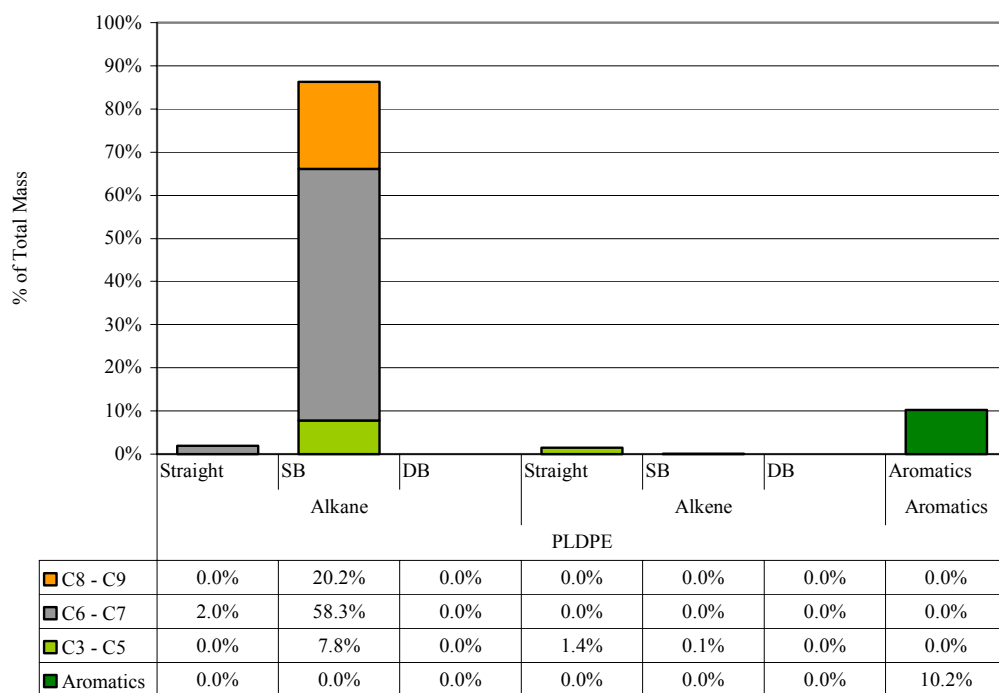
Figure 5.19: Degradation products of pure LDPE and Fulcat 435 at 400ºC (% of Total Mass)

257

Even at the lower temperature of 400ºC, Figure 5.19 appears to show that the heating of LDPE in the presence of Fulcat 435 clay catalyst has reduced the amount of straight chain alkanes by 30% in comparison to thermal degradation. The proportion of alkenes was reduced dramatically from 35% of the total mass to less than 2%. No double-branched products were formed, however, an increase in the yield of aromatics (10% of total mass) was observed. The main products for the degradation of LDPE in the presence of Fulcat 435 clay were single-branched alkanes (86%) with 58% of those being C_6-C_7 length.

| | Alkane | | | Alkene | | | Aromatics |
	Straight	SB	DB	Straight	SB	DB	Aromatics
				PLDPE			
C8 - C9	0.0%	8.6%	0.0%	0.0%	0.0%	0.0%	0.0%
C6 - C7	2.5%	60.2%	0.0%	1.2%	8.7%	0.0%	0.0%
C3 - C5	0.0%	10.3%	0.0%	2.7%	3.0%	0.0%	0.0%
Aromatics	0.0%	0.0%	0.0%	0.0%	0.0%	0.0%	2.8%
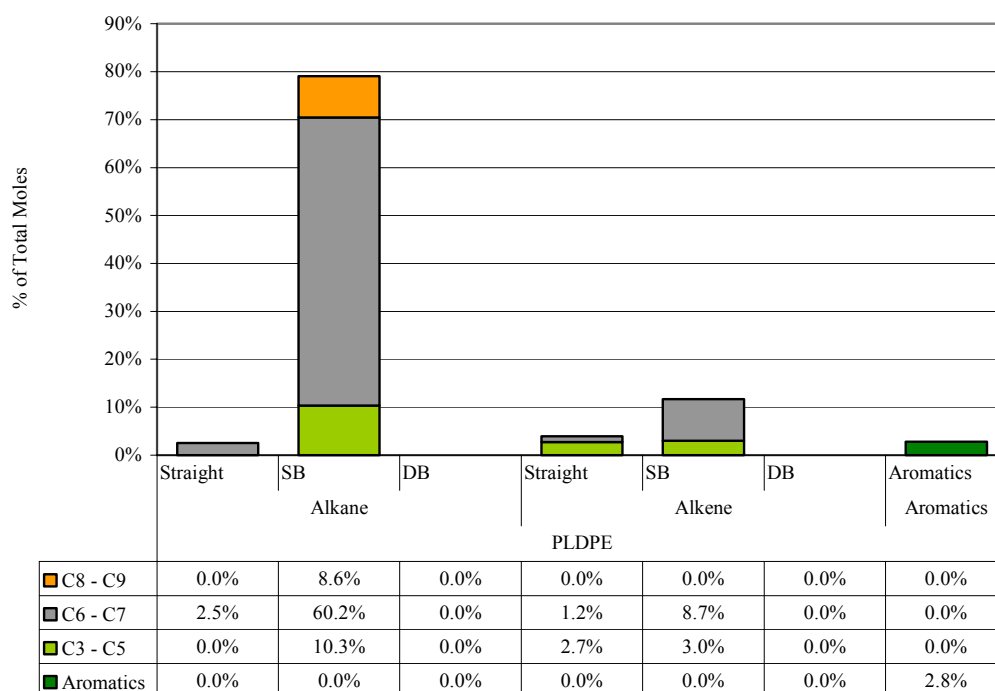
Figure 5.20: Degradation products of pure LDPE and Fulcat 435 at 450ºC (% of Total Moles)

	Straight	SB	DB	Straight	SB	DB	Aromatics
		Alkane			Alkene		Aromatics
				PLDPE			
■ C8 - C9	0.0%	11.0%	0.0%	0.0%	0.0%	0.0%	0.0%
■ C6 - C7	2.4%	62.5%	0.0%	1.1%	8.5%	0.0%	0.0%
■ C3 - C5	0.0%	8.3%	0.0%	1.4%	2.3%	0.0%	0.0%
■ Aromatics	0.0%	0.0%	0.0%	0.0%	0.0%	0.0%	2.4%

Figure 5.21: Degradation products of pure LDPE and Fulcat 435 at 450ºC (% of Total Mass)

From Figure 5.21, increasing the temperature of degradation of LDPE in the presence of Fulcat 435 appears to almost halve the amount of C_8-C_9 single-branched alkanes (from 20% to 11% of the total mass) and increased the total amount of alkene products from less than 2% to 13%. The yield of aromatics was reduced from 10% at 400ºC to 2.4% at 450ºC, but this may be due to the increase in alkene formation. Single-branched alkanes still remained as the most abundant product at almost 82% of the total mass, with the C_6-C_7 content of this remaining at around 60% (as seen at 400ºC).

	Straight	SB	DB	Straight	SB	DB	Aromatics
		Alkane			Alkene		Aromatics
			PLDPE				
■ C8 - C9	0.0%	5.5%	0.0%	0.0%	0.0%	0.0%	0.0%
■ C6 - C7	1.5%	57.0%	0.0%	3.1%	14.7%	0.0%	0.0%
■ C3 - C5	0.0%	9.7%	0.0%	3.3%	2.9%	0.0%	0.0%
■ Aromatics	0.0%	0.0%	0.0%	0.0%	0.0%	0.0%	2.4%
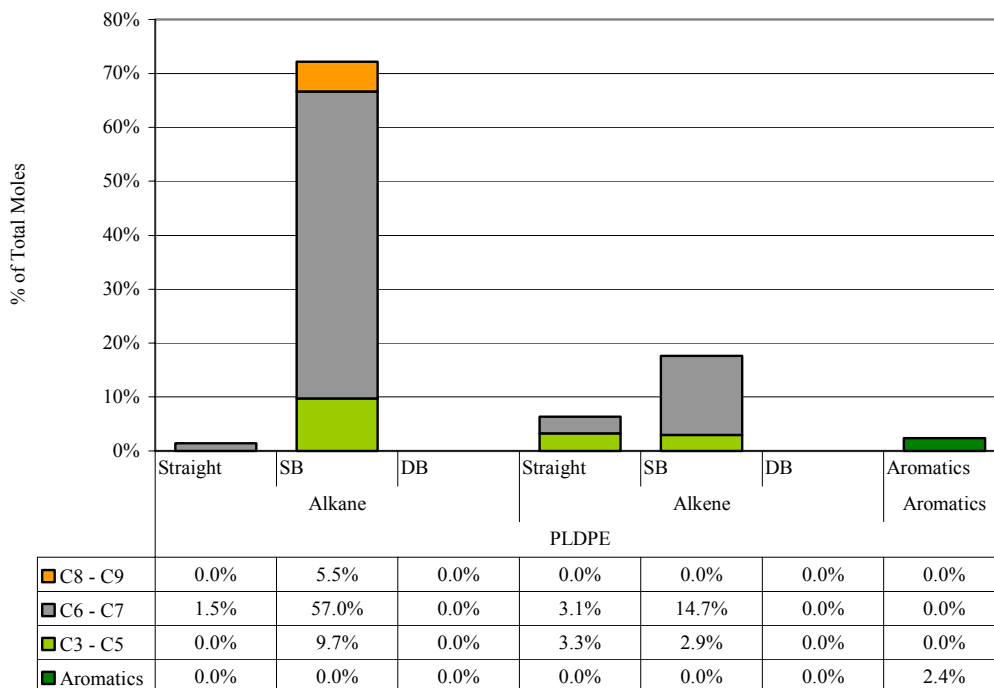
Figure 5.22: Degradation products of pure LDPE and Fulcat 435 at 500ºC (% of Total Moles)

	Straight	SB	DB	Straight	SB	DB	Aromatics
		Alkane			Alkene		Aromatics
			PLDPE				
■ C8 - C9	0.0%	7.1%	0.0%	0.0%	0.0%	0.0%	0.0%
■ C6 - C7	1.6%	59.5%	0.0%	3.2%	14.7%	0.0%	0.0%
■ C3 - C5	0.0%	7.9%	0.0%	1.6%	2.3%	0.0%	0.0%
■ Aromatics	0.0%	0.0%	0.0%	0.0%	0.0%	0.0%	2.1%
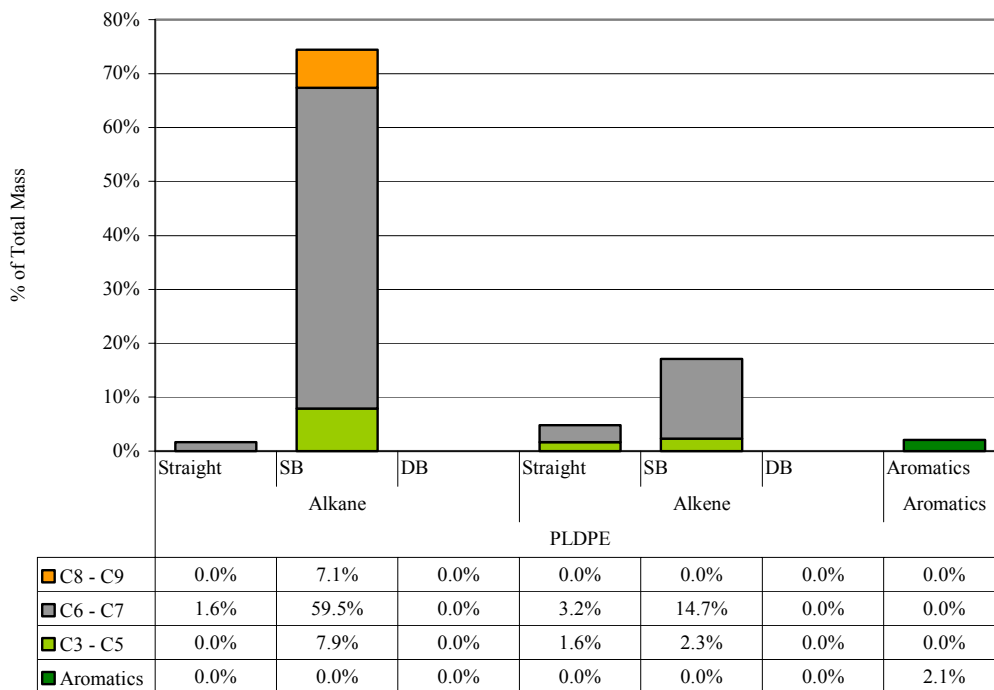
Figure 5.23: Degradation products of pure LDPE and Fulcat 435 at 500ºC (% of Total Mass)

By increasing the temperature of degradation of LDPE and Fulcat 435 to 500ºC (Figure 5.23), the total amount of single-branched alkanes has reduced slightly from 82% to 74.5%, with the C_3-C_5 content remaining constant at 8%. An increase in the number of alkenes was observed, with these making up almost 22% of the total mass. The aromatic content still remained very low (2%). No double-branched alkanes or alkenes were formed at decomposition temperatures of 400ºC, 450ºC or 500ºC.

	Straight	SB	DB	Straight	SB	DB	Aromatics
		Alkane			Alkene		Aromatics
				PPB			
■ C8 - C9	0.0%	0.0%	0.0%	0.0%	0.0%	0.0%	0.0%
■ C6 - C7	0.0%	51.4%	0.0%	4.0%	20.5%	0.0%	0.0%
■ C3 - C5	0.0%	12.1%	0.0%	8.7%	1.4%	0.0%	0.0%
■ Aromatics	0.0%	0.0%	0.0%	0.0%	0.0%	0.0%	1.9%
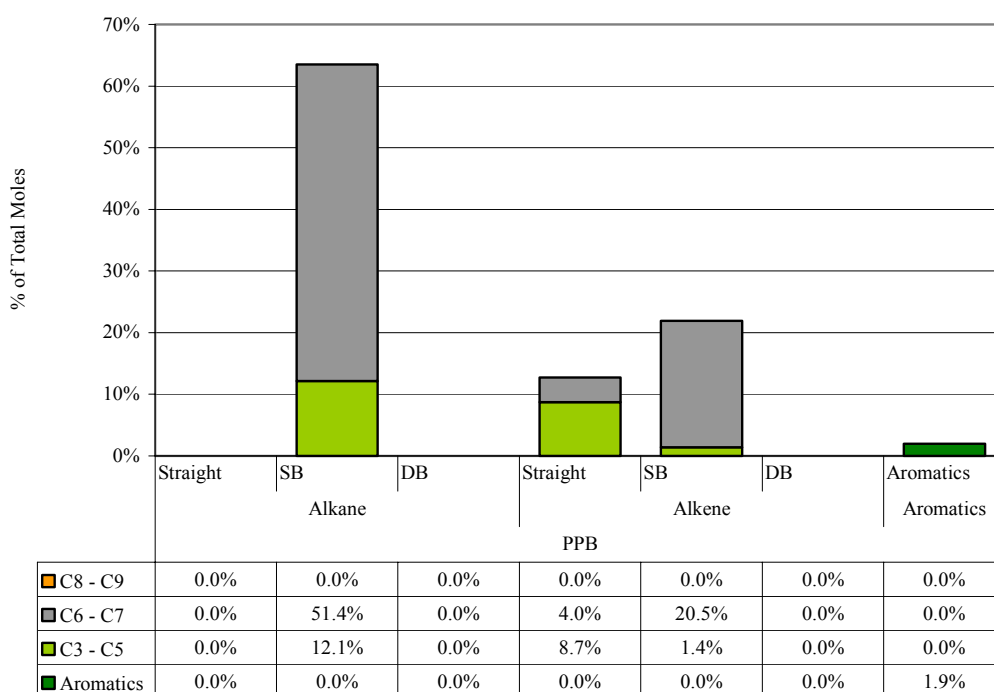
Figure 5.24: Degradation products of pure PPB and Fulcat 435 at 500ºC (% of Total Moles)

	Straight	SB	DB	Straight	SB	DB	Aromatics
		Alkane			Alkene		Aromatics
				PPB			
■ C8 - C9	0.0%	0.0%	0.0%	0.0%	0.0%	0.0%	0.0%
■ C6 - C7	0.0%	55.5%	0.0%	4.2%	21.3%	0.0%	0.0%
■ C3 - C5	0.0%	10.2%	0.0%	5.9%	1.1%	0.0%	0.0%
■ Aromatics	0.0%	0.0%	0.0%	0.0%	0.0%	0.0%	1.7%
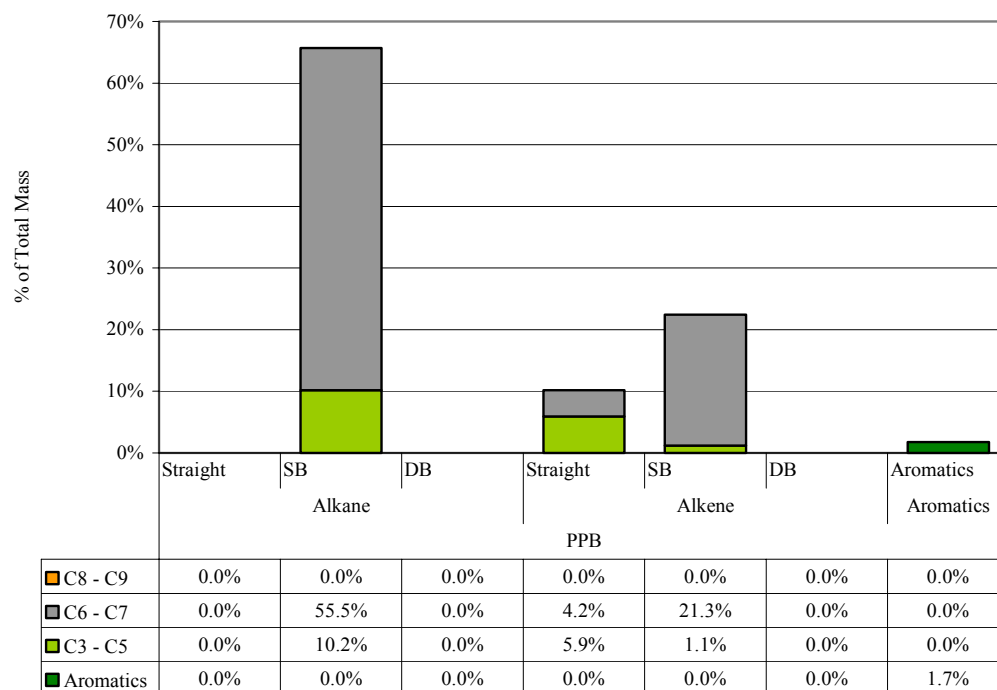
Figure 5.25: Degradation products of pure PPB and Fulcat 435 at 500ºC (% of Total Mass)

The decomposition of polypropylene with Fulcat 435 at 500ºC (Figure 5.25), found that no C_8-C_9 alkane products were formed. The amount of single-branched alkanes had been reduced from 74.5% of the total to 65.7% of the total mass, whilst the proportion of alkenes had increased from 22% to 32%. A larger proportion of straight chain alkenes were formed (10%) than for LDPE (5%) at the same temperature. The aromatic content still remained very low at 1.7% of the total mass.

5.2.4.2.3 23z

	Straight	SB	DB	Straight	SB	DB	Aromatics
		Alkane			Alkene		Aromatics
				PPB			
■ C8 - C9	0.0%	0.0%	0.0%	0.0%	0.0%	0.0%	0.0%
■ C6 - C7	5.8%	52.1%	0.0%	4.3%	18.1%	0.0%	0.0%
■ C3 - C5	0.0%	6.3%	0.0%	3.7%	1.3%	0.0%	0.0%
■ Aromatics	0.0%	0.0%	0.0%	0.0%	0.0%	0.0%	8.5%
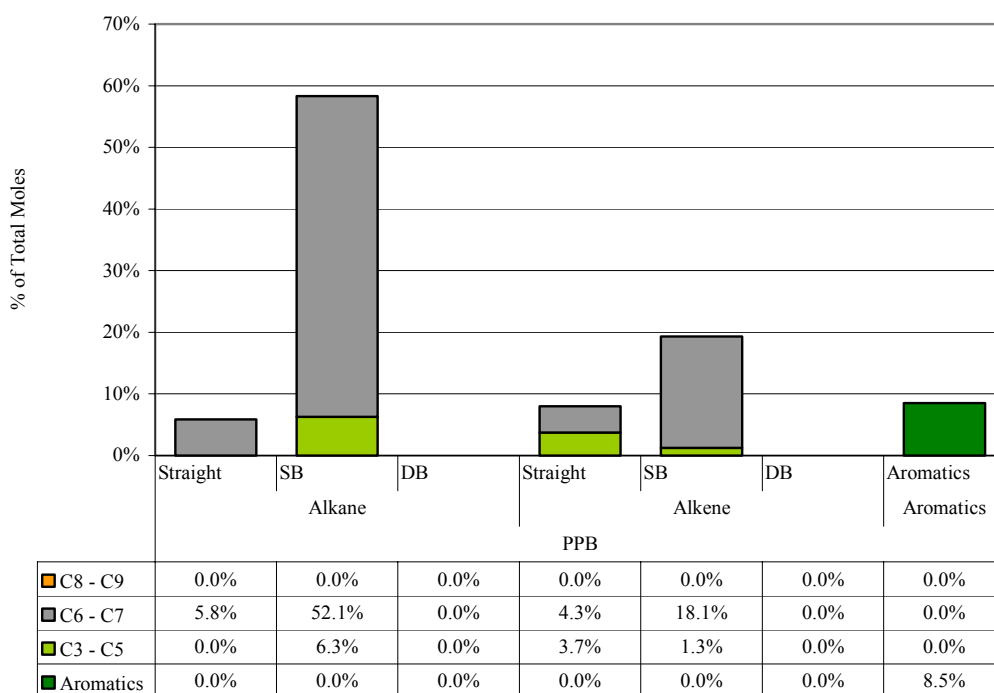
Figure 5.26: Degradation products of pure PPB and 23z at 450ºC (% of Total Moles)

	Straight	SB	DB	Straight	SB	DB	Aromatics
		Alkane			Alkene		Aromatics
				PPB			
■ C8 - C9	0.0%	0.0%	0.0%	0.0%	0.0%	0.0%	0.0%
■ C6 - C7	5.8%	54.6%	0.0%	4.5%	18.4%	0.0%	0.0%
■ C3 - C5	0.0%	5.1%	0.0%	2.2%	1.0%	0.0%	0.0%
■ Aromatics	0.0%	0.0%	0.0%	0.0%	0.0%	0.0%	8.3%
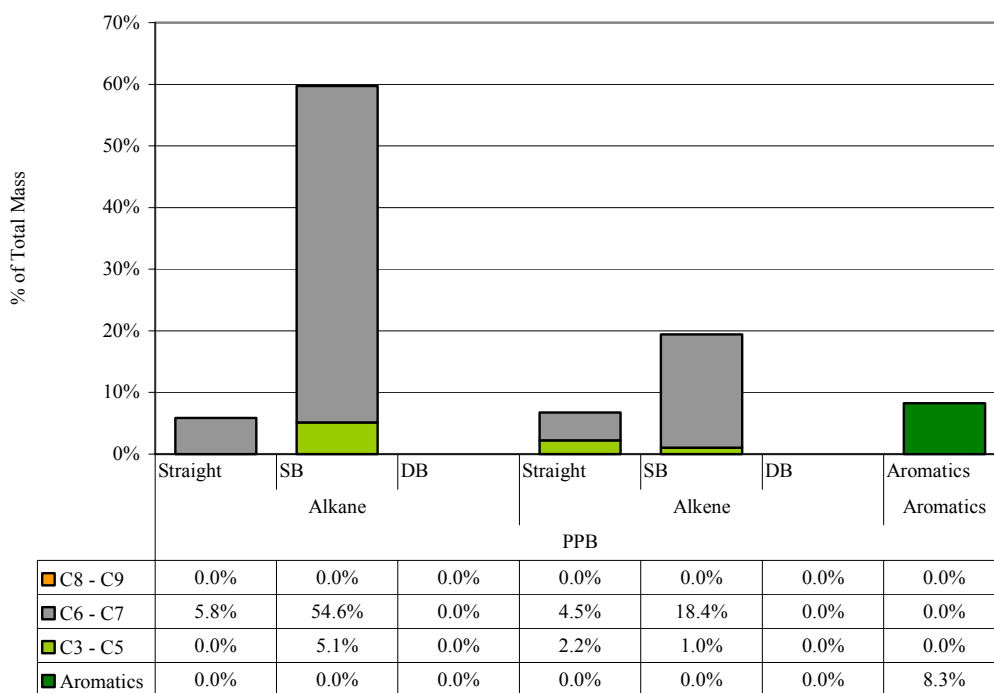
Figure 5.27: Degradation products of pure PPB and 23z at 450ºC (% of Total Mass)

263

Figure 5.27 shows the degradation products of polypropylene in the presence of ZSM-5 zeolite catalyst, 23z, at 450ºC. This resulted in the formation of 59% single-branched alkanes (54% C_6-C_7 length), along with a small proportion of straight chain alkanes of C_6-C_7 length (6%). Alkenes made up 26% of the total mass of products, with 18% of those being single-branched C_6-C_7 products. The aromatic content increased noticeably to 8%. No double-branched products or C_8-C_9 alkanes or alkenes were formed.

	Straight	SB	DB	Straight	SB	DB	Aromatics
		Alkane			Alkene		Aromatics
				PPB			
C8 - C9	0.0%	0.0%	0.0%	0.0%	0.0%	0.0%	0.0%
C6 - C7	5.2%	47.8%	0.0%	5.7%	22.0%	0.0%	0.0%
C3 - C5	0.0%	4.5%	0.0%	2.2%	1.5%	0.0%	0.0%
Aromatics	0.0%	0.0%	0.0%	0.0%	0.0%	0.0%	11.1%
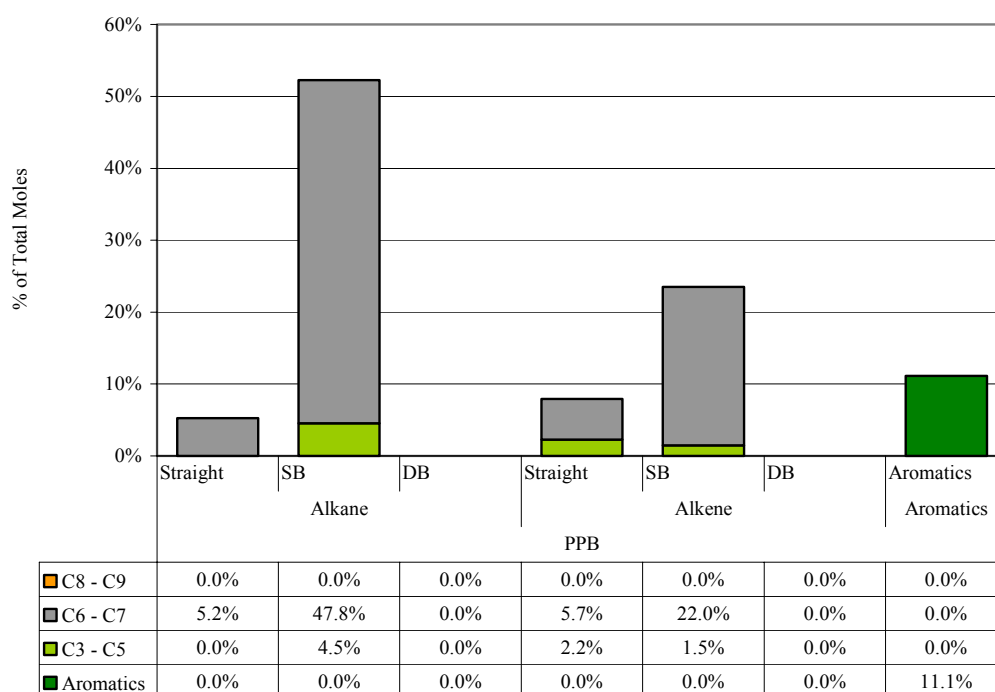
Figure 5.28: Degradation products of pure PPB and 23z at 500ºC (% of Total Moles)

| | Straight | SB | DB | Straight | SB | DB | Aromatics |
| | Alkane | | | Alkene | | | Aromatics |
				PPB			
■ C8 - C9	0.0%	0.0%	0.0%	0.0%	0.0%	0.0%	0.0%
■ C6 - C7	5.3%	49.8%	0.0%	6.0%	22.3%	0.0%	0.0%
■ C3 - C5	0.0%	3.6%	0.0%	1.3%	1.1%	0.0%	0.0%
■ Aromatics	0.0%	0.0%	0.0%	0.0%	0.0%	0.0%	10.5%
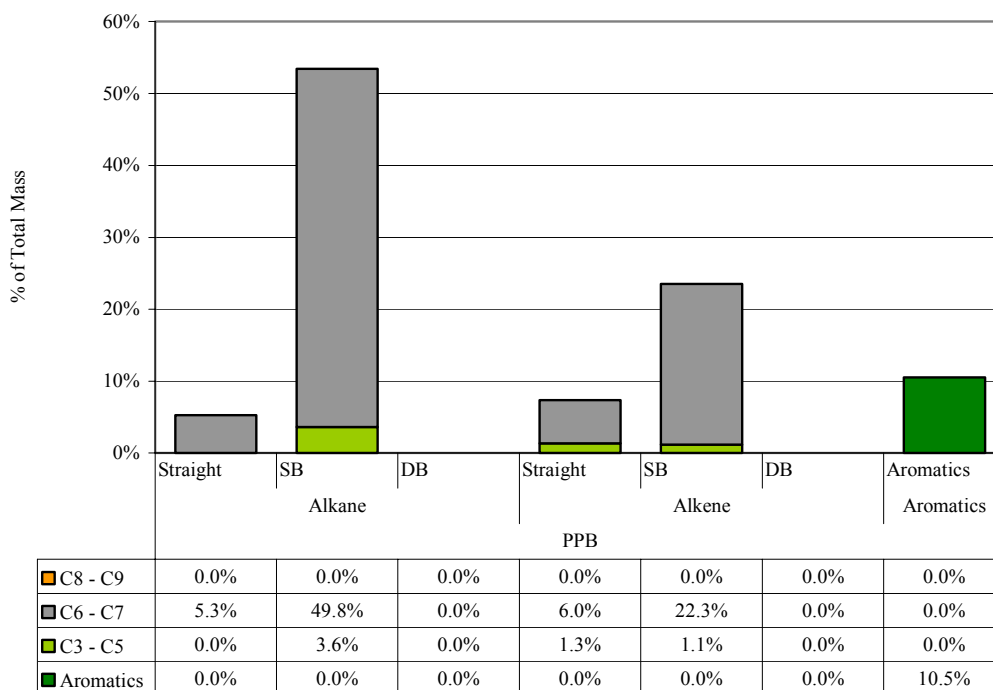
Figure 5.29: Degradation products of pure PPB and 23z at 500ºC (% of Total Mass)

Increasing the degradation temperature of polypropylene and 23z from 450ºC to 500ºC resulted in the amount of straight chain alkanes remaining constant at around 5%, whilst the proportion of single-branched alkanes reduced from 59% to 53%. The total yield of alkenes was found to increase slightly from 26% to 30.7%. The aromatic content increased noticeably in comparison to degradation in the presence of Fulcat 435, giving an 11% yield in comparison to 2% when polypropylene was degraded at 500ºC with the clay. Again, no double-branched products or C_8-C_9 alkanes or alkenes were formed (see Figure 5.29).

	Straight	SB	DB	Straight	SB	DB	Aromatics
		Alkane			Alkene		Aromatics
				PLDPE			
■ C8 - C9	24.6%	17.6%	0.0%	0.0%	0.0%	0.0%	0.0%
■ C6 - C7	0.0%	18.5%	0.0%	0.0%	8.5%	0.0%	0.0%
■ C3 - C5	0.0%	10.4%	0.0%	1.1%	1.1%	0.0%	0.0%
■ Aromatics	0.0%	0.0%	0.0%	0.0%	0.0%	0.0%	18.2%
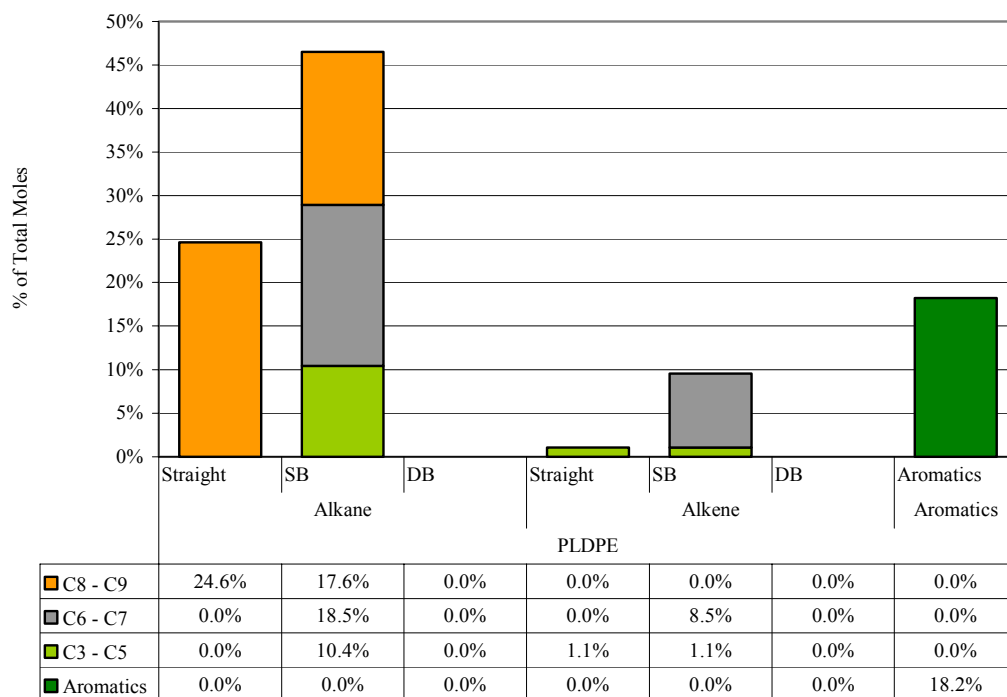
Figure 5.30: Degradation products of pure LDPE and 280z at 400ºC (% of Total Moles)

	Straight	SB	DB	Straight	SB	DB	Aromatics
		Alkane			Alkene		Aromatics
				PLDPE			
■ C8 - C9	29.4%	21.7%	0.0%	0.0%	0.0%	0.0%	0.0%
■ C6 - C7	0.0%	16.6%	0.0%	0.0%	6.6%	0.0%	0.0%
■ C3 - C5	0.0%	7.2%	0.0%	0.7%	0.7%	0.0%	0.0%
■ Aromatics	0.0%	0.0%	0.0%	0.0%	0.0%	0.0%	17.0%
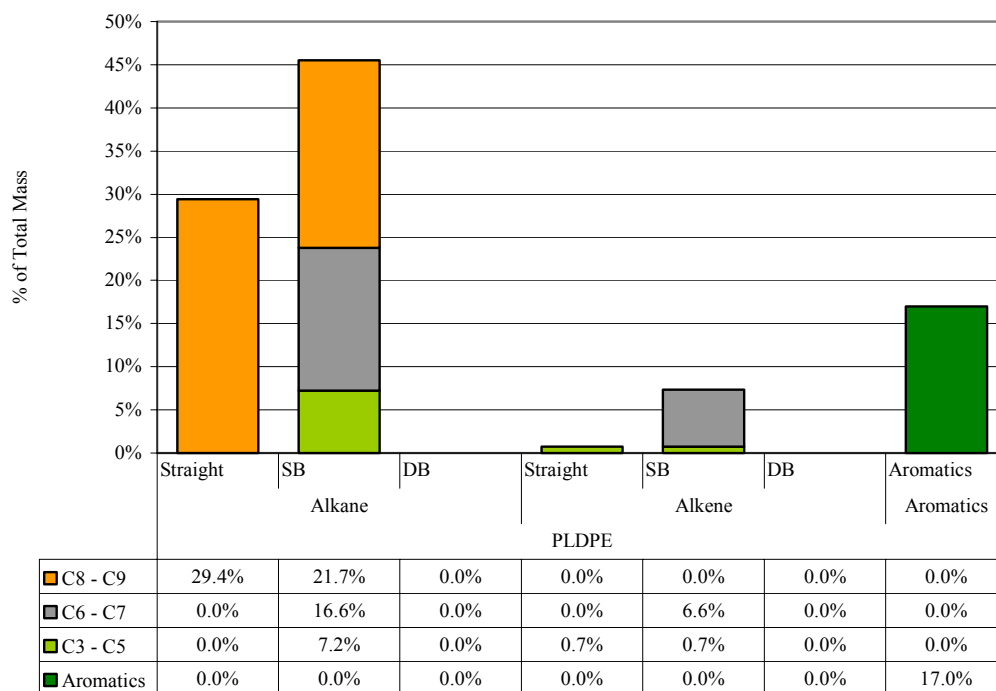
Figure 5.31: Degradation products of pure LDPE and 280z at 400ºC (% of Total Mass)

266

The degradation of LDPE in the presence of 280z zeolite produced some very interesting results (Figure 5.31). Noticeable differences were observed between the products formed with this catalyst in comparison to those formed in the presence of 23z zeolite and Fulcat 435 clay. At 400ºC, 51% of the total mass was C_8-C_9 alkanes (either straight chain or single-branched), whereas for the other catalysts, only a very small proportion, if any, of C_8-C_9 products were detected. Additionally, the yield of aromatics increased to 17%, at the expense of alkene formation, which reduced to 8% of the total mass.

| | Alkane | | | Alkene | | | Aromatics |
	Straight	SB	DB	Straight	SB	DB	Aromatics
C8 - C9	0.0%	2.9%	0.0%	0.0%	0.0%	0.0%	0.0%
C6 - C7	5.5%	33.6%	0.0%	4.4%	5.8%	0.0%	0.0%
C3 - C5	0.0%	5.3%	0.0%	2.9%	0.8%	0.0%	0.0%
Aromatics	0.0%	0.0%	0.0%	0.0%	0.0%	0.0%	38.7%
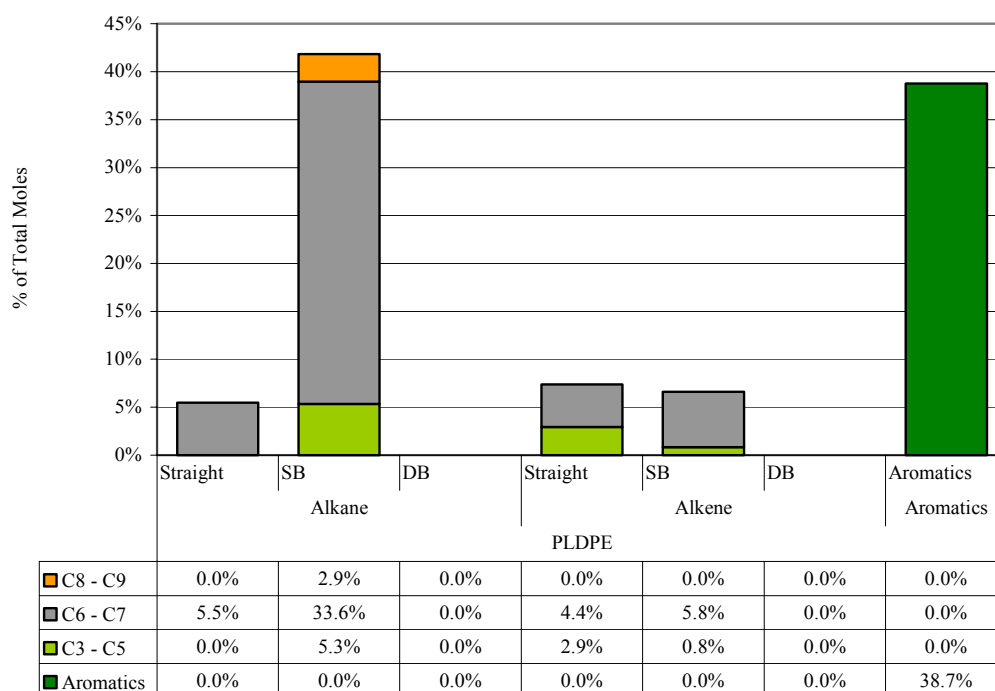
Figure 5.32: Degradation products of pure LDPE and 280z at 450ºC (% of Total Moles)

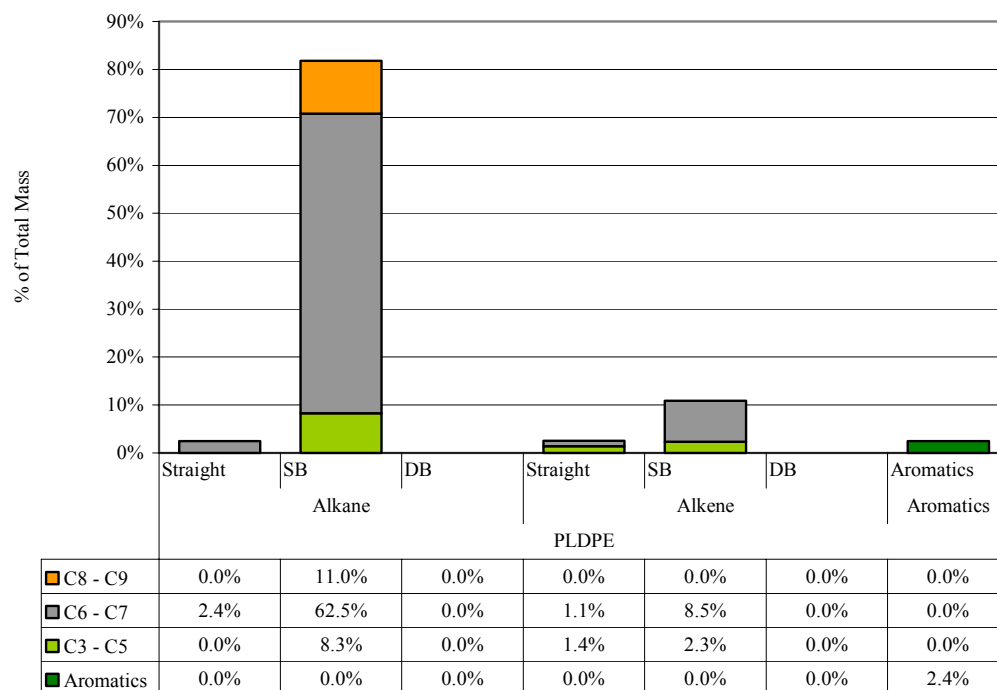|	Straight	SB	DB	Straight	SB	DB	Aromatics
		Alkane			Alkene		Aromatics
				PLDPE			
■ C8 - C9	0.0%	3.5%	0.0%	0.0%	0.0%	0.0%	0.0%
■ C6 - C7	5.3%	33.3%	0.0%	4.7%	5.6%	0.0%	0.0%
■ C3 - C5	0.0%	4.2%	0.0%	1.7%	0.6%	0.0%	0.0%
■ Aromatics	0.0%	0.0%	0.0%	0.0%	0.0%	0.0%	41.1%
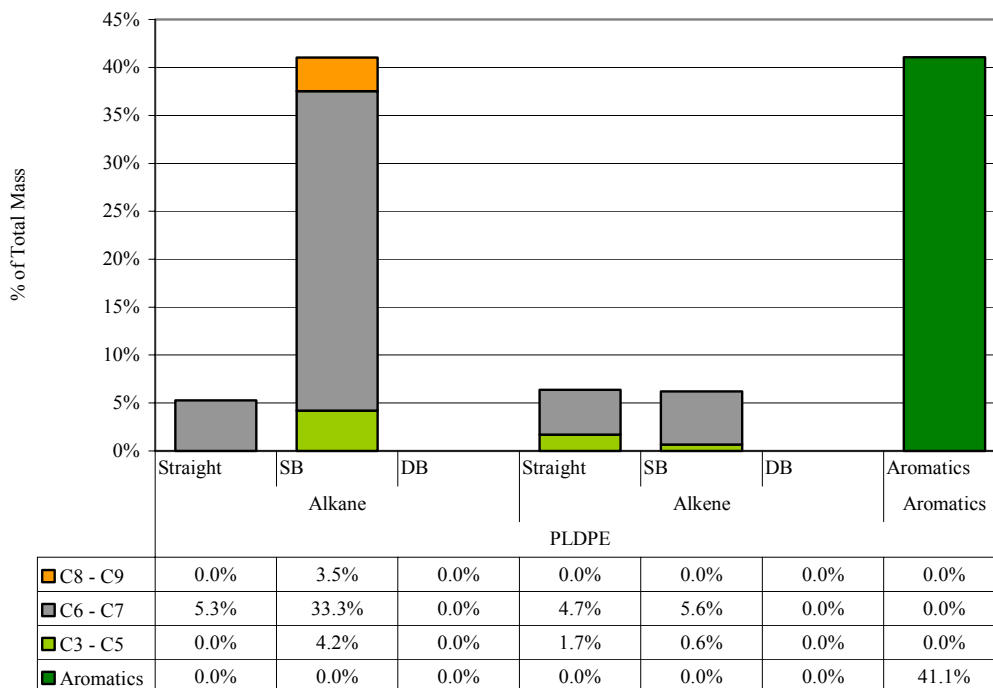
Figure 5.33: Degradation products of pure LDPE and 280z at 450ºC (% of Total Mass)

As shown in Figure 5.33, increasing the temperature of degradation of LDPE and 280z from 400ºC to 450ºC reduced the total amount of C_8-C_9 products drastically, from a total of 51% to only 3.5%. This resulted in the total amount of C_6-C_7 alkanes (straight chain and single-branched) increasing from 16% to 38%. The amount of alkene products still remained relatively low at 13% (8% at 400ºC), whilst the aromatic content increased dramatically from 17% at 400ºC to 41% of the total mass at 450ºC. No double-branched alkanes or alkenes were produced.

	Straight	SB	DB	Straight	SB	DB	Aromatics
	Alkane			Alkene			Aromatics
			PLDPE				
□ C8 - C9	0.0%	0.0%	0.0%	0.0%	0.0%	0.0%	0.0%
□ C6 - C7	7.0%	35.8%	0.0%	3.3%	12.6%	0.0%	0.0%
□ C3 - C5	0.0%	7.0%	0.0%	2.7%	1.2%	0.0%	0.0%
■ Aromatics	0.0%	0.0%	0.0%	0.0%	0.0%	0.0%	30.4%
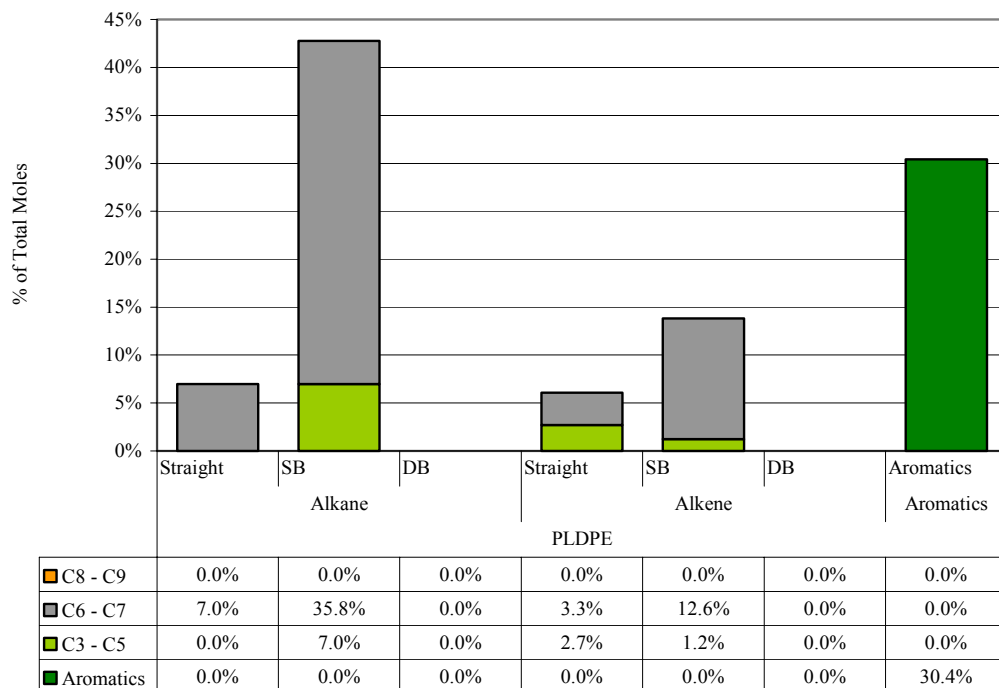
Figure 5.34: Degradation products of pure LDPE and 280z at 500ºC (% of Total Moles)

	Straight	SB	DB	Straight	SB	DB	Aromatics
	Alkane			Alkene			Aromatics
			PLDPE				
□ C8 - C9	0.0%	0.0%	0.0%	0.0%	0.0%	0.0%	0.0%
□ C6 - C7	6.8%	36.2%	0.0%	3.5%	12.8%	0.0%	0.0%
□ C3 - C5	0.0%	5.6%	0.0%	1.5%	0.9%	0.0%	0.0%
■ Aromatics	0.0%	0.0%	0.0%	0.0%	0.0%	0.0%	32.6%
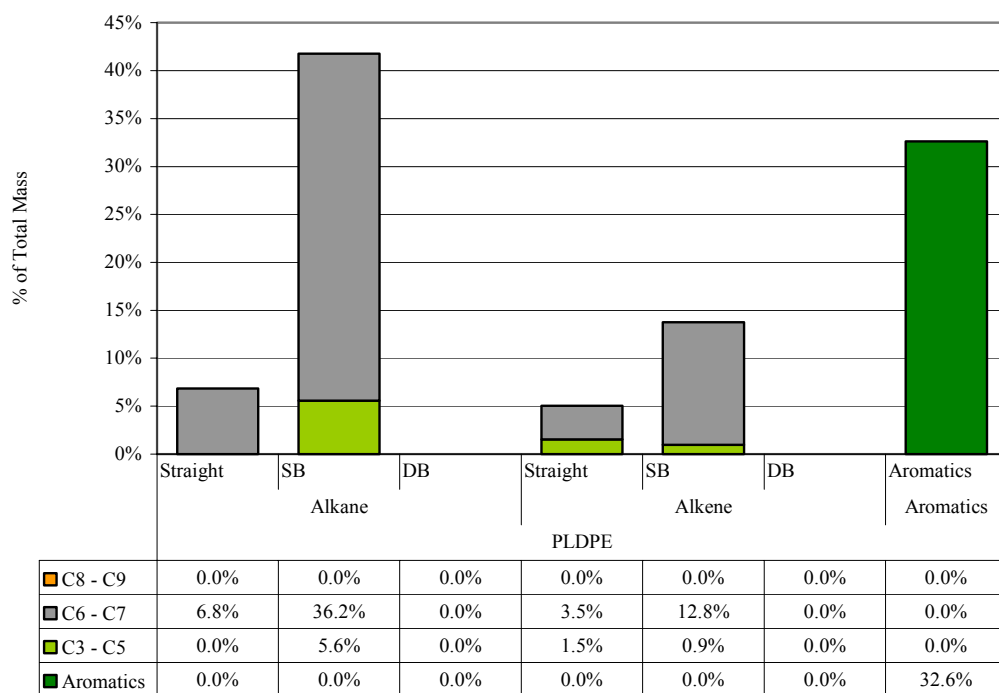
Figure 5.35: Degradation products of pure LDPE and 280z at 500ºC (% of Total Mass)

The degradation of LDPE in the presence of 280z at 500ºC (Figure 5.35) appeared to produce a constant amount of single-branched alkanes as that seen at 450ºC (but with no small C_8-C_9 fraction). The amount of single-branched alkenes increased from 6% to nearly 14% at the higher temperature. The proportion of aromatics reduced from 41% at 450ºC to 32.6% at 500ºC, which could account for the increase in alkene products. No double-branched alkanes or alkenes were produced.

5.2.4.3 Discussion of Non-Isothermal Results

The un-catalysed thermal degradation of low-density polyethylene at 450ºC produced 66% alkanes, 33% alkenes and 1% aromatics, whilst at 500ºC, the proportions were 56% alkanes, 40% alkenes and 4% aromatics. A larger proportion of C_8-C_9 products were formed when no catalyst was present than in the catalytic degradation with Fulcat 435 clay or 23z zeolite. The formation of alkanes and alkenes and the increase of aromatics with temperature was in agreement with Williams and Williams.[276] This was not in agreement with Breen et al.,[277] who found that the degradation of LDPE without a catalyst produced C_4-C_{22} alkanes, but no branched alkanes.

In comparison with LDPE, the thermal degradation of polypropylene produced few straight chain alkanes (2%) but a large increase in single-branched alkanes of C_8-C_9 length (48%). The longer length alkanes observed with the degradation of PP is consistent with the findings of Onu et al.,[278] who found a greater scission of C-C chains for polyethylene than for polypropylene.

In the presence of the clay catalyst (Fulcat 435), the majority of the products formed appeared to be single-branched alkanes (predominantly C_6-C_7), at the expense of the

formation of alkenes and aromatics. In contrast, decomposition in the presence of 23z zeolite appeared to increase the total alkene fraction and aromatic content in relation to the clay. The increase in alkane production with the Fulcat 435 catalyst could be due to the cancelling out of the alkene C=C double bond with two hydrogen atoms picked up from either the acid activation of the clay, a proton from the Brønsted acid or a hydride ion from the Lewis acid.

The most interesting results appeared to occur when LDPE was degraded at 400ºC, 450ºC and 500ºC in the presence of 280z zeolite catalyst. At 400ºC a large proportion of C_8-C_9 alkanes were produced, with this figure decreasing dramatically with increasing temperature. The formation of a large aromatic content (a maximum of 41% of the total mass at 450ºC) in the presence of zeolites is well documented in the literature (see Appendix A), and is said to be the result of the catalyst having large intra-crystalline pore channels and strong acidity.[279]

From the literature,[72,238] liquid products are often collected from the degradation of PE and PP at temperatures of 400-500ºC. This is not in agreement with the results of this study as the decomposition products were all gaseous at this temperature. This was due to the design of the experiment, in which the sample holder was placed inside the furnace with half of the sample tube above the heated zone. This encouraged larger decomposition products to reflux back down into the heated end of the tube (rather than continue on to the cold trap), resulting in further cracking and rearrangement of products into lighter, gaseous components.

5.2.4.4 Conclusions for Non-Isothermal Experiments

The increase in single-branched alkane products from the degradation of pure LDPE with Fulcat 435 is thought to be due to the addition of two hydrogen atoms across the alkene C=C double bond. Fulcat 435 has undergone acid activation in order to develop Brønsted and Lewis acid sites, which could be responsible for the formation of predominantly alkane products.

In contrast, the degradation of low-density polyethylene in the presence of 280z zeolite produced a large proportion of aromatics components (41% of total mass at 450ºC). The LDPE molecules during decomposition were sufficiently small enough to enter the active sites of the ZSM-5 catalyst where they underwent aromatisation. This increased the relative octane number (RON) of the total products formed, hence 280z catalyst could be very effective when attempting to recycle waste plastics into high-grade fuel.

5.2.4.5 Results of Isothermal GC-MS Experiments

The degradation products for the isothermal experiments were collected every ten minutes over a period of up to 340 minutes. The relative proportions of each component type were calculated and represented as a bar chart. All 'bars' were then placed together to represent the changes in the decomposition products as a percentage of the total mass or moles for the entire experiment. The components were stacked in the order: aromatics, double-branched alkanes, single-branched alkanes, double-branched alkenes, single-branched alkenes, straight chain alkanes and straight chain alkenes (bottom to top). The isothermal results of the degradation of LDPE with 280z (400ºC and 450ºC) are displayed from Figure 5.36 to Figure 5.39. The isothermal results of the degradation of LDPE with Fulcat 435 (400ºC and 450ºC) are displayed

from Figure 5.40 to Figure 5.43. The isothermal results of the degradation of polypropylene with Fulcat 435 clay (450ºC) are displayed from Figure 5.44 to Figure 5.45 below.

Comparing the degradation of LDPE in the presence of Fulcat 435 at 400ºC and 450ºC, it can be seen that only a very small amount of straight chain alkenes and single branched alkenes are produced at the lower of the two temperatures. A marked increase in the number of alkenes was observed when LDPE was held at 450ºC. The major component at 400ºC was single branched alkanes, whereas at 450ºC, although single branched alkanes did appear to be the most common products, the total alkene component (straight chain and single branched) was of a comparable quantity. The amount of aromatics did not appear to alter significantly with increasing temperature. No double branched products were formed at either temperature.

Relating the degradation products of LDPE when heated with Fulcat 435 clay at 450ºC with a similar experiment conducted with polypropylene at 450ºC, the relative abundance of alkanes to alkenes, and straight chain products to single-branched products were found to be similar between the two polymers. For LDPE degraded in the presence of 280z zeolite, an increase in the relative amount of aromatics in relation to the other products was noted at 400ºC. This trend did not appear to occur at 450ºC, however at 400ºC, a marked increase in the yield of aromatics is seen as the run continues. This suggests that as low-density polyethylene is held at a constant temperature of 400ºC, after approximately 180 minutes (3 hours), a greater proportion of aromatic compounds begin to be produced.
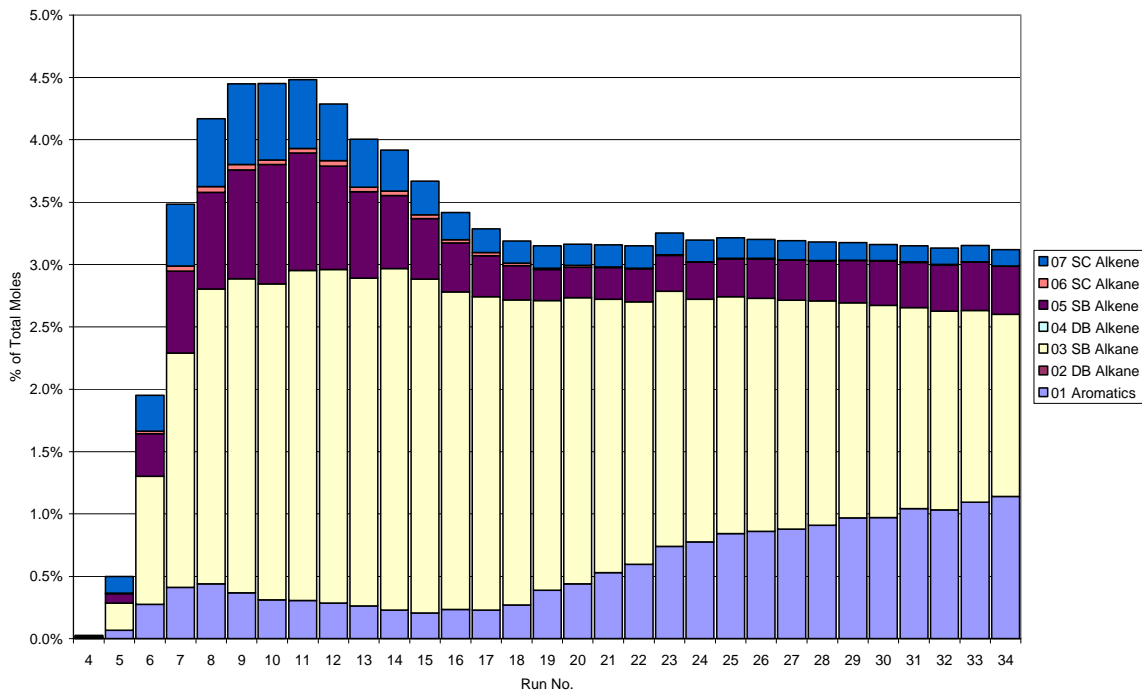
Figure 5.36: Degradation of LDPE with 280z zeolite at 400ºC (% of Total Moles)
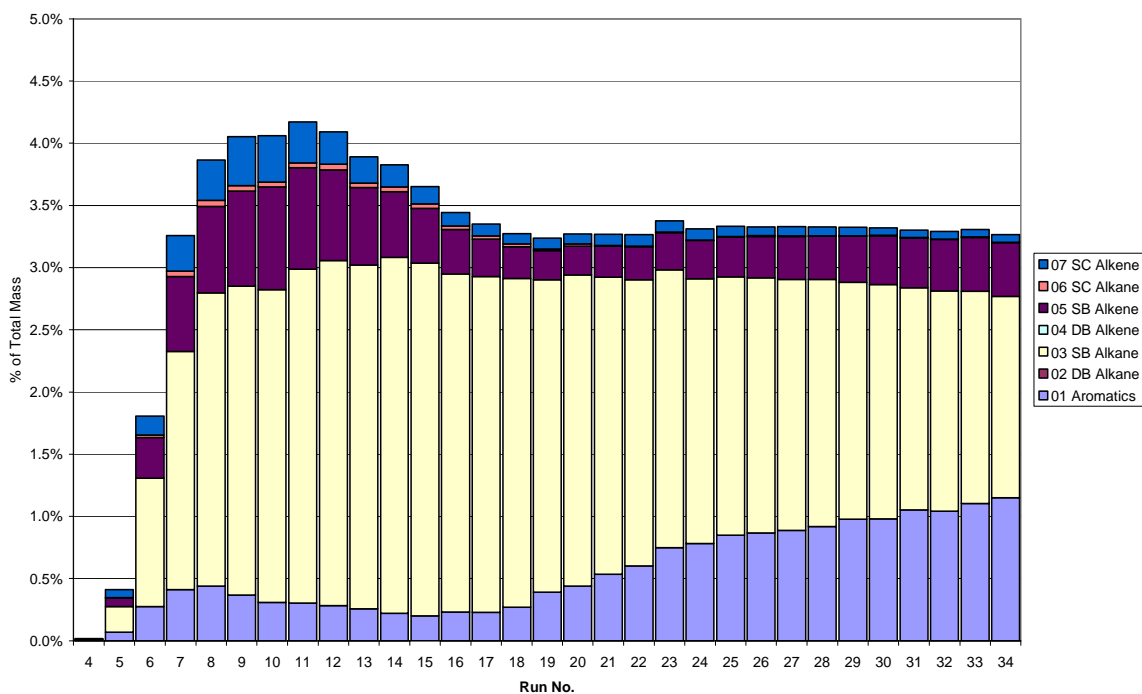
Figure 5.37: Degradation of LDPE with 280z zeolite at 400ºC (% of Total Mass)

274
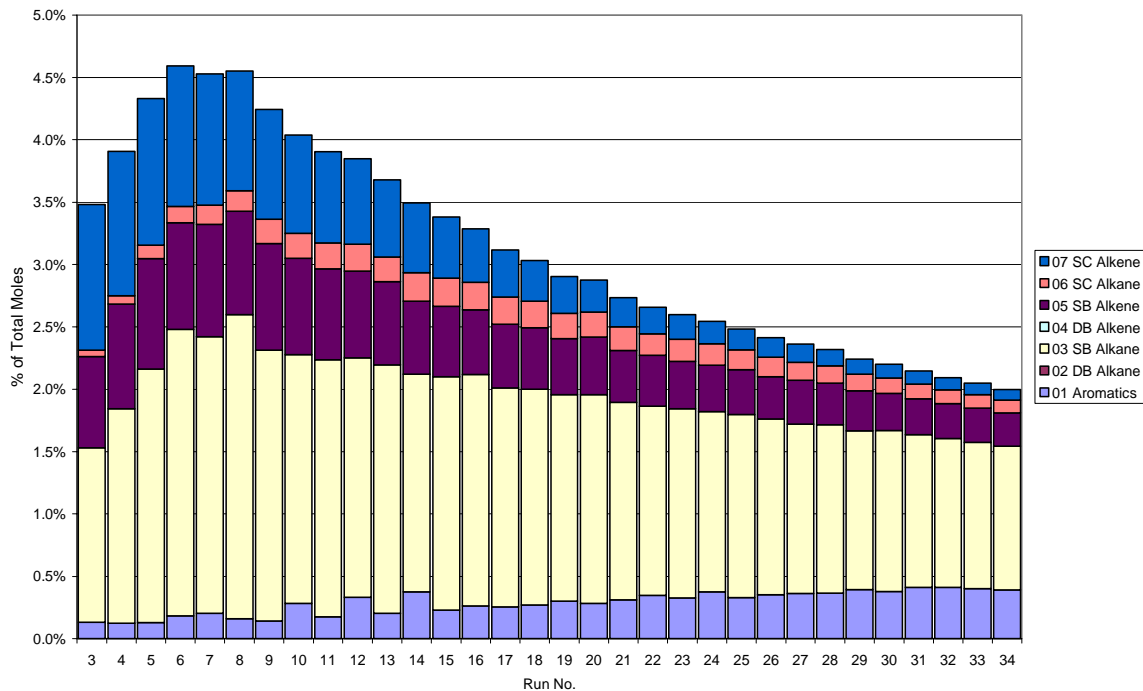
Figure 5.38: Degradation of LDPE with 280z zeolite at 450ºC (% of Total Moles)
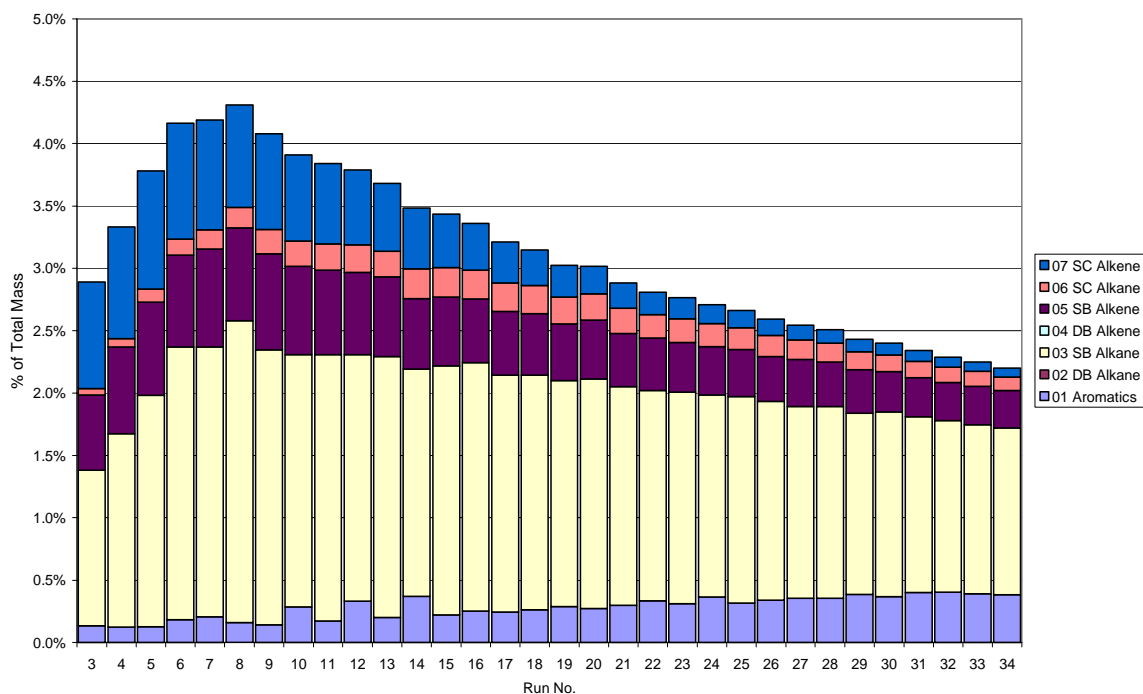
Figure 5.39: Degradation of LDPE with 280z zeolite at 450ºC (% of Total Mass)
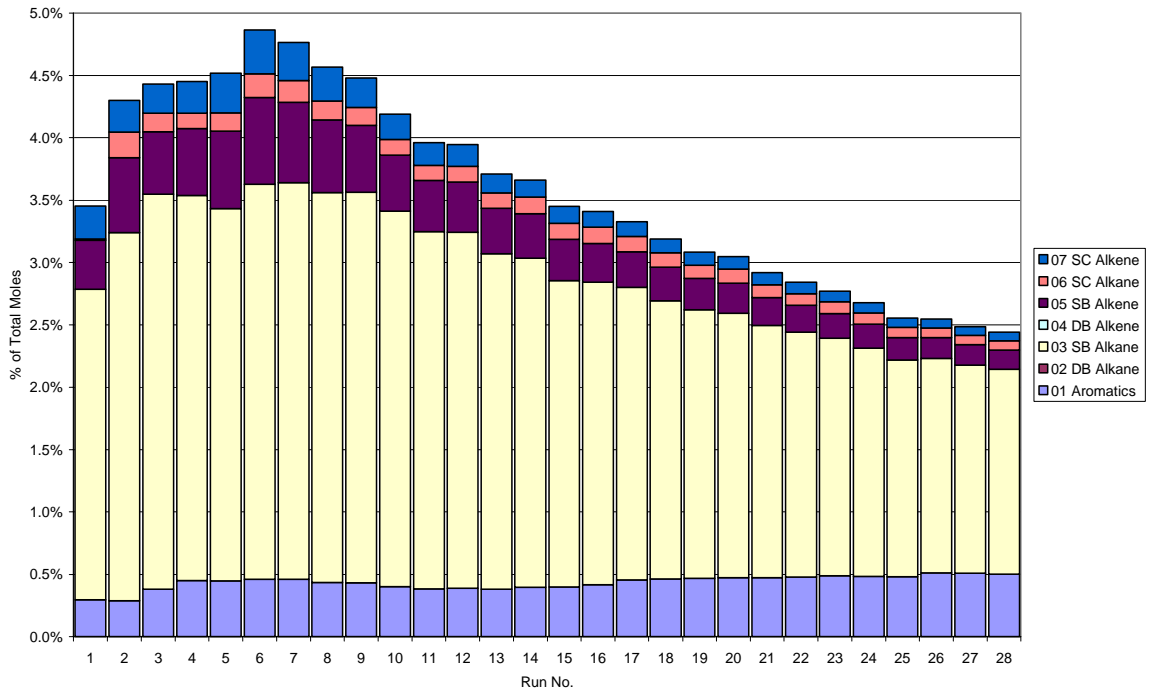
Figure 5.40: Degradation of LDPE with Fulcat 435 at 400ºC (% of Total Moles)
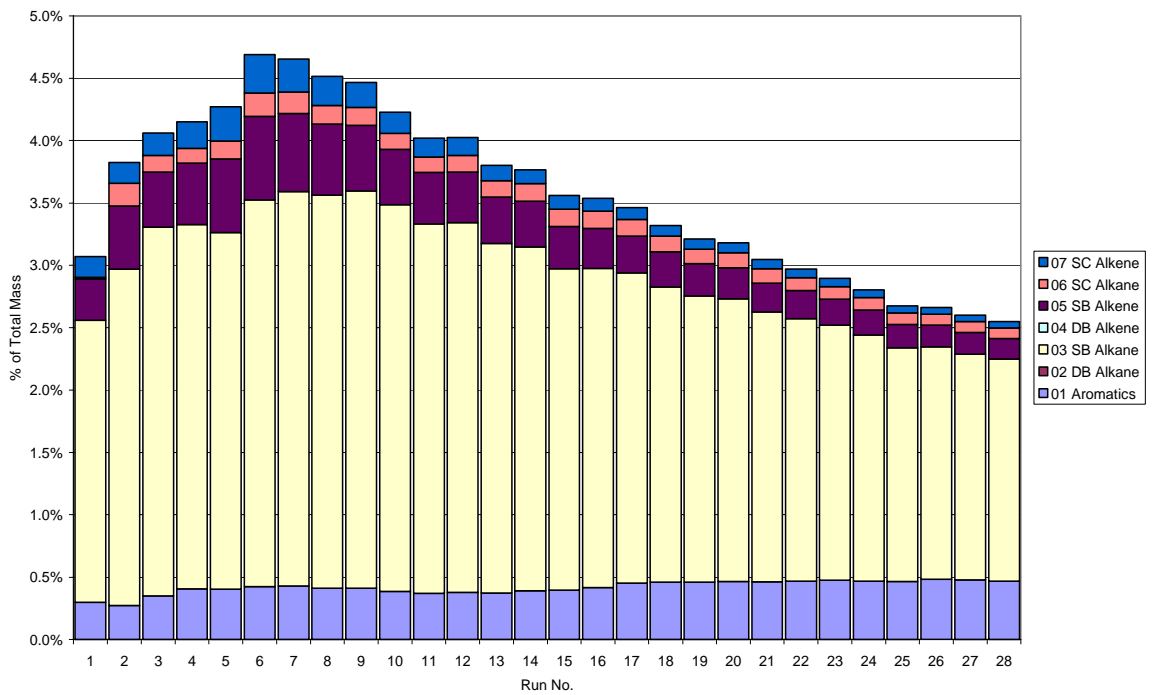
Figure 5.41: Degradation of LDPE with Fulcat 435 at 400ºC (% of Total Mass)

276
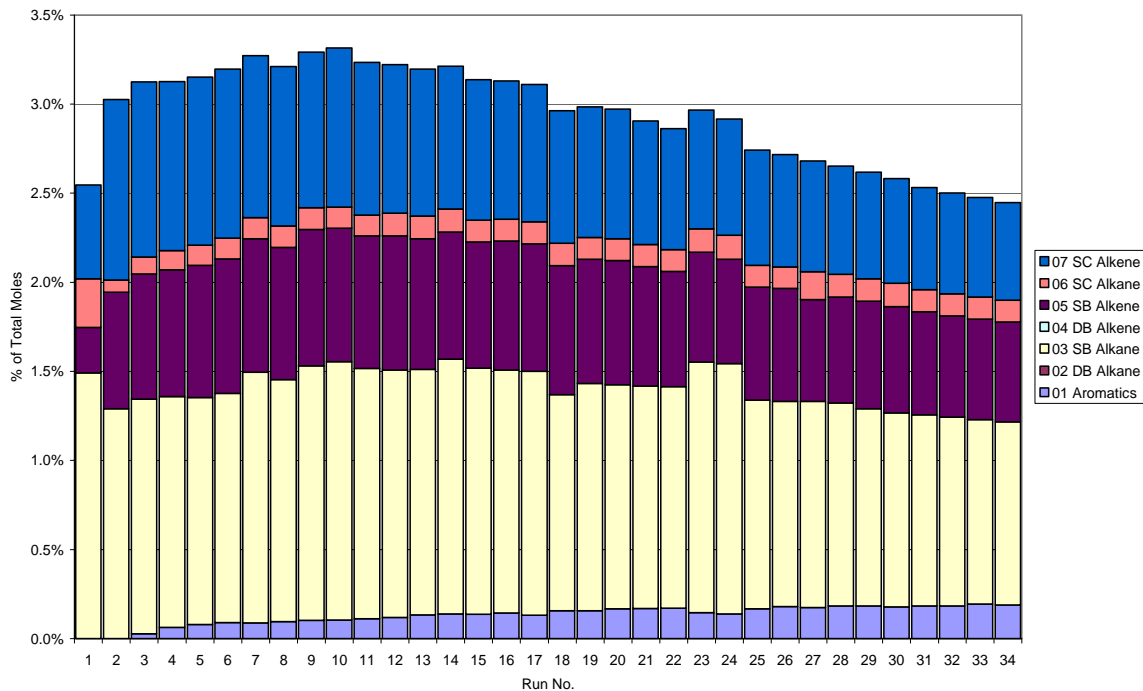
Figure 5.42: Degradation of LDPE with Fulcat 435 at 450ºC (% of Total Moles)
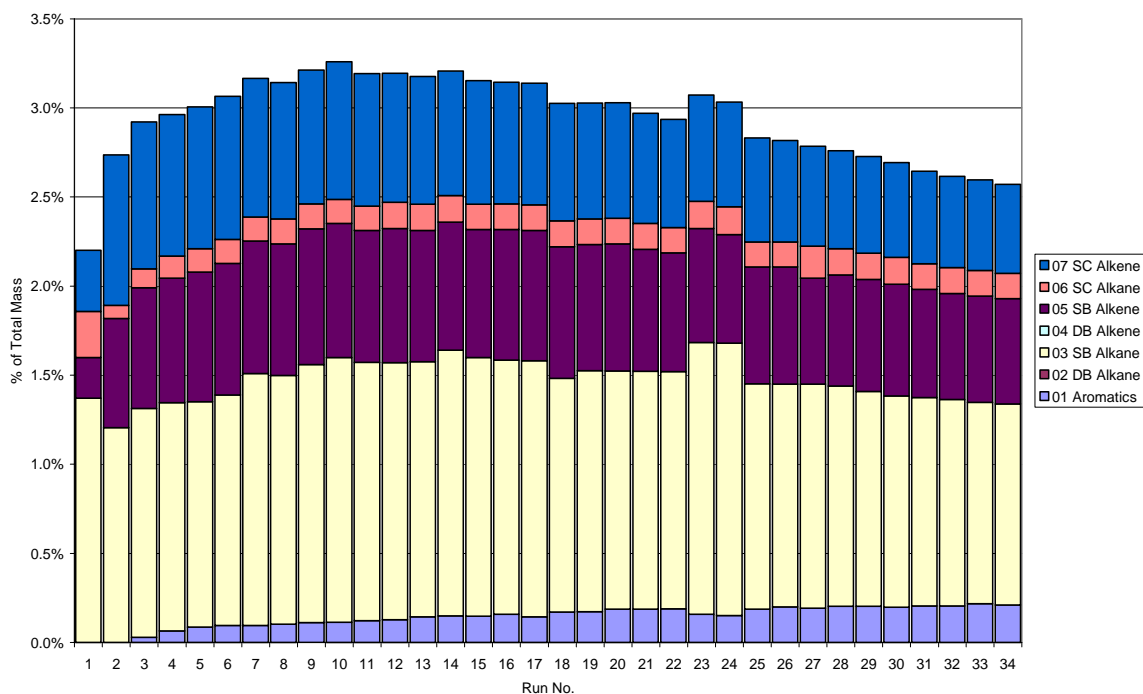
Figure 5.43: Degradation of LDPE with Fulcat 435 at 450ºC (% of Total Mass)
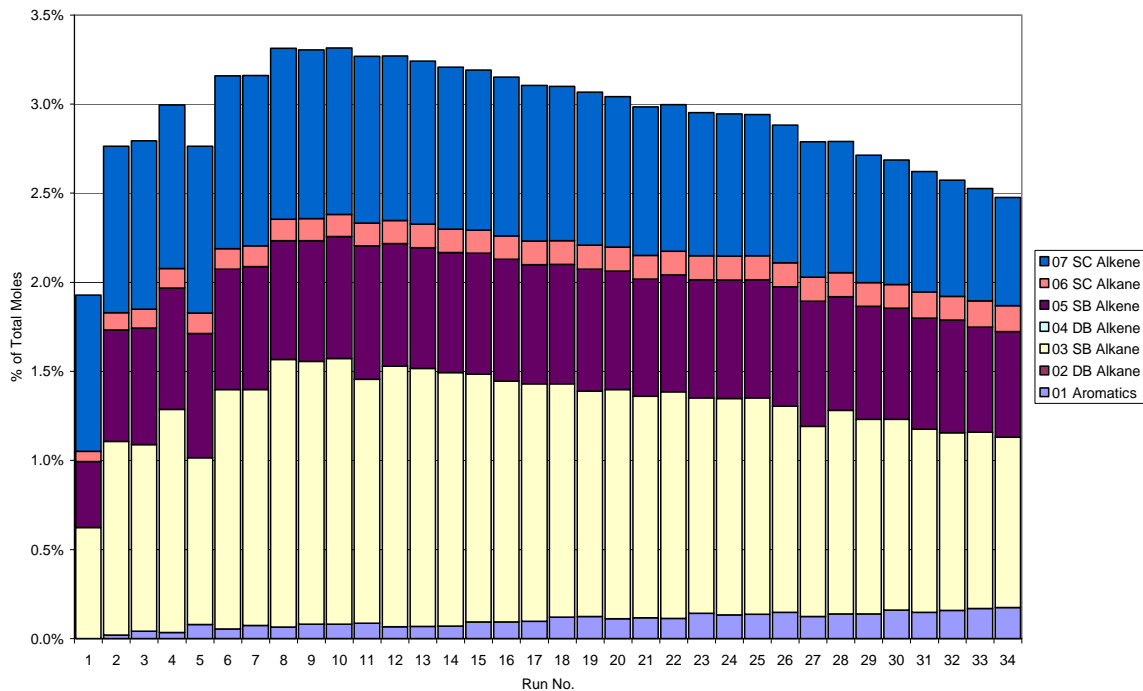
Figure 5.44: Degradation of polypropylene with Fulcat 435 at 450ºC (% of Total Moles)
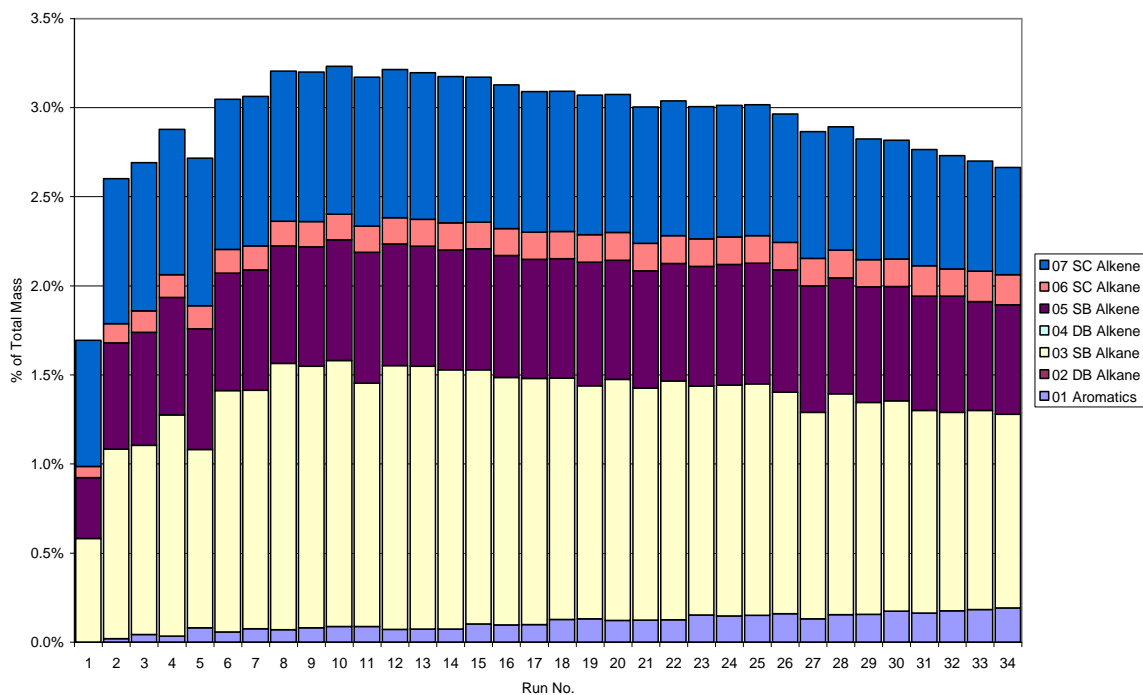
Figure 5.45: Degradation of polypropylene with Fulcat 435 at 450ºC (% of Total Mass)

5.2.4.6 Conclusions of Isothermal GC-MS Experiments

Isothermal measurements provide an alternative approach to observing the decomposition products formed at different temperatures than dynamic experiments. By holding a polymer and catalyst mixture at a certain temperature for a length of time, it is possible that the components of degradation have a longer time to interact with the catalytic sites of the zeolite or clay, and hence may improve the selectivity of the products. Only a small range of isothermal measurements were carried out in this study, but the method does appear to have provided useful information into the formation of different compounds and how they alter throughout the duration of the degradation reaction.

5.2.4.7 Pyroprobe Results

The pyroprobe produced greater separation in the GC than that seen by the other pyrolysis methods attempted. Time constraints meant that only a small number of runs were carried out with the pyroprobe. However, the results obtained were promising and proved to be a successful way of analysing solid polymer samples.

The results for the degradation of pure low-density polyethylene and pure polypropylene in the presence of two different catalysts were compared. The polymer and catalyst had been held at a temperature of 350°C for thirty minutes before the chromatograms were recorded. The chromatograms for the degradation of pure LDPE and PPB in the presence of 280z zeolite at 350°C are displayed in Figure 5.46. The chromatograms for the degradation of pure LDPE and PPB in the presence of Fulcat 435 clay at 350°C are displayed in Figure 5.47. The main peaks of the chromatograms were identified and displayed in Table 5.6.
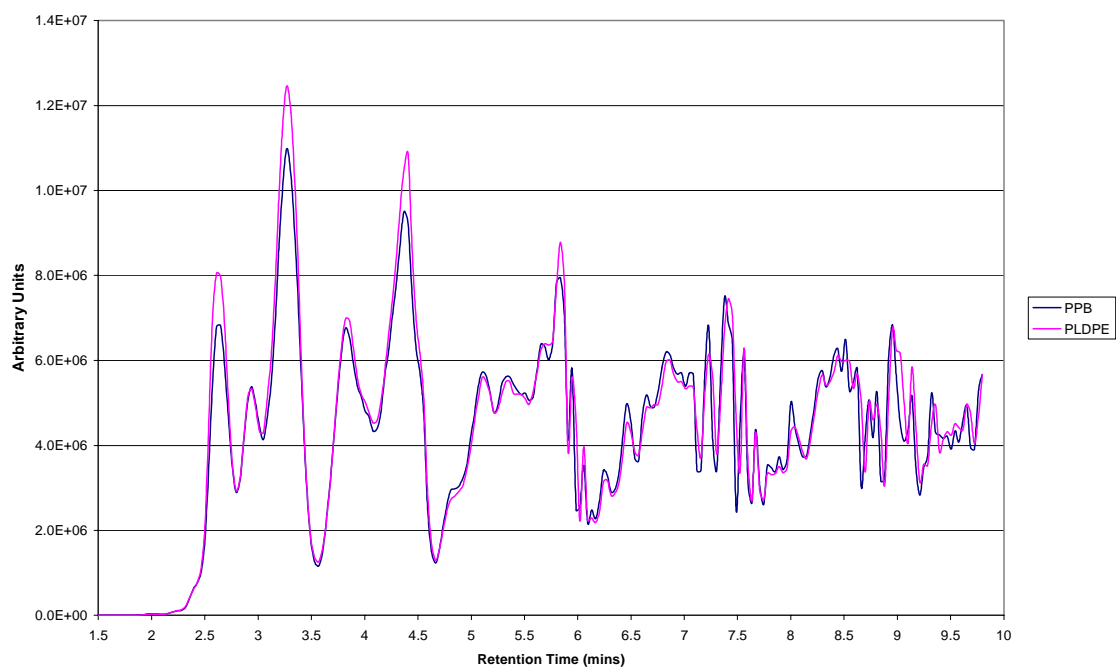
Figure 5.46: Chromatograms for the degradation of pure LDPE and PP at 350ºC in the presence of 280z
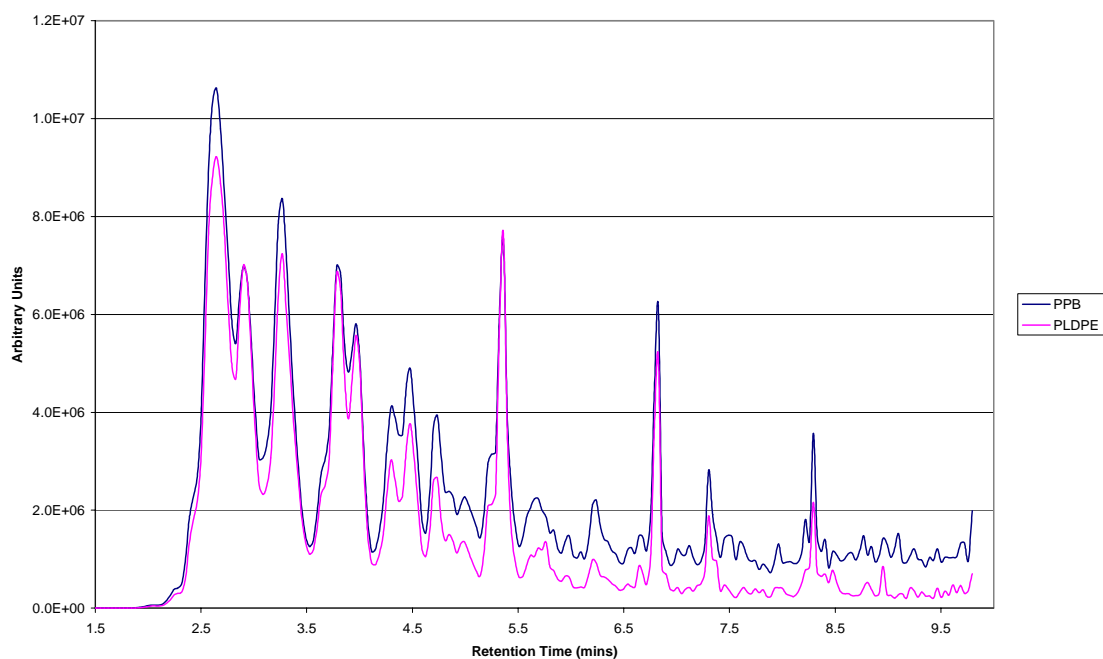
Figure 5.47: Chromatograms for the degradation of pure LDPE and PP at 350ºC in the presence of Fulcat 435

Table 5.6: Components identified from the chromatograms of polymer degradation

R.T (mins)	Component	LDPE + Fulcat	PP + Fulcat	LDPE + 280z	PP + 280z
2.61	3-methylene-pentane	X	X	X	
2.65	3,methyl-2-pentene				X
2.90	1,4-hexadiene			X	
3.27	3-methyl-2-hexene (c,t)	X	X	X	X
3.78	1-methylethylidene cyclobutane			X	X
3.82	2-methyl-3-heptene	X			
4.41	3-octene	X	X		
4.44	2-ethyl-3-methylcyclopentene			X	X
4.74	1,4-dimethyl-1-cyclohexene				X
5.10	2,6-dimethyl-3-heptene	X			
5.36	1,2-dimethylbenzene			X	X
5.84	trans-4-nonene	X	X		
6.83	1-ethyl-2-methylbenzene			X	X
6.86	3-tridecene	X			
7.23	2-decene (z)	X	X		
7.34	1,2,3-trimethylbenzene	X		X	X
7.56	trans-3-decene	X			
8.26	1-methyl-3-propylbenzene			X	
8.95	5-dodecene	X	X		
9.40	tridecene	X			

It can be seen from Table 5.6 that the presence of Fulcat 435 catalyst produced predominantly straight chain alkenes and single-branched alkenes, whereas in the presence of the zeolite (280z), a higher proportion of aromatics were formed in the degradation products. The greater production of aromatics in the presence of 280z was expected from the previous GC-MS experiments. This pyroprobe study was limited in size, however, the ease of the technique would have allowed a thorough study of polymer decomposition products in the presence of a variety of catalysts, had I had more time.

Chapter 6

Degradation of Biomaterials

6   Degradation of Biomaterials

Biomass may be converted to a variety of energy forms such as heat, steam, electricity, hydrogen ethanol, methanol and methane. Compared to other fossil fuels, methane produces few atmospheric pollutants and generates less carbon dioxide per unit energy, making it an attractive option.[280]

Landfilling large amounts of biomass without control can cause important environmental problems. The biomass would undergo anaerobic fermentation, resulting in the formation of methane. Methane has twenty-three times the absorption capacity of infrared radiation in comparison to CO_2, thus its influence on the greenhouse effect would be very high. Also, methane causes the formation of tropospheric (ground-level) ozone which can affect human health, vegetation and building materials. These problems have led to much research into using biomass residues to substitute fossil fuels for heat and electricity generation.

Several aspects must be taken into consideration when pyrolysing biomass. Sulphur dioxide (SO_2) emissions result in acid rain which causes damage to health and the environment. Soot particles from the combustion of biomass contribute to global warming, due to the dark coloured particles increasing the absorption of solar radiation.

This short study investigated the feasibility of using waste biomass together with its packaging as a source of fuel. Vegetable samples (tomato, apple, white cabbage, onion)

with and without their plastic packaging underwent thermal analysis and bomb calorimetry to gain information into the amount of energy available when these samples were degraded. Tomato vine, straw silage and manure were also tested.

6.1 Previous Research into the Degradation of Biomaterials

6.1.1 Tomato

Tegelaar and de Leeuw[281] studied the flash pyrolysis of tomato and found the protective outer layers of the tomato (cutins and suberins) to be insoluble high molecular weight polyesters. Tegelaar and de Leeuw undertook Curie-point pyrolysis-gas chromatography/mass spectrometry (Py-GC/MS) at 770ºC, and found the main pyrolysis products of the cutin to be vinylphenol, six 16:2 fatty acid isomers and one 16:1 hydroxy fatty acid, all produced by rearrangement of six-membered rings.

Mangut *et al.*,[282] undertook a thermogravimetric study of the pyrolysis of biomass residues from the tomato processing industry. They found that lignin decomposition was complex and took place over a range of temperatures. Slight decomposition at very low temperatures was said to be due to the scission of the lateral groups that form the lignin polymer. Cellulose (leaves and stems) decomposition was found to occur in two steps, with the final residue accounting for 16.6% of the initial weight. Tomato peel and seeds were found to have low sulphur and ash contents, a high volatile content and higher heating value (HHV), with the latter relating to the oil content of the residues. The best pyrolysis results of the thermal degradation of tomato peel and tomato seed residue was found for a mixture of 55.3 wt.% peels and 44.7 wt.% seeds.

6.1.2 Apple

A press-cake is the part of apple that remains after juice has been extracted from the crushed fruit and generally contains a high concentration of sugar. Pyrolysis of press-cakes transforms this sugar to caramel. Walter and Sherman[283] air-dried moist apple press-cake in a fumehood, with the loss of 76% water. Once dried, the press-cake was combusted and found to produce 7960 Btu/lb (33.3 kJ/g) of energy. Suárez-García, Martínez-Alonso and Tascó air-dried apple pulp residues from cider manufacture. Thermogravimetric analysis of the apple showed that the fruit exhibited weight-loss steps, ascribable to decomposition of light fractions such as hemicellulose, cellulose decomposition and lignin decomposition.[284]

6.1.3 Vegetable Samples with Plastic Packaging

For each vegetable sample, the weight of the packaging as a percentage of the total weight was calculated. Fourier Transform Infrared (FTIR) Spectroscopy was carried out on the plastic packaging (bag, tray, wrap, mesh). The IR spectra identified the apple bag, cabbage wrap and onion mesh as being made of polyethylene (PE) whilst the tomato samples were packaged in polypropylene (PP) bags and punnets/trays. The packaging as a percentage of the total weight of the fruit and vegetable samples was displayed in Table 6.1.

Table 6.1: Packaging as a % of the total weight of the fruit and vegetable samples

Vegetable Sample	Plastic Packaging	Packaging as % of Total Weight
Tomato 1 (Spanish Family Pack)	Bag Tray	0.93
Tomato 2 (Family Value Pack)	Bag Punnet	2.30
Apple	Bag	0.43
White Cabbage	Wrap	0.49
Onion	Mesh	0.45

6.1.4 Thermal Analysis

Thermogravimetric (TG) analysis with a Shimadzu TGA-50 was carried out on the five fruit and vegetable samples (Figure 6.1). Each sample was heated in a nitrogen atmosphere at 10ºC/min from room temperature to 120ºC and held at this temperature until the weight loss became stable. This enabled the water content of each vegetable or fruit to be established.
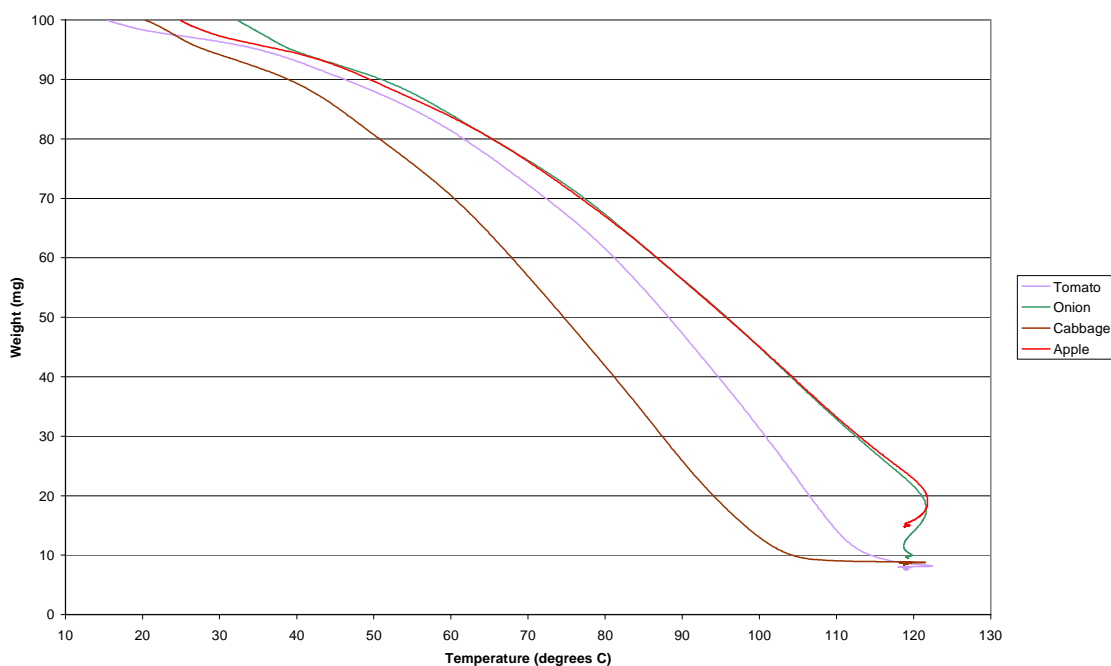
Figure 6.1: TG curves for the degradation of fruit and vegetable samples

Differential Thermal Analysis with a Shimadzu DTA-50 was carried out on the five fruit or vegetables in order to establish the total enthalpy change associated with the loss of water from the samples (Figure 6.2). The vegetables were heated in a nitrogen atmosphere at 10ºC/min from room temperature to 120ºC.
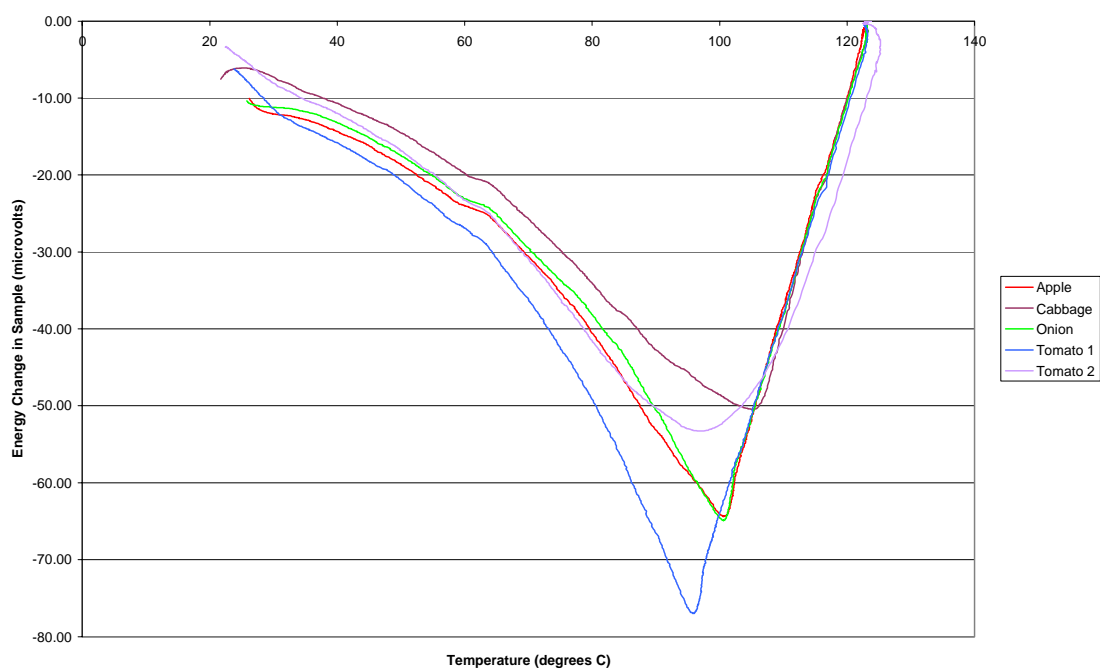
Figure 6.2: DTA curves of fruit and vegetable samples

6.1.5 Bomb Calorimetry

For optimal results, the sample under investigation should be dried before combustion, without the drying process volatilising or destroying any of the combustible material. The five fruit and vegetable samples were freeze-dried under vacuum overnight to remove all water. No preparation of the plastic packaging was necessary.

6.1.6   Results of Analysis of Vegetable Samples

Bomb calorimetry of the fruit and vegetable/packaging mixtures was undertaken using a Gallenkamp Calorimeter CBA-305 (previously calibrated, see Section 4.6.2). However, due to the very low weight of the packaging in relation to the total weight of the fruit or vegetable plus packaging ($\geq$ 1%), the presence of the packaging had a negligible effect on the heat of combustion. However, increasing the relative plastic content by drying the samples would give an energy lying between the values obtained for pure fruit or vegetable and pure plastic combustion. Table 6.2 displays the results for the TGA, DTA and bomb calorimetry experiments undertaken on the fruit and vegetable samples, whilst Table 6.3 displays the TGA, DTA and bomb calorimetry results for the plastic packaging.

Table 6.2: TGA, DTA and bomb calorimetry results for the fruit and vegetable samples

Sample	TGA Weight Loss (%)	DTA Energy (J/g)	DTA Peak (ºC)	Bomb Calorimetry* (kJ/g)
Tomato 1	88	-1890	96	40 ± 3
Tomato 2	92	-1860	97	47 ± 4
Apple	85	-1250	101	32 ± 2
Cabbage	91	-1750	105	45 ± 4
Onion	90	-1400	101	36 ± 2

* measured at constant volume

Table 6.3: TGA, DTA and bomb calorimetry results for the fruit and vegetable samples

Sample	Bomb Calorimetry* (kJ/g)
Tomato 1 Bag	49 ± 2
Tomato 1 Tray	45 ± 2
Tomato 2 Bag	43 ± 2
Tomato 2 Punnet	47 ± 2
Apple Bag	44 ± 2
Cabbage Wrap	43 ± 2
Onion Mesh	44 ± 2

* measured at constant volume

All of the fruit or vegetable samples contained a high proportion of water (85-92%) which was removed successfully *via* freeze-drying under vacuum overnight. This did not appear to degrade the fruit or vegetable samples and enabled almost total combustion of the organic material (> 95%). Bomb calorimetry of the fruit and vegetable samples gave heats of combustion varying from 32 ± 2 kJ/g (apple) to 47 ± 4 kJ/g (tomato 2). Results for the plastic packaging varied from 43 ± 2 kJ/g (tomato 2 bag and cabbage wrap) to 49 ± 2 kJ/g (tomato 1 bag).

6.1.7   Results of Analysis into Tomato Vines, Straw Silage and Manure

The tomato vine, straw silage and manure samples were heated up to 550ºC in a nitrogen atmosphere (50 ml/min). TG analysis and differential thermal analysis was carried out and the results averaged and reported in Table 6.4.

Table 6.4: TGA and DTA results for biomass samples

Sample	Weight Loss due to water (%)	Energy Loss due to water (J/g)	Weight Loss up to 550ºC (%)
Tomato Vine	87.2	-1550	92.6
Straw Silage	20.2	-370	69.4
Manure	74.3	-965	89.8

For bomb calorimetry, the samples needed to be as dry as possible, therefore different preparations were attempted to discover whether this had a significant effect on the energy of combustion. Tomato Vine (1) was pressed fresh and dried in a fume hood overnight whilst Tomato Vine (2) was oven dried at 80ºC for two hours. The straw silage sample was pellitised fresh and undried, whilst Manure (1) and Manure (2) followed the same sample preparations as for Tomato Vine (1) and (2) respectively. The results of the bomb calorimetry of the biomass samples are displayed in Table 6.5.

Table 6.5: Bomb calorimetry results for biomass samples

Sample	Bomb Calorimetry* (kJ/g)
Tomato Vine (1)	24 ± 2
Tomato vine (2)	38 ± 3
Straw Silage	17 ± 1
Manure (1)	19 ± 1
Manure (2)	19 ± 1

* measured at constant volume

6.1.8   Conclusions of Biomass Study

The combustion of most fruit and vegetable samples produced approximately half of the energy as that seen for the combustion of the packing, with the exception of the second tomato vine, which produced a comparable energy of combustion to that of the plastic. The fruit, vegetable and biomass samples required the removal of water before combustion could be achieved. The latent heat of vapourisation of water is 2.26 kJ/g (2260 kJ/kg), therefore the heat released on combustion of the fruit and vegetables must be greater than this to achieve a net positive production of energy.   All bomb calorimetry results from the food waste produced energy from 32 ± 2 kJ/g (dried apple) to 47 ± 4 kJ/g (dried tomato). The energy released from the combustion of biomass ranged from 17 ± 1 kJ/g (untreated straw silage) to 38 ± 3 kJ/g (dried tomato vine). All waste food and biomass samples were found to release energy on heating that far exceeded the 2.26 kJ/g required for the removal of water prior to combustion. It is hoped that the combustion of waste fruit and vegetables, along with their packaging, could be utilised as a localised energy source for supermarkets, whereby the discarded produce is combusted on-site. The energy would then be used for heating, lighting, refrigeration, *etc*.

6.2   Anaerobic Digestion

Anaerobic digestion is a complex biological process by which almost any waste can be converted in the absence of oxygen. It requires specific environmental conditions with mixed bacterial populations to degrade the organic compounds into high energy biogas of mainly methane (CH_4) and carbon dioxide (CO_2). Anaerobic digestion can take place over a wide temperature range from 4ºC to 100ºC and at a variety of moisture contents from 60% to more than 99%. This distinguishes the methane bacteria favourably from

most aerobic micro-organisms involved in the composting process. The anaerobic treatment of wastes can be performed in different reactor systems, in single phase, two phase or multiphase configuration. In single phase operation, different groups of micro-organisms are developed in the same environment, with each group of bacteria establishing is own operating conditions (pH, temperature, retention period). Two phase operation involves two distinct phases (acid formation and methane formation) and allows wastes with toxic elements to be handled. Since optimal environmental conditions for micro-organisms vary, in multi-stage digestion, biological reactions can occur separately.

6.2.1   Anaerobic Digestion in Practice

Co-digestion of organic solid wastes is often used to improve biogas yields, due to positive synergisms established in the digestion medium and the supply of missing nutrients.[285]   At Amiens in France, biodegradable organic wastes are processed by anaerobic digestion. The plant is particularly suited for treating the fermentation fraction of municipal solid wastes and produces, on average, 210-240 m^3 methane per tonne of volatile solids introduced into the digester.[286]   The municipality of Velenje underwent a full-scale experiment where their organic waste was co-digested with municipal sludge. The anaerobic digestion led to virtually complete degradation of the organic waste, with an 80% increase in biogas quantity, with the biogas producing 45% more heat energy and 130% more electrical energy.[287]

The waste generated from the fruit and vegetable industry contains very high C/N ratios and a high water content (>80%). Lastella *et al*.,[288] found that the anaerobic treatment of this semi-solid organic waste lowered the pollution potential and improved biogas

production and methane content. Gómez et al.,[289] studied the anaerobic co-digestion of primary sludge and the fruit and vegetable fraction of municipal solid waste, by measuring total solids, volatile solids, pH and daily biogas production. The presence of the fruit and vegetable fraction in the feed led to an increase in the production of biogas.

On 11th March 2008, I visited a tomato farm in Cheshire, UK, which was piloting a scheme in which waste tomato leaves were digested anaerobically to produce fuel. I was informed that the tomato farm produced approximately $20m^3$ of tomato leaf waste per week, along with $3m^3$ of waste fruit (damaged, out of specification). The leaves and fruit were compressed to $8m^3$, macerated and then pumped through a series of tanks. Tank 1 controlled the feed to the system, Tank 2 heated the waste to 55ºC to hydrolyse and break down the cellulose, with the final three tanks acting as digesters at 35ºC. Initial trials had produced more CO_2 gas than methane, with the produced methane being used to generate electricity to drive the fans in the greenhouses of the tomato farm.

It is hoped that research into the generation of energy from biomass and plastic waste will continue and that the residual energy left in the non-biodegraded residues, such as cellulose and plastic packaging, can be released in a useful manner.

Chapter 7

Experimental

7 Experimental

7.1 Samples and Standards

7.1.1 Polymers

Pure low-density polyethylene (LDPE), high-density polyethylene (HDPE), polyethylene terephthalate (PET) and polystyrene pellets were purchased from Sigma-Aldrich. Pure isotactic polypropylene (PP) with molecular weights of 12,000 and 190,000 were purchased from Sigma-Aldrich. Thirteen waste polymers were sourced from everyday household waste (see Chapter 3).

7.1.2 Catalysts

The Envirocat catalysts, EPZE, EPZG and EPZ10, were a gift from Contract Chemicals and were identified as Lewis acidic salts deposited on a K10 acid activated clay substrate. Fulacolor, Fulcat 435 and Fulmont were a gift from Rockwood and were identified as acid activated montmorillonite clays.

CeY and LaY were synthesised by a colleague at the University of Central Lancashire and were known to be cerium-exchanged and lanthanum-exchanged Y-zeolites respectively. 23z and 280z were purchased from Zeolyst International and were ZSM-5 zeolites of the ammonium form.

7.1.3 Standards

D3170 Qualitative Calibration Mix was purchased from Supelco.

7.2 Polymer Identification

To identify the polymers collected from everyday household waste, a model FT/IR-400 single-beam spectrometer with Golden Gate^{TM} attachment was used to obtain an Attenuated Total Reflectance (ATR) spectrum for each polymer sample. The spectra were collected over sixty-four scans and displayed as transmittance (%) *vs.* wavenumber (cm^{-1}).

7.3 Scanning Electron Microscopy – Energy Dispersive X-Ray

Each powdered catalyst was pressed into a disk and the catalyst pellet was placed into the Quanta 200 SEM. An image of the sample topography was acquired. EDX analysis led to problems with charging of the surface of the aluminosilicate insulators and resulted in the signal falling off rapidly. By carrying out the experiments in low vacuum mode, the addition of water vapour dissipated the charge and the use of high kV radiation allowed all excitation energies. However, the disadvantages with low vacuum mode included heating of the sample (due to the high kV energy) and beam spread (from scattering caused by collision between the electrons and gas atoms from the water vapour molecules).

7.4 Nitrogen Desorption

Nitrogen desorption of the ten powdered catalysts was undertaken using a Micromeretics ASAP 2010 Accelerated Surface Area and Porosimetry System. To

check the accuracy of the equipment, two silica-alumina standards of known surface area were run. Each powdered catalyst was left to degas at 100ºC overnight. Clays were found to take approximately four hours to degas fully, whilst the zeolite samples took up to 36 hours. Once degassing of the sample had been achieved, it was transferred to a clean, dry sample tube for analysis. The Micrometrics System produced data for the Surface Area (m^2/g), Total Pore Volume of Pores < 665 Å (cm^3/g) and Average Pore Diameter (Å) of each of the ten catalysts.

7.5 Surface Acidity

To determine the surface acidity of the clays and zeolites in this study, the catalysts were heated to 200ºC in order to remove any water present, then stored in an oven at 110ºC to prevent the absorption of water vapour from the atmosphere. Four anhydrous potassium bromide (KBr) disks were then made to a series of catalyst concentrations (0.8-1.2%) for each clay and zeolite. This was achieved by placing 20g of KBr in a flask and heating it on a vacuum line for 30 minutes at 200ºC, then transferring the powder to an oven held at 110ºC. This ensured the KBr was free of any absorbed water. In order to make the disks of specific concentration, the amount of catalyst had to be weighed very accurately, then ground in a pestle and mortar with the correct amount of KBr to ensure homogeneity. The disks, weighing 100mg, were made by transferring the mixture of fine particles of KBr (~99%) and catalyst (~1%) to a press where a pressure of six tonnes was applied for twenty seconds.

The KBr disks of varying catalyst concentrations were then placed in an enclosed saturated atmosphere of pyridine vapour for seven days to ensure complete migration through the KBr pellet; previous work having shown that equilibrium was achieved

within 3-4 days. FT-IR analysis using a Perkin Elmer Spectrum RX1 instrument was then undertaken on all the disks (four per catalyst). A pure KBr disk was used as a background in order to reduce any effects that were not attributable to the catalysts. Each disk was measured four times, rotating by 90º each time, to improve the reproducibility of results by eliminating any directional effects of the pellet manufacture. The peak areas obtained from the IR absorbance spectra 470 cm^{-1} (Si-O) and 523 cm^{-1} (Al-O) were recorded for the four quarter rotations of each disk and a graph of average absorbance *vs*. catalyst concentration was plotted. Equally, for the characteristic Brønsted frequency (1545 cm^{-1}) and Lewis frequency (1455 cm^{-1}) a plot of average absorbance *vs*. catalyst concentration for each catalyst at each of the frequencies was constructed, allowing the average Brønsted site concentration and average Lewis site concentration to be calculated.

7.6   Thermogravimetric Analysis

The thermogravimetric analysis of six polymers and thirteen waste polymers was undertaken with a Shimadzu TGA-50 instrument. The TGA could be used over a temperature range from room temperature to 1,000°C and employed a chromel-alumel thermocouple. The instrument was of a deflection-type, and when the weight of the sample was changed by heating, the beam supported by the taut band inclined. This inclination was detected by the photoelectric elements and amplified, whilst a current flowed to the feedback coil to provide a uniform magnetic field to balance with the moment of rotation based on the mass change of the sample. This 'zero-position method' meant that the beam position was fixed and the torque was directly proportional to the current. By sampling and recording the current, the mass changes of the sample could be continuously and accurately measured.[290]

Thermogravimetric analysis was carried out in a fixed atmosphere flow to prevent a rise or drop of partial pressure (for better data reproducibility) and to prevent secondary reactions occurring. Nitrogen at a flow rate of 50 ml/min was selected as the inert gas to prevent oxidation. An aluminium pan was employed as the sample container and the solid polymer samples were subjected to heating from room temperature to 550°C at a heating rate of 10°C/min. The sample size (1-10 mg) was small enough in size to try to ensure temperature uniformity during decomposition.

Table 7.1: Experimental parameters for the Shimadzu TGA-50

Atmosphere	Nitrogen
Atmosphere Flow Rate	50 ml/min
Sample Holder	Aluminium Pan (no lid)
Sample Weight	1-10 mg
Temperature Programme	Room Temperature to 550°C
Heating Rate	10°C/min

Thermogravimetric analysis was undertaken for the six pure polymers and thirteen waste polymers without the presence of a catalyst. These plastic samples were then analysed in the presence of each of the ten catalysts (at a polymer-to-catalyst weight ratio of 2:1). Sample preparation was kept to a minimum and involved no grinding or shredding of the plastic into small fragments. The catalyst powder was placed in the bottom of the aluminium sample pan and a small piece of untreated polymer (<10 mg) was placed directly on top of the catalyst. No mixing of the polymer and catalyst was undertaken in order to simulate how plastics could be recycled in the future with next to

no initial preparation. The effects on the onset temperatures and activation energies of the decomposition steps of the polymers were recorded and compared.

7.7 Differential Thermal Analysis

The differential thermal analysis of six pure polymers and thirteen waste polymers was undertaken with a Shimadzu DTA-50 instrument. The DTA could be used over a temperature range from room temperature to 1,500°C and employed a platinum-platinum rhodium 10% thermocouple to measure the sample temperature, T_s. The thermocouple on the reference material side was used for temperature control. Both T_s and T_r signals were amplified by a factor of 200 and input to the A/D converter after addition of a room temperature compensating signal.

Differential thermal analysis was carried out in a fixed atmosphere flow to prevent a rise or drop of partial pressure (for better data reproducibility) and to prevent secondary reactions occurring. Nitrogen at a flow rate of 20 ml/min was selected as the inert gas to prevent oxidation. Aluminium pans were employed as the sample and reference container. A blank test of heating the pans without any sample or reference material was carried out to observe the baseline and gain information as to possible contamination of the apparatus, deterioration of the thermocouple and magnitude of noise. The DTA was also calibrated by means of the melting point and heat of fusion of pure substances such as indium (156.6°C, 28.59 J/g) and zinc (419.6°C, 111.4 J/g).[291]

For the heating of polymer samples, a blank reference pan was employed. The solid polymer samples were subjected to heating from room temperature to 550°C at a heating rate of 10°C/min. The sample size (1-10 mg) was small enough in size to try to

ensure temperature uniformity during decomposition. The six pure polymers were also heated with the catalysts at a polymer-to-catalyst ratio of 2:1. In these cases, the same weight of catalyst was used as the reference material. Sample preparation was kept to a minimum and involved no grinding or shredding of the plastic into small fragments. The catalyst powder was placed in the bottom of the aluminium sample pan and a small piece of untreated polymer (<10 mg) was placed directly on top of the catalyst. No mixing of the polymer and catalyst was undertaken.

Table 7.2: Experimental parameters for the Shimadzu DTA-50

Atmosphere	Nitrogen
Atmosphere Flow Rate	20 ml/min
Sample Holder	Aluminium Pan (no lid)
Sample Weight	1-10 mg
Temperature Programme	Room Temperature to 550°C
Heating Rate	10°C/min

7.8 Bomb Calorimetry

A Gallenkamp Autobomb Calorimeter CBA-305 was used to determine the heat capacity of the environmental samples. The samples were weighed accurately and placed in a crucible. A piece of nickel chromium firing wire was stretched between the electrodes of the bomb and a strand of cotton was tied from the wire to the sample to aid ignition. The bomb was filled with oxygen and then submerged into a known volume of water in the calorimeter vessel. The temperature of the system was left to stabilise and once constant, the sample was ignited by depressing the 'FIRE' button. The heat of the burning sample was absorbed by the water in the calorimeter and the temperature

rise of the water was recorded. The bomb was removed from the calorimeter and the residual carbon in the crucible was weighed.

7.9 Mass Spectrometry

Initial experiments involved the use of a Hiden Mass Spectrometer and a U-shaped stainless steel tube of ¼" diameter. The empty sample tube was weighed, then 0.25g of catalyst was added to the tube, followed by 0.5 g of untreated polymer (plastic-to-catalyst ratio of 2:1). One end of the U-tube was connected to a Mass Flow Controller, which regulated the flow rate of helium through the tube to 50 ml/min. The sample tube was positioned inside a temperature controlled furnace. The other end of the U-tube was connected to a cold trap *via* stainless steel tubing wrapped in a heated coil which kept the temperature at around 200ºC to avoid condensation of any decomposition gases. The glass cold trap was immersed in an ice bath and allowed the condensation of any heavier gaseous components into a liquid. Non-condensed gases travelled through the cold trap for detection at the mass spectrometer. After the run, any condensate collected in the cold trap could be extracted for analysis. The U-tube was also weighed in order to calculate if any solid polymer remained after heating. The furnace used was a Eurotherm 2408 Temperature Programmer and was able to be heated at any rate between 1ºC/min and 50ºC/min, or to be held at any temperature up to 1000ºC. Initially, experiments were carried out at a heating rate of 10ºC/min up to 550ºC where the furnace was held at this temperature. After a number of experiments, the flow rate of the helium carrier gas was reduced to 20 ml/min in order to prevent loss of catalyst escaping from the sample tube. To improve the rearrangement of decomposition products into lighter and more-branched gaseous components, the experimental set-up was modified. The ¼" stainless steel U-tube was replaced with a ¾" straight tube. By

positioning only the bottom half of the tube into the heated furnace, the top section of the steel tube remained at a lower temperature. Any heavier decomposition products, instead of passing straight out of the tube and across the heated line and into the cold trap, would reach the cooler section of the sample tube and reflux back down into the furnace for further decomposition and possible rearrangement into branched products by the catalyst. By using a straight tube of ¾" diameter, the flow rate of the carrier gas could be increased from 20 ml/min back up to 50 ml/min without the catalyst escaping from the tube.

7.10 Pyrolysis-Gas Chromatography

The ¾" stainless steel straight tube was used as the sample reactor. The bottom of the tube had a removable stopper that allowed the remains of the degraded polymer to be removed after each run and for the tube to be cleaned properly. Once the plastic and catalyst sample had been added to the tube, the reactor was placed into the furnace, with half of the tube submerged in the heated zone, whilst the other half remained unheated to allow any possible reflux of the decomposition products for further reactions in the furnace.

Table 7.3: Experimental parameters for the GC-MS set-up

Carrier Gas	Helium
Carrier Gas Flow Rate	50 ml/min
MS Mass Range	15-100
GC Temperature	40°C
Split Flow	45 ml/min
Split Ratio	30

7.11 Pyroprobe Studies

A small number of pyrolysis experiments were undertaken using the CDS Analytical 5200 Pyroprobe coupled to the Perkin Elmer AutoSystem XL Gas Chromatograph with Turbomass mass spectrometer. The sample holder was a quartz tube within which a small amount of polymer and catalyst (< 1 mg) was placed and held in position by glass wool at either end. The volatile organic compounds were purged to a trap where they were concentrated and then thermally desorbed for transfer to the GC-MS. This produced greater separation in the GC than that seen by the other pyrolysis methods attempted. The mass spectrometer was programmed to detect masses in the range 45 – 300, and the split ratio was set at 1/40 so as to send only a fraction of the products to the GC (and therefore not overload the detector).

Table 7.4: Experimental parameters for pyroprobe studies

Interface Oven Rest Temperature	50°C
Carrier Gas	Helium
Trap Absorb Temperature	50ºC
Trap Desorb Temperature	280ºC
Transfer Line Temperature	310ºC
Valve Oven Temperature	310°C
Heating Rate	10ºC/min
Detector	MS

Chapter 8

Conclusions

8   Conclusions

Historically, waste has simply been dumped and forgotten about. However, with an increase in the generation of waste, a reduction in the amount of land available, and the synthesis of more hazardous products such as pesticides, landfills are bigger and more toxic than ever before. The future of waste disposal must be based on the underlying principle of sustainable development and must not pose a risk to human health or the environment, either now or in the future. An effort must be made to conserve non-renewable resources to the maximum extent possible and wastes should be managed in a way that does not place a burden on future generations. When buried in landfill, plastics remain inert. Is it not wasteful of our finite resources to bury products of the petro-chemical industry which could be recycled?
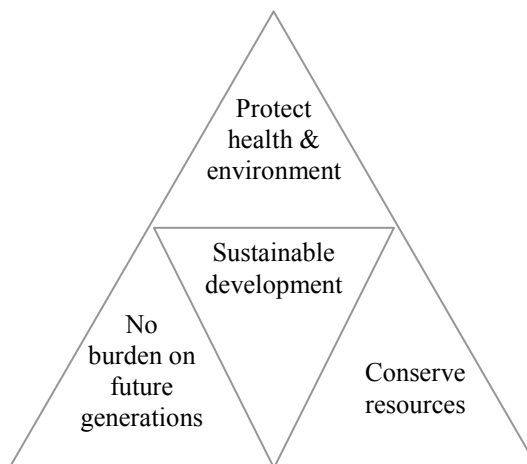
Figure 8.1: Principles for sustainable development and waste management.[4]

This study aimed to investigate the thermal degradation of a variety of waste polymers in the presence of catalysts in an attempt to convert this valuable waste stream into high-grade fuel.

In order to determine their likely effectiveness, certain characteristics of the clay and zeolite catalysts chosen were tested. These characteristics included: elemental composition, silicon-to-aluminium ratio, surface area, pore size and surface acidity. It was important to examine the results obtained for each catalyst as a whole in order to establish which were the most likely to be good candidates for the catalytic degradation of polymers. Correlation of the specificity and activity of each catalyst towards each polymer, with the catalyst's characteristic properties, was made and is summarised in Table 8.1.

Table 8.1: Catalytic properties related to polymer degradation

Property:	Surface Area, m^2g^{-1}	Pore Diameter (Å)	Si/Al_{tot}	Si/Al_{tet}	Si/Al_{oct}	Surface Acidity (mmol/g)		Main polymer degradation observations:		
Catalyst:						Lewis	Brønsted	PE	PP	Other Polymers
Fulacolor	329	39	5.1	20.8	6.8	0.1128	0.3124	LDPE: T_{onset} reduced by 52°C. Initiated carbocation catalytic degradation mechanism for pure and waste LDPE and HDPE.	178°C reduction in T_{onset} of PPA. Initiated carbocation degradation mechanism for pure and waste PP.	Reduced T_{onset} effectively for most polymers.
Fulcat 435	360	39	4.3			0.0421	0.1099	Greatest reduction of T_{onset} for waste LDPE (78°C). Initiated carbocation degradation mechanism for pure and waste LDPE and HDPE. Studied further: forms mostly C_6-C_7 single-branched alkanes.	Best reducer of T_{onset} of pure PPA: 188°C. Best reducer of E_a of free radical mechanism of PPB. Initiated carbocation degradation mech. for waste PP.	One of the best reducers of E_a for free radical deg. mechanism. Initiated carbocation degradation mechanism for pure PS.
Fulmont	243	63	5.3	12.9	9.1	0.0926	0.2364	Initiated catalytic degradation mechanism for pure and waste LDPE and HDPE.	Initiated catalytic degradation mechanism for pure and waste PP.	Initiated catalytic degradation mechanism for pure PET and waste PS

Property:	Surface Area, m^2g^{-1}	Pore Diameter (Å)	Si/Al_{tot}	Si/Al_{tet}	Si/Al_{oct}	Surface Acidity (mmol/g)		Main polymer degradation observations:		
Catalyst:						Lewis	Brønsted	PE	PP	Other Polymers
EPZE	287	56	5.8	29.9	7.2	0.1111	0.2943	Initiated carbocation degradation mechanism for pure HDPE and waste LDPE.	PPA: 97ºC reduction in T_{onset}. PPB: 171ºC reduction in T_{onset}. Initiated carbocation degradation mechanism for pure and waste PP.	PU(RC35): Two T_{onset} reduced to one. Initiated carbocation degradation mechanism for pure PS and waste PET.
EPZG	203	60	4.3	37.0	4.9	0.0889	0.2329	Initiated carbocation degradation mechanism for pure HDPE and Brønsted-catalysed reaction for waste LDPE and HDPE	Initiated catalytic degradation mechanism for pure PPB and waste PP.	PU(RC35): Two T_{onset} reduced to one. Initiated carbocation degradation mech. for waste PET.
EPZ10	200	69	5.6	29.4	6.9	0.0236	0.0760	Waste HDPE: change in TG curve gradient suggests mechanism change. Initiated carbocation degradation mechanism for pure LDPE and Brønsted-catalysed reaction for pure HDPE and waste LDPE and HDPE.	PPA and PPB: T_{onset} reduced by 178ºC and 106ºC respectively. Initiated catalytic degradation mech. for all PP.	PS: Reduction in T_{onset} of 136ºC. Initiated carbocation degradation mechanism for pure PS.

Property:	Surface Area, m^2g^{-1}	Pore Diameter (Å)	Si/Al_{tot}	Si/Al_{tet}	Si/Al_{oct}	Surface Acidity (mmol/g)		Main polymer degradation observations:		
Catalyst:						Lewis	Brønsted	PE	PP	Other Polymers
23z	301	19	10.9			0.0045	0.0085	Pure LDPE: T_{onset} reduced by 70ºC. Pure HDPE: T_{onset} reduced by 63ºC. Initiated carbocation degradation mechanism for all PE samples. Studied further: Increase in alkene and aromatic fraction from single-branched alkanes.	Pure PPB: T_{onset} reduced by 79ºC. Waste PP: T_{onset} reduced by 67ºC	First T_1 of PU(RC35) reduced by 74ºC. Initiated Brønsted-catalysed deg. mech. for pure PET.
280z	460	20	61.7			0.0024	0.0046	Pure LDPE: T_{onset} reduced by 77ºC. Initiated catalytic degradation mechanism for all PE samples. Studied further: Formation of large aromatic content – increase in RON.	Pure PPB: T_{onset} reduced by 70ºC. Initiated carbocation degradation mech. for pure PPB, waste PP.	Waste PET: best reducer of T_{onset} (31ºC), initiated Brønsted-catalysed degradation mech.
CeY	569	19	2.5			0.0030	0.0039	Initiated catalytic degradation mechanism for pure and waste LDPE and HDPE.	Waste PP: T_{onset} reduced by 88ºC. Initiated carbocation deg. mech. for all PP.	
LaY	428	21	2.4			0.0079	0.0155	PLDPE: T_{onset} reduced by 75ºC. Initiated carbocation degradation mech. for waste LDPE and HDPE.	Initiated carbocation degradation mech. for waste PP.	Initiated carbocation degradation mech. for pure PS.

The results of the catalyst characterisation experiments led to the construction of Table 2.10 which rated the catalysts' overall performance in terms of desirable properties. Fulacolor clay (acid-activated montmorillonite) was found to show the most potential as a successful catalyst, due to its good surface area (329 m^2g^{-1}) and moderate pore size (39 Å) measurements and for exhibiting the highest concentration of Brønsted- and Lewis-acid sites in relation to all the other catalysts tested. The performance of Fulacolor in the thermogravimetric analysis of all the pure and waste polymers was very promising, with the clay proving to be a good reducer in the onset temperature of a number of the plastics, especially for low molecular weight polypropylene (PPA) where the onset temperature of degradation was reduced by 178ºC. Fulacolor was also seen to initiate a Brønsted (Si-OH protonation of the polymer) or Lewis (removal of hydride ions) degradation mechanism for all of the pure polymers (excluding PET) and the seven waste polymers that degraded *via* a single decomposition step. The high concentrations of both Brønsted- and Lewis-acid sites in comparison to the other catalysts, along with good surface area and pore diameter measurements appeared to enable the clay to effectively alter the degradation mechanism of many everyday household plastics.

EPZE ($AlCl_3$ and $ZnCl_2$ deposited on acid-activated montmorillonite K10 clay) was rated the second highest in terms of catalyst performance. For the thermogravimetric experiments, EPZE generally exhibited a good level of success in reducing the onset temperature of decomposition and the activation energy of a free radical mechanism, whilst initiating a carbocation degradation mechanism for pure PPA, pure PS, waste LDPE, HDPE and PP, and a Brønsted-catalysed reaction for waste PET. The success of EPZE in altering the degradation mechanism to a catalytic process is consistent with the

clay displaying the second greatest concentration of Brønsted- and Lewis-acid sites of all the catalysts.

Some of the most significant changes in the activation energies of degradation were associated with Fulcat 435 (acid-activated montmorillonite clay). Fulcat 435 was found to initiate a catalytic degradation mechanism for ten of the polymer samples and was also very effective in reducing the activation energy of a free radical process and the onset temperature of decomposition of the plastics. The success of Fulcat 435 was thought to be attributed to its good surface area and surface acidity properties. Additionally, the flexible sheet structure of the clay could allow more complex polymer molecules to access the active catalytic sites than would be possible for the restricted rigid structure of a zeolite.

EPZ10 ($ZnCl_2$ on acid-activated montmorillonite K10 clay) exhibited the lowest surface area (200 m^2g^{-1}) and the greatest average pore diameter (69 Å) of all the catalysts investigated and was found to produce some very large reductions in the onset temperature of degradation for a number of polymers (*i.e.* 178ºC reduction for PPA and 106ºC for PPB). EPZ10 was also found to initiate a Brønsted- or Lewis- acid degradation mechanism for twelve of the polymers, despite the clay displaying an average concentration of acid sites in relation to the other catalysts. This could suggest that pore diameter is a significant characteristic when evaluating the success of a catalyst for the degradation of plastics.

On some occasions, the rare-earth Y-zeolites (CeY, LaY), were found to be very effective in initiating a catalytic degradation mechanism (often of lower energy than

other catalysts) despite their below average ranking in the catalyst characterisation experiments. One possible explanation is that, on heating of the catalyst, the removal of water exposed previously hidden Lewis sites on the Ce or La cations (which also have f-orbitals available for interactions with intermediates) or on the Y-zeolites themselves, prompting them to be more effective at higher temperatures. However, their tendency to produce a large amount of residue on polymer decomposition made these catalysts the least desirable in terms of plastic recycling. In comparison, the ZSM-5 zeolites (23z, 280z) were found to be good reducers in the onset temperatures of degradation of a variety of polymers, whilst also initiating Brønsted- and/or Lewis-catalysed degradation mechanisms for pure and waste polyethylene. 280z appeared slightly more successful in the thermogravimetric experiments than 23z. This was consistent with Table 2.10 in which 280z was ranked just above 23z, based on its superior surface area measurement.

Due to time constraints, only a selection of the catalysts could be chosen for the next stage of experimentation. Fulcat 435 was selected as the one clay to analyse further in relation to the recycling of plastic, due to its significant effects on the onset temperature of degradation and its ability to change the degradation mechanism from a free radical process to a Brønsted- and/or Lewis-acid catalysed mechanism in some cases. GC-MS analysis of the degradation of LDPE and Fulcat 435 produced a large proportion of C_6-C_7 single-branched alkanes. The combination of a good surface area, average pore diameter and higher relative concentrations of Lewis acidic catalytic sites in relation to the other clay catalysts could explain the success of this catalyst even though it has lower overall acidity.

The low Al content of the ZSM-5 catalysts, 23z and 280z, suggests that there will be fewer catalytic sites available in these zeolite catalysts and their low pore size in comparison to the acid-activated clays could result in larger organic molecules being prevented from reaching the active sites. However, this was not found to be the case. The thermogravimetric analysis of polymers in the presence of both zeolites produced good reductions in the onset temperature of degradation of a variety of plastics. For the GC-MS experiments, 280z was found to be extremely successful in forming high RON aromatics from the degradation of LDPE. The average pore diameter of 20 Å did not appear to hinder the hydrocarbon polymer chains from entering the sites and forming aromatics (benzene, toluene, ethylbenzene and xylene). This may be somewhat attributable to the large surface area of 280z, which may have negated the effects of low Al content and small pore diameter.

Catalytic degradation of polymers showed a marked reduction in the onset temperature of decomposition. However, it was also important to determine the amount of energy required for the decomposition of the plastic to occur and offset this with the energy expelled on combustion. These energy balance calculations give insight as to whether certain reactions are energetically viable, and hence environmentally sound. Differential Thermal Analysis and Bomb Calorimetry provided the necessary energy values for the endothermic and exothermic processes and suggested that the catalytic degradation of the five pure polymers tested (LDPE, HDPE, PP, PS and PET) was energetically viable, with a net 25 kJ/g of energy remaining (the endothermic value of forming degradation products was found to be overwhelmingly compensated by the energy released on combustion of the polymer).

The most desired products of polymer decomposition would be those with high Relative Octane Number (RON). Aromatics (*i.e.* benzene, toluene), *iso*-paraffins (highly branched) and olefins have high RON values, whilst mixed paraffins (*i.e. iso*-paraffins with limited branching) and naphthenes (*i.e.* cyclohexane) exhibit intermediate values of RON. Paraffins such as *n*-heptane exhibit low RON values (defined as 0 for this case). In general, high octane number is increased with the degree of branching and the number of double bonds, as more stable radicals are formed allowing slower, smoother reactions. The formation of over 40% aromatics by mass from the degradation of LDPE in the presence of 280z zeolite at 450ºC, is a very positive result in terms of formulating high RON fuel from the recycling of plastic. The design of the experiment, in which the sample holder was placed inside the furnace with half of the sample tube above the heated zone, encouraged reflux of intermediate fractions and further cracking and rearrangement of products into lighter, gaseous components. Additionally, isothermal experiments where LDPE was held at 400ºC in the presence of 280z displayed a marked increase in the yield of aromatics as the run continued for 340 minutes. This suggested that as low-density polyethylene is held at a constant temperature of 400ºC, after approximately three hours, a greater proportion of high RON products are formed.

In summary, the ZSM-5 zeolites - 23z and 280z - proved to be the most promising catalysts with high yields of products, large reduction in T_{onset} relative to thermal cracking, high aromatic and C_6-C_8 branched alkane yield and low proportions of undesirable alkenes and straight chain alkanes. The acid-activated montmorillonite clay Fulcat 435 was very effective at reducing the temperature of reactions and formed a very large proportion of single-branched alkanes, but a very low amount of high RON aromatics. The Envirocat catalysts (EPZ**) were a little disappointing in that they did

312

not appear to out-perform the ZSM-5 zeolites (as would have been expected from the results of the catalyst characterisation experiments). However, EPZE, EPZG and EPZ10 did initiate Brønsted- and/or Lewis-catalysed reactions for eleven, nine and twelve of the polymers respectively, suggesting that the Envirocats show good promise in relation to plastic recycling. Overall, from the large thermogravimetric study taken, every catalyst appeared to have at least one outstanding effect on one of the polymers it was used to degrade (be it a large reduction in T_{onset} or a significant effect on E_a).

In conclusion, this study has provided a useful insight into the degradation of many different polymers in the presence of clay and zeolite catalysts. A comprehensive thermal analysis of polymer and catalyst mixtures was undertaken and revealed that onset temperatures of degradation were reduced dramatically in relation to free-radical thermal degradation. The activation energies for decompositions that occurred at temperatures below the T_{onset} value obtained with a catalyst were found to correspond to Si-OH protonation (Brønsted) of the polymer and/or Lewis-acid removal of hydride ions from the polymer. Although in some cases the activation energies of a reaction were higher than for the free-radical degradation mechanism (especially in relation to deprotonation energy), it was hoped that the decomposition products would be more favourable. This was found to be the case in relation to the formation of a greater number of single-branched alkanes (Fulcat 435) and an increase in the aromatic yield (280z) compared to thermal (non-catalytic) degradation of low-density polyethylene.

Future Work in this area would involve greater analysis of the degradation of polymers in the presence of Fulacolor and EPZ10 clays in particular, due to their promising catalytic properties (see Table 8.1) and their effects on polymer decomposition seen from thermogravimetry.

More detailed energy balance calculations would also be undertaken. This study used a basic comparison between the energy required to decompose the polymer (endothermic process) from DTA measurements and the energy of combustion of the polymer (exothermic process) from bomb calorimetry experiments. However, this calculation could be improved greatly by analysing the calorific value of the degradation products (identified from GC-MS). A C—H bond requires 99 kcal/mol (414 kJ/mol) to break, whilst C—C and C=C bonds require 83 kcal/mol (347 kJ/mol) and 146 kcal/mol (610 kJ/mol) to rupture respectively. Therefore, accurate energies of the degradation products could be determined. A combined TGA/DTA system would allow precise mass and energy measurements whilst the polymer degraded at an elevated temperature.

To determine the success of 280z zeolite and Fulcat 435 clay for the degradation of waste polymers on an industrial scale, the experiment must be scaled-up to dimensions where kilograms of mixed waste plastics can be added to the furnace instead of the grams used in this study. The larger furnace, containing a base-layer of chosen catalyst, or mixture of catalysts, could be held at a constant temperature (determined from the thermogravimetric results) and waste polymers added. Once the majority of waste plastic has been converted to gaseous products, further waste could be added, with the cycle continuing as long as the catalyst remains active.

It is hoped that more research continues in this field so that the problems of plastic waste and shortages of fuel move ever closer to being resolved.

Appendix A

Table A.1: Summary of past research into the degradation of different polymers

AUTHOR	CATALYST	CONDITIONS	MAIN PRODUCTS	COMMENTS
POLYETHYLENE				
Ayame et al.[292]	CaX zeolite	452-526ºC for 3 hours	C_3, C_4, iso-C_4	Olefin-to-paraffin ratio decreased with increasing temperature and contact time.
Wampler and Levy[293]	None	600-1000ºC	Alkadiene, alkene and alkane triplet peaks on GC	Decreasing alkane and increasing diene with increasing temperature.
Songip et al.[294]	HZSM-5 zeolite HY and REY zeolites Silica-alumina	450ºC	C_3 C_4 C_4	C_4 olefins created due to the penetration of the molecules into the larger pore size HY and REY zeolites and silica alumina catalyst.
Masuda et al.[295]	Ni and REY zeolites HY and HZSM-5	450ºC	Gaseous compounds and gasoline	Ni-REY zeolite produced highest gasoline yield (64%).
Schirmer, Kim and Klemm[296]	No catalyst HZSM-5and Y-zeolites		No catalyst - Wax (C_{15}) Zeolites - Large C_5-C_7 yield	Low yields of oils and gases with no catalyst present. Catalytic degradation yielded 70 wt.% oil fraction.
POLYETHYLENE WAX				
You, Kim and Seo[297]	No catalyst MFI zeolite	400ºC 350ºC	No catalyst - 3% gas Zeolite - 78% liquid	C_3-C_5 major gas component C_5-C_9 major liquid component.
LINEAR LOW-DENSITY POLYETHYLENE				
McCaffrey, Kamal and Cooper[298]	No catalyst	425-450ºC	Liquid portion of straight-chain hydrocarbons	Thermolysis of LLDPE said to be a random scission mechanism.

AUTHOR	CATALYST	CONDITIONS	MAIN PRODUCTS	COMMENTS
Manos et al.[299]	Al pillared saponite and montmorillonite		Gases mainly butenes, propene and then pentene	Conversion to liquid >70%
Gobin and Manos[300]	No catalyst Zeolites Clays		No catalyst - no liquid products Zeolites - lighter H/Cs Clays - most liquid, heavier H/Cs	No catalyst: 5% polymer conversion Zeolites: 90% polymer conversion Clays: 98% polymer conversion
LOW-DENSITY POLYETHYLENE				
Uemichi, Kashiwaya and Ayame[301]	Activated carbon Silica-alumina		C_6-C_7 C_3-C_5	More aromatics with activated carbon – radical mechanism so few branched alkanes and alkenes.
Ohkita et al.[302]	Silica alumina Zeolites	400ºC	Aromatics with HZSM-5	
Mordi, Field and Dwyer[303]	HZSM-5, HMOR, H-Theta-1 zeolites	Polymer-to-catalyst ratio 5:1	HZSM-5 highest gas (C_1-C_5) fraction and most aromatics	Initiation on external catalyst surface as LDPE molecule too large to enter zeolite pores.
Blazśo and Zelei[304]	Fe(II) and Cu(I) chlorides	400ºC 600ºC 1000ºC	600ºC – catalysts decreased aliphatic volatiles and increased aromatics 1000ºC - mainly aromatic volatiles	Promote chain scission and double bond formation Increased char.
Williams and Williams[305]	No catalyst	500-700ºC	Alkanes, alkenes	More gases and aromatics at higher temps.
Behie and Berruti[306]	No catalyst	780-860ºC	Gas >90%, olefins > 75 wt.%	Methane and ethane increased with temp., butane and butadiene decreased at higher T.
Marcilla, Beltran and Conesa[307]	MCM1			Decomposition temperature reduced by 50ºC with 2% of MCM1 catalyst.
Bagri and Williams[308]	Fixed zeolite bed	500ºC	Oils (alkadiene, alkene, alkane) - Aromatics (toluene, ethylbenzene, xylene)	Production of two- and three-ring naphthalene and phenanthrene and methyl derivatives.
De la Peunte, Klocker and Sedran[309]	FCC catalysts at 500ºC	LDPE dissolved in toluene	Light olefins, isoparaffins, aromatics	Wide product distribution due to formation of carbenium ions.
Zhou et al.[310]	ZSM-5 and La^{3+} exchanged ZSM-5	390ºC	Increase in olefins, decrease in aromatics, double isoparaffins	La^{3+} ions said to increase number of weak acid sites and decrease strong acid sites.
Serrano et al.[311]	Nanocrystalline ZSM5 ZSM-5 Al-MCM-41		n-ZSM5: no olefins or paraffins above C_6	Reduced max. rate of decomposition by 81ºC Reduced max. rate of decomposition by 34ºC Reduced max. rate of decomposition by 70ºC

AUTHOR	CATALYST	CONDITIONS	MAIN PRODUCTS	COMMENTS
HIGH-DENSITY POLYETHYLENE				
Garforth et al.[311]	Mesoporous and microporous catalysts	30-600ºC	Generation of Brønsted- and Lewis-acid sites	Reduced activation energy of decomposition from 255 kJ/mol to 77-201 kJ/mol.
Garforth et al.[312]	Mesoporous and microporous catalysts	290-430ºC fluidised bed	Large mesopores (supercages) and low acidity gave broad C_3-C_8	HZSM-5 and HMOR with smaller channels gave narrow C_3-C_5 distribution (over 80%).
Sakata et al.[313]	No catalyst Mesoporous silica (KFS-16)	430ºC	No catalyst: C_3, C_2 and a little C_4 KFS-16: decrease in C_2 and C_3, increase in C_4 and C_5	No catalyst: liquid products (C_5-C_{22}) paraffins and olefins, no aromatics Catalytic degradation: increased C_4-C_{10} and aromatics and decreased >C_{12}
Lin et al.[314]	US-Y zeolite	Up to 500ºC	Production of lots of coke	Average activation energy of 101 kJ/mol
Breen and Last[315]	Bed of acid-activated clay		Maximum C_{13}-C_{16} alkanes, branched alkanes up to C_{20}	Pillared clays produced the most aromatics due to dehydrocyclisation.
Park et al.[316]	Solid acid catalysts		Narrow liquid distribution C_5-C_{13}	HZSM-5: high Brønsted sites, giving 75% aromatics, RON 93.3%
Breen et al.[277]	Bed of acid-activated clay	420ºC and 650ºC in TG	No catalyst: C_4-C_{22} alkanes and alkenes with no branched alkanes	Catalytic degradation gave maximum distribution at C_{11}-C_{18}, branched alkanes up to C_{20} and aromatics
Ali et al.[317]	Bed of acid-activated clay or zeolite	360ºC and 450ºC	ZSM-5 yielded 83 wt.% olefins in C_3-C_5 range	US-Y supercages produced C_3-C_8 of paraffins and olefins but more coke.
Park, Kim and Seo[318]	MOR, MFI, BEA, FAU, MWW zeolites		BEA and FAU gave high liquid yields due to weak acidities and rapid diffusion into pores	MWW gave slow diffusion in pores yielding high gas products. MOR rapidly blocked by char.
Seo, Lee and Shin[279]	ZSM-5, zeolite-Y		Enhanced formation of aromatics and branched hydrocarbons	Due to large intracrystalline pore channels and strong acidity.
COMPARISON OF LDPE AND HDPE				
Uddin et al.[319]	Silica-alumina catalysts		No catalyst gave C_3, C_2 and C_4 and liquids C_5-C_{25}. Catalytic degradation gave C_5-C_{15}	Branched polymers degrade more easily to liquid hydrocarbons. Catalysts increased gas and liquid yields.

AUTHOR	CATALYST	CONDITIONS	MAIN PRODUCTS	COMMENTS
Horvat and Ng[320]	No catalyst	400-460ºC	Gases C_3-C_4, liquids C_2-C_{20} Average liquid chain C_{11}-C_{15}	TGA data – activation energies for alkane and alkene fractions. LDPE showed fastest thermolysis rate.
Ballice[321]	No catalyst	Non-isothermal	1-olefin and paraffin production	Activation energies of products calculated.
Schirmer, Kim and Klemm[322]	No catalyst HZSM-5 and Y-type zeolites	400ºC	Wax $>C_{15}$, low oil and gases (no catalyst). HZSM-5 gave high yields of C_5-C_6 oils, Y-zeolite gave more wax.	Y-zeolite had less acid sites therefore less effect on degradation temperature and increased coking. HZSM-5 channel structure not as prone to coking.
Van Grieken et al.[323]	HZSM-5, HY zeolites, MCM-41		65 wt.% of gas seen with HZSM-5 and LDPE at 380ºC. 50 wt.% of liquid with MCM-41 at 420ºC.	MCM-41large pores prevent rapid deactivation. Poor HY performance due to coke formation. MCM-41 produced greatest wax fraction for HDPE.
Manos et al.[324]	Montmorillonite and saponite clays, pillared clays, Y-zeolite		70% conversion to liquids (C_6-C_{10} alkenes) with clays. 50% conversion to liquids with Y-zeolite	Greater selectivity with clays. Zeolite had more acidity and stronger external sites but suffered coke formation.
Marcilla et al.[325, 326]	MCM-41, HZSM-5, HUSY			Greater branching on LDPE gave lower decomposition temperature.
Marcilla, Beltrán and Navarro[327]	HZSM-5 and HUSY zeolites		Greater loss of activity with LDPE when catalyst suffered coking	Branched LDPE entered inner active sites of catalyst while HDPE reacted with external sites.
Serrano et al.[328]	Three HZSM-5 zeolites	340ºC for 2hrs		Cracking of LDPE more than HDPE due to branching.
POLYPROPYLENE				
Schooten and Wijga[329]	No catalyst			Rapid decomposition of PP at 320ºC
Chan and Balke[330]			Activation Energy of 328 kJ/mol	Associated with random scission throughout PP
Audisio and Silvani[331]	Silica, alumina, silica-alumina and zeolites	200ºC, 400ºC and 600ºC		Ionic and radical mechanisms occurring with silica, alumina and Z-Na-Y.
Mordi, Fields and Dwyer[332]	HZSM-5	Polymer-to-catalyst ratio 5:1		Cracking of PP initially on surface then at the inside cavities of catalysts
Zhao et al.[333]	Zeolites		Mainly olefinic hydrocarbons	Due to an intra-molecular free-radical transfer mechanism.

AUTHOR	CATALYST	CONDITIONS	MAIN PRODUCTS	COMMENTS
Cardona and Corma[334]	Large pore zeolites Amorphous and ordered silica-aluminas	Introduction of catalyst at 380ºC		Neither the total amount or strength of acid sites on the catalysts were the most determinant factors for cracking PP as the cracking was initiated on the external surface.
Jakab, Várhegyia and Faix[335]	Wood-derived materials		Charcoal found to promote formation of monomer and dimer.	
Hwang et al.[336]	Zeolites	Heated to 400ºC	No catalyst: wide ranging C_4-C_{26}. Catalytic degradation: gasoline range C_4-C_{12}	Initiation of PP degradation at external surface of zeolite, decomposed fragments diffused into pores for further cracking to iso-paraffins (C_8-C_{11}), olefins (C_6-C_9) or aromatics (C_8-C_{10}).
Kim et al.[337]	Clinoptilolite zeolites	400ºC		Acid sites of medium strength necessary for formation of carbenium ions.
Marcilla et al.[338]	ZSM-5 zeolite E-cat (FCC catalyst)	500-775K	Addition of E-cat reduced decomposition temperature by over 100ºC.	
Durmus et al.[339]	BEA, ZSM-5, MOR zeolites			Reduction in activation energy of degradation with catalysts.

COMPARISON OF PE AND PP

AUTHOR	CATALYST	CONDITIONS	MAIN PRODUCTS	COMMENTS
Uddin et al.[340]	Non-acidic mesoporous silica (FSM)	380ºC and 430ºC	Increase in rate of degradation in presence of catalyst	Absence of strong acid sites prevented over-cracking to gaseous products, producing 86 wt.% liquid hydrocarbons.
Onu et al.[278]	HZSM-5 and PZSM-5 (modified with orthophosphoric acid)		Greater scission of C-C chains for PE than PP, resulting in more gaseous products.	HZSM-5 increased liquid yield and aromatics for PE and PP. PZSM-5 had fewer silanol groups and Brønsted-acid sites, decreasing acidity but increasing paraselectivity.
Sakata, Uddin and Muto[341]	Solid acid and non-acid catalysts	PE at 430ºC PP at 380ºC	Non-catalytic degradation: C_5-C_{25} liquids. Silica-alumina: C_5-C_{15} rich in unsaturated H/Cs (olefins)	Strong acid sites on ZSM-5 gave more gases and less liquid.
Aguado et al.[342]	Zeolite beta	400ºC	HDPE selectivity to form C_5-C_{12} LDPE and PP gave 62% of C_5-C_{12} and lighter C_1-C_4	Presence of tertiary carbons on LDPE and PP provided favourable positions for initiation of polymer chain cracking.

AUTHOR	CATALYST	CONDITIONS	MAIN PRODUCTS	COMMENTS
Zhou et al.[343]	Modified ZSM-5 zeolite	330ºC, 380ºC and 430ºC	Non-catalytic degradation yielded C_4-C_{20}. Catalytic degradation produced 23% conversion of LDPE at 330ºC.	LDPE gave narrower carbon distribution due to interaction with the zeolites inner sites, whereas PP was hindered due to the presence of the side-chain methyl groups.

POLYSTYRENE

AUTHOR	CATALYST	CONDITIONS	MAIN PRODUCTS	COMMENTS
Grassie and Kerr[344]	No catalyst	280ºC and 330ºC	Monomer to pentamer volatile products	Depolymerise via depropagation (formation of monomer) and intra- or inter-molecular transfer.
Simard, Kamal and Cooper[345]	No catalyst	370ºC-420ºC	Liquid products – styrene, styrene dimer, styrene trimer, toluene, α-methylstyrene, ethylbenzene and 1,3-diphenylpropane	Up to 70% conversion of PS into styrene produced, with yield increasing with temperature. Activation energy of depolymerisation said to be 166 kJ/mol.
Zhang et al.[346]	Solid acids and bases		No catalyst: 70% styrene. Catalyst: styrene monomer and dimer, benzene and ethylbenzene.	Aromatics from further cracking and hydrogenation of the styrene yield.
Carniti et al.[347]	Zeolites, silica-aluminas		Catalytic degradation gave a 10-20 times faster rate of formation of radicals.	No catalyst: toluene, ethylbenzene and styrene. Catalyst: high selectivity to benzene and toluene, possibly due to Lewis-acid sites.
Zhibo et al.[348]	Solid acid catalysts	623K	Cracking of styrene into benzene	Hydrogenation of styrene into ethylbenzene.
Guoxi et al.[349]	Metal powders (Al, Zn, Fe, Ni, Cu)	Polymer-to-catalyst, 10:1	Activation energies decreased in presence of most catalysts	Cu powder found to hinder degradation of PS.
De la Peunte and Sedran[350]	Acid catalysts		Brønsted sites said to yield large amounts of styrene and some benzene, toluene, ethylbenzene and C_{9+} aromatics	Brønsted sites greatly reduced over 600ºC.
Serrano, Aguado and Escola[351]	Acid catalysts		Thermal cracking – styrene and corresponding dimers and trimers	Thermal cracking of PS: radical mechanism. Acid catalysed cracking of a carbenium nature associated with Brønsted-acid sites.
Karaduman et al.[352]	No catalyst	700-875ºC	Liquid yield maximised at 750ºC (48% benzene, 18% styrene, 8% toluene)	Styrene yield greatest at 825ºC (no benzene content).

AUTHOR	CATALYST	CONDITIONS	MAIN PRODUCTS	COMMENTS
Karmore and Madras[353]	Lewis-acid solutions			Degradation rate dependent on electronegativity of Lewis acid.
COMPARISON OF PE AND PS				
Zhibo et al[354]	Solid bases Solid acids		Bases - More oil with PE, low RON 80wt.% to styrene monomer and trimer with PS	Acids - Less oil with PE but rich in aromatics and branched isomers (high RON).
Mertinkat et al.[355]	FCC catalyst	370-515ºC	PS – produced BTX-aromatics and ethylbenzene rather than styrene	PE – iso-compounds in the gas and oil fractions, mainly methylpropane, propene, propane and methylbutenes.
Faravelli et al.[356]	No catalyst	370ºC and 410ºC	HDPE –alkanes, alkenes, dialkenes PS –monomer, dimer and trimer	PS degradation independent from presence of PE
COMPARISON OF PS, PE AND PP				
Peterson, Vyazovkin and Wight[357]	No catalyst	TGA on PE, PS and PP	Activation energies: PS (200 kJ/mol), PP (150-200 kJ/mol), PE (150-240 kJ/mol)	PS: single reaction step. PP and PE: lower values from initiation processes at weak links, higher values from degradation by random scission.
Lee et al.[358]	FCC catalysts	HDPE, LDPE, PP and PS at 400ºC	80-90% liquid yields for polymers (PS>PP>PE). Gas yields (PE>PP>PS)	PS produced 97% aromatics in liquid yield due to its polycyclic structure, including C_7-C_9 of single benzene ring structure.
Walendziewski[359]	Cracking catalyst	0-10% catalyst	PE and PP gave light H/Cs, PS gave mainly styrene derivatives (C_6-C_9)	
Demirbas[360]	No catalyst	Waste PE, PP and PS	PS gave higher liquids (65 wt.% styrene)	Higher gaseous products with PE and PP (56 wt.% and 50 wt.% respectively).
POLYETHYLENE TEREPHTHALATE				
Buxbaum[361]	No catalyst	PET in molten state at 280ºC	Gaseous products (280-306ºC) – acetaldehyde major product	Cyclic oligomers (mainly the trimer) formed during thermal degradation.
Goodings[362]	No catalyst	288ºC	CH_3CHO 80% of total gas	From mass spectrometry of products.

AUTHOR	CATALYST	CONDITIONS	MAIN PRODUCTS	COMMENTS
Ritchie[363]	No catalyst	400-550ºC	CO_2 from breakdown of vinyl ester end-groups and decarbonylation of acetaldehyde.	Description of thermal degradation of PET.
Masuda et al.[364]	No catalyst	Steam atmosphere	Degradation in steam said to weaken C-O bonds, accelerating hydrolysis	Monomers of PET produced with little carbonaceous residue (<1%).
Masuda et al.[365]	FEOOH, Fe_2O_3, $Ni(OH)_2$, NiO		Attempt to convert terephthalic acid from thermal degradation of PET	FeOOH found to show high activity for successful decomposition of PET.
POLYVINYL CHLORIDE				
[366,367]	No catalyst		(1) 305ºC: release of hydrogen chloride, (2) 468ºC: benzene, chlorobenzene, dichlorobenzene and trichlorobenzene	Chlorinated aromatics very stable, trimer pathway found to be major pyrolysis pathway of PVC degradation. Dehydrochlorination said to follow chain reaction mechanism.
[368]	Ferric chloride and aluminium chloride catalysts		Cl linked to tertiary carbon atom can be easily removed to form a double bond and give an allylic structure from which HCl is removed	Presence of metal chlorides found to bring about radical-type decomposition by providing unsaturated centres through an ionic mechanism.
Müller and Dongmann[369]	Lewis acids: $FeCl_3$, $GaCl_3$, $SbCl_3$, $BiCl_3$, $ZnCl_2$ Copper halides		All catalysts found to reduce the formation of aromatics. Crosslinking found to occur at 253ºC	Positively charged carbon atom reacted with an electron rich polyene sequence (reacting with double bond, producing a C-C bond), crosslinking two polymer chains.
COMPARISON OF PE AND PVC				
Wu et al.[370]	No catalyst	Different HCl concentrations	Pyrolysis of HDPE in presence of HCl gas.	Increase in amount of HCl found to inhibit the conversion of HDPE.
Bockhorn, Hornung and Hornung[371]	No catalyst		PE: E_a = 268 kJ/mol PVC: E_a of Dehydrochlorination = 190 kJ/mol, E_a of 2nd step = 163 kJ/mol	Dehydrochlorination of PVC accompanied by benzene formation.
POLYAMIDE				

AUTHOR	CATALYST	CONDITIONS	MAIN PRODUCTS	COMMENTS
[372]	No catalyst		Nylon-6 underwent major degradation from 300-400ºC	Melting peak at 240ºC and decomposition endotherm at 450ºC.
Kachi and Jellinek[373]	No catalyst	35-65ºC	Nylon-66 films	Degradation *via* random chain scission in amorphous and interfacial regions.
Strauss and Wall[374]	No catalyst	310-380ºC	Maximum rate of volatilisation occurred at 30-40% volatilisation	Activation energy of 42 kcal/mol representative of a free radical mechanism.

POLYBUTADIENE

[375]	No catalyst		Two distinct weight loss steps – first due to volatile depolymerisation	Second step attributed to degradation of a residue due to cyclised and cross-linked butadiene rubber.
[376]	No catalyst	325-425ºC	Pyrolysis products mainly CH_4	Yield of monomers found to be small, therefore scissions of C-C bonds in chain accompanied by hydrogen transfer.
Straus and Madorsky[377]	No catalyst		Activation energy of polybutadiene = 62 kcal/mol	

POLYACRYLONITRILE

Burlant and Parsons[378]	No catalyst	200-320ºC	Above 210ºC, HCN vapour evolved. At 280ºC, the maximum 8% of ammonia was liberated	Pyrolysis at 250ºC yielded non-monomer liquid (10-15% weight of polymer) with unsaturated bonds present.
Nagao *et al.*[379]	No catalyst	200-350ºC in nitrogen or air	Considerable amount of HCN evolved.	
Houtz[380]	No catalyst	400ºC	Only a trace of HCN evolved.	
National Bureau of Standards [381]	No catalyst	Pyrolysis at 500ºC-800ºC	500ºC: black powder residue of 75% carbon, 4% hydrogen and 21% nitrogen. 800ºC: residue not completely carbonised	Thermal degradation of PAN in two steps: (1) rapid evolution of HCN, acrylonitrile and acetonitrile with activation energy of 31 kcal/mol (2) slower rate of evolution.
Chatterjee *et al.*[382]	No catalyst	DTA and TGA	250-400ºC: small amount of ammonia, HCN and hydrogen. 425-680ºC: 68% mass loss of PAN	DTA results revealed exotherms relating to intrachain polymerisation of nitrile groups and aromatisation.

AUTHOR	CATALYST	CONDITIONS	MAIN PRODUCTS	COMMENTS
Frankoski and Siggia[383]	No catalyst	Furnace at 150ºC	Liberation of ammonia	
Zhao and Jang[384]	No catalyst	PAN fibres	Mass loss of PAN fibres at 260ºC	Due to cyclisation of original PAN structure.

POLYMETHYL METHACRYLATE

AUTHOR	CATALYST	CONDITIONS	MAIN PRODUCTS	COMMENTS
[385,386]	No catalyst	500ºC	Degraded primarily to monomer	Monomer is methyl methacrylate (MMA).
Hirata, Kashiwagi and Brown[387]	No catalyst		Two stages of weight loss: (1) 160ºC, E_a = 31 kJ/mol (2) E_a = 233 kJ/mol	(1) end initiation (2) random scission initiation
Kashiwagi and Inabi[388]	No catalyst		Degradation of PMMA via β-scission at pendant position, not backbone.	
Jellinek and Luh[389]	No catalyst	300-400ºC	E_a of isotactic PMMA = 36 kcal/mol	
Barlow, Lehrle and Robb[390]	No catalyst		E_a for degradation of thin film of PMMA = 25 kcal/mol	
Zhang and Blum[391]	Silica		Degradation of isotactic PMMA easier to start but easier to interrupt	Syndiotactic PMMA more stable to degradation due to chain stiffness in polymer backbone.
Wang and Smith[392]	No catalyst	Styrene/methyl methacrylate copolymers	Presence of MMA found to improve thermal resistance to nonpolar solvents	
Bate and Lehrle[393]	No catalyst	Pyrolysis of PMMA:PS blend at 550ºC	PS:PMMA ratio (1:1) stabilised each polymer due to cross-termination reaction	Predominance of cross-termination rather than chain transfer due to lower reactivity of PMMA radical in relation to poly(alkyl acrylate) radical with relation to H abstraction from PS molecules.

POLYURETHANE

AUTHOR	CATALYST	CONDITIONS	MAIN PRODUCTS	COMMENTS
Day, Cooney and MacKinnon[394]	No catalyst		E_a for 10% weight loss for two steps of PU degradation: 122 kJ/mol and 182 kJ/mol respectively	Presence of contamination (rust, copper, dirt) in PU reduced weight loss temperature from 263ºC to 255ºC.

AUTHOR	CATALYST	CONDITIONS	MAIN PRODUCTS	COMMENTS
Molero, de Lucas and Rodríguez[395]	Diethanolamine (DEA), titanium (IV) butoxide, potassium octoate, calcium octoate		Glycolysis of PU foams	All catalysts allowed complete recovery of polyols from the PU matrix.

AUTHOR	CATALYST	CONDITIONS	MAIN PRODUCTS	COMMENTS
MIXED WASTE				
Ibrahim, Hopkins and Seehra[396]	No catalyst		Co-mingled plastic, 90% PE and 10% PP	Average activation energy of degradation: 39 kcal/mol.
Ramdoss and Tarrer[397]	No catalyst	475-525ºC	Co-mingled plastic – decomposition complete by 500ºC	Selectivity for formation of light oil decreased from 32% to 24% as temperature increased.
Ballice[398]	No catalyst	Different LDPE:PP ratios	Maximum product release temperature: 440ºC giving straight and branched paraffins and olefins, dienes and aromatics (C_1-C_{27}).	Increasing ratio of LDPE produced greater amount of C_{16+} paraffins.
Marcilla et al.[399]	HZSM-5 zeolite, FCC	PE and PP mixtures	Catalyst provoked an advance in the degradation of both polymers and their mixture	FCC catalyst produced better separation between HDPE and PP cracking processes
Albano and de Freitas[400]			Activation energy of pure PP: 259 kJ/mol. E_a of PP:PE mix lower	Suggesting one of the polymers accelerated the process of decomposition of the other.
Koo and Kim[401]	No catalyst		PE and PS mixtures: maximum oil production from high T and low PE content	Maximum gas production from high pyrolysis temperatures and high mixing ratio of PE.

AUTHOR	CATALYST	CONDITIONS	MAIN PRODUCTS	COMMENTS
Kiran, Ekinci and Snape[402]	No catalyst	TGA up to 700ºC Ratios of PE:PS	PE – main products wax and gas, E_a of 218 kJ/mol. PS – E_a = 269 kJ/mol. PE:PS mix – Less oil as PE increased	PE degradation *via* free radical formation and hydrogen abstraction steps. PS degraded *via* radical chain process. In PE:PS mixture, PE favoured production of low MW aliphatics (C_7-C_{11}).
Kaminsky, Schlessmann and Simon[403]	No catalyst	Mixture of PE, PP and PS at 700ºC	Gas fraction 51 wt.% - ethane, propene, C_4-olefins Liquid – styrene and benzene	For higher monomer yields, each component in mixture would need its own pyrolysis temp.: 500-550ºC for PS, 700-750ºC for polyolefins.
Kaminsky, Schlessmann and Simon[404]	No catalyst	Mixture of PE, PP and PS	Gas 35 wt.% - methane, ethane, ethene, propene. Aromatic oils 44 wt.% - benzene, xylene, styrene	Calorific value of gas fraction: 50 MJ/kg
Pinto *et al.*[405]	No catalyst	Mixtures of PE, PP and PS	Highest gas yields with PE 100%, lowest gas with more PS. Greater aromatic content in liquid seen with PS	100% PE: 20% alkenes and 80% alkanes in gas Presence of PP favoured formation of alkenes Presence of PS favoured formation of aromatics.
Pinto *et al.*[405]	Zeolites	68% PE, 16% PP, 16% PS	Large quantities of ethylbenzene and toluene	Presence of zeolites found not to significantly affect results of previous study[251]
Kim, Yoon and Park[406]	Zeolites Silica-alumina	PP and PS mixture	Zeolite gave good conversion and low coking. All catalysts gave highly aromatic oils	Strong Brønsted-acid sites allowed crosslinking reactions among adjacent polymer chains. Presence of PP accelerated PS degradation by carbenium ions.
Ciliz, Ekinci and Snape[407]	No catalyst	PE:PP and PS:PP mixes	Virgin polymers gave E_a of 167-181 kJ/mol. PE:PP mix gave high values of gas and residue and low liquid yield.	Liquid yield for PE:PP mix reduced with increasing PP, but more C_7-C_{11} aliphatics. Addition of PP increased alkene/alkane ratio for C_2 and C_3.
Wu *et al.*[408]	No catalyst	Different HCl concentrations	Pyrolysis of HDPE in presence of HCl gas.	Increase in amount of HCl found to inhibit the conversion of HDPE.
Bate and Lehrle[409]	No catalyst	Pyrolysis of PMMA:PVC and PMMA:PE, PMMA:PS blends at 500ºC	PMMA:PVC blend produced no change from degradation of individual polymers. PMMA:PE blends produced no cross-products	PMMA:PS blend formed no cross-products but strongly stabilised the depropagation of each of the polymers, reducing the rate of monomer formation.

AUTHOR	CATALYST	CONDITIONS	MAIN PRODUCTS	COMMENTS
Murty et al.[410]	No catalyst	PET:LDPE and PVC:LDPE mixtures	TGA of individual polymers and then polymer mixtures showed degradation curve shifted to the right for the mixtures	Shift in TGA curve for mixtures indicated a delay in the onset of degradation.
Sakata et al.[411]	No catalyst	PE:PVC and PE:PET mixtures at 430ºC	PE:PVC and PE:PET mixes decreased yield of liquid products and increased gases and residues.	PE:PVC mix decreased C_{13}-C_{25} and increased C_7-C_{12} fraction.
Sakata et al.[412]	Silica-alumina	PE:PP:PS:PVC:ABS:PET mix at 410ºC	Non-catalytic liquids were in the C_5-C_{15} range. No real change seen for catalytic degradation	Presence of PVC and PET in waste resulted in large amounts of solid residues. PS and ABS thought to have deactivated the catalyst.
Kim, Kaminsky and Schlesselmann[413]	No catalyst	Plastic waste at 638ºC, 690ºC and 735ºC	Feed material: 79-75% polyolefin, 25-30% PS and 0-5% PVC: gas fraction chiefly methane, ethene and propene.	At 690ºC, 20 wt.% BTX-aromatics, 30 wt.% aliphatics. 638ºC and 690ºC product oil contained 20 ppm of Cl. 735ºC gave very low Cl content in oil.
Ding, Liang and Anderson[414]	ZSM-5 zeolite	HDPE and post-consumer plastic waste, 400-435ºC	No catalyst: gases C_1-C_4, oils C_5-C_{27} with higher paraffins and olefins than naphthenes and aromatics.	Catalytic degradation gave oil products containing large amounts of aromatics and naphthenes at expense of olefins and paraffins.
Williams and Williams[415]	No catalyst	LDPE:HDPE:PP:PS:PVC and PET mixture, 500-700ºC	500ºC: major gas was propene with small amounts of ethane. Amount of ethane increased with T while propene decreased.	500ºC: aliphatic oil from PE and PP made up 60% of sample, alkenes present. Aromatic concentrations increased with T. Oxygen from PET evolved as CO_2.
Williams and Williams[416]	No catalyst	LDPE:HDPE:PP:PS:PVC and PET mixture, 500-700ºC	Yield and composition of products in plastic mix said to be related to the proportion of each type of polymer.	Some evidence of interaction of the plastics resulted in a change in the composition of the pyrolysis products.
Bockhorn, Hornung and Hornung[417]	No catalyst	PVC:PS:PE, PE:PS and PA:PE mixes	Degradation of PA at same time as dehydrochlorination of PVC	Decomposition of PA catalysed by HCl. Styrene dimer yield reduced in presence of PA (increase in styrene dimmer and trimer).
Bockhorn et al.[418]	No catalyst	Electronic plastic scrap	Waste consisted of polyester resins, phenolic plastics and ABS.	Maximum evolution at 280ºC.

AUTHOR	CATALYST	CONDITIONS	MAIN PRODUCTS	COMMENTS
Blazsó[419]	Cu(I) and Fe(II) chlorides	LDPE, PP, PVC, PS, PMMA, polycarbonate and epoxy resin	Formation of chlorides in polymer mixtures containing PVC as evolved HCl reacted with metals and metal oxides.	Catalyst had no effect on fast radical depolymerisation reactions of PP, PS and PMMA..
Kaminsky and Kim[420]	No catalyst	685-738ºC	Mixture of polyolefins (78%), PS (14%), PVC (4%), polyester (7%) and paper	Maximum oil product: 50 wt.% methane, ethane, propene and CO. Calorific content of gas = 45-50 MJ/kg.
Vasile *et al.*[421]	ZSM-5 zeolites	Pure plastic waste mixture	HDPE (24%), LDPE (39%), PP (21.5%), PS (10%), ABS (4%), PET (1.5%)	No catalyst: wax (87 wt.%), gas (12 wt.%), residue (1 wt.%). Catalyst: reduced high MW products from C_{35} to C_{20}. Increase in low MW aromatics, *iso*alkanes, *iso*aalkenes, naphthenes.
Masuda *et al.*[422]	FeOOH catalyst, Ni-REY zeolite	PE:PET mix (15:2 ratio)	FeOOH increased oil and CO_2. Ni-REY converted oil $>C_{20}$ to gasoline and kerosene	FeOOH aided decomposition of wax.
Seo and Shin[423]	No catalyst	Shredded waste plastic pyrolysed at 400-500ºC	PE (50-60%), PP (20-30%), PS (10-20%), PVC (10%) gave pyrolysis oil of toluene (49-68%) and other aromatics.	Aromatics in oil said to be partly due to PS in feed but likely some other effect in the pyrolysis process contributed too.

Appendix B

Table B.1: Average Weight % of atomic elements from SEM-EDX

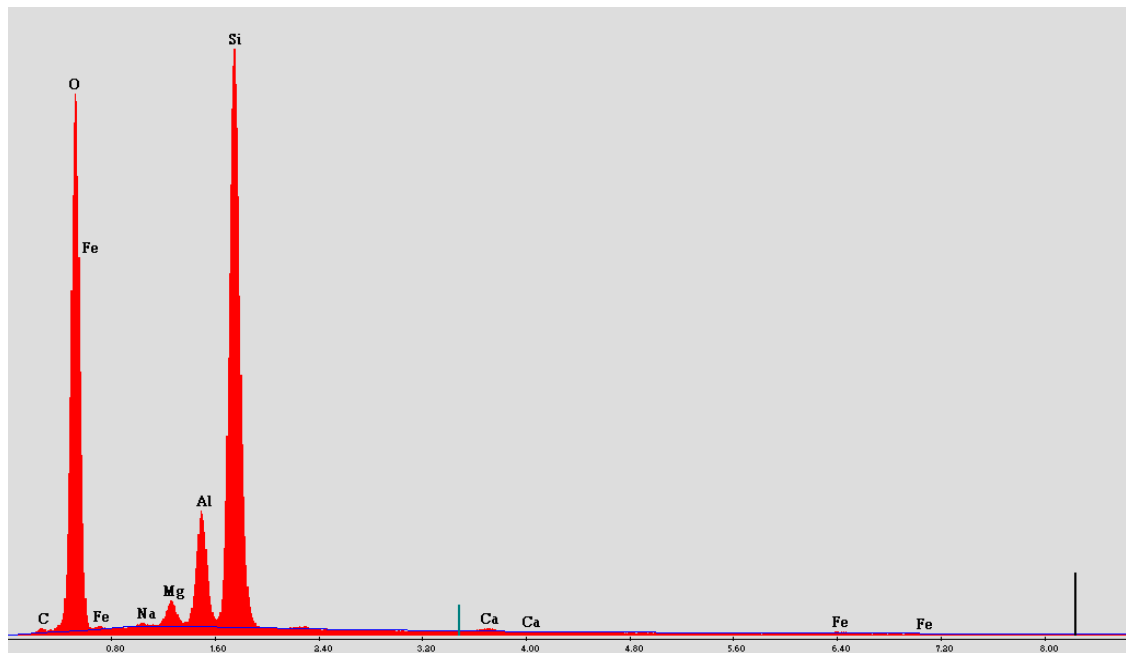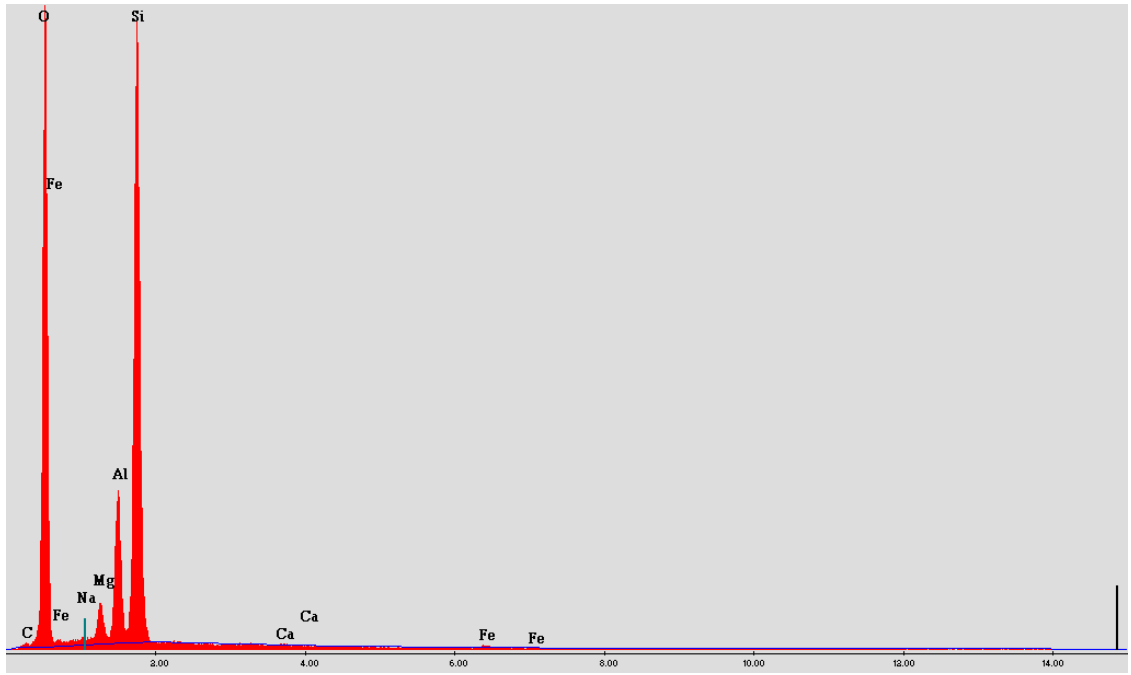|	Fulacolor	Fulcat	Fulmont	CeY	LaY	EPZE	EPZG	EPZ10	23z	280z
N				4.3	2.9					
O	51.3	51.9	49.2	52.0	50.9	48.0	48.8	41.7	50.5	48.6
Na	0.7	0.5	0.8	2.0	1.8	1.4	0.7	4.5		
Mg	1.9	2.3	1.8	0.6	0.3	1.4	1.2	1.3		
Al	7.0	7.8	6.0	9.4	10.4	5.2	7.8	4.4	4.0	0.7
Si	37.4	35.7	33.0	25.0	25.6	31.8	34.9	25.7	45.4	50.7
S			1.9			3.3		3.1		
Cl						1.2	1.9	7.0		
K			0.6			0.3	1.1	0.3		
Ca	0.5	0.3	2.0			3.5	0.2	3.6		
Ti			0.5			0.4		0.3		
Fe	1.1	1.4	4.2			1.7	3.4	1.4		
Zn						1.7		6.8		
Ce				6.7						
La					8.2					

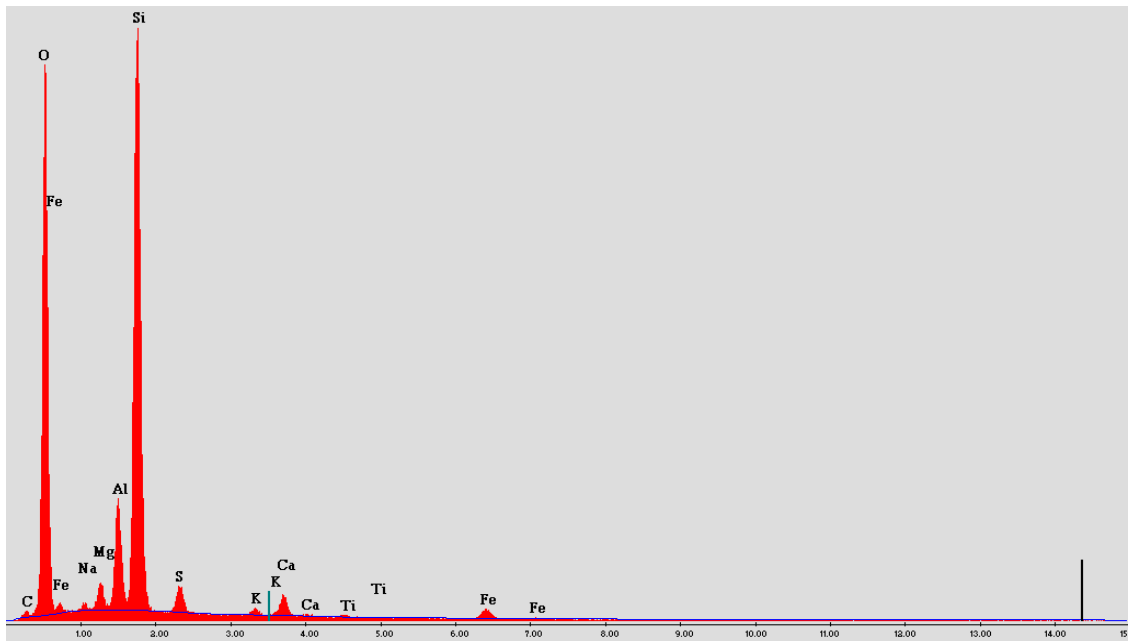**Figure B.1: Fulacolor clay**

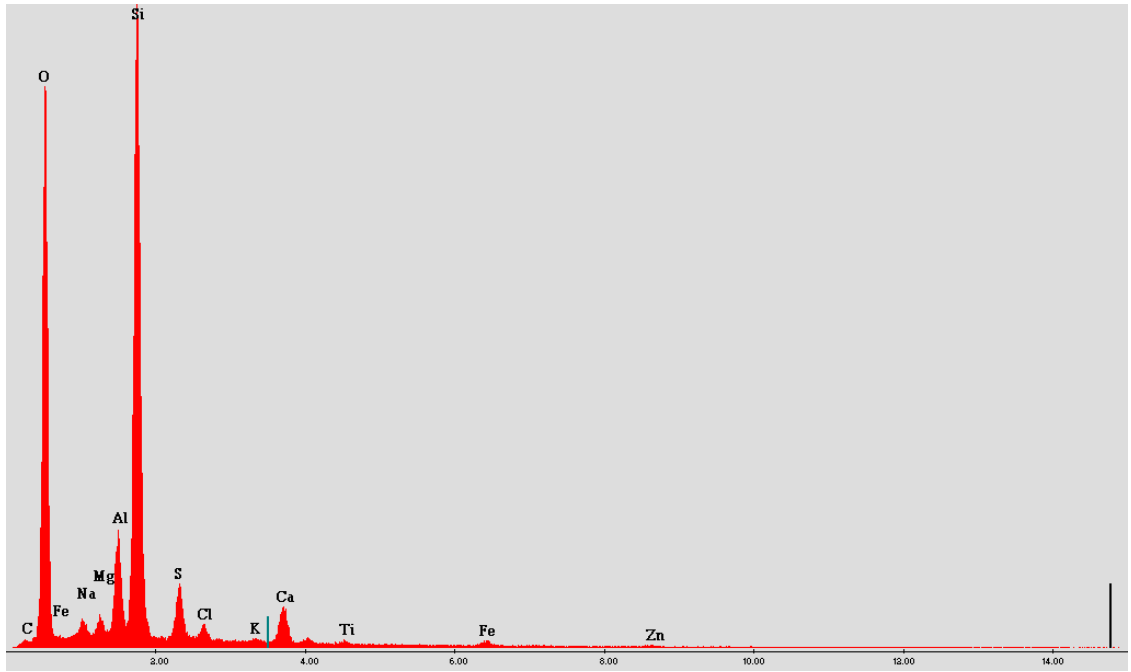**Figure B.2: Fulcat 435 clay**

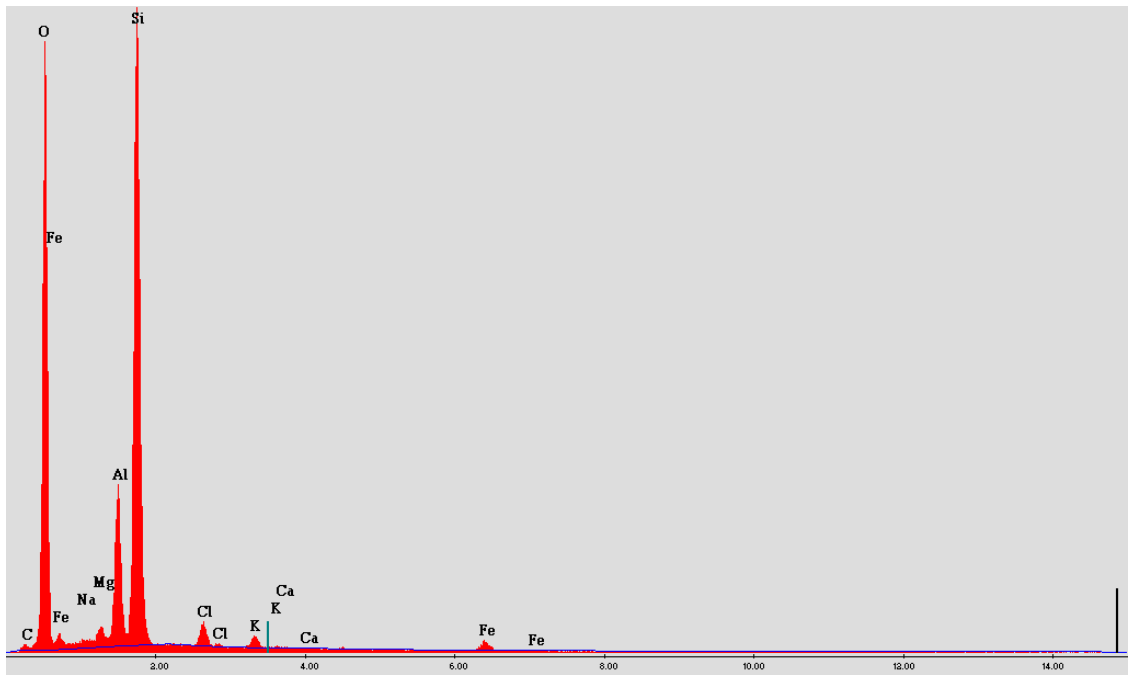**Figure B.3: Fulmont clay**

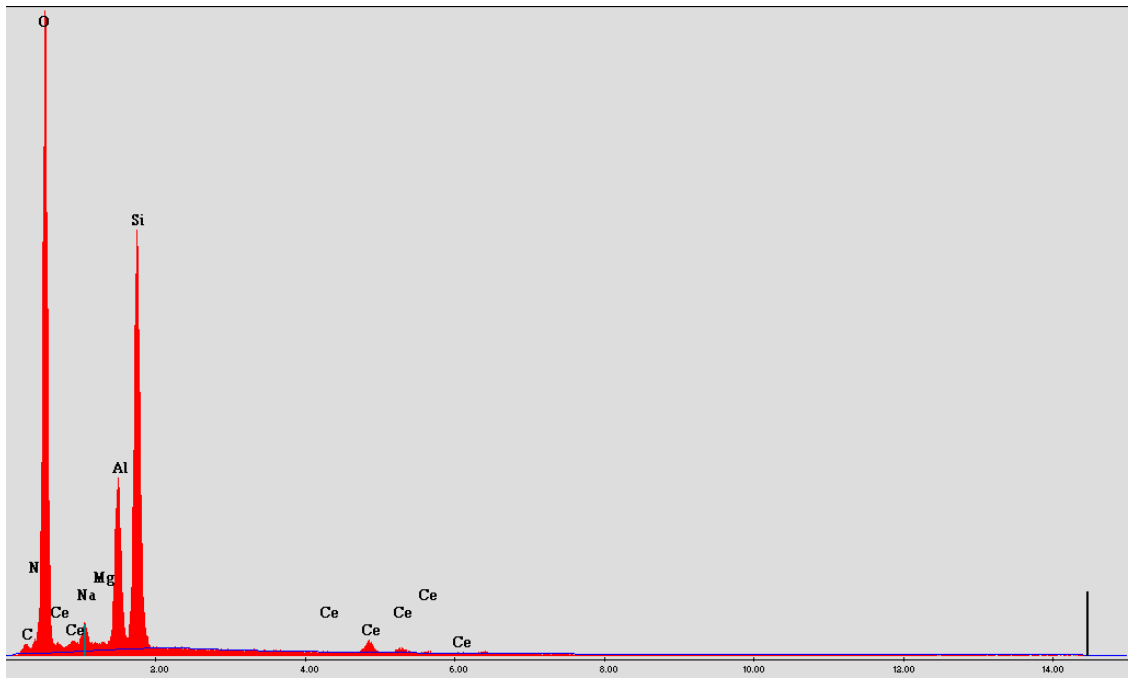**Figure B.4: EPZE clay**

Figure B.5: EPZG clay
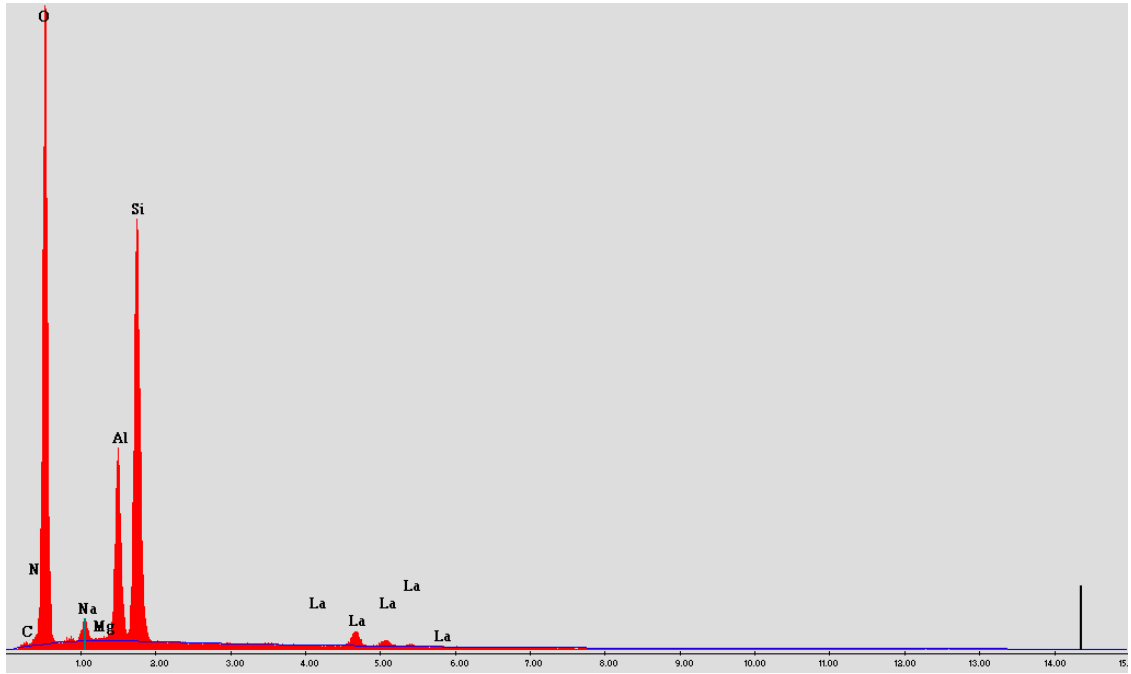
Figure B.6: CeY zeolite
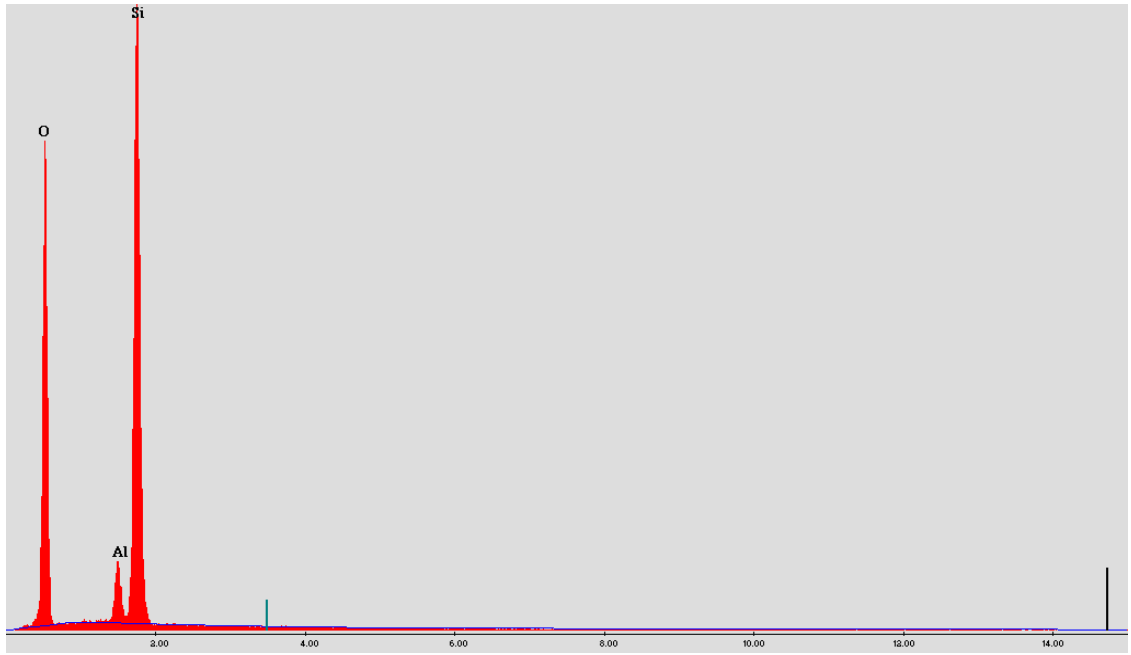

Figure B.7: LaY zeolite

Figure B.8: 23z zeolite
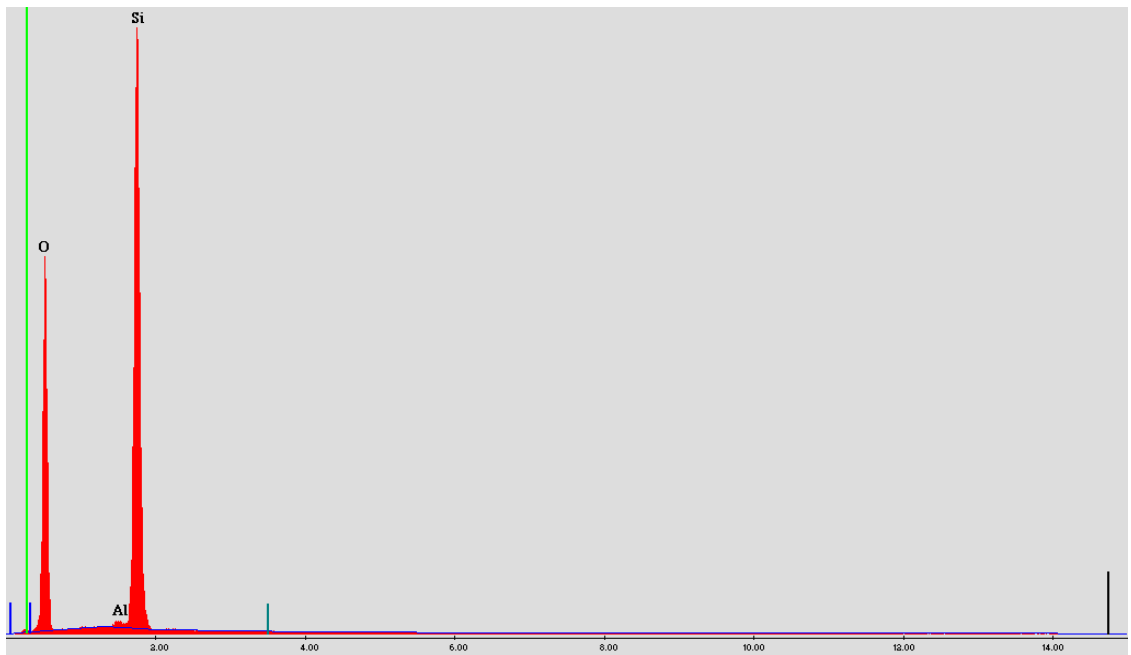
Figure B.9: 280z zeolite

Appendix C

Table C.1: Surface Area of the catalysts

Sample	BET Surface Area (m²/g)	Langmuir Surface Area (m²/g)	T-Plot Micropore Volume (cm³/g)	T-Plot Micropore Area (m²/g)	T-Plot External Surface Area (m²/g)
Si-Al (1)	227 ± 1	314 ± 6			
Si-Al (2)	232 ± 1	319 ± 6	0.011	27	204
Fulacolor	329 ± 1	452 ± 9	0.018	47	282
Fulcat 435	360 ± 1	493 ± 11	0.016	42	318
Fulmont	243 ± 1	334 ± 6	0.018	43	200
EPZE	287 ± 1	397 ± 8	0.007	22	266
EPZG	203 ± 1	282 ± 6	0.003	12	191
EPZ10 (1)	196 ± 1	274 ± 7	-0.004	-3	199
EPZ10 (2)	204 ± 1	285 ± 7	-0.002	0.9	203
23Z (1)	125 ± 2	166 ± 1	0.053	115	10
23Z (2)	327 ± 6	432 ± 1	0.014	301	26
23Z (3)	292 ± 6	385 ± 1	0.130	280	21
23Z (4)	310 ± 6	410 ± 1	0.129	277	33
280Z (1)	468 ± 6	642 ± 22	0.054	130	338
280Z (2)	453 ± 6	618 ± 21	0.057	132	321
CeY (1)	562 ± 10	742 ± 1	0.249	534	29
CeY (2)	575 ± 10	759 ± 1	0.250	536	39
LaY (1)	444 ± 8	587 ± 1	0.188	404	40
LaY (2)	413 ± 7	545 ± 1	0.177	379	33

Table C.2: Pore Volume and Pore Diameter of the catalysts

Sample	Single Point Surface Area at P/P_0 (m^2/g)	Single Point Adsorption Total Pore Volume of Pores < 665 Å (cm^3/g)	Adsorption Average Pore Diameter (Å)
Si-Al (1)	220	0.60	106
Si-Al (2)	224	0.62	107
Fulacolor	319	0.32	39
Fulcat 435	349	0.35	39
Fulmont	237	0.39	63
EPZE	277	0.40	56
EPZG	195	0.31	60
EPZ10 (1)	188	0.35	71
EPZ10 (2)	195	0.34	67
23Z (1)	130	0.06	21
23Z (2)	341	0.16	19
23Z (3)	305	0.13	18
23Z (4)	323	0.16	20
280Z (1)	461	0.23	20
280Z(2)	450	0.23	20
CeY (1)	589	0.26	19
CeY (2)	601	0.27	19
LaY (1)	463	0.23	21
LaY (2)	431	0.21	20

Appendix D

Thermogravimetric Analysis of Polymers and Catalysts

One-step degradation – 150ºC to 550ºC
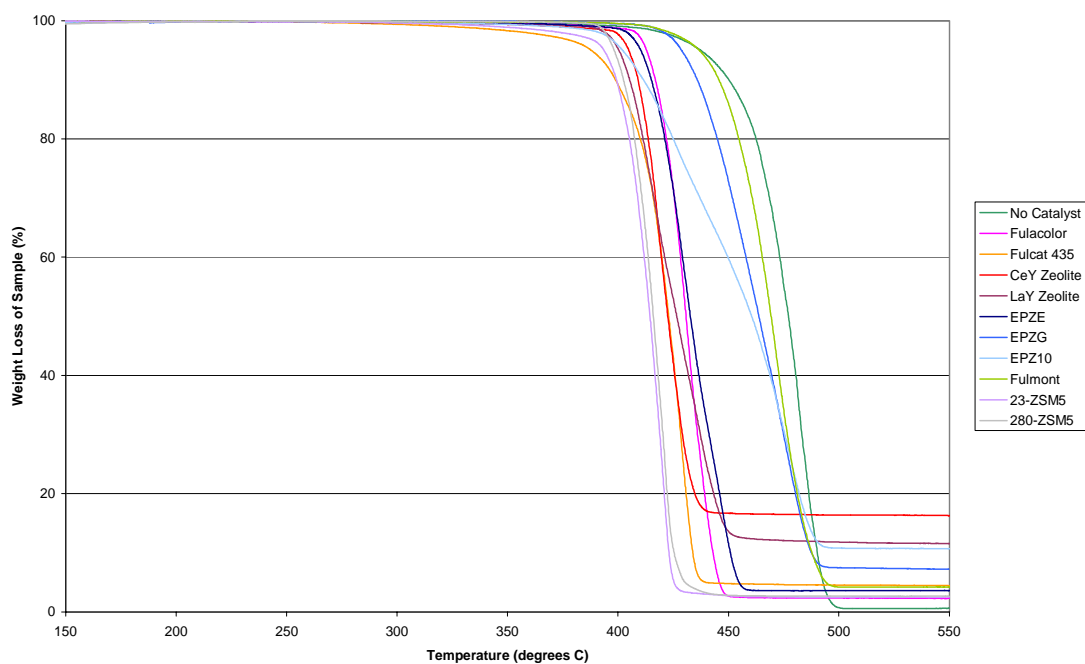
Figure D.1: TG curves for pure high-density polyethylene (PHDPE)
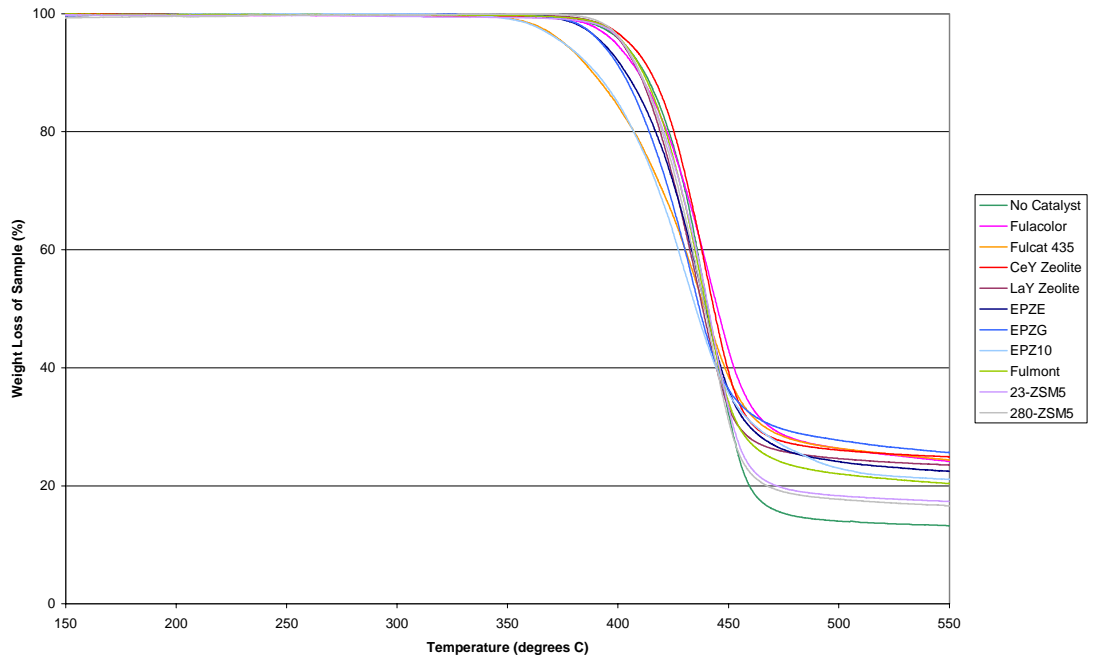
Figure D.2: TG curves for pure polyethylene terephthalate (PPET)
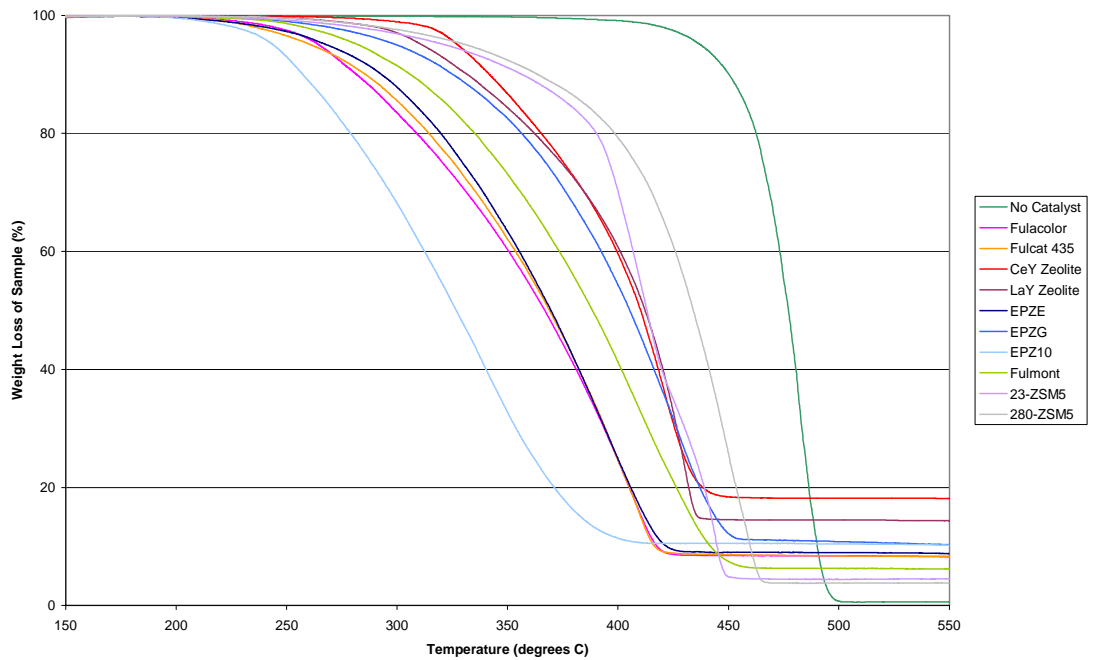
Figure D.3: TG curves for pure polystyrene (PPS) – 200ºC to 550ºC
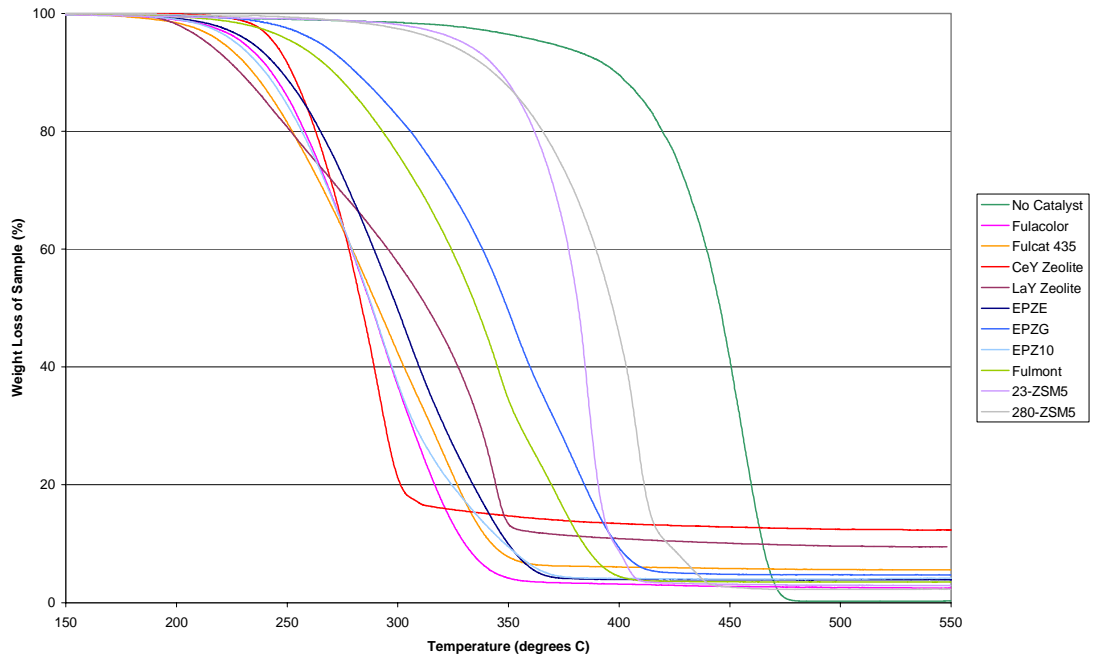
Figure D.4: TG curves for pure low-molecular weight polypropylene (PPPA)
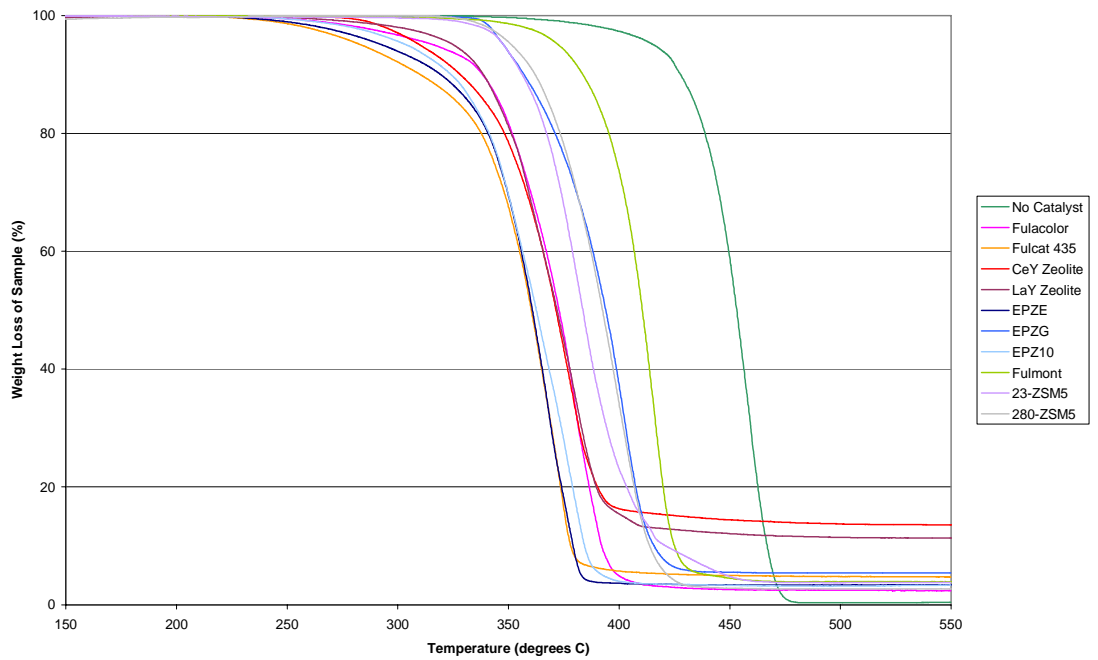
Figure D.5: TG curves for pure high-molecular weight polypropylene (PPPB)

D-3
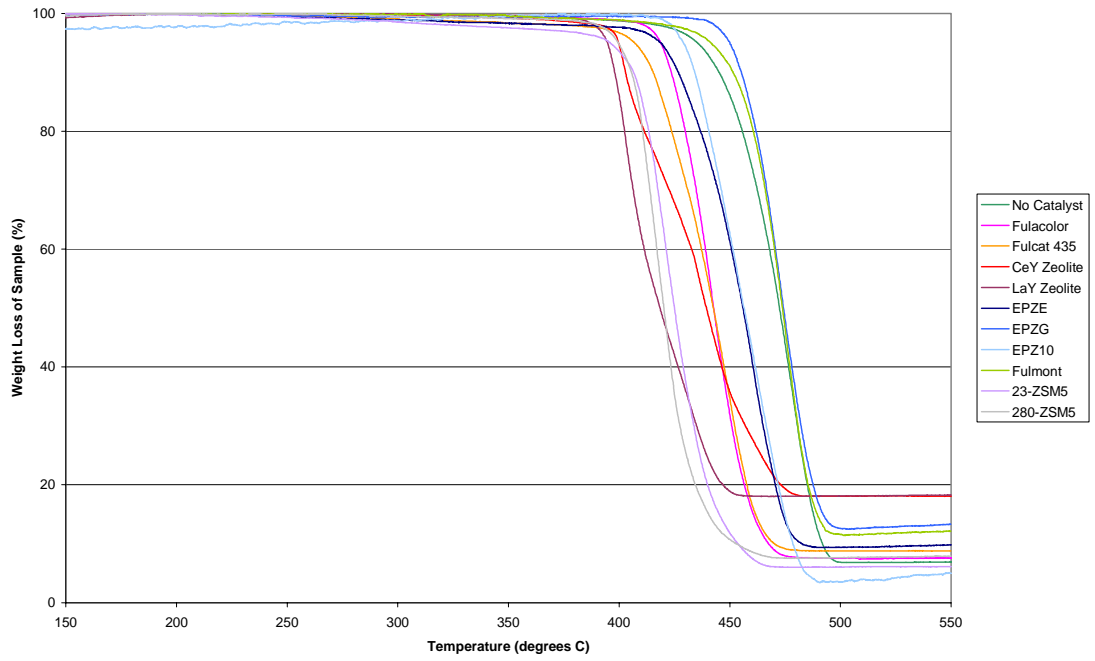
Figure D.6: TG curves for waste low-density polyethylene (LDPE)
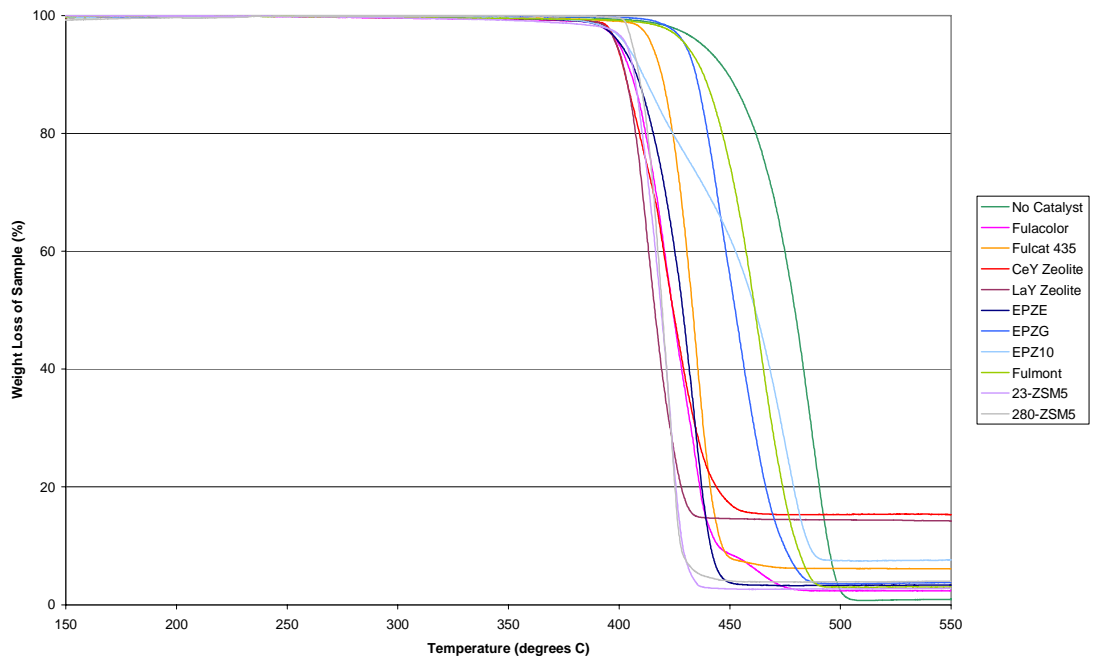
Figure D.7: TG curves for waste high-density polyethylene (HDPE)
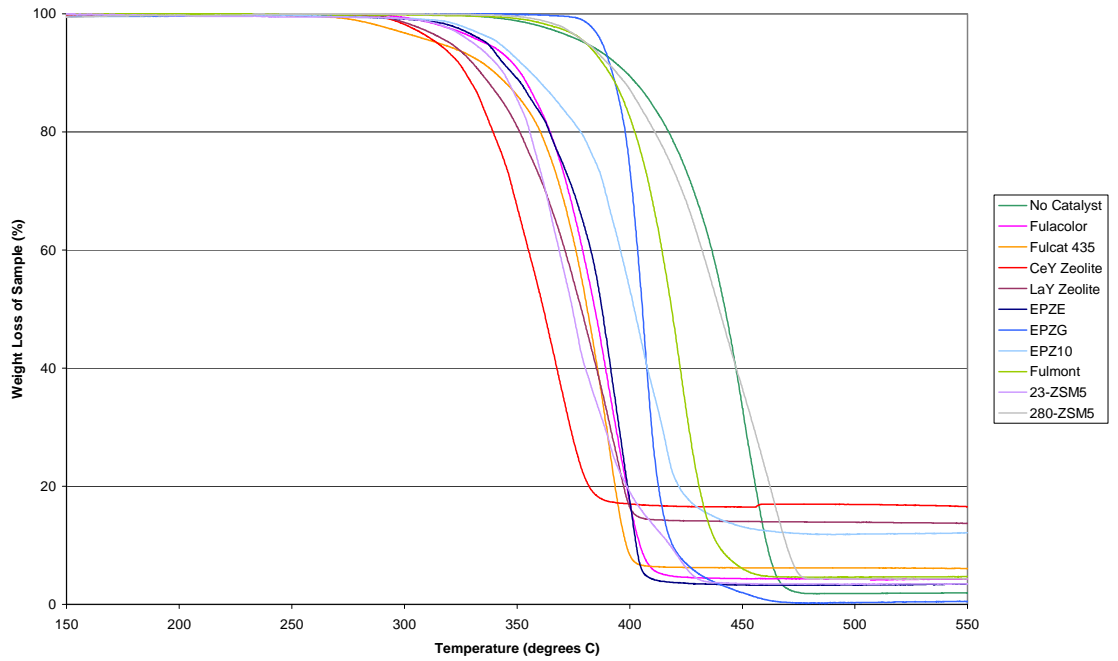
Figure D.8: TG curves for waste polypropylene (PP)
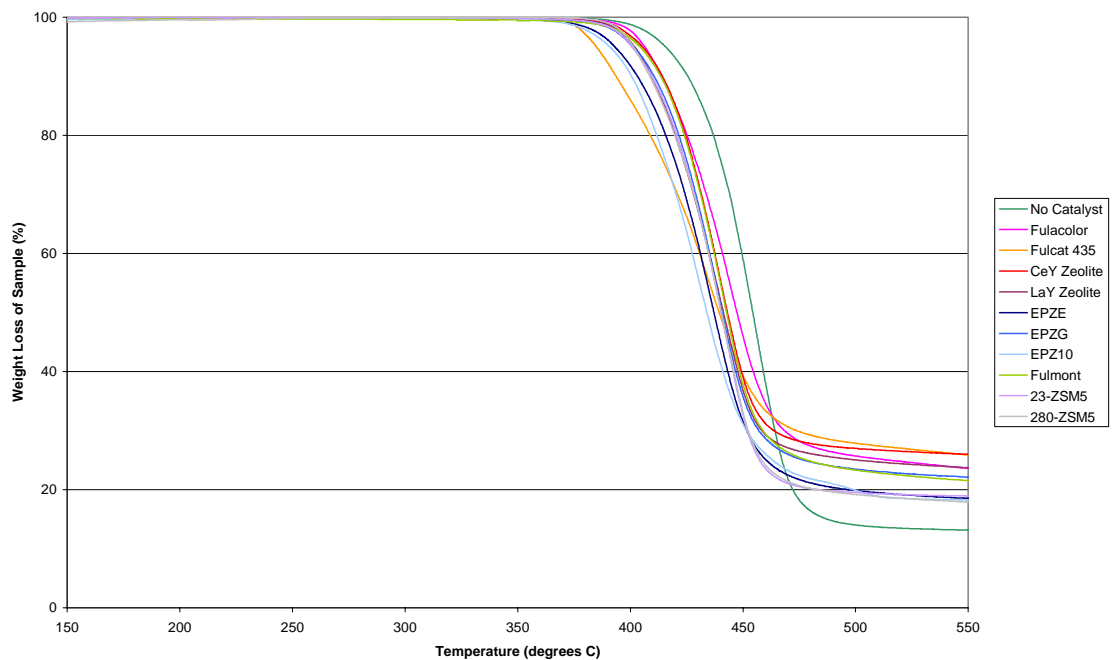
Figure D.9: TG curves for waste polyethylene terephthalate (PET)

D-5
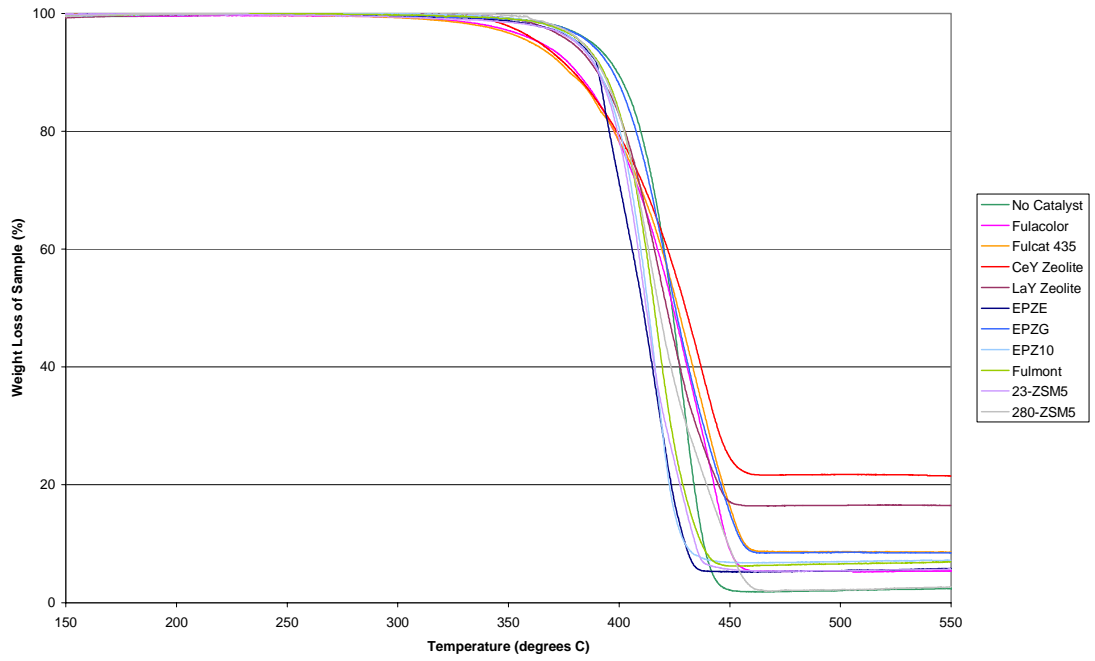
Figure D.10: TG curves for waste polystyrene (PS)
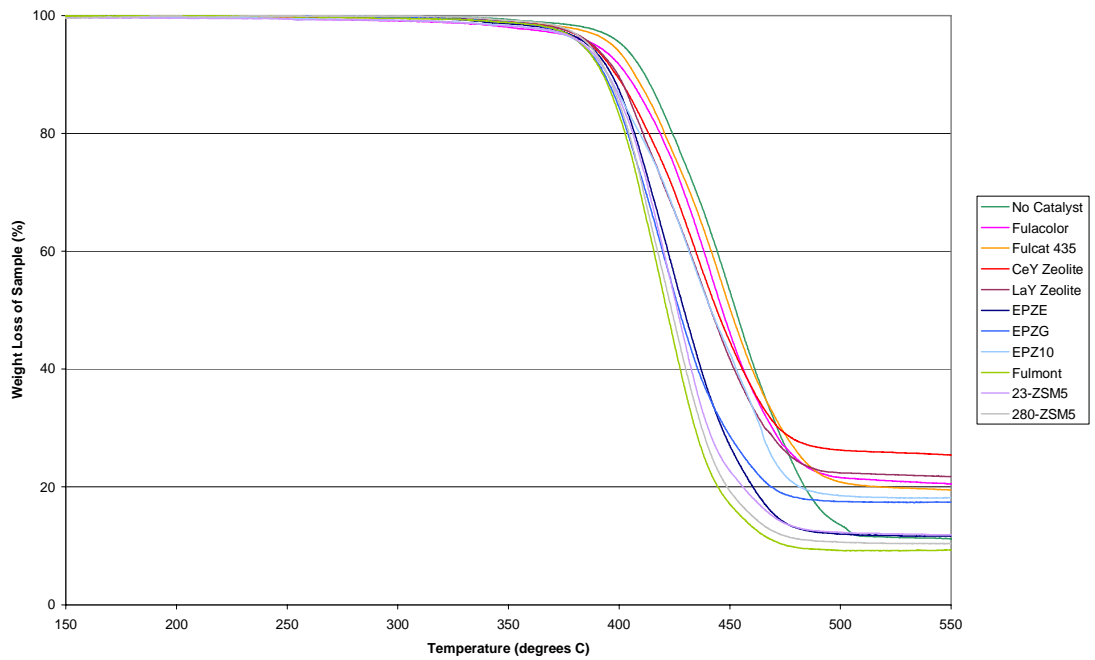
Figure D.11: TG curves for waste polyamide (PA)
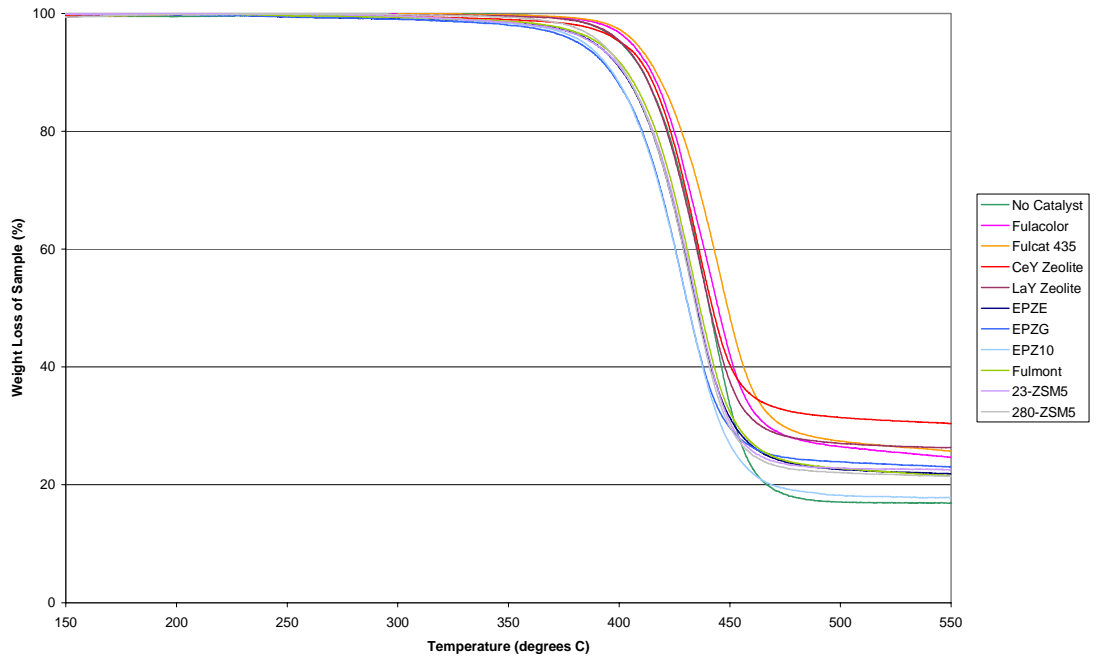
Figure D.12: TG curves for waste polyester (PE)

Two-step degradation – 150ºC to 550ºC
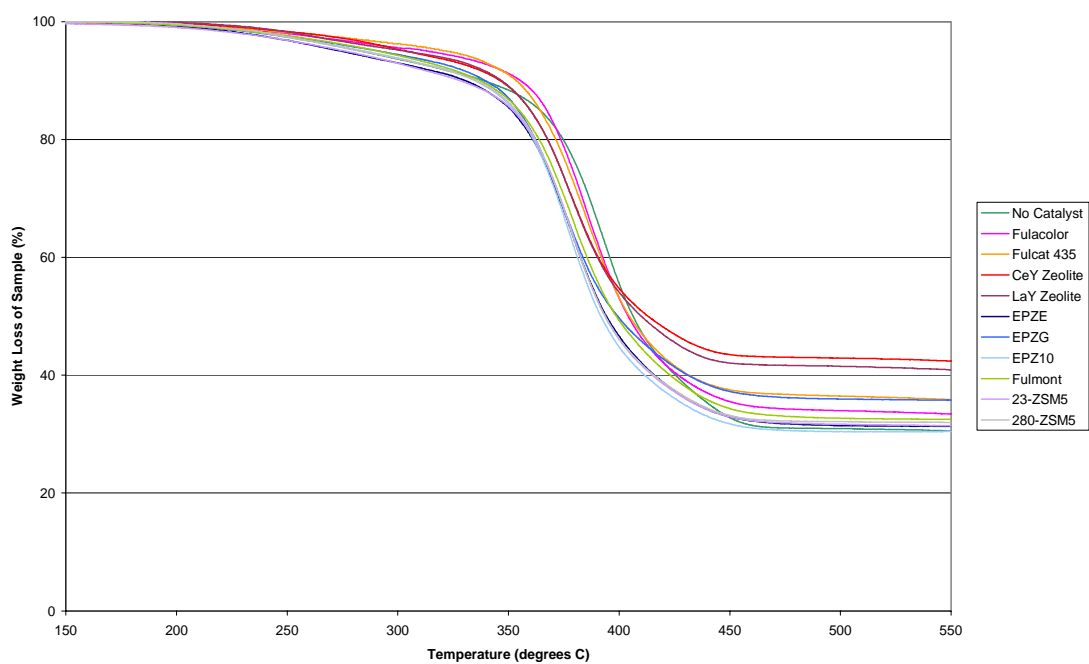
Figure D.13: TG curves for waste polybutadiene (PB)
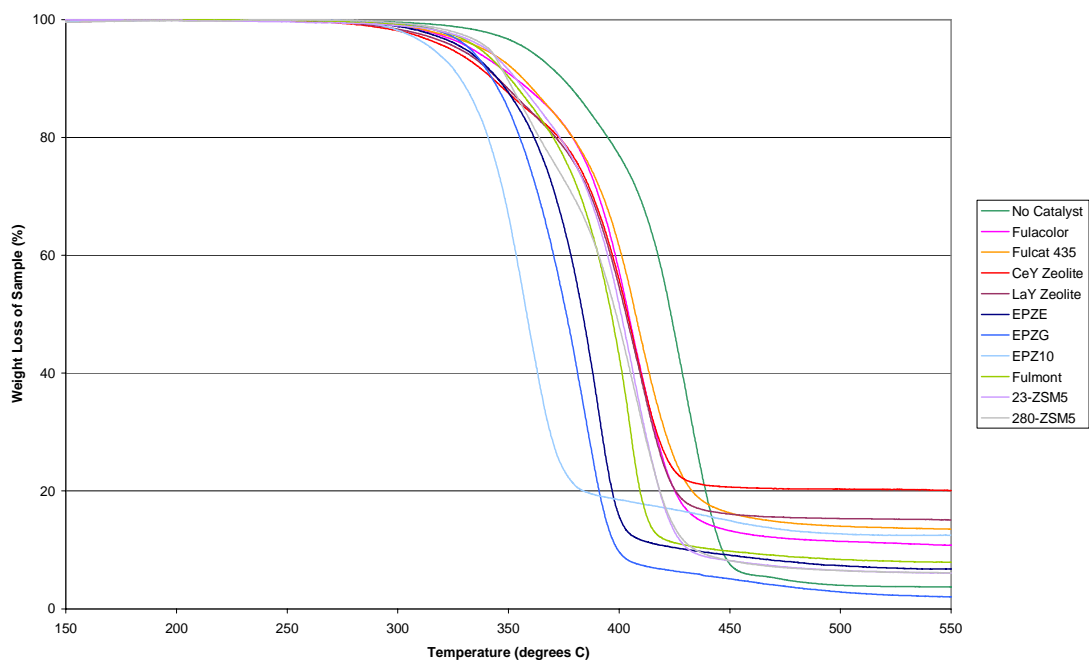
Figure D.14: TG curves for waste polyurethane (PU(RC35))
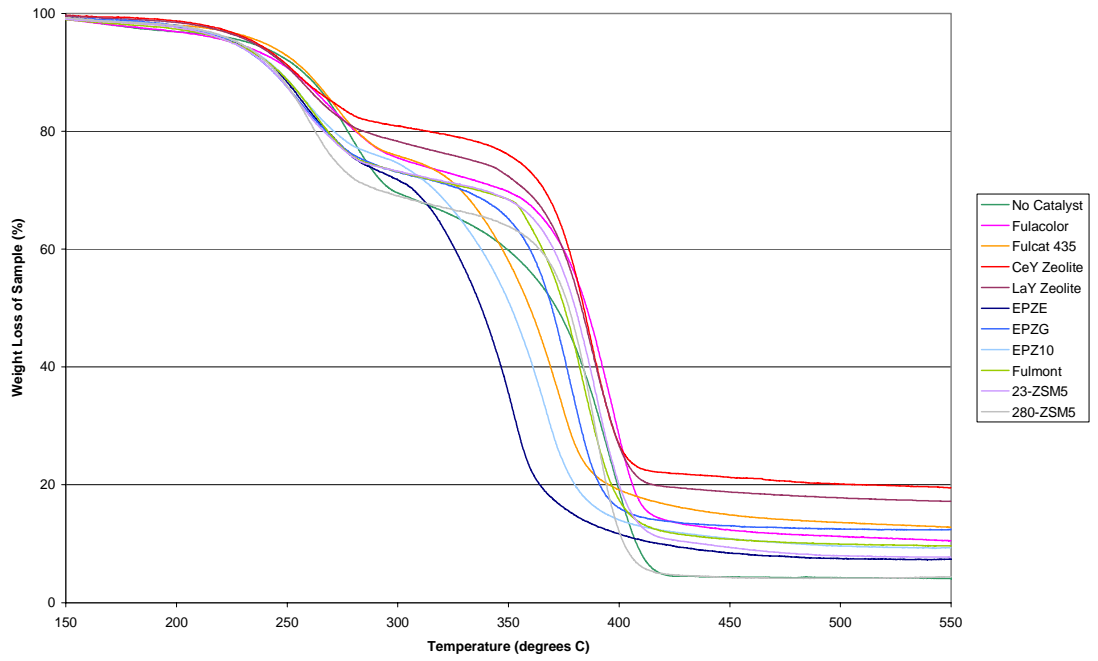
Figure D.15: TG curves for waste polyurethane foam (PU foam)
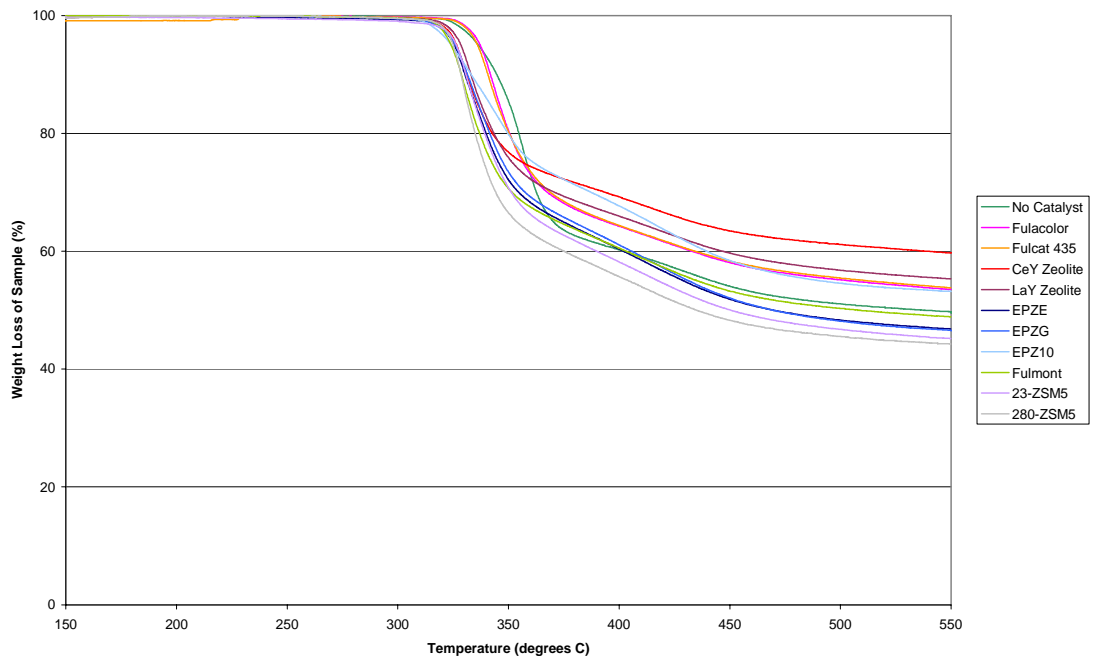
Figure D.16: TG curves for waste polyacrylonitrile (PAN)

D-9

Three-step degradation – 150ºC to 550ºC
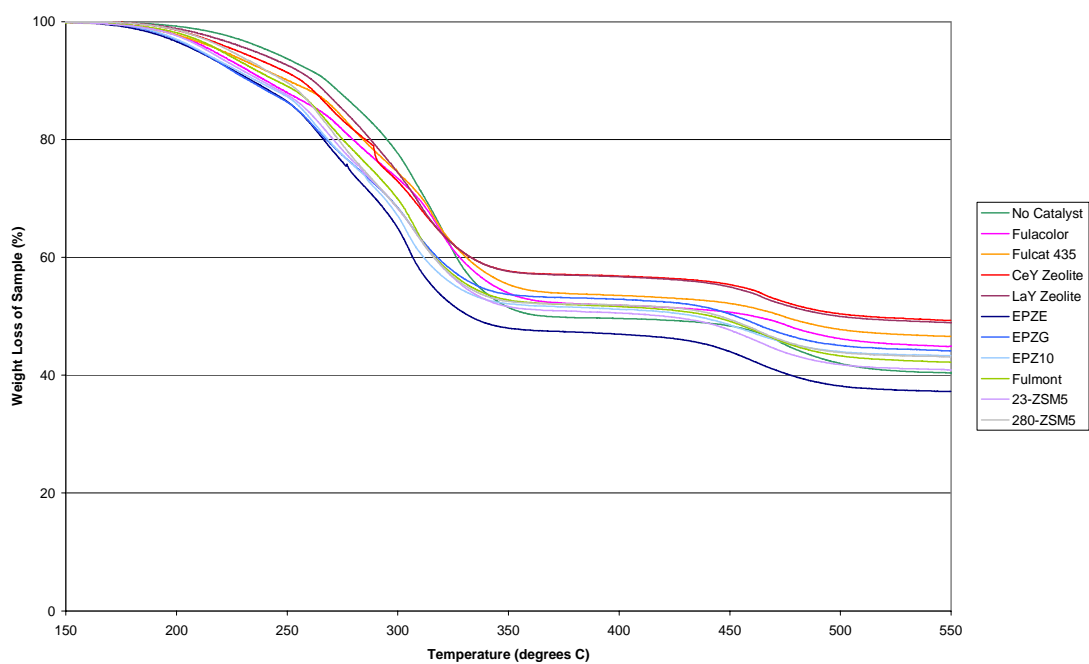
Figure D.17: TG curves for waste polyvinyl chloride (PVC)
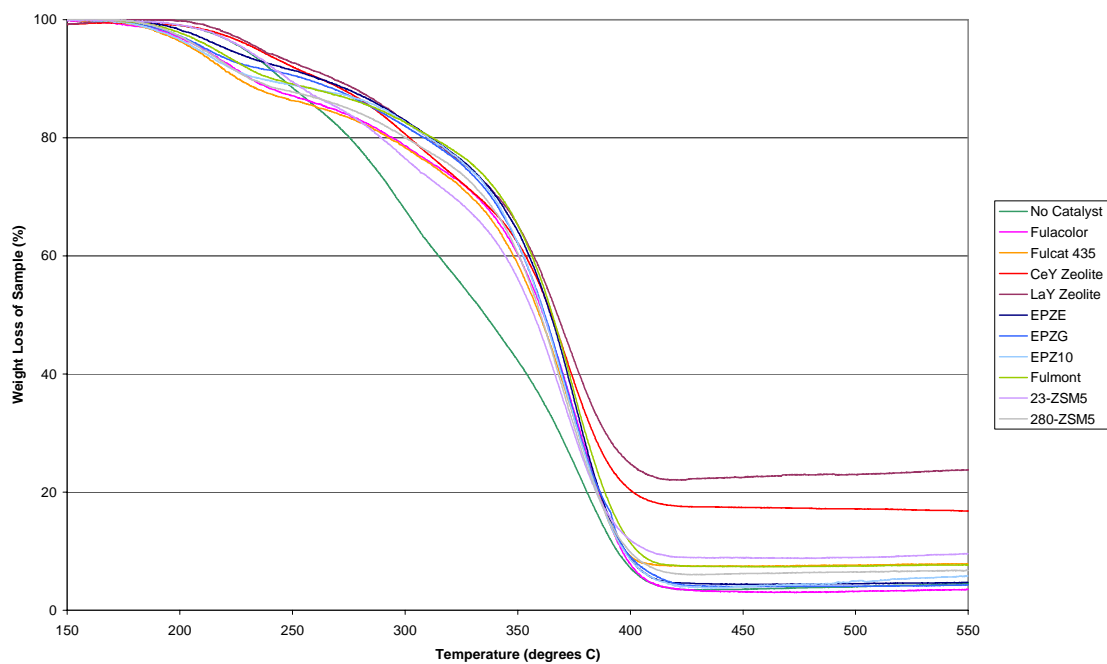
Figure D.18: TG curves for waste polymethyl methacrylate (PMMA)

U-Tube Furnace Results

Table E.1: Ten most common gaseous products detected from the degradation of pure polymers in the presence of catalysts

	PLDPE	PLDPE-Fulcat	PHDPE	PHDPE-Fulcat	PHDPE-EPZ10	PHDPE-CeY	PHDPE-23z	PHDPE-280z	PPPA	PPPA-Fulcat	PPPB	PPPB-Fulcat	PPPB-EPZG	PPPB-EPZ10
Butene	1	1	1	1	2	4	1	2	1	1	1	1	1	1
2,2-dimethylpropane														
2-methylbutane														
*Iso*butene														
(Z)-2-pentene	5	7	5	5	7	10	7	8	4	6	5	7	6	6
1-pentene		6			1	1	3	1	9	10	8	2	8	7
Pentane	8	9	9	9		9			8	9	10		10	10
2-methylbut-1-ene	3	4	4	4	5	5	5	4	3	3	3	5	4	5
2-methylbut-2-ene	9	10	6	6	10		9	10		7	9	9	9	9
3-methylbut-1-ene	6	3	2	2	3		4	5	6	2	7	3	2	2
Butane	2	2	7	7	4	2	6	6	2	5	2	6	5	4
Propene	4	5	3	3	6	7	2	3	5	4	4	4	3	3
Propane														
n-butane	10					8								
Methane					9	3	10	9				10		
Ethene	7	8	8	8	8	6	8	7	7	8	6	8	7	8
Ethane														
Methylbutene			10	10					10					

Straight-Tube Results

Table E.2: Ten most common gaseous products detected from the degradation of pure LDPE in the presence of catalysts

	PLDPE	PLDPE-Fulcat	PLDPE-280z	PLDPE-LaY	PLDPE-EPZE	PLDPE-EPZG	PLDPE-EPZ10a	PLDPE-EPZ10b
1-Butene								9
*Iso*butane								
trans-2-butene								
o-xylene								
m-xylene								
p-xylene								
Ethylbenzene								
cis-2-butene	2	2	2	2	2	2	2	2
2,2-dimethylpropane								
2-methylbutane	9	8	9	7	9	8	9	
*Iso*butene								10
(Z)-2-pentene	5	7	7	8	8	7	6	6
1-pentene	8		8				8	8
Pentane	3	3	4	3	3	3	4	5
2-methylbut-1-ene	6	4	5	5	5	5	5	4
2-methylbut-2-ene	7	6	6	4	6	6	7	7
3-methylbut-1-ene	4	5	3	9	4	4	3	3
Butane								
Propene	1	1	1	1	1	1	1	1
Propane	10		10				10	
n-butane		10		6	10	9		
Methane								
Ethene								
Ethane		9		10	7	10		

Table E.3: Ten most common gaseous products detected from the degradation of pure PPB in the presence of catalysts

	PPB	PPB-Fulacolor	PPB-Fulcat	PPB-Fulmont	PPB-EPZG	PPB-EPZG	PPB-EPZ10	PPB-280z	PPB-23z
1-Butene									
*Iso*butane									
trans-2-butene									
o-xylene									
m-xylene									
p-xylene									
Ethylbenzene									
cis-2-butene	2	2	2	2	2	2	2	2	2
2,2-dimethylpropane									
2-methylbutane	10	10	8	8	10	10	8	10	10
*Iso*butene									
(Z)-2-pentene	4	6	7	6	6	6	6	8	7
1-pentene	8	8	9=	9	9	9	10		
Pentane	3	4	3	4	4	4	4	3	3
2-methylbut-1-ene	5	3	5	5	5	5	5	5	4
2-methylbut-2-ene	6	7	6	7	7	7	7	7	5
3-methylbut-1-ene	7	5	4	3	3	3	3	4	6
Butane									
Propene	1	1	1	1	1	1	1	1	1
Propane									
n-butane	9		9=	10			9	9	9
Methane									
Ethene									
Ethane		9			8	8		6	8

Mixtures of Plastics

Table E.4: Ten most common gaseous products detected from the degradation of polymer mixtures in the presence of a variety of catalysts

	PLDPE+PPPB +280z	WHDPE+PPPB +23z	WHDPE+PLDPE +PPB+23z	WHDPE+PLDPE +PPB+Fulcat
1-Butene				
*Iso*butane				
trans-2-butene				
o-xylene				
m-xylene				
p-xylene				
Ethylbenzene				
cis-2-butene	2	2	2	2
2,2-dimethylpropane				
2-methylbutane				8
*Iso*butene				
(Z)-2-pentene	7	7	7	7
1-pentene	9	9		10
Pentane	5	4	3	3
2-methylbut-1-ene	3	3	4	4
2-methylbut-2-ene	6	5	5	6
3-methylbut-1-ene	4	6	6	5
Butane				
Propene	1	1	1	1
Propane	10	10	10	
n-butane			9	9
Methane				
Ethene				
Ethane	8	8	8	

Appendix F

ASTM D3170 Qualitative Calibration Mix
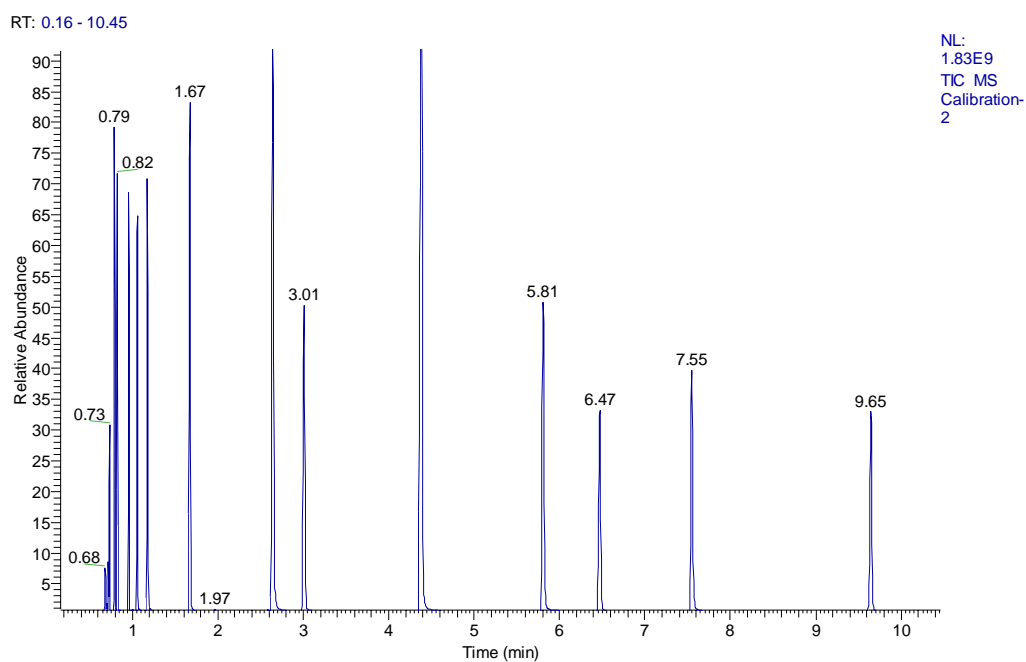
Figure F.1: Chromatogram of D3170 Quantitative Calibration Mix

Table F.1: Identification of components in D3170 Quantitative Calibration Mix

Retention Time (mins)	Component
0.72	*n*-propane
0.73	2-methylpropane
0.73	*n*-butane
0.79	2-methylbutane
0.82	*n*-pentane
0.96	2-methylpentane
1.06	*n*-hexane
1.18	2,4-dimethyl pentane
1.67	*n*-heptane
2.64	toluene
3.01	*n*-octane
4.39	*p*-xylene
5.81	propyl-benzene
6.47	*n*-decane
7.55	butyl-benzene
9.65	*n*-dodecane
11.08	*n*-tridecane
12.43	*n*-tetradecane
13.70	*n*-pentadecane

References

[1] *Council Directive 91/156/EEC of 18 March 1991.*

[2] *Kyoto Protocol to the United Nations Framework Convention on Climate Change*, http://unfcc.int/resource/docs/convkp/kpeng.html.

[3] *Official Journal of the European Communities, 28.12.2000, L332/96-L332/99.*

[4] S. Otoma, Y. Mori, A. Terazono, T. Aso, R. Sameshima, *Resources, Conservation and Recycling*, 1997, **20**, pp 95-117.

[5] P. McKendry, *Bioresource Technology*, 2002, **83**, pp 37-46.

[6] B. Baum, C. H. Parker, *in Solid Waste Disposal, Volume 1: Incineration and Landfill.*

[7] A. F. M. Barton, *Resource Recovery and Recycling*, 1979, John Wiley & Sons.

[8] DEFRA, *Municipal Waste Management Survey 2003/04*, 2005, Department for the Environment, Food and Rural Affairs, UK.

[9] Biffa Waste Services, *Future Perfect - an Analysis of Britain's Waste Production and Disposal Account, with Implications for Industry and Government for the next Twenty Years*, 2003, pp 1-105.

[10] J. Singer, *Resources, Conservation and Recycling*, 1995, **14**, pp 133-155.

[11] Environmental Resources Ltd., *Economic Instruments and Recovery of Resources from Waste*, 1992, Department of Trade and Industry, Department of the Environment.

[12] A. Parkes, *Journal of the Franklin Institute*, 1863, **75**, p 69.

[13] W. C. Ferguson, *in Plastics and the Environment*, 1974, Ed. J. J. P. Staudinger, Hutchinson & Co.

[14] *Official Journal of the European Communities*, 1994, pp 10-23

[15] *Official Journal of the European Communities*, 2000.

[16] Waste Watch & Recoup, *Plastics in the UK Economy*, 2003, http://www.wasteonline.org.uk/resources/WasteWatch/PlasticsUKEconomy.pdf

[17] www.defra.gov.uk/Environment/waste/topics/packaging.

[18] R. J. Sperber, S. L. Rosen, *Polymer Plastic Technology Engineering*, 1974, **3**, pp 215-239.

[19] A. G. R. Manser, A. A. Keeling, *Practical Handbook of Processing and Recycling Municipal Waste*, 1996, CRC Press, Inc.

[20] H. Shent, R. J. Pugh, E. Forssberg, *Resources, Conservation and Recycling*, 1999, **25**, pp 85-109.

[21] S. Ashley, *Mechanical Engineering*, 1995, p 117.

[22] G. Paula, *Mechanical Engineering*, 1997, p 119.

[23] J. G. Poulakis, C. D. Papaspyrides, *Resources, Conservation and Recycling*, 1997, **20**, pp 31-41.

[24] G. Pappa et al., *Resources, Conservation and Recycling*, 2001, **34**, pp 33-44.

[25] *Organic Chemistry - Structure and Reactivity*, 1999, Houghton Mifflin Company, pp 1024-1064.

[26] Jr. F. W. Billmeyer, *Textbook of Polymer Science*, 1971, John Wiley & Sons, Inc., ed. Second.

[27] J. W. Nicholson, *The Chemistry of Polymers*, 1991, Royal Society of Chemistry.

[28] A. D. Baker, R. Engel, *Organic Chemistry*, 1992, West Publishing Company.

[29] R. B. Seymour, Jr. C. E. Carraher, *Polymer Chemistry: An Introduction*, 1992, Marcel Dekker, Inc., ed. Third.

[30] S. L. Madorsky, *Thermal Degradation of Organic Polymers*, 1964, John Wiley & Sons, Inc.

[31] M. Herrera, G. Matuschek, A. Kettrup, *Journal of Analytical and Applied Pyrolysis*, 2003, **70**, pp 35-42.

[32] F. C.-Y. Wang, *Journal of Chromatography*, 2000, pp 199-210.

[33] B. C. Gates, *in Catalytic Chemistry*, 1992, John Wiley & Sons, Inc.

[34] B. C. Gates, *in Catalytic Chemistry*, 1992, John Wiley & Sons, Inc.

[35] E. B. M. Daesburg, J. H. C. van Hooff, *in Catalysis - An Integrated Approach to Homogeneous, Heterogeneous and Industrial Catalysis*, 1993, Eds. J. A. Moulijn, P. W. N. M. van Leeuwen, R. A. van Santen, Elsevier Science.

[36] J. Cejka, S. Zones, A. Corma, *Zeolites and Catalysis: Volume 1*, 2010, Wiley-VCH, p 496.

[37] J. A. Rabo, C. L. Angell, V. Schomaker, *Proceedings of the Fourth International Congress on Catalysis*, 1968, pp 96-113.

[38] L. V. C. Rees, *in Proceedings of the First European Symposium on Thermal Analysis*, 1976, Ed. D. Dollimore, Heyden & Son Ltd.

[39] F. Lemos, F. R. Ribeiro, M. Kern, G. Giannetto, M. Guisnet, *Applied Catalysis*, 1987, **29**, pp 43-54.

[40] D. E. Akporiaya, K. Daasvatn, J. Solberg, M. Stöcker, *Heterogeneous Catalysis and Fine Chemicals III*, 1993, pp 521-526.

[41] H. S. Sherry, *Journal of Physical Chemistry*, 1966, **70**, pp 1158-1168.

[42] J. W. Ward, *Journal of Catalysis*, 1966, **13**, pp 321-327.

[43] M. Malinowski, S. Krzyzanowski, *in Proceedings of the DFirst European Symposium on Thermal Analysis*, 1976, Ed. D. Dollimore, Heyden & Son Ltd.

44 C. Gauthier, B. Chiche, A. Finiels, P. Geneste, *Journal of Molecular Catalysis A: Chemical*, 1989, **50**, pp 219-229.

45 F. Lemos, F. R. Ribeiro, M. Kern, G. Giannetto, M. Guisnet, *Applied Catalysis*, 1988, **39**, pp 227-238.

46 R. Carvajal, P. J. Chu, J. H. Lunsford, *Journal of Catalysis*, 1990, **125**, pp 123-131.

47 K. Gaare, D. Akporiaye, *Journal of Molecular Catalysis A: Chemical*, 1996, **109**, pp 177-187.

48 E. F. T. Lee, L. V. C. Rees, *Zeolites*, 1987, **7**, pp 143-147.

49 E. F. T. Lee, L. V. C. Rees, *Zeolites*, 1987, **7**, pp 446-450.

50 J. G. Nery, Y. P. Mascarenhas, T. J. Bonagamba, N. C. Mello, E. F. Souza-Aguiar, *Zeolites*, 1997, **18**, pp 44-49.

51 A. Chatterjee, D. Bhattacharya, T. Iwasaki, T. Ebina, *Journal of Catalysis*, 1999, **185**, pp 23-32.

52 H. C. Woo, K. H. Lee, J. S. Lee, *Applied Catalysis A: General*, 1996, **134**, pp 147-158.

53 J. S. Buchanan, *Catalysis Today*, 2000, **55**, pp 207-212.

54 R. W. McCabe, *in Inorganic Materials*, 1996, Eds. D. W. Bruce and D. O'Hare, John Wiley & Sons Ltd.

55 J. N. Ganguli, B. Bhagawati, *in Catalysis in Petroleum and Petrochemical Industries*, 2005, Eds. K. G. Bhattacharyya, A. K. Talukdar, Narosa Publishing House.

56 C. L. Thomas, J. Hickey, G. Stecker, *Industrial and Engineering Chemistry Research*, 1950, **42**, pp 866-871.

57 D. N. Todor, *Thermal Analysis of Minerals*, 1976, Abacus Press.

58 R. C. Mackenzie, *in Physiochemical Methods of Mineral Analysis*, 1975, Ed. A. W. Nicol, Plenum Press, New York.

59 B. V. Liengme, W. K. Hall, *Transactions of the Faraday Society*, 1966, **62**, pp 3229-3243.

60 J. B. Uytterhoeven, L. G. Christner, W. K. Hall, *Journal of Physical Chemistry*, 1965, **69**, pp 2117-2126.

61 S. Guggenheim, A. F. Koster van Groos, *Clays and Clay Minerals*, 2001, **49**, pp 433-443.

62 T. A. Korneva, T. S. Yusupov, *in Proceedings of the First European Symposium on Thermal Analysis*, 1976, Ed. D. Dollimore, Heyden & Son Ltd.

63 J. A. Moulijn, A. E. van Diepen, F. Kapteijn, *Applied Catalysis A: General*, 2001, **212**, pp 3-16.

64 R. G. Haldeman, M. C. Botty, *Journal of Physical Chemistry*, 1959, **63**, pp 489-496.

65 S. M. Holmes, A. Garforth, B. Maunders, J. Dwyer, *Applied Catalysis A: General*, 1997, **151**, pp 355-372.

66 P. D. Hopkins et al., *Applied Catalysis A: General*, 1996, **136**, pp 29-48.

67 Y. San You, J. H. Kim, G. Seo, *Polymer Degradation and Stability*, 2000, **70**, pp 365-371.

68 W. C. McCaffrey, M. R. Kamal, D. G. Cooper, *Polymer Degradation and Stability*, 1995, **47**, pp 133-139.

69 K. Gobin, G. Manos, *Polymer Degradation and Stability*, 2004, **83**, pp 267-279.

70 P. T. Williams, E. A. Williams, *Journal of Analytical and Applied Pyrolysis*, 1999, **51**, pp 107-126.

71 B. J. Milne, L. A. Behie, F. Berruti, *Journal of Analytical and Applied Pyrolysis*, 1999, **51**, pp 157-166.

72 Y. Sakata et al., *Journal of Analytical and Applied Pyrolysis*, 1997, **43**, pp 15-25.

73 C. Breen, P. M. Last, S. Taylor, P. Komadel, *Thermochimica Acta*, 2000, **363**, pp 93-104.

74 L. Ballice, *Fuel*, 2001, **80**, pp 1923-1935.

75 Y. San You, J. H. Kim, G. Seo, *Polymer Degradation and Stability*, 2000, **70**, pp 365-371.

76 W. C. McCaffrey, M. R. Kamal, D. G. Cooper, *Polymer Degradation and Stability*, 1995, **47**, pp 133-139.

77 K. Gobin, G. Manos, *Polymer Degradation and Stability*, 2004, **83**, pp 267-279.

78 Y. Sakata et al., *Journal of Analytical and Applied Pyrolysis*, 1997, **43**, pp 15-25.

79 C. Breen, P. M. Last, S. Taylor, P. Komadel, *Thermochimica Acta*, 2000, **363**, pp 93-104.

80 G. Manos, I. Y. Yusof, N. H. Gangas, N. Papayannakos, *Energy and Fuels*, 2002, **16**, pp 485-489.

81 Y. Uemichi, Y. Kashiwaya, A. Ayame, H. Kanoh, *Chemistry Letters*, 1984, pp 41-44.

82 H. Ohkita et al., *Industrial and Engineering Chemistry Research*, 1993, **32**, pp 3112-3116.

83 A. Ayame, Y. Uemichi, T. Yoshida, H. Kanoh, *Journal of Japanese Petroleum Instrumentation*, 1979, **22**, pp 280-287.

84 G. Audisio and A. Silvani, *Journal of Analytical and Applied Pyrolysis*, 1984, **7**, pp 83-90.

85 W. Zhao et al., *Polymer Degradation and Stability*, 1996, **53**, pp 129-135.

86 S. C. Cardona and A. Corma, *Applied Catalysis B: Environmental*, 2000, **25**, pp 151-162.

87 E. Y. Hwang, J. R. Kim, J. K. Choi, H. C. Woo, D. W. Park, *Journal of Analytical and Applied Pyrolysis*, 2002, **62**, pp 351-354.

88 M. Azhar Uddin et al., *Microporous and Mesoporous Materials*, 1998, **21**, pp 557-564.

89   P. Onu, C. Vasile, S. Ciocilteu, E. Iojoiu, H. Darie, *Journal of Analytical and Applied Pyrolysis*, 1999, **49**, pp 145-153.

90   Y. Sakata, M. Uddin, A. Muto, *Journal of Analytical and Applied Pyrolysis*, 1999, **51**, pp 135-155.

91   J. Aguado, D. P. Serrano, J. M. Escola, E. Garagorri, J. A. Fernandez, *Polymer Degradation and Stability*, 2000, **69**, pp 11-16.

92   Q. Zhou, L. Zheng, Y. Z. Wang, G. M. Zhao, B. Wang, *Polymer Degradation and Stability*, 2004, **84**, pp 493-497.

93   N. Grassie, W. W. Kerr, *Transactions of the Faraday Society*, 1957, **53**, pp 234-239.

94   Y. D. M. Simard, M. R. Kamal, D. G. Cooper, *Journal of Applied Polymer Science*, 1995, **58**, pp 843-851.

95   A. Karaduman, E. H. Simsek, B. Cicek, A. Y. Bilgesu, *Journal of Analytical and Applied Pyrolysis*, 2001, **60**, pp 179-186.

96   P. Carniti, A. Gervasini, P. L. Beltrame, G. Audisio, F. Bertini, *Applied Catalysis A: General*, 1995, **127**, pp 139-155.

97   Z. Zhang et al., *Industrial and Engineering Chemistry Research*, 1995, **34**, pp 4514-4519.

98   P. Carniti, A. Gervasini, P. L. Beltrame, G. Audisio, F. Bertini, *Applied Catalysis A: General*, 1995, **127**, pp 139-155.

99   Z. Zhibo et al., *Catalysis Today*, 1996, **29**, pp 303-308.

100   G. de la Puente and U. Sedran, *Applied Catalysis B: Environmental*, 1998, **19**, pp 305-311.

101   D. P. Serrano, J. Aguado, J. M. Escola, *Applied Catalysis B: Environmental*, 2000, **25**, pp 181-189.

102   J. D. Peterson, S. Vyazovkin, C. A. Wight, *Macromolecular Chemical Physics*, 2001, **202**, pp 775-784.

103   K. H. Lee, N. S. Noh, D. H. Shin, Y. Seo, *Polymer Degradation and Stability*, 2002, **78**, pp 539-544.

104   J. Walendziewski, *Fuel*, 2002, **81**, pp 473-481.

105   A. Demirbas, *Journal of Analytical and Applied Pyrolysis*, 2004, **72**, pp 97-102.

106   J. J. Maurer, *in Thermal Characterisation of Polymeric Materials*, 1981, Ed. E. A. Turi, Academic Press, Inc.

107   H. F. Mark, E. H. Immergut, *in Thermal Degradation of Organic Polymers - Volume 7*, 1964, Ed. S. L. Madorsky, John Wiley & Sons, Inc.

108   S. Straus, S. L. Madorsky, *Journal of Research of the National Bureau of Standards - A.Physics and Chemistry*, 1958, **61**, pp 77-81.

[109] F. C.-Y. Wang, P. B. Smith, *Analytical Chemistry*, 1996, **68**, pp 425-430.

[110] S. L. Madorsky, *in Thermal Degradation of Organic Polymers - Volume 7*, 1964, Ed. S. L. Madorsky, John Wiley & Sons, Inc.

[111] Z. Wolkóber, *in High Temperature Resistance and Thermal Degradation of Polymers - S. C. I. Mongoraph No. 13*, 1961, Ed. Society of Chemical Industry, Page Bros. (Norwich) Ltd.

[112] J. Muller, G. Dongmann, *Journal of Analytical and Applied Pyrolysis*, 1998, **45**, pp 59-74.

[113] J. Schirmer, J. S. Kim, E. Klemm, *Journal of Analytical and Applied Pyrolysis*, 2001, **60**, pp 205-217.

[114] S. L. Madorsky, *in Thermal Degradation of Organic Polymers - Volume 7*, 1964, Eds. H. F. Mark and E. H. Immergut, John Wiley & Sons, Inc.

[115] S. L. Madorsky and S. Straus, *Journal of Research of the National Bureau of Standards - A.Physics and Chemistry*, 1959, pp 216-268.

[116] E. A. Radell and H. C. Strutz, *Analytical Chemistry*, 1959, **31**, pp 1890-1891.

[117] J. Strassburger, G. M. Brauer, M. Tryon, A. F. Forziati, *Analytical Chemistry*, 1960, **32**, pp 454-457.

[118] T. Hirata, T. Kashiwagi, J. E. Brown, *Macromolecules*, 1985, **18**, pp 1410-1418.

[119] T. Kashiwagi and A. Inabi, *Polymer Degradation and Stability*, 1989, **26**, pp 161-184.

[120] L. H. Buxbaum, *Angew.Chem.Internat.Edit.*, 1968, **7**, pp 182-190.

[121] E. P. Goodings, *in High Temperature Resistance and Thermal Degradation of Polymers - S. C. I. Mongoraph No. 13*, 1961, Ed. Society of Chemical Industry, Page Bros. (Norwich) Ltd.

[122] P. D. Ritchie, *in High Temperature Resistance and Thermal Degradation of Polymers - S. C. I. Mongoraph No. 13*, 1961, Ed. Society of Chemical Industry, Page Bros. (Norwich) Ltd.

[123] T. Masuda et al., *Polymer Degradation and Stability*, 1997, **58**, pp 315-320.

[124] E. M. Pearce, Y. P. Khanna, D. Raucher, *in Thermal Characterisation of Polymeric Materials*, 1981, Ed. E. A. Turi, Academic Press, Inc.

[125] S. Straus, L. A. Wall, *Journal of Research of the National Bureau of Standards - A.Physics and Chemistry*, 1958, **60**, pp 39-45.

[126] M. Day, J. D. Cooney, M. MacKinnon, *Polymer Degradation and Stability*, 1995, **48**, pp 341-349.

[127] C. Molero, A. de Lucas, J. F. Rodriguez, *Polymer Degradation and Stability*, 2006, **91**, pp 894-901.

[128] N. Kiran Ciliz, E. Ekinci, C. E. Snape, *Waste Management*, 2004, **24**, pp 173-181.

[129] N. Kiran Ciliz, E. Ekinci, C. E. Snape, *Waste Management*, 2004, **24**, pp 173-181.

[130] N. Kiran Ciliz, E. Ekinci, C. E. Snape, *Resources, Conservation and Recycling*, 2000, **29**, pp 273-283.

[131] A. Marcilla, J. C. Garcia-Quesada, S. Sanchez, R. Ruiz, *Journal of Analytical and Applied Pyrolysis*, 2005, **74**, pp 387-392.

[132] L. Ballice, *Fuel*, 2002, **81**, pp 1233-1240.

[133] F. Pinto, P. Costa, I. Gulyurtlu, I. Cabrita, *Journal of Analytical and Applied Pyrolysis*, 1999, **51**, pp 39-55.

[134] J. R. Kim, J. H. Yoon, D. W. Park, *Polymer Degradation and Stability*, 2002, **76**, pp 61-67.

[135] Y. Sakata, M. A. Uddin, K. Koizumi, K. Murata, *Polymer Degradation and Stability*, 1996, **53**, pp 111-117.

[136] Y. Sakata et al., *Polymer Recycling*, 1996, **2**, pp 309-315.

[137] J. A. Moulijn, R. A. Sheldon, H. van Bekkum, P. W. N. M. van Leeuwen, *in Catalysis - An Integrated Approach to Homogeneous, Heterogeneous and Industrial Catalysis*, 1993, Eds. J. A. Moulijn, P. W. N. M. van Leeuwen, R. A. van Santen, Elsevier Science.

[138] S. Van der Baan, *in Modern Petroleum Technology*, 1962, Ed. The Institute of Petroleum.

[139] S. R. M. Ellis, M. F. Mohtadi, *in Modern Petroleum Technology*, 1962, Ed. The Institute of Petroleum.

[140] D. L. Samuel, *in Modern Petroleum Technology*, 1962, Ed. The Institute of Petroleum.

[141] The Shell Petroleum Company Limited, *The Petroleum Handbook*, 1948, Ed. The Petroleum Handbook, James Truscoff and Son Limited.

[142] I. D. G. Berwick, *in Petroleum Based Fuels and Automotive Applications*, 1986.

[143] W. A. Gruse, D. R. Stevens, *Chemical Technology of Petroleum*, 1960, McGraw-Hill Book Company, Inc., pp 343-399.

[144] B. J. Mair, *in Chemical Technology of Petroleum*, 1960, Eds. W. A. Gruse, D. R. Stevens, McGraw-Hill Book Company, Inc.

[145] E. V. Murphee, G. Ciprios, *in Modern Petroleum Technology*, 1962, Ed. The Institute of Petroleum.

[146] C. R. Reddy, Y. S. Bhat, G. Nagendrappa, B. S. Jai Prakash, *Catalysis Today In Press*, Corrected Proof.

[147] T. Masuda et al., *Chemical Engineering Journal*, 2001, **82**, pp 173-181.

[148] W. A. Gruse, D. R. Stevens, *Chemical Technology of Petroleum*, 1960, McGraw-Hill Book Company, Inc., pp 343-399.

[149] J. H. Gary, G. E. Handwerk, *Petroleum Refining Technology and Economics, Second Edition*, 1984, Marcel Dekker, Inc.

¹⁵⁰ J. W. Scott, A. G. Bridge, *in Origin and Refining of Petroleum*, 1971, Ed. R. F. Gould, American Chemical Society.

¹⁵¹ F. W. B. Porter, P. T. White, *Modern Petroleum Technology*, 1962, Ed. The Institute of Petroleum.

¹⁵² J. G. Speight, *The Chemistry and Technology of Petroleum*, 1999, Marcel Dekker, Inc.

¹⁵³ S. Sisvasanker, *Catalysis in Petroleum and Petrochemical Industries*, 2005, Eds. K. G. Bhattacharyya, A. K. Talukdar, Narosa Publishing House.

¹⁵⁴ E. V. Murphee, G. Ciprios, *Modern Petroleum Technology*, 1962, The Institute of Petroleum.

¹⁵⁵ S. Ghosh, S. K. Ray, *Catalysis in Petroleum and Petrochemical Industries*, 2005, Eds. K. G. Bhattacharyya, A. K. Talukdar, Narosa Publishing House.

¹⁵⁶ The Shell Company Limited, *The Petroleum Handbook*, 1948, James Truscott and Son Limited, pp 220-237.

¹⁵⁷ http://www.rockwoodspecialities.com; accessed on 27/05/2011.

¹⁵⁸ http://www.scprod.com/product_bulletins/PBFulcat435.pdf; accessed on 27/05/2011.

¹⁵⁹ http://www.amcuk.ltd.uk/bleaching_earth.htm; accessed on 06/07/2011.

¹⁶⁰ J. A. Gardner, Ph.D. Thesis, University of Central Lancashire, 2004.

¹⁶¹ G. Bond, J. A Gardner, R. W. McCabe, D. J. Shorrock, *Journal of Molecular Catalysis A: Chemical*, 2007, **278**, Issues 1-2, pp 1-5.

¹⁶² http://www.chemelab.ucsd.edu/methanol/memos/ZSM-5.html.

¹⁶³ C. Albano, E. de Freitas, *Polymer Degradation and Stability*, 1998, **61**, pp 289-295

¹⁶⁴ D. M. Bate, R. S. Lehrle, *Polymer Degradation and Stability*, 1998, **62**, pp 57-66

¹⁶⁵ M. Landau, A. Molyneux, *in Differential Thermal Analysis, Volume 2*, 1972, Ed. R. C. Mackenzie, Academic Press Inc. Ltd.

¹⁶⁶ M. S. Spencer, *in Catalyst Handbook*, 1996, Ed. M. V. Twigg, Manson Publishing Ltd.

¹⁶⁷ H. M. F. Freundlich, *Journal of Physical Chemistry,* 1909, **57**, pp385-470.

¹⁶⁸ I. Langmuir, *Journal of the American Chemical Society*, 1916, 38, pp 2221-2295.

¹⁶⁹ S. Brunauer, P. H. Emmett, E. Teller, *Journal of the American Chemical Society*, 1938, **60**, pp 309-319.

¹⁷⁰ J. J. F. Scholten, "*The Use of Adsorption Methods for the Assessment of the Surface Area and Pore Size Distribution of Heterogeneous Catalysts*", in J. A. Moulijn, P.W.N.M. van Leeuwen, R. A van Santen, "*Catalysis: An Integrated Approach to Homogeneous, Heterogeneous and Industrial Catalysis*", Elsevier Science, 1993.

[171] E. W Washburn, *Physics Review*, 1921, **17**, p 273.

[172] W. T. Thomson, *Phil. Mag.*, 1871, **42**, p 448.

[173] J. P. Oliver, W. B. Conklin, *International Symposium on the Effects of Surface Heterogeneity in Adsorption and Catalysis on Solids*, Poland, July 1992.

[174] C. R. Reddy, Y. S. Bhat, G. Nagendrappa, B. S. Jai Prakash, *Catalysis Today In Press*, Corrected Proof.

[175] F. Arena, R. Dario, A. Parmaliana, *Applied Catalysis A: General*, 1998, **170**, pp 127-137.

[176] E. Selli, L. Forni, *Microporous and Mesoporous Materials*, 1999, **31**, pp 129-140.

[177] F. Arena, R. Dario, A. Parmaliana, *Applied Catalysis A: General*, 1998, **170**, pp 127-137.

[178] M. Azhar Uddin et al., *Microporous and Mesoporous Materials*, 1998, **21**, pp 557-564.

[179] Y. Sakata, M. Uddin, A. Muto, *Journal of Analytical and Applied Pyrolysis*, 1999, **51**, pp 135-155.

[180] A. Marcilla, J. C. Garcia-Quesada, S. Sanchez, R. Ruiz, *Journal of Analytical and Applied Pyrolysis*, 2005, **74**, pp 387-392.

[181] J. H. Clark, S. R. Cullen, S. J. Barlow, T. W. Bastock, *Journal of the Chemical Society - Perkin Transactions*, 1994, **2**, pp 1117-1130.

[182] G. L. Miessler, D. A. Tarr, *Inorganic Chemistry*, Second Edition, Prentice-Hall, 1998.

[183] C. A. Emeis, *Journal of Catalysis*, 1993, **141**, pp 347-354.

[184] G. L. Woolery, G. H. Kuehl, H. C. Timken, A. W. Chester, J. C. Vartuli, *Zeolites*, 1997, **19**, pp 288-296.

[185] K. Tanabe, *Solid Acids and Bases: Their Catalytic Properties*, 1970, Academic Press, Inc., pp 1-3

[186] R. S. Drago, S. C. Dias, M. Torrealba, L. de Lima, *Journal of the American Chemical Society*, 1997, **119**, pp 4444-4452

[187] G. K. Misra, K. G. Bhattacharyya, S. Sivasanker, in *Catalysis in Petroleum and Petrochemical Industries*, 2005, Eds. K. G. Bhattacharyya, A. K. Talukdar, Narosa Publishing House

[188] J. W. Ward, *Journal of Catalysis*, 1967, **9**, pp 225-236.

[189] Jr. P. E. Eberly, *Journal of Physical Chemistry*, 1968, **72**, pp 1042-1047.

[190] R. Ch. Deka, in *Catalysis in Petroleum and Petrochemical Industries*, 2005, Eds. K. G. Bhattacharyya, A. K. Talukdar, Narosa Publishing House.

[191] E. Falabella Sousa-Aguiar, V. L. D. Camorim, F. M. Z. Zotin, R. L. Correa dos Santos, *Microporous and Mesoporous Materials*, 1998, **25**, pp 25-34.

[192] D. Ballivet, P. Pichat, D. Barthomeuf, *Molecular Sieves*, 1973, pp 469-479

¹⁹³ M. C. Maldonado et al., *in Catalyst Deactivation, C. H. Bartholomew and G. A. Fuentes*, 1997, Eds. C. H. Bartholomew, G. A. Fuentes, Elsevier Science B. V.

¹⁹⁴ D. R. Brown, C. N. Rhodes, *Thermochimica Acta*, 1997, **294**, pp 33-37.

¹⁹⁵ E. Selli, L. Forni, *Microporous and Mesoporous Materials*, 1999, **31**, pp 129-140.

¹⁹⁶ W. Kaminsky, *Journal of Analytical and Applied Pyrolysis*, 1985, **8**, pp 439-448.

¹⁹⁷ G. Engelhardt, *in Studies in Surface Science and Catalysis*, 2001, Eds. H. van Bekkum, E. M. Flanigen, P. A. Jacobs, J. C. Jansen.

¹⁹⁸ J. Klinowski, *Colloids and Surfaces*, 1989, **36**, pp 133-154.

¹⁹⁹ M. Hunger, *Solid State Nuclear Magnetic Resonance*, 1996, **6**, pp 1-29.

²⁰⁰ C. J. Pouchert, *The Aldrich Library of Infrared Spectra*, Second Edition, Aldrich Chemical Co., 1975.

²⁰¹ C. J. Keattch, *in Proceedings of the First European Symposium on Thermal Analysis*, 1976, Ed. D. Dollimore, Heyden & Son Ltd.

²⁰² W. W. Wendlandt, P. K. Gallagher, *in Thermal Characterization of Polymeric Materials*, 1981, Ed. E. A. Turi, Academic Press, Inc.

²⁰³ D. Dollimore, *in Thermal Analysis - Techniques and Applications*, 1992, Eds. E. L. Charsley, S. B. Warrington, The Royal Society of Chemistry.

²⁰⁴ M. E. Brown, *Introduction to Thermal Analysis Techniques and Applications*, 1988, Chapman and Hall Ltd.

²⁰⁵ A. W. Coats, J. P. Redfern, *Analyst*, 2005, **88**, pp 906-924.

²⁰⁶ S. St. J. Warne, *in Thermal Analysis - Techniques and Applications*, 1992, Eds. E. L. Charsley, S. B. Warrington, The Royal Society of Chemistry.

²⁰⁷ A. C. Norris, M. I. Pope, M. Selwood, *in Proceedings of the First European Symposium on Thermal Analysis*, 1976, Ed. D. Dollimore, Heyden & Son Ltd.

²⁰⁸ A. C. Norris, M. I. Pope, M. Selwood, *in Proceedings of the First European Symposium on Thermal Analysis*, 1976, Ed. D. Dollimore, Heyden & Son Ltd.

²⁰⁹ H. C. Anderson, *in Techniques and Methods of Polymer Evaluation, Volume 1*, 1966, Eds. Jr. P. E. Slade, L. T. Jenkins, Marcel Dekker, Inc.

²¹⁰ A. E. Newkirk, *Analytical Chemistry*, 1960, **32**, pp 1558-1563.

²¹¹ H. C. Anderson, *Journal of Polymer Science: Part C*, 1963, pp 175-182.

²¹² S. Glasstone, *in Textbook of Physical Chemistry*, 1948, Ed. S. Glasstone, Macmillan and Company Limited.

²¹³ W. Gomes, *Nature*, 1961, **192**, pp 865-866.

[214] C. D. Doyle, *Journal of Applied Polymer Science*, 1961, **5**, pp 285-292.

[215] E. S. Freeman, B. Carroll, *Journal of Physical Chemistry*, 1958, **62**, pp 394-397.

[216] A. W. Coats, J. P. Redfern, *Nature*, 1964, **201**, pp 68-69.

[217] J. H. Sharp, S. A. Wentworth, *Analytical Chemistry*, 1969, **41**, pp 2060-2062

[218] H. Horowitz, G. Metzger, *Analytical Chemistry*, 1963, **35**, pp 1464-1468.

[219] C. Albano, E. de Freitas, *Polymer Degradation and Stability*, 1998, **61**, pp 289-295.

[220] H. Bockhorn, A. Hornung, U. Hornung, P. Jakobstroer, *Journal of Analytical and Applied Pyrolysis*, 1999, **49**, pp 53-74.

[221] P. Carniti, A. Gervasini, S. Bernardelli, *Polymer Degradation and Stability*, 1997, **57**, 3, pp 301-306.

[222] L. A. Pérez-Maqueda, P. E. Sánchez-Jiménez, J. M. Criado, *Polymer*, 2005, **46**, 9, pp 2950-2954.

[223] H. Bockhorn, A. Hornung, U. Hornung, *Journal of Analytical and Applied Pyrolysis*, 1999, **50**, pp 77-101.

[224] A. K. Kaw, E. Kalu, *Numerical Methods with Applications*, 2008, autarkaw.com.

[225] C. Albano, E. de Freitas, *Polymer Degradation and Stability*, 1998, **61**, pp 289-295.

[226] H. Bockhorn, A. Hornung, U. Hornung, *Journal of Analytical and Applied Pyrolysis*, 1998, **46**, pp 1-13.

[227] S. Straus, S. L. Madorsky, *Journal of Research of the National Bureau of Standards - A.Physics and Chemistry*, 1958, **61**, pp 77-81.

[228] J. J. Maurer, *in Thermal Characterisation of Polymeric Materials*, 1981, Ed. E. A. Turi, Academic Press, Inc.

[229] H. Bockhorn, A. Hornung, U. Hornung, *Journal of Analytical and Applied Pyrolysis*, 1999, **50**, pp 77-101.

[230] T. Hirata, T. Kashiwagi, J. E. Brown, *Macromolecules*, 1985, **18**, pp 1410-1418.

[231] J. A. Lercher, R. A. van Santen, H. Vinek, *Catalysis Letters*, 1994, **27**, pp 91-96.

[232] V. B. Kazansky, *Catalysis Today*, 1999, **51**, pp 419-434.

[233] I. Milas, M. A. C. Nascimento, *Chemical Physical Letters*, 2003, **373**, pp 379-384.

[234] X. Zheng, P. Blowers, *Journal of Molecular Catalysis A: Chemical*, 2005, **229**, pp 77-85.

[235] X. Zheng, P. Blowers, *Journal of Molecular Catalysis A: Chemical*, 2006, **246**, pp 1-10.

[236] J. Macht, R. T. Carr, E. Iglesia, *Journal of Catalysis*, 2009, **264**, pp 54-66.

[237] A. Ayame, Y. Uemichi, T. Yoshida, H. Kanoh, *Journal of Japanese Petroleum Instrumentation*, 1979, **22**, pp 280-287.

[238] N. Horvat, F. T. T. Ng, *Fuel*, 1999, **78**, pp 459-470.

[239] L. Ballice, *Fuel*, 2001, **80**, pp 1923-1935.

[240] A. Garforth et al., *Thermochimica Acta*, 1997, **294**, pp 65-69.

[241] Y.-H. Lin, P. N. Sharratt, A. A. Garforth, J. Dwyer, *Thermochimica Acta*, 1997, **294**, pp 45-50.

[242] H. Bockhorn, A. Hornung, U. Hornung, D. Schawaller, *Journal of Analytical and Applied Pyrolysis*, 1999, **48**, pp 93-109.

[243] N. Kiran, E. Ekinci, C. E. Snape, *Conservation and Recycling*, 2000, **29**, pp 273-283.

[244] J. H. Chan, S. T. Balke, *Polymer Degradation and Stability*, 1997, **57**, pp 135-149.

[245] A. Durmus, S. Naci Koc, G. Selda Pozan, A. Kasgoz, *Applied Catalysis B: Environmental*, 2005, **61**, pp 316-322.

[246] J. D. Peterson, S. Vyazovkin, C. A. Wight, *Macromolecular Chemical Physics*, 2001, **202**, pp 775-784.

[247] Y. Kodera, B. J. McCoy, *Energy and Fuels*, 2002, **16**, pp 119-126.

[248] M. Day, J. D. Cooney, M. MacKinnon, *Polymer Degradation and Stability*, 1995, **48**, pp 341-349.

[249] H. H. G. Jellinek, M. D. Luh, *Journal of Physical Chemistry*, 1966, **70**, pp 3672-3680.

[250] A. Barlow, R. S. Lehrle, J. C. Robb, *Polymer*, 1961, **2**, pp 267-281.

[251] Jr. P. E. Slade, L. T. Jenkins, *in Techniques & Methods of Polymer Evaluation, Volume 1*, 1966, Marcel Dekker, Inc.

[252] W. W. Wendlandt, P. K. Gallagher, *in Thermal Characterization of Polymeric Materials*, 1981, Ed. E. A. Turi, Academic Press, Inc.

[253] B. D. Mitchell, A. C. Birnie, *in Differential Thermal Analysis, Volume 1*, 1970, Ed. R. C. Mackenzie, Academic Press Inc. Ltd.

[254] V. J. Griffin, P. G. Laye, *in Thermal Analysis - Techniques and Applications*, 1992, Eds. E. L. Charsley, S. B. Warrington, The Royal Society of Chemistry.

[255] M. I. Pope, M. D. Judd, *Differential Thermal Analysis - A Guide to the Technique and its Applications*, 1977, Heyden & Son Ltd.

[256] A. D. Cunningham, F. W. Wilburn, *in Differential Thermal Analysis - Volume 1*, 1970, Ed. R. C. Mackenzie, Academic Press Inc. Ltd.

[257] R. C. Mackenzie, B. D. Mitchell, *Analyst*, 1962, **87**, pp 420-434.

²⁵⁸ M. E. Brown, *Introduction to Thermal Analysis Techniques and Applications*, 1988, Chapman and Hall Ltd.

²⁵⁹ D. J. David, *Analytical Chemistry*, 1964, **36**, pp 2162-2166.

²⁶⁰ http://www.anasys.co.uk/library/dsc2.htm.

²⁶¹ J. H. Sharp, *in Differential Thermal Analysis, Volume 2*, 1972, Ed. R. C. Mackenzie, Academic Press Inc. Ltd.

²⁶² H. E. Kissinger, *Analytical Chemistry*, 1957, **29**, pp 1702-1706.

²⁶³ H. J. Borchardt, F. Daniels, *Journal of the American Chemical Society*, 1956, **79**, pp 41-46.

²⁶⁴ D. J. David, *in Techniques & Methods of Polymer Evaluation, Volume 1*, 1966, Eds. Jr. P. E. Slade, L. T. Jenkins, Marcel Dekker, Inc.

²⁶⁵ R. N. Walters, S. M. Hackett, R. E. Lyon, *"Heats of Combustion of High Temperature Polymers"*, Federal Aviation Administration.

²⁶⁶ L. M. Harwood, T. D. W. Claridge, *Introduction to Organic Spectroscopy*, 1997, Oxford University Press.

²⁶⁷ S. F. Dyke, A. J. Floyd, M. Sainsbury, R. S. Theobald, *in Organic Spectroscopy - an Introduction*, 1971, Penguin Books Ltd.

²⁶⁸ J. W. Cooper, *in Spectroscopic Techniques for Organic Chemists*, 1980, John Wiley & Sons, Inc.

²⁶⁹ E. W. Neumann, H. G. Nadeau, *Analytical Chemistry*, **35**, <u>10</u>, 1963, pp 1454-1457.

²⁷⁰ B. Groten, *Analytical Chemistry*, 1964, **36**, pp 1206-1212.

²⁷¹ C. E. Roland Jones, A. F. Moyles, *Nature*, 1961, **191**, pp 663-665.

²⁷² B. C. Cox, B. Ellis, *Analytical Chemistry*, 1964, **36**, pp 90-96.

²⁷³ G. J. Mol, R. J. Gritter, G. E. Adams, *in Applications of Polymer Spectroscopy*, 1978, Ed. E. G. Jr. Brame, Academic Press, Inc.

²⁷⁴ J. C. J. Bart, *Journal of Analytical and Applied Pyrolysis*, 2001, pp 3-28.

²⁷⁵ S. Tsuge, H. Ohtani, *Polymer Degradation and Stability*, 1997, **58**, pp 109-130.

²⁷⁶ P. T. Williams, E. A. Williams, *Journal of Analytical and Applied Pyrolysis*, 1999, **51**, pp 107-126.

²⁷⁷ C. Breen, P. M. Last, S. Taylor, P. Komadel, *Thermochimica Acta*, 2000, **363**, pp 93-104.

²⁷⁸ P. Onu, C. Vasile, S. Ciociteu, E. Iojoiu, H. Darie, *Journal of Analytical and Applied Pyrolysis*, 1999, **49**, pp 145-153.

²⁷⁹ Y. H. Seo, K. H. Lee, D. H. Shin, *Journal of Analytical and Applied Pyrolysis*, 2003, **70**, pp 383-398.

[280] D. P. Chynoweth, J. M. Owens, R. Legrand, *Renewable Energy*, 2001, **22**, pp 1-8.

[281] E. W. Tegelaar, J. W. de Leeuw, *Journal of Analytical and Applied Pyrolysis*, 1989, **15**, pp 289-295.

[282] V. Mangut et al., *Fuel Processing Technology*, 2006, **87**, pp 109-115.

[283] R. H. Walter, R. M. Sherman, *Journal of Agricultural Food Chemistry*, 1976, **24**, pp 1244-1245.

[284] F. Subrez-GarcÆa, A. MartÆnez-Alonso, J. M. D. Tasc£n, *Journal of Analytical and Applied Pyrolysis*, 2002, **62**, pp 93-109

[285] J. Mata-Alvarez, S. Mace, P. Llabres, *Bioresource Technology*, 2000, **74**, pp 3-16

[286] V. K. Sharma, C. Testa, G. Castelluccio, *Energy Conversion and Management*, 1999, **40**, pp 369-384.

[287] G. D. Zupancic, N. Uranjek-Zevart, M. Ros, *Biomass and Bioenergy In Press*, Corrected Proof.

[288] G. Lastella et al., *Energy Conversion and Management*, 2002, **43**, pp 63-75.

[289] X. Gomez, M. J. Cuetos, J. Cara, A. Moran, A. I. Garcia, *Renewable Energy*, 2006, **31**, pp 2017-2024.

[290] *TGA-50 Thermogravimetric Analyzer Instruction Manual*, 1989, Shimadzu Corporation, pp 11-21.

[291] *Service Manual of DTA-50 Differential Thermal Analyzer*, 1989, Shimadzu Corporation.

[292] A. Ayame, Y. Uemichi, T. Yoshida, H. Kanoh, *Journal of Japanese Petroleum Instrumentation*, 1979, **22**, pp 280-287.

[293] *Journal of Japanese Petroleum Instrumentation*, 1986, **111**, pp 1065-1067.

[294] A. R. Songip, T. Masuda, H. Kuwahara, K. Hashimoto, *Applied Catalysis B: Environmental*, 1993, **2**, pp 153-164.

[295] T. Masuda, H. Kuwahara, S. Mukai, K. Hashimoto, *Chemical Engineering Science*, 1999, **54**, pp 2773-2779.

[296] J. Schirmer, J. S. Kim, E. Klemm, *Journal of Analytical and Applied Pyrolysis*, 2001, **60**, pp 205-217.

[297] Y. San You, J. H. Kim, G. Seo, *Polymer Degradation and Stability*, 2000, **70**, pp 365-371.

[298] W. C. McCaffrey, M. R. Kamal, D. G. Cooper, *Polymer Degradation and Stability*, 1995, **47**, pp 133-139.

[299] G. Manos, I. Y. Yusof, N. H. Gangas, N. Papayannakos, *Energy and Fuels*, 2002, **16**, pp 485-489.

[300] K. Gobin, G. Manos, *Polymer Degradation and Stability*, 2004, **83**, pp 267-279.

[301] Y. Uemichi, Y. Kashiwaya, A. Ayame, H. Kanoh, *Chemistry Letters*, 1984.

[302] H. Ohkita et al., *Industrial and Engineering Chemistry Research*, 1993, **32**, pp 3112-3116.

[303] R. C. Mordi, R. Fields, J. Dwyer, *Journal of Analytical and Applied Pyrolysis*, 1994, **29**, pp 45-55.

[304] M. Blazso, B. Zelei, *Journal of Analytical and Applied Pyrolysis*, 1996, **36**, pp 149-158.

[305] B. J. Milne, L. A. Behie, F. Berruti, *Journal of Analytical and Applied Pyrolysis*, 1999, **51**, pp 157-166.

[306] A. Marcilla, M. Beltran, J. A. Conesa, *Journal of Analytical and Applied Pyrolysis*, 2001, pp 117-126.

[307] R. Bagri, P. T. Williams, *Journal of Analytical and Applied Pyrolysis*, 2002, **63**, pp 29-41.

[308] G. de la Puente, C. Klocker, U. Sedran, *Applied Catalysis B: Environmental*, 2002, **36**, pp 279-285.

[309] Q. Zhou, Y. Z. Wang, C. Tang, Y. H. Zhang, *Polymer Degradation and Stability*, 2003, **80**, pp 23-30.

[310] D. P. Serrano, J. Aguado, J. M. Escola, J. M. Rodriguez, G. San Miguel, *Journal of Analytical and Applied Pyrolysis*, 2005, **74**, pp 370-378.

[311] A. Garforth et al., *Thermochimica Acta*, 1997, **294**, pp 65-69.

[312] A. A. Garforth, Y.-H. Lin, P. N. Sharratt, J. Dwyer, *Applied Catalysis A: General*, 1998, **169**, pp 331-342.

[313] Y. Sakata et al., *Journal of Analytical and Applied Pyrolysis*, 1997, **43**, pp 15-25.

[314] Y.-H. Lin, P. N. Sharratt, A. A. Garforth, J. Dwyer, *Thermochimica Acta*, 1997, **294**, pp 45-50.

[315] C. Breen, P. M. Last, *Journal of Materials Chemistry*, 1999, **9**, pp 813-818.

[316] D. W. Park et al., *Polymer Degradation and Stability*, 1999, **65**, pp 193-198.

[317] S. Ali, A. A. Garforth, D. H. Harris, D. J. Rawlence, Y. Uemichi, *Catalysis Today*, 2002, **75**, pp 247-255.

[318] J. W. Park, J. H. Kim, G. Seo, *Polymer Degradation and Stability*, 2002, **76**, pp 495-501.

[319] M. A. Uddin, K. Koizumi, K. Murata, Y. Sakata, *Polymer Degradation and Stability*, 1997, **56**, pp 37-44.

[320] N. Horvat, F. T. T. Ng, *Fuel*, 1999, **78**, pp 459-470.

[321] L. Ballice, *Fuel*, 2001, **80**, pp 1923-1935.

322 J. Schirmer, J. S. Kim, E. Klemm, *Journal of Analytical and Applied Pyrolysis*, 2001, **60**, pp 205-217.

323 R. van Grieken, D. P. Serrano, J. Aguado, R. Garcia, C. Rojo, *Journal of Analytical and Applied Pyrolysis*, 2001, pp 127-142.

324 G. Manos, I. Y. Yusof, N. Papayannakos, N. H. Gangas, *Industrial and Engineering Chemistry Research*, 2001, **40**, pp 2220-2225.

325 A. Marcilla, A. Gomez, A. N. Garcia, M. Mar Olaya, *Journal of Analytical and Applied Pyrolysis*, 2002, **64**, pp 85-101.

326 A. Marcilla, M. I. Beltran, F. Hernandez, R. Navarro, *Applied Catalysis A: General*, 2004, **278**, pp 37-43.

327 A. Marcilla, M. I. Beltran, R. Navarro, *Journal of Analytical and Applied Pyrolysis*, 2005, **74**, pp 361-369.

328 D. P. Serrano, J. Aguado, J. M. Escola, J. M. Rodríguez, *Journal of Analytical and Applied Pyrolysis*, 2005, **74**, pp 353-360.

329 J. V. Schooten, P. W. O. Wijga, *in High Temperature Resistance and Thermal Degradation of Polymers - S. C. I. Mongoraph No. 13*, 1961, Ed. Society of Chemical Industry, Page Bros. (Norwich) Ltd.

330 J. H. Chan, S. T. Balke, *Polymer Degradation and Stability*, 1997, **57**, pp 135-149.

331 G. Audisio, A. Silvani, *Journal of Analytical and Applied Pyrolysis*, 1984, **7**, pp 83-90.

332 R. C. Mordi, J. Dwyer, R. Fields, *Polymer Degradation and Stability*, **46**, 1, 1994, pp 57-62.

333 W. Zhao et al., *Polymer Degradation and Stability*, 1996, **53**, pp 129-135.

334 S. C. Cardona, A. Corma, *Applied Catalysis B: Environmental*, 2000, **25**, pp 151-162.

335 E. Jakab, G. Varhegyi, O. Faix, *Journal of Analytical and Applied Pyrolysis*, 2000, **56**, pp 273-285.

336 E. Y. Hwang, J. R. Kim, J. K. Choi, H. C. Woo, D. W. Park, *Journal of Analytical and Applied Pyrolysis*, 2002, **62**, pp 351-364.

337 J. R. Kim, Y. A. Kim, J. H. Yoon, D. W. Park, H. C. Woo, *Polymer Degradation and Stability*, 2002, **75**, pp 287-294.

338 A. Marcilla, A. Gomez, J. A. Reyes-Labarta, A. Giner, F. Hernandez, *Journal of Analytical and Applied Pyrolysis*, 2003, pp 476-480.

339 A. Durmus, S. Naci Koc, G. Selda Pozan, A. Kasgoz, *Applied Catalysis B: Environmental*, 2005, **61**, pp 316-322.

340 M. Azhar Uddin et al., *Microporous and Mesoporous Materials*, 1998, **21**, pp 557-564.

341 Y. Sakata, M. Uddin, A. Muto, *Journal of Analytical and Applied Pyrolysis*, 1999, **51**, pp 135-155.

342 J. Aguado, D. P. Serrano, J. M. Escola, E. Garagorri, J. A. Fernandez, *Polymer Degradation and Stability*, 2000, **69**, pp 11-16.

343 Q. Zhou, L. Zheng, Y. Z. Wang, G. M. Zhao, B. Wang, *Polymer Degradation and Stability*, 2004, **84**, pp 493-497.

344 N. Grassie, W. W. Kerr, *Transactions of the Faraday Society*, 1957, **53**, pp 234-239.

345 Y. D. M. Simard, M. R. Kamal, D. G. Cooper, *Journal of Applied Polymer Science*, 1995, **58**, pp 843-851.

346 Z. Zhang et al., *Industrial and Engineering Chemistry Research*, 1995, **34**, pp 4514-4519.

347 P. Carniti, A. Gervasini, P. L. Beltrame, G. Audisio, F. Bertini, *Applied Catalysis A: General*, 1995, **127**, pp 139-155.

348 Z. Zhibo et al., *Catalysis Today*, 1996, **29**, pp 303-308.

349 X. Guoxi, R. Liang, T. Qinhu, L. Jinghua, *Journal of Applied Polymer Science*, 1999, **73**, pp 1139-1143.

350 G. de la Puente, U. Sedran, *Applied Catalysis B: Environmental*, 1998, **19**, pp 305-311.

351 D. P. Serrano, J. Aguado, J. M. Escola, *Applied Catalysis B: Environmental*, 2000, **25**, pp 181-189.

352 A. Karaduman, E. H. Simsek, B. Cicek, A. Y. Bilgesu, *Journal of Analytical and Applied Pyrolysis*, 2001, **60**, pp 179-186.

353 V. Karmore, G. Madras, *Industrial and Engineering Chemistry Research*, 2002, **41**, pp 657-660.

354 Z. Zhibo et al., *Catalysis Today*, 1996, **29**, pp 303-308.

355 J. Mertinkat, A. Kirsten, M. Predel, W. Kaminsky, *Journal of Analytical and Applied Pyrolysis*, 1999, **49**, pp 87-95.

356 T. Faravelli, G. Bozzano, M. Colombo, E. Ranzi, M. Dente, *Journal of Analytical and Applied Pyrolysis*, 2003, **70**, pp 761-777.

357 J. D. Peterson, S. Vyazovkin, C. A. Wight, *Macromolecular Chemical Physics*, 2001, **202**, pp 775-784.

358 K. H. Lee, N. S. Noh, D. H. Shin, Y. Seo, *Polymer Degradation and Stability*, 2002, **78**, pp 539-544.

359 J. Walendziewski, *Fuel*, 2002, **81**, pp 473-481.

360 A. Demirbas, *Journal of Analytical and Applied Pyrolysis*, 2004, **72**, pp 97-102

361 L. H. Buxbaum, *Angew.Chem.Internat.Edit.*, 1968, **7**, pp 182-190.

362 E. P. Goodings, *in High Temperature Resistance and Thermal Degradation of Polymers - S. C. I. Mongoraph No. 13*, 1961, Ed. Society of Chemical Industry, Page Bros. (Norwich) Ltd.

363 P. D. Ritchie, *in High Temperature Resistance and Thermal Degradation of Polymers - S. C. I. Mongoraph No. 13*, 1961, Ed. Society of Chemical Industry, Page Bros. (Norwich) Ltd.

364 T. Masuda et al., *Polymer Degradation and Stability*, 1997, **58**, pp 315-320.

365 T. Masuda, Y. Miwa, K. Hashimoto, Y. Ikeda, *Polymer Degradation and Stability*, 1998, **61**, pp 217-224.

366 F. C.-Y. Wang, P. B. Smith, *Analytical Chemistry*, 1996, **68**, pp 425-430.

367 S. L. Madorsky, *in Thermal Degradation of Organic Polymers - Volume 7*, 1964, Eds. H. F. Mark and E. H. Immergut, John Wiley & Sons, Inc.

368 Z. Wolkóber, *in High Temperature Resistance and Thermal Degradation of Polymers - S. C. I. Mongoraph No. 13*, 1961, Ed. Society of Chemical Industry, Page Bros. (Norwich) Ltd.

369 J. Muller, G. Dongmann, *Journal of Analytical and Applied Pyrolysis*, 1998, **45**, pp 59-74.

370 C. H. Wu, C. Y. Chang, J. P. Lin, Y. Liang, *Journal of Hazardous Materials*, 1998, **58**, pp 105-205.

371 H. Bockhorn, A. Hornung, U. Hornung, *Journal of Analytical and Applied Pyrolysis*, 1999, **50**, pp 77-101.

372 E. M. Pearce, Y. P. Khanna, D. Raucher, *in Thermal Characterisation of Polymeric Materials*, 1981, Ed. E. A. Turi, Academic Press, Inc.

373 H. Kachi, H. H. G. Jellinek, *Journal of Polymer Science: Polymer Science Edition 17*, 1979, pp 2031-2038.

374 S. Straus, L. A. Wall, *Journal of Research of the National Bureau of Standards - A.Physics and Chemistry*, 1958, **60**, pp 39-45.

375 J. J. Maurer, *in Thermal Characterisation of Polymeric Materials*, 1981, Ed. E. A. Turi, Academic Press, Inc.

376 H. F. Mark, E. H. Immergut, *in Thermal Degradation of Organic Polymers - Volume 7*, 1964, Ed. S. L. Madorsky, John Wiley & Sons, Inc.

377 S. Straus, S. L. Madorsky, *Journal of Research of the National Bureau of Standards - A.Physics and Chemistry*, 1958, **61**, pp 77-81.

378 W. J. Burlant, J. L. Parsons, *Journal of Polymer Science*, 1956, **22**, pp 249-256

379 S. L. Madorsky, *in Thermal Degradation of Organic Polymers - Volume 7*, 1964, Eds. H. F. Mark and E. H. Immergut, John Wiley & Sons, Inc.

380 R. C. Houtz, *Textile Research Journal*, November 1950, pp 786-800.

381 S. L. Madorsky, S. Straus, *Journal of Research of the National Bureau of Standards - A.Physics and Chemistry*, 1959, pp 261-268.

382 N. Chatterjee, S. Basu, S. K. Palit, M. M. Maiti, *Journal of Polymer Science: Part B: Polymer Physics*, 1995, **33**, pp 1705-1712.

383 S. P. Frankoski, S. Siggia, *Analytical Chemistry*, 1972, **44**, pp 2078-2080.

384 L. Zhao, B. Z. Jang, *Journal of Materials Science*, 1995, **30**, pp 4535-4540.

385 E. A. Radell, H. C. Strutz, *Analytical Chemistry*, 1959, **31**, pp 1890-1891.

386 J. Strassburger, G. M. Brauer, M. Tryon, A. F. Forziati, *Analytical Chemistry*, 1960, **32**, pp 454-457.

387 T. Hirata, T. Kashiwagi, J. E. Brown, *Macromolecules*, 1985, **18**, pp 1410-1418.

388 T. Kashiwagi, A. Inabi, *Polymer Degradation and Stability*, 1989, **26**, pp 161-184.

389 H. H. G. Jellinek, M. D. Luh, *Journal of Physical Chemistry*, 1966, **70**, pp 3672-3680.

390 A. Barlow, R. S. Lehrle, J. C. Robb, *Polymer*, 1961, **2**, pp 267-281.

391 B. Zhang, F. D. Blum, 2001, **42**, p 2.

392 F. C.-Y. Wang, P. B. Smith, *Analytical Chemistry*, 1996, **68**, pp 3033-3037.

393 D. M. Bate, R. S. Lehrle, *Polymer Degradation and Stability*, 1997, **55**, pp 295-299.

394 M. Day, J. D. Cooney, M. MacKinnon, *Polymer Degradation and Stability*, 1995, **48**, pp 341-349.

395 C. Molero, A. de Lucas, J. F. Rodriguez, *Polymer Degradation and Stability*, 2006, **91**, pp 894-901.

396 M. M. Ibrahim, E. Hopkins, M. S. Seehra, *Fuel Processing Technology*, 1996, **49**, pp 65-73.

397 P. K. Ramdoss, A. R. Tarrer, *Fuel*, **77**, 4, 1998, pp 239-299.

398 L. Ballice, *Fuel*, 2002, **81**, pp 1233-1240.

399 A. Marcilla, J. C. Garcia-Quesada, S. Sanchez, R. Ruiz, *Journal of Analytical and Applied Pyrolysis*, 2005, **74**, pp 387-392.

400 C. Albano, E. de Freitas, *Polymer Degradation and Stability*, 1998, **61**, pp 289-295.

401 K. Ja-Kong, K. Seok-Wan, *Waste Management & Research*, 1993, **11**, pp 515-529.

402 N. Kiran, E. Ekinci, C. E. Snape, *Conservation and Recycling*, 2000, **29**, pp 273-283.

403 W. Kaminsky, B. Schlesselmann, C. Simon, *Journal of Analytical and Applied Pyrolysis*, 1995, **32**, pp 19-27.

404 W. Kaminsky, B. Schlesselmann, C. M. Simon, *Polymer Degradation and Stability*, 1996, **53**, pp 189-197.

405 F. Pinto, P. Costa, I. Gulyurtlu, I. Cabrita, *Journal of Analytical and Applied Pyrolysis*, 1999, **51**, pp 39-55.

[406] J. R. Kim, J. H. Yoon, D. W. Park, *Polymer Degradation and Stability*, 2002, **76**, pp 61-67.

[407] N. Kiran Ciliz, E. Ekinci, C. E. Snape, *Waste Management*, 2004, **24**, pp 173-181.

[408] C. H. Wu, C. Y. Chang, J. P. Lin, Y. Liang, *Journal of Hazardous Materials*, 1998, **58**, pp 195-205.

[409] D. M. Bate, R. S. Lehrle, *Polymer Degradation and Stability*, 1998, **62**, pp 57-66.

[410] M. V. S. Murty, P. Rangarajan, E. A. Grulke, D. Bhattacharyya, *Fuel Processing Technology*, 1996, **49**, pp 75-90.

[411] Y. Sakata, M. A. Uddin, K. Koizumi, K. Murata, *Polymer Degradation and Stability*, 1996, **53**, pp 111-117.

[412] Y. Sakata *et al.*, *Polymer Recycling*, 1996, **2**, pp 309-315.

[413] J. S. Kim, W. Kaminsky, B. Schlesselmann, *Journal of Analytical and Applied Pyrolysis*, 1997, pp 365-372.

[414] W. Ding, J. Liang, L. L. Anderson, *Fuel Processing Technology*, 1997, **51**, pp 47-62.

[415] E. A. Williams, P. T. Williams, *Journal of Analytical and Applied Pyrolysis*, 1997, pp 347-363.

[416] P. T. Williams, E. A. Williams, *Journal of the Institute of Energy*, 1998, **71**, pp 81-93.

[417] H. Bockhorn, A. Hornung, U. Hornung, *Journal of Analytical and Applied Pyrolysis*, 1998, **46**, pp 1-13.

[418] H. Bockhorn, A. Hornung, U. Hornung, P. Jakobstroer, M. Kraus, *Journal of Analytical and Applied Pyrolysis*, 1999, **49**, pp 97-106.

[419] M. Blazso, *Journal of Analytical and Applied Pyrolysis*, 1999, **51**, pp 73-88.

[420] W. Kaminsky, J. S. Kim, *Journal of Analytical and Applied Pyrolysis*, 1999, **51**, pp 127-134.

[421] C. Vasile et al., *Journal of Analytical and Applied Pyrolysis*, 2001, **57**, pp 287-303.

[422] T. Masuda et al., *Chemical Engineering Journal*, 2001, **82**, pp 173-181.

[423] Y. H. Seo, D. H. Shin, *Fuel*, 2002, **81**, pp 2103-2112.